The behaviour of reinforced concrete beams under cyclic temperature profiles

Richardson, Michael

THE BEHAVIOUR OF REINFORCED CONCRETE BEAMS UNDER CYCLIC TEMPERATURE PROFILES

by

Michael Richardson

To Bill and Val

ABSTRACT

On a hot summer day, high levels of solar radiation are incident on concrete bridge decks, causing non-linear variations in temperature through the depths of the structures. The changes in temperature lead to axial expansion and curvature of decks. In addition, self-equilibrating stresses arise from the non-linearity of the temperature profiles. In continuous structures, where axial expansion and curvature may be restrained, secondary thermal stresses are induced also.

Tests are described in which reinforced concrete beams were subjected to daily cycles of heating. Applied temperature profiles were similar to maximum positive profiles for the United Kingdom.

It was found that a linear elastic analysis, based on the uncracked section, generally gave an adequate prediction of thermal strains of non-loaded and loaded single span beams during heating cycles. Changes in curvature, during heating, were substantially modified in the early stages of loading, due to the existence of creep curvatures. Two span beams were tested also, with special regard to changes in support reactions during heating. No evidence was found in any of the tests of increases in the extent of cracking as a result of heating.

Daily heating cycles were imposed over several weeks and evidence was found of a steady increase in the coefficient of thermal expansion, attributed to drying.

Changes in curvature resulting from non-uniform shrinkage were observed, these being greatest in non-heated beams. Creep curvatures were found to increase roughly in proportion to the time-averaged beam temperature. Creep results were compared with prediction methods, including an incremental rate of creep analysis.

Additional tests are described in which variations in moisture content and in the coefficient of thermal expansion within members were identified, using a segmentation technique.

ACKNOWLEDGEMENTS

I am grateful to Dr. A.R. Selby for his help and advice, during his supervision of this project.

I should like to express gratitude to those members of the technical staff of this department who were involved with the project. They include Mr. B.P. Scurr, Mr. T. Nancarrow, Mr. F. Emery and Mr. W.C. Roscamp. Thanks are due also to Miss L.A. Graham and Mr. P.R. Nicholson for their assistance during the preparation of this thesis.

Finally, I am grateful to Mr. J.M. Terrill for his invaluable assistance with the moisture content tests.

THE BEHAVIOUR OF REINFORCED CONCRETE BEAMS UNDER CYCLIC TEMPERATURE PROFILES

by

Michael Richardson

Thesis Submitted for the Degree of

Doctor of Philosophy

in the Faculty of Science

University of Durham

April 1986

LIST OF CONTENTS

CHAPTER IV

COMPUTER PROGRAMS AND SENSITIVITY STUDY

CHAPTER V

VARIATIONS IN MOISTURE CONTENT IN MEMBERS

CHAPTER VIII

RESULTS AND DISCUSSION OF LONG-TERM BEAM RESPONSE

CHAPTER IX

CONCLUSIONS AND SUGGESTIONS FOR FURTHER WORK

LIST OF FIGURES

LIST OF PHOTOGRAPHS

LIST OF GRAPHS OF EXPERIMENTAL RESULTS

No material contained in this thesis has previously been submitted for a degree in this or any other university.

CHAPTER I

INTRODUCTION

In common with most materials, concrete expands when heated. In cases where the expansion is restrained, thermal stresses are induced. The effects of temperature differences in concrete structures have been considered by a number of workers. The storage cells, used in certain types of North Sea oil platforms, experience temperature differentials when they are filled with hot oil or gas (1). The example is cited (2) of thermal stresses in silos used for the storage of initially hot cement grains. Chimneys experience severe temperature differences as a result of the passage of hot flue gases. Since the advent of the nuclear power industry, attention has been paid to thermal stresses in pressurised water reactor vessels. Structures experience temperature differences also as a result of climatic effects. Evidence is reported of thermally induced cracking in retaining walls (3) and in the columns of a multi-storey car park (4). The effects of variations in ambient conditions have been considered also in relation to concrete roofs (5) and water tanks (6). Since the early 1970's considerable attention has been drawn to temperatures in concrete bridge decks.

Before 1973, specifications for the loads on bridge decks (7) included an overall temperature range and a maximum temperature difference between components. The temperature range was used to define the overall expansion or contraction of members and was thus of interest in the choice of expansion joints. The temperature difference was available for the calculation of thermal curvatures and stresses.

During the 1960's and 1970's, the Transport and Road Research Laboratory undertook an extensive study of temperatures in bridge decks. Much of this work was concerned with effective bridge temperatures for the purpose of setting bearings and expansion joints (eg 8). The work was extended to include the variations in temperature which occur within members. A calculation method was developed to predict temperature profiles, using known meteorological data, and findings were supported by results from structures in service. It was demonstrated that highly non-linear temperature profiles could occur as a result of diurnal environmental variations (eg 9). Similar conclusions were drawn by Priestley (eg 10), working in New Zealand.

In 1973, Technical Memorandum BE5/73 (11) was issued, recommending non-linear design temperature profiles. Similar design profiles are included in the present bridge code, BS5400.

The inclusion of the non-linear temperature profile is of particular importance in consideration of design stresses. A non-uniform linear profile does not in itself require any consideration of thermal stresses, unless external restraint to thermal strains is present. However, a non-linear temperature profile necessarily induces thermal stresses, due to the internal restraint of thermal strains. Also, as before, the external restraint of overall thermal movements causes the secondary thermal stresses.

It has been argued (12,13,14) that thermal stresses are not an ultimate limit state problem. The thermal load emanates from a strain, not a force. As ultimate is approached, the gradient of the load/deflection curve for concrete becomes much reduced, so that, for

a given thermal strain, the corresponding change in stress is slight. The proposition has been investigated experimentally using single span and continuous beams (15). It was found that the existence of severe temperature profiles did not affect the ultimate moment of members.

It appears then that temperature effects are primarily a serviceability problem. Here the design requirements for reinforced concrete have become less stringent. Whereas previously stresses of up to a third of the cube strength were permitted, the current limit state permits stresses of up to $0.5f_{cu}$.

There is no doubt that non-linear temperature profiles, of the type specified in the code, do actually occur in bridge decks, but there are a number of questions to be answered regarding their effects at service loads. These include :

i. Can thermal strains be predicted on the basis of an uncracked section analysis ?

ii. How sensitive are predictions to variations in parameters such as the coefficient of thermal expansion, the elastic modulus or the degree of cracking ?

iii. Does creep modify strains induced by temperature profiles ?

iv. Are cracks initiated during heating and are existing cracks affected ?

v. What changes in support reactions of two span continuous beams result from temperature profiles ?

vi. In the case of a member with a moisture concentration profile, how much does the coefficient of thermal expansion vary within the member and what is the effect on thermal strains ?

In order to investigate these matters, a series of tests was performed on reinforced concrete beams. The beams were subjected to daily cycles of heating, producing temperature profiles corresponding to summer conditions in the United Kingdom. Initial tests were performed on single span beams, where temperature profiles and strains were monitored during heating. Tests were conducted on continuous two span beams, where thermally induced changes in support reactions were recorded. Non-loaded companion beams were included in the tests.

Each test was extended over several weeks, during which time the long-term strains were observed. In this way, it was possible also to detect age dependent trends in the daily thermal response.

To provide the predictions of the daily thermal strains in test beams, a computer analysis was developed. The program is briefly described in Chapter IV, where a sensitivity study can be found also. In addition, descriptions of the creep prediction programs are given in Chapter IV.

Chapter V deals with the variations in moisture content and in the coefficient of thermal expansion which occur within members. These results have a bearing on the main test results which follow and they raise the matter of potentially damaging stresses due to shrinkage behaviour during non-uniform drying. The main tests are described and discussed in Chapters VI, VII and VIII. The most important results from this project, regarding the daily thermal response of beams, are described in Chapter VII. The long-term results, of secondary interest, are described in Chapter VIII.

CHAPTER II

TEMPERATURES IN CONCRETE BRIDGE DECKS

2.1 Introduction

Bridge decks experience changes in temperature due to seasonal climatic variations, with a superimposed diurnal fluctuation. These temperature changes cause longitudinal strains, which may be accommodated at expansion joints or by the flexure of piers. Also, due to the transient nature of environmental conditions, there exist temperature differences within the deck which induce curvatures. The magnitude of such curvatures is roughly proportional to the difference in temperature between the top surface and the soffit. Since the variation of temperature with depth is generally non-linear, thermal stresses occur and, if the longitudinal movement or curvature are restrained, then additional secondary thermal stresses result.

Over recent years, a greater understanding of these effects has been sought in order to improve design recommendations. In the U.K., a great deal of work on the subject has been performed at the T.R.R.L. and the major findings of this work will be described. These will be compared, where possible, with results obtained by other workers. The terminology which will be used here is consistent with that of Emerson (9).

2.2 Factors Affecting Bridge Temperatures

The factors which influence bridge temperatures are extrinsic, or environmental, and intrinsic, relating to the materials and construction of the member. Figure 1 shows the major environmental factors which influence bridge temperatures. As far as climatic influences are concerned, radiation and in particular direct solar

radiation are generally of greatest importance. The rays of the sun fall onto the surface of the structure in the form of short-wave radiation with an additional contribution of diffuse short-wave radiation from the day-time sky. The latter is known as indirect solar radiation. The member emits some of its acquired heat energy in the form of long-wave radiation but this type of radiation, which is emitted by surrounding objects and the atmosphere, is also absorbed by the member.

In addition to radiation, heat energy exchange at the surface of the member takes place by convection and conduction and these processes are influenced by the temperature of the air. Wind speed is also of importance here since it affects the layer of air which is in close proximity to the concrete surface.

Considering the intrinsic factors, the exchange of radiation energy is affected by the absoptivity and emissivity of the surface of the member. Within the member, the transfer of heat is by conduction. The rate at which temperatures change is governed by the thermal diffusivity. For concrete, its magnitude is relatively small. Due to this, and the fact that concrete members are relatively massive, the average temperature of a bridge deck changes slowly, lagging behind ambient conditions. A further important consequence of this is that highly non-linear temperature variations can occur through the depth of the member.

2.2.1 Radiation and Reradiation

The levels of solar radiation which reach the atmosphere vary between 1300 Wm^{-2} and 1400 Wm^{-2}, depending on the distance of the Earth from the Sun (12). Some of this is absorbed by the atmosphere

but the majority penetrates and, on clear days in the U.K., intensities approaching 1000 W/m ^{2} have been recorded. As well as the seasonal variation, the solar intensity varies through the daylight hours. Emerson (16) assumes a variation in solar intensity given by :

$$I(t) = \frac{2S}{T} \sin^2 \frac{\pi t}{T}$$

where: I(t) is the intensity of solar radiation at time t

S is the total solar radiation for the day

T is the length of the solar day

On a clear day in summer, when the length of the solar day is 18 hours, the total radiation may be taken as 7950 Wh/m^2 with a peak intensity of approximately 850 W/m^2 (16). This may be compared with a maximum value of 1050 W/m^2 mentioned by Priestley (10) for Christchurch, New Zealand. Not all of this energy passes into a member ; the proportion which does is termed the absorptivity of the surface and, for a bridge deck surface, its value is approximately 0.9.

During the hours of darkness, energy is emitted to the night sky in the form of long-wave radiation. According to Emerson (16), published values of night-time reradiation lie between 95 W/m^2 and 125 W/m^2 and so a value of 110 W/m^2 is assumed in calculations. This figure must be multiplied by the emissivity of the surface to arrive at the actual energy loss. Emerson states that since emissivity is not affected by the colour or texture of the surface a value of 0.9 may be assumed for both surfaced and unsurfaced concrete. The actual value is a function of wavelength, but it is interesting to note that a C.E.B. Bulletin (17) quotes values of 0.6 and 0.88 for asphalt and

concrete repectively in relation to long-wave radiation.

2.2.2 Windspeed

The exchange of heat energy at the surface of a member by mechanisms other than radiation is dependent upon windspeed : the greater the windspeed, the more rapidly the temperature of the member approaches the temperature of the surrounding air. This feature is reflected in the values of the top surface heat transfer coefficient assumed in thermal calculations. This coefficient relates to heat transfer by both radiation and convection, but its magnitude is greatly affected by the amount of forced convection, which is a function of wind speed. Priestley (10) takes a value of approximately 13 $W/m^2/^0C$ for no wind, rising linearly to approximately 76 $W/m^2/^0C$ for a windspeed of 16 ms^{-1}. Emerson (16) considers windspeeds of between 2.2 ms^{-1} and 3.0 ms^{-1} as representative of normal exposure in the U.K., with an accompanying surface heat transfer coefficient of 23 $W/m^2/^0C$.

The effect of variations in wind speed on bridge temperatures has been calculated by Priestley (10), who found that an increase in wind speed from zero to 4 ms^{-1} resulted in a reduction in the maximum temperature difference from 27 ^0C to 12.5 ^0C in a 1524 mm deep deck. Emerson (18) also performed calculations on a surfaced, 1000 mm deep deck in which the wind speed increased from 2.5 ms^{-1} to 14.7 ms^{-1}. The resulting reduction in the maximum temperature difference was from 13 ^0C to 5 ^0C. Both workers found that the influence was of greatest significance to temperatures in the upper fibres.

2.2.3 Shade Temperatures

Variations in shade temperature occur on a seasonal and daily

basis. The daily minimum temperature occurs at approximately 05.00 hours and the maximum at around 15.00 hours, although there is a great deal of variability (19). As far as temperature profiles are concerned, variations in shade temperature are of greatest importance to bridge temperatures in the lower fibres of a deck. This has been demonstrated by Priestley (10) and Emerson (9). However, shade temperatures may be used to give an indication of the thermal response of the member as a whole.

The T.R.R.L. undertook a study to determine the correlation between shade temperature and effective bridge temperature for design purposes (8,20,21). Shade temperature was selected as a convenient parameter since, compared to other climatic features, it is easy to measure. Concrete members are slow to respond to changes in the ambient temperature, so a shade temperature history was considered. Correlations were thus found between the 48 hour mean shade temperature and the instantaneous effective bridge temperature. A second correlation was established between the 48 hour mean shade temperature and the daily minimum shade temperature. The procedure was repeated for maximum temperature conditions and so with a knowledge of extreme values of shade temperature, over a suitable return period, it is possible to estimate the maximum range of effective bridge temperature.

2.2.4 Surfacing

Surfacing has a two-fold influence on the temperatures of concrete bridge decks. Firstly, since surfacing is much darker than the bare concrete, it is able to absorb more radiation. The proportion of radiation absorbed is known as the absorptivity, which

for surfacing has a value of 0.9 (16,20,21). This may be compared with the value for bare concrete which is 0.5 (16) or 0.7 (22). On the other hand, the surfacing acts as an insulating layer to concrete. The extreme temperature difference condition may arise during construction, when a black waterproof membrane is applied to the concrete prior to the bituminous layer, as a high absorptivity coexists with virtually no insulation.

Emerson (9,18) calculated the maximum temperature differences beneath various thicknesses of surfacing under positive and reversed temperature profiles. It was found that the insulation effect predominates over the absorptivity effect for depths of surfacing in excess of 50 mm. A depth of 76 mm is suggested by Reynolds and Emanuel (23) but this relates to exposure in the United States. In consideration of 'critical temperature gradients', Priestley (22) calculated that for depths of surfacing between zero and 50 mm, the concrete top surface temperature decreases linearly with depth of surfacing. Presumably, the unsurfaced condition included the waterproof membrane.

2.2.5 Depth and Shape of Construction

The rate of overall thermal response of a bridge deck is greatly affected by the depth of construction, with thinner members responding more rapidly to climatic variations. In so far as temperature differences during day-time conditions are concerned, temperatures in the upper 500 mm are governed largely by incident solar radiation and in the lower 300 mm, the shade temperature is of greatest importance (9). In thinner members the two features overlap, but, for a member of sufficient depth, the temperature of the inner fibres is controlled

by the climatic conditions of the previous day or two. It follows also that the non-linearity of the temperature profile increases with the depth of the member.

The shape of the member influences the direction of heat flow and it therefore influences temperatures, but the author has been able to find little evidence of this effect. The results collected by Emerson (19) from the Coldra Viaduct include readings from two thermocouples placed at approximately the same depth, in the top flange of an I-section member, one at the centre and the other near the edge. Both gave very similar temperature readings. Also, Priestley (10) claims that the transverse flow of heat in bridge decks is negligible.

A considerable amount of solar radiation may fall onto the vertical surfaces of a member. For example, from June figures (24), the total solar intensity falling onto a horizontal surface is 7870Wh/m^2, compared with 4570Wh/m^2 for a vertical surface. It is interesting to compare values of the combined heat transfer coefficient for the various surfaces. It has been mentioned that Emerson assumes a value of 23 W/$m^2/^0$C for the top surface, under normal exposure. She also assumes a value of 9 W/$m^2/^0$C for the bottom surface. The values suggested for vertical walls range from approximately 10 W/$m^2/^0$C to 19 W/$m^2/^0$C, depending on orientation (25). However, a bridge deck offers more horizontal surface area to incoming solar radiation and the proportion of the radiation which is absorbed is greater for surfaced concrete. Also, the vertical surfaces may be shaded, as can be the case for the web of a T-section member.

As far as box section decks are concerned, Priestley (10)

recorded increased temperatures in the deck over an enclosed air cell compared to a solid deck, due to the insulating effect of the stagnant air within. Further results (26) reveal that the web temperature is related to the air cell temperature. In the U.K., daily fluctuations in air cell temperature in the order of 1 or 2 ^{0}C have been recorded but, in New Zealand, Wood (26) recorded a fluctuation of approximately 8 ^{0}C.

These points are of consequence to the choice of calculation method for predicting temperatures and will be discussed later in that context.

2.3 Calculation of Temperature Profiles

The transient thermal response of bridge decks may be predicted using a Fourier heat flow equation which applies ideally to a homogeneous isotropic solid. The equation may be expressed as :

$$K\left[\frac{\partial^2\theta}{\partial x^2}+\frac{\partial^2\theta}{\partial y^2}+\frac{\partial^2\theta}{\partial z^2}\right]=\frac{\partial\theta}{\partial t}$$

where θ is the temperature

x,y,z are the Cartesian coordinates

t is time

K is the thermal diffusivity

The solution of the heat flow equation depends on the boundary condition, which in its more general form may be expressed as :

$$k\frac{\partial\theta}{\partial n}-q+h(\theta_a-\theta_0)=0$$

where k is the thermal conductivity

h is the surface heat transfer coefficient

q is the radiation

n is the normal to the surface of heat transfer

θ_a is the ambient temperature

θ_0 is the surface temperature

The boundary condition is a function largely of climatic conditions and, during the day-time, the radiation term, q, is equal to the incident solar radiation multiplied by the absorptivity of the surface. However, under reversed temperature conditions, its magnitude is equal to the reradiation value, e.g. $-110\ Wm^{-2}$ (9), multiplied by the emissivity of the surface.

Unfortunately, there is no general direct solution of the heat flow equation so numerical methods are required such as the two-dimensional finite element analysis developed by Buckle and Lanigan (27). However, it may be reasonable to ignore any transverse flow of heat and then apply a linear or one-dimensional analysis in which the heat flow equation becomes :

$$K \frac{\partial^2 \theta}{\partial x^2} = \frac{\partial \theta}{\partial t}$$

In this form, finite difference approximations provide a convenient method of solution. Dividing the member into a series of layers and time into increments, it is possible to make the approximations:

$$\frac{\partial^2 \theta}{\partial x^2} = \frac{\theta_{n+1,p} + \theta_{n-1,p} - 2\theta_{n,p}}{\Delta x^2} \quad \text{and}$$

$$\frac{\partial \theta}{\partial t} = \frac{\theta_{n,p+1} - \theta_{n,p}}{\Delta t}$$

where the subscript n refers to the layer number and p to the increment of time.

This approach is employed by Emerson (16) to incorporate her assumptions on climatic influences and subsequently developed into a computer program by Jones (28). The program assumes a single material of construction, but allowance can be made for surfacing. An improved method, due to Hunt and Cooke (29), performs the iterations for two materials and, with the use of more elaborate difference expressions, is unconditionally stable. The former method requires that the value of $K\Delta t/\Delta x^2$ is less than 0.5 for stability.

An alternative approach is adopted by Hambly (30), in which the temperature fluctuations are are given by the expression :

$$\Delta T=\Delta T'.\exp(-x\sqrt{(\gamma/2K)}).\sin(\gamma t-x\sqrt{(\gamma/2K)})$$

where ΔT is the temperature fluctuation

$\Delta T'$ is the amplitude of surface temperature fluctuation

x is the depth below the surface

t is time

K is the thermal diffusivity

γ is $2\pi/24$ hour^{-1}

This method has the limitation that it applies only to the case of a sinusoidally fluctuating top surface temperature and, in the case of a member which is less than 600 mm deep, it is necessary to superimpose the influence of the lower surface temperature fluctuation (30).

With the exception of simple slab members, some transverse flow of heat is inevitable. However, Priestley (10,22,31) suggests that it is reasonable to consider even quite complicated cross-sections in terms of parallel and independent linear heat flow lines. Hambly adopts a similar approach but then guesses the temperature contours in

corners where the linear heat flow assumption is least applicable.

Moving on to decks of cellular construction, Emerson (16) assumes that the instantaneous flow of heat from the top flange to the air cell is equal to the instantaneous flow from the air cell to the lower flange and the flow of heat through the webs is neglected. Alternatively, simple conduction through the air cell may be assumed (27,29). Hambly (30) suggests that, since fluctuations in air cell temperature are small, it is probably reasonable to assume a constant air cell temperature for calculations. As pointed out earlier, this assumption may not be reasonable as appreciable daily temperature differences within an air cell have been recorded. Also, Wood (26) notes that the one-dimensional computation fails to yield an accurate prediction of mid-height web temperature, as the differences in air cell temperature cause transverse heat flow.

In conclusion, the linear models are generally thought to be adequate in predicting bridge temperatures for most purposes. Any benefits which might be obtained as a result of a more elaborate method are out-weighed by the greater complexity of the computer programs which are required and the increased time for the preparation of input data. However, it must be remembered that the success of any method is dependent upon the accuracy of meteorological information and this may be more of a problem than the actual method of analysis.

2.4 The Calculation of Thermal Stresses and Strains

The three-dimensional thermal stress problem may be approached using the theory of elasticity as described, for example, by Timoshenko and Goodier (32). However, this method becomes very complicated for all but the most simple boundary conditions, so it is

more usual to consider reinforced concrete bridge decks in terms of a simplified two-dimensional approach. The analysis may be performed by considering strains (33) or stresses (34), although both approaches yield the same final stress distribution. The method which will be described is that which forms the basis of the computer program SACRAK, to be described in Chapter IV, and it is the stress approach.

In this analysis, the following are assumed :

i. Plane sections remain plane.

ii. Temperature is constant in the plane which is parallel to the heated surface.

iii. The section is located remote from end effects.

iv. The materials are elastic and isotropic.

To begin, consider the effect of a non-linear temperature profile on a simply supported beam composed of one material. Generally, the beam exhibits a longitudinal movement and a change in curvature, and there will be also internal thermally induced stresses. For the following discussion, it may be useful to refer to figure 2.

The temperature, at any depth, is multiplied by the coefficient of thermal expansion to yield the FREE STRAIN PROFILE. This represents the strains which would be assumed by the fibres of the member in the absence of any restraint between adjacent fibres. Associated with this is the FREE STRESS PROFILE which is obtained by multiplying the free strains by the elastic modulus :

$$\sigma_f(x)=\alpha(x).E(x).T(x)$$

where $\sigma_f(x)$ is the free stress

$\alpha(x)$ is the coefficient of thermal expansion

$E(x)$ is the elastic modulus

T(x) is the temperature

x is the distance from the heated surface

Since plane sections are to remain plane, the free strain profile cannot be realised unless it is linear. Instead, there is the ACTUAL STRAIN PROFILE. In order to evaluate the actual strains, it is necessary to return to the free stress profile. The average free stress over the area of the section determines the magnitude of the AVERAGE STRESS PROFILE, given by :

$$\sigma_a(x) = \frac{1}{A} \int_0^d \sigma_f(x).b(x).dx$$

where $\sigma_a(x)$ is the average stress

A is the total cross-sectional area

b(x) is the width of the section at a given depth

d is the overall depth

The free stress and average stress profiles are in axial force equilibrium but they are not in moment equilibrium and so it is necessary to introduce the MOMENT BALANCE STRESS PROFILE to restore the equilibrium. The moment balance stresses are given by :

$$\sigma_{mb}(x) = \frac{(M_a - M_f).x}{I}$$

where $\sigma_{mb}(x)$ is the moment balance stress

M_a is the moment due to the average stress profile

M_f is the moment due to the free stress profile

I is the second moment of area

Associated with the latter two components of stress are the AVERAGE STRAIN PROFILE and MOMENT BALANCE STRAIN PROFILE which are effectively the longitudinal movement and the curvature. Their

combined effect is therefore the ACTUAL STRAIN PROFILE.

The longitudinal movement may be prevented, in which case the average stress profile is realised as actual stresses. Should the curvature be prevented, then the moment balance stresses become actual stresses. In either case, the restraint may only be partial, so that reduced stresses are induced.

Provided the temperature profile is linear, then no further stresses are induced, but, in the more general case of a non-linear profile, there is an additional regime of 'locked-in' or SELF-EQUILIBRATING stress. The latter term arises from the fact that these stresses provide no nett axial force or moment to the section. They are given by :

$$\sigma_{se}(x)=\sigma_f(x)-\sigma_a(x)-\sigma_{mb}(x)$$

where $\sigma_{se}(x)$ is the self-equilibrating stress

A further refinement is to allow for the presence of reinforcement. The free strain of the reinforcement is simply its temperature multiplied by its coefficient of thermal expansion and further multiplication with the elastic modulus yields the free stress. This is superimposed on the free stress profile for the concrete to give the total free stress profile. The method may then proceed as already described using the transformed cross-section in the equilibrium calculations. As a first approximation, or where it can be assumed that the coefficients of thermal expansion of the steel and concrete are identical, the free strains may be considered also in terms of a transformed section.

Cracking may be allowed for by setting to zero all stress in the concrete in the cracked region.

2.5 Estimates of Thermal Stresses

A rather extreme example of thermal stresses in service, reported by De Serio (2), relates to a cylindrical concrete silo where wall temperature differences of up to 77 ^{0}C were estimated. With theoretical tensile stresses of -15 N/mm^2, it is not surprising that cracking was observed in the structure. Priestley (6) estimated tensile stresses of -6 N/mm^2 in concrete water tanks, as a result of ambient thermal loading.

Bridge structures usually experience much less severe stresses when subjected to ambient thermal loading, with most stress estimates below the tensile strength of concrete. In such structures, the internal stresses are not only dependent on the temperature differences, but also on the non-linearity of the temperature profiles which are, in practice, a function of member depth.

Blythe and Lunniss (14) considered the positive temperature profile suggested by the T.R.R.L. and calculated maximum tensile and compressive stresses of -1.17 N/mm^2 and 3.95 N/mm^2 respectively for a 1000 mm deep section. These figures are close to the -1.03 N/mm^2 and 3.47 N/mm^2 arrived at by Church and Clark (35) with regard to the BS5400 temperature profile, which is based on the T.R.R.L. recommendations. Hambly (30) used the same temperature profile to calculate maximum stresses of -1.1 N/mm^2 and 3.2 N/mm^2, this time for a cracked section.

Radolli and Green (36) considered climatic conditions in Toronto, Canada and their estimates of maximum tensile and compressive stresses in a 1000 mm deep member are approximately -1.1 N/mm^2 and 3.6 N/mm^2 respectively. They also point out that the magnitude of

self-equilibrating stresses diminishes for shallower members where the temperature profiles are less non-linear. In a 200 mm deep member, for instance, extreme stresses of around -0.5 N/mm^2 and 1.0 N/mm^2 were calculated. In all of the cases mentioned, the maximum compressive stresses were found to exist at the top surface of the deck.

Priestley and Buckle (37) considered the effect of a 5th order parabolic temperature distribution on a double cell box-girder bridge deck. Here, the maximum tensile stress, occurring in the web, was -3.07 N/mm^2 and the maximum compressive stress, at the deck surface, was 2.88 N/mm^2. Hunt and Cooke (29) employed an elasticity method in reaching broadly similar results to the above authors.

It may be noted that, as well as the longitudinal stresses, it may be necessary to consider transverse effects. As an example, Priestley and Buckle calculated a transverse tensile stress of -2.41 N/mm^2, occurring at the bottom of the deck slab, as a result of the differential expansion between the deck and soffit slabs.

It is interesting also to consider the self-equilibrating stresses which develop as heat is generated by hydration of cement in slabs. Thurston et al. (38) calculated a maximum tensile stress of over -3 N/mm^2 in a 3600 mm deep foundation pad. No doubt much larger stresses are possible in more massive structures.

2.6 Secondary Thermal Stresses

A number of secondary effects are possible when overall thermal movements are fully or partially restrained. In bridge decks, thermally induced longitudinal movements may be accommodated with the inclusion of expansion joints. However, this may not be the case in

certain types of framed structure. Clarke (39) considered the differential expansion of a black-topped upper slab compared with the lower slabs of a multi-storey car park and estimated resulting theoretical tensile stresses in columns of -7 N/mm^2.

In continuous decks, additional stresses emanate from the restraint of thermal curvatures, although these stresses may be reduced or eliminated with suitably located construction joints. The magnitude of these continuity stresses is proportional to the product of the free thermal curvature and the depth of the member (12,36). However, greater depths of construction do not generally result in greater continuity stresses, as thermal curvature is itself a function of member depth. Thus, Radolli and Green (36) calculated the greatest continuity stresses for a 380 mm deep member. White (12) considered several design profiles and found the product of free thermal curvature and member depth to reduce with member depth. Only depths in excess of 500 mm were considered.

Cracking reduces flexural stiffness and would thus be expected to reduce continuity stresses. Thurston et al. (40) report a 50 % reduction in their model test.

2.7 Temperature Effects in Design

The temperature clauses, which are to be found in section 5.4 of BS5400 part 2 (41), contain specifications relating to overall thermal movement and to the effects of non-linear temperature profiles.

It has been mentioned that overall movements are governed by the effective bridge temperature and that this correlates with shade temperature. Therefore, the code contains maps of isotherms of maximum and minimum shade temperature from which values may be

obtained for the area of interest. These are translated into the maximum and minimum effective bridge temperature using tables 10 and 11 of the code, with suitable adjustment for depth of surfacing and location. To calculate the movement, a coefficient of thermal expansion of 12 $\mu\epsilon/^0C$ is recommended, except for concretes which contain limestone aggregate where a value of 7 $\mu\epsilon/^0C$ is advised. This must be multiplied by the partial safety factor γ_{fL}.

Where the movement is restrained, the code advises that the stresses induced by the temperature changes should be taken as the nominal load. However, Clark (13) argues that, according to the terminology of the code, it is consistent to treat the thermal movements themselves as the nominal loads.

Example specifications for non-linear temperature differences for concrete bridge decks are shown in figure 3. These were based on the T.R.R.L profiles. The code states that the effects of these temperature variations are the nominal values which are to be multiplied by γ_{fL} to give the design effect. This again is an inconsistent use of terminology and Clark suggests that the latter should be regarded as design loads.

In combination, maximum positive temperature differences are considered to coexist with effective bridge temperatures above 15 ^0C and maximum reversed differences with bridge temperatures upto 2 ^0C below the maximum effective bridge temperature.

CHAPTER III

MATERIAL PROPERTIES OF CONCRETE

3.1 Introduction

Several of the material properties of concrete, of relevance to this project, will be discussed. The discussion will begin with the properties that control the short-term response of concrete. Moisture migration, creep and shrinkage will be discussed in the later sections.

3.2 Effect of Temperature on Compressive Strength, Tensile Strength and the Modulus of Elasticity

Firstly, temperature affects the rate of hydration of cement and it therefore affects the development of strength. For example, Pihlajavaara (42) found the compressive strength of specimens cured at temperatures of between 40 ^{0}C and 50 ^{0}C to be greater than those of specimens cured at room temperature.

As well as the effect on the rate of hydration, temperature affects the compressive strength of mature concrete. A number of investigators (43,44,45,46,47) have observed losses in strength at elevated temperature and following exposure to elevated temperature. It must be borne in mind however that the majority of the work referenced above relates to tests conducted at temperatures greatly in excess of those which might be climatically induced. The effect of heating at moderate temperatures is less clear, although it does appear to be of less significance. In fact, Nasser (48) found no influence from temperature in the range 21 ^{0}C to 96 ^{0}C, for mature specimens. Kaplan and Roux (49) noted that, in most cases, a 6 hour heating cycle at 100 ^{0}C resulted in a reduction in compressive

strength of up to 20 %. They also detected a slight increase in strength in specimens of low strength.

Reductions in tensile strength and flexural strength at elevated temperatures have been noted also (44,45,47,49), although Sullivan and Poucher (45) observed an increase in flexural strength of mortar specimens at 140 ^{0}C. They found a slight decrease for concrete specimens at 200 ^{0}C.

The modulus of elasticity has been found to decrease with temperature (44,45,46,47,49,50). However, Nasser (48) detected no such decrease for mature specimens. Hannant (50) observed an 8 % decrease in the modulus at 50 ^{0}C compared with that at 27 ^{0}C. The same worker also found evidence of a recovery, where the modulus increased upon cooling.

A complicating factor arises in the case of a specimen which is not fully sealed. The rate of moisture loss from such a specimen depends upon temperature, and moisture content also affects mechanical properties. Under normal circumstances, the strength of mature concrete increases with increased drying, although this may not be the case if the drying is rapid (51). Also, the elastic modulus decreases with initial drying (51), although continued drying may reverse this trend (52).

Lankard et al. (44) found that the detrimental effects of temperature on mechanical properties were greatest for sealed specimens. Furthermore, they concluded that heating of unsealed specimens may even produce a slight increase in compressive strength, in the absence of thermal shock.

However, as was stated earlier, these variations in the

mechanical properties were observed at high temperatures and it is unlikely that the influence of climatically induced temperatures is of any great significance.

3.3 Thermal Diffusivity

Thermal diffusivity is a measure of the facility with which a solid will undergo a change in temperature. It is therefore of relevance to the prediction of temperature profiles in concrete structures. It was not necessary to evaluate this property for the purposes of the present project as temperatures were measured directly. However, a brief description of thermal diffusivity will be given.

Thermal diffusivity depends on a number of other material properties and is given by :

$$K = k/(\rho.c)$$

where K is thermal diffusivity

k is thermal conductivity

ρ is density

c is specific heat

Increased moisture content increases both the conductivity (53,54,55) and the specific heat (54) of concrete, and therefore has a reduced influence on thermal diffusivity. Marshall (54) reports decreases in thermal diffusivity of up to 16 %, with an increase in moisture content corresponding to 8 % of the concrete weight. Diffusivity has been found to decrease with temperature (54,55). Marshall reports a 21 % decrease as temperature is increased from 10 ^{0}C to 65 ^{0}C.

3.4 The Coefficient of Thermal Expansion

A knowledge of the coefficient of thermal expansion is necessary

in order to determine the stresses and strains in a member as it undergoes changes of temperature. It is usual to assume a constant value which is typically 12 $\mu\varepsilon/^0C$. However, the thermal dilation of concrete is a phenomenon of great complexity which is affected by several factors. These factors will be discussed.

3.4.1 Factors Influencing the Coefficient of Thermal Expansion

3.4.1.1 The Influence of Aggregate

Generally, the aggregate occupies from 65 % to 80 % of the volume of the concrete. Further, its elastic modulus is some 5 times greater than that of the cement matrix. It follows that the aggregate is the most important parameter in determining the coefficient of thermal expansion of the composite, and, as one might expect, the magnitude of the coefficient varies in proportion to the amount of aggregate present (56).

The magnitude of the thermal coefficient of aggregate varies between 0.9 $\mu\varepsilon/^0C$ and 16 $\mu\varepsilon/^0C$ (54), depending upon the rock type, and it is usually lower than that of the surrounding cement. Values for various rock groups, together with the coefficient for the resulting concrete, are given in the table below (57).

Rock Group	Silica Content (% by weight)	Average Thermal Coefficient ($\mu\varepsilon/^0C$)	
		Rock	Concrete
Chert	94	11.8	13.2
Quartzite	94	10.3	12.1
Sandstone	84	9.3	11.4
Granite	66	6.8	9.6
Limestone	Negligible	5.5	8.6

A rough correlation exists between the silica content of a rock

and its thermal coefficient. This is indicated in the table. Higher coefficients are obtained where the silica is present in its free form, as in chert, quartzite or sandstones. Limestones, which contain very little silica, exhibit considerably lower thermal coefficients, although the range of values obtained is wide. Aggregates composed of ignious materials have thermal coefficients of intermediate value.

The thermal response of certain rocks is complicated by the anisotropy of their crystal structure. For example, the calcite crystal has a coefficient of thermal expansion of 14.3 $\mu\epsilon/^0C$ along one axis and a negative coefficient of 2.8 $\mu\epsilon/^0C$ along the orthogonal axis. There is evidence (58) to suggest that this feature causes damage to rock undergoing thermal movement as expanding and contracting faces are in contact. Internal strains are also generated in sedimentary materials due to the varying thermal coefficients of the constituent grains and their cementing matrix.

Bonnell and Harper (59) performed tests on a range of rocks, to investigate the effect of water content on the coefficient of thermal expansion. Their results show a slight reduction in the coefficient for the saturated specimens compared to the dry specimens.

Loubser and Bryden (60) developed a more elaborate apparatus to perform similar tests. They found a higher thermal expansion in their saturated specimens. Both investigations included granite and sandstones. It is not clear whether the discrepancy between the two sets of results was due to differences in experimental procedure or whether it was due to the different characteristics of the rocks tested.

3.4.1.2 The Influence of Moisture Content

The observed thermal dilations of cement paste may be considered as two separate components. There is the kinetic movement, which is associated with the change in kinetic energy of the constituent molecules, and a further movement which is a function of moisture content.

Bonnell and Harper (59) observed a reduced thermal expansion in saturated and dry specimens, compared to those of intermediate moisture content. Meyers (58) confirmed this and found that, for a young paste, the maximum thermal expansion occurred at a relative humidity of approximately 70 %. His findings are shown in figure 4. This variability was affected by the age of the specimen and the method of curing. Specimens which were 15 years old exhibited a reduced maximum thermal coefficient occurring at a relative humidity of approximately 50 %. No variation at all was observed for autoclaved specimens.

This evidence suggests that the moisture dependent thermal dilation is a feature of the gel and so is absent in the case of an autoclaved specimen in which the products of hydration are crystalline. It also follows that the maximum coefficient diminishes with age as the structure tends to crystallinity.

Several explanations for this behaviour have been proposed. For example, it is suggested (51) that, as the temperature of a specimen is increased, the capillary tension of the water held within the gel decreases and swelling results. Powers (61) suggests that the amount of water that gel may adsorb increases as the temperature decreases. Hence, if the moisture content is held constant, an increase in

temperature leads to a relatively more saturated state which causes swelling.

More recent considerations incorporate a thermodynamic approach. Bazant (62) divides thermal dilations into three components: the pure thermal movement; a movement due to differences in latent heat and entropy along the so-called diffusable layers; a movement due to changes in relative humidity with temperature. This latter movement accounts for the shape of figure 4. All three components are time dependent: the first two leading to a delayed recovery and the third to continued dilation.

3.4.1.3 The Influence of Extreme Temperature

In the interval 0 ^{0}C to 60 ^{0}C the coefficient of thermal expansion of cement is sensibly constant (57). Outside of this range, other effects come into play. Some aspects of the behaviour at temperatures near to and below the freezing point of water, and at temperatures in excess of 60 ^{0}C, will be discussed.

Wittmann and Lukas (63) observed a reduced thermal coefficient in the interval between -10 ^{0}C and +10 ^{0}C. Further, the value below -10 ^{0}C exceeded that obtained above +10 ^{0}C. The reduction occurred only in saturated specimens. Those specimens which were tested at a relative humidity of 90 % showed a continuous increase in the coefficient between -20 ^{0}C and +10 ^{0}C.

Marachel (64) observed an expansion as quartzite aggregate concrete was cooled from -18 ^{0}C to -50 ^{0}C. He suggested that water contained within the smaller pores of the gel supercools at temperatures down to -18 ^{0}C. Below this, ice forms and causes an expansion of the concrete. Concretes with lower water/cement ratios,

and hence fewer capillary pores, are less susceptible to this feature.

The variation between the thermal expansion of aggregates and that of the cement matrix has been mentioned. In concretes containing limestone aggregate, the difference is sufficient to cause cracking when the temperature is in excess of 60 ^{0}C (57). A resulting loss of strength of 40 % is reported.

Specimens which are free to lose water to the surroundings experience rapid drying at elevated temperatures. The resulting shrinkage reduces the thermal expansion.

3.4.1.4 The Influence of Age and Curing Conditions

The coefficient of thermal expansion of concrete changes with age. Any such changes may be due to the development of the microstructure of the cement paste. However, it must be remembered that a variation in the moisture condition usually accompanies the aging process and, as stated above, this has a significant influence on the magnitude of the thermal coefficient.

Berwanger and Sarkar (65) measured the thermal expansion of concrete specimens of 7 and 84 days of age. They report increases in the coefficient of 12 % and 7 % for air-dried and saturated specimens. The increases in tests conducted below 0 ^{0}C were 20 % and 13 % respectively. There is no mention of the application of a sealant to the specimens before testing and so the results obtained were, presumably, affected by moisture exchange with the environment.

Bonnell and Harper (59) report a slight reduction in the coefficient with age for air cured concrete and little change for wet cured concrete, for the period between 3 months and 1 year.

The nature of the dependence on age may be influenced by the

temperature at which the coefficient is measured. Wittmann and Lukas (63) found that, for saturated specimens, the coefficient at room temperature increased with age, but decreased with age at temperatures below $-10\ ^{0}C$.

The effect of wet or dry curing has been mentioned. The evidence suggests that dry curing results in higher thermal coefficients, but this may owe more to the reduced moisture content than to the actual progress of hydration.

3.4.1.5 The Influence of Reinforcement

For a uniform temperature increase, the presence of reinforcement can affect the overall thermal expansion only when the coefficients of the steel and the plain concrete are different. Both mild steel and high tensile steel have a coefficient of 12 $\mu\epsilon/^{0}C$, which is identical to the commonly quoted value for plain concrete. However, in the case of concretes which contain a substantial quantity of limestone aggregate, and hence have a low thermal coefficient, the inclusion of reinforcement increases the overall thermal expansion. Since the elastic modulus for steel is much greater than that of plain concrete, the increase may be large. Berwanger and Sarkar (65) found that, for plain concrete with a thermal coefficient of 7.2 $\mu\epsilon/^{0}C$, the addition of 5 % reinforcement increased the coefficient by some 16 %.

Concretes with thermal coefficients in excess of that for steel are less common but, clearly, the addition of reinforcement would reduce the overall thermal expansion.

3.5 The Movement of Moisture in Concrete

Since the behaviour of concrete is greatly influenced by the presence of moisture, a knowledge of the migration of moisture is of

importance. A distinction is made here between the flow of water through the material under saturated conditions and moisture migration during drying. The commonly quoted figures for permeability relate to the former process. The latter process involves variations in moisture content and is thus considerably more complicated.

3.5.1 The Permeability of Concrete

The uniaxial movement of water through a saturated body may be represented by the D'Arcy equation :

$$\frac{dm}{dt} = A.K.\frac{dp}{dx}$$

where dm/dt is the mass flow rate

dp/dx is the pressure gradient

A is the cross-sectional area of flow

K is the coefficient of permeability

It is difficult to suggest a typical value for the coefficient as wide variations are reported. Browne and Baker (66) suggest values of between 10^{-8} m/s and 10^{-12} m/s, depending on the quality of the concrete.

In fact, the movement of moisture through concrete depends on the permeabilities of both the cement matrix and the aggregate particles. Values for various rock types are shown below (66) :

Rock Type	Permeability
Dense Trap	2.47×10^{-14} m/s
Quartz Dolerite	8.24×10^{-14}
Granite I	5.35×10^{-11}
Sandstone	1.23×10^{-10}
Granite II	1.56×10^{-10}

Clearly, there are large variations between various rocks, but it is suggested (51) that it is the permeability of the paste which is of greatest importance. If it is assumed that the permeability of the aggregate is much lower than that of the surrounding cement, then the effect of the aggregate is to reduce the effective cross-sectional area of flow and to increase the flow path, as water has to circumvent the aggregate particles.

Powers et al. (67) investigated the factors which influence the permeability of cement and found that the degree of hydration was of major importance. They reported a hundred-fold decrease in permeability of specimens which were cured for 6 days, compared with those cured for 24 hours. An increase in the initial water/cement ratio was found to increase permeability, the effect being much greater for ratios in excess of 0.5. A seventy-fold increase in permeability was observed in specimens which previously had been dried to 70 % r.h. before resaturation and testing.

It is suggested (67) that the permeability of the gel itself is approximately 7×10^{-16} m/s, considerably below the overall permeability of the paste. It appears then that a high proportion of the flow occurs through the capillary pore system. The relationship between permeability and capillary porosity is shown in figure 5. Thus, the capillary porosity is of importance to permeability, especially when the porosity exceeds 30 %. The continuity of the pore system is affected by the initial water/cement ratio and pore discontinuity occurs at ratios below 0.5 (67). The increase in permeability due to the prior drying is attributed to the rupture of the gel webs between capillary pores.

3.5.2 The Drying of Concrete

Two types of drying will be discussed. These are the diffusion of moisture to the environment under uniform temperature and diffusion caused by a temperature gradient. The discussion will begin with the former condition.

Consider the idealised drying curve of an initially saturated material, shown in figure 6. The first phase of drying, AB, proceeds as an adequate supply of water is able to reach the surface, so that the free water surface condition is effectively maintained. The linearly declining region, BC, occurs as insufficient water reaches the surface to maintain the free surface condition. At point C, the surface is in moisture equilibrium with the environment and, beyond this, the plane of evaporation recedes away from the surface of the member.

Consider next the mechanism by which this movement of moisture takes place. Initially the movement of saturated liquid predominates, but at more advanced stages vapour diffusion becomes more important. Arumugasaamy and Swamy (69) propose a four stage sequence of drying mechanisms. The first stage involves the movement of saturated liquid. From this condition to that of 90 % r.h., moisture transfer is due exclusively to liquid flow, although the moisture containing pores are no longer saturated. Between 90 % r.h. and 40 % r.h. liquid and water vapour flow occur and, in the final stage, below 40 % r.h., the transfer of moisture is exclusively by means of water vapour diffusion.

A number of workers (68,70,71,72) have attempted to model moisture migration by application of the simple diffusion equation :

$$K.\left[\frac{\partial^2 C}{\partial x^2}+\frac{\partial^2 C}{\partial y^2}+\frac{\partial^2 C}{\partial z^2}\right]=\frac{\partial C}{\partial t}$$

where C is the evaporable moisture concentration

x, y, z are the Cartesian coordinates

t is time

K is the coefficient of diffusion

Hughes et al. (68) compared the weights of spheres drying at uniform temperatures of between 50 ^{0}C and 95 ^{0}C with a series solution of the simple diffusion equation. They found good agreement, except in cases where there was an insufficient rate of removal of moisture from the surface of the sphere. In such instances it was claimed that the surface mass-transfer rate was the controlling factor. These results suggested also that the coefficient of diffusion increases with temperature and water/cement ratio, and decreases with curing time.

In addition, tests were conducted on spheres at 30 ^{0}C (72). A major conclusion of this work was that the coefficient of diffusion depends on moisture concentration. This might follow from the dependence of the mechanism of moisture transfer on relative humidity, mentioned earlier. A diffusion equation which allows the coefficient to be a function of moisture content would be non-linear, although linearity can be maintained by allowing the coefficient to be time dependent.

It may be noted that, in the work referenced, overall measurements from specimens were used in comparison with theory. No attempt was made to compare the distribution of moisture content in specimens with theory.

3.5.3 Moisture Migration Under Temperature Gradients

The interest in moisture migration under temperature gradients arises from the use of reactor vessels in the nuclear power industry. The temperatures involved may exceed the boiling point of water and so the conclusions drawn from the associated research may not be appropriate to more conventional structures. However, some of this work will be discussed.

A non-uniform temperature distribution in a saturated or a partially saturated member produces a pore pressure gradient which provides the driving force to moisture movement. This is in addition to the normal drying process described in the previous section.

England et al. (73,74,75) conducted tests on concrete cylinder specimens which were laterally sealed so as to ensure nett uniaxial migration of moisture. The cylinders were subjected to base temperatures of up to 200 ^{0}C, some with the opposite ends left unsealed. Moisture migration was monitored by means of pore pressure measurements taken from porous inclusions within specimens and by direct weighing. As expected, two drying regions were detected moving into the specimen, one from the exposed surface and the other from the heated surface. Drying was accompanied by reductions in the pore pressure gradient.

Ross and Parkinson (76) used the attenuation of microwaves as a means of measuring the moisture content of concrete cylinders. With base temperatures of up to 95 ^{0}C, moisture loss at the heated end greatly exceeded that at the exposed end.

England and Sharpe (75) found that the diffusion equation was incapable of predicting moisture distributions under such conditions

so instead they used the D'Arcy equation. It was thought necessary to consider two forms of the equation, one relating to gases and the other to incompressible fluids. Thus, account was taken of the migration of water, water vapour and air. The approach yielded good agreement with experimental observations, except for near the cold end of the cylinder where diffusion was of greater importance.

3.5.4 The Measurement of Relative Humidity in Members

Several workers (69,77,78) have measured the relative humidity at various locations within members. For this purpose, Monfore (78) developed a probe-type gauge which was inserted into pre-formed wells within the specimens. The wells were normally sealed to allow them to reach moisture equilibrium with the concrete. The probe itself utilised a Dacron thread whose length increased with relative humidity. This movement was transmitted to a conducting advance wire whose resistance was measured.

Monfore used the probe to measure the relative humidity at the axis of mortar cylinders of 19 mm, 76 mm and 152 mm diameter which were allowed to dry in air at 50 % r.h. The small cylinder had effectively reached moisture equilibrium with the environment by the 25th day from first exposure. At this stage, the large cylinder was at 100 % r.h. and the intermediate cylinder was at a humidity of 90 %.

Hanson (77) used the Monfore Gauge to measure the relative humidity distribution in drying concrete members which were moist cured for 7 days before exposure at 50 % r.h. After 28 days the humidity had fallen to 67 % r.h., where the cover was 6 mm, and to 90 % r.h., where the cover was 67 mm. It took approximately 2 years for the humidity to fall to 60 % r.h. at the greater depth.

Arumugasaamy and Swamy (69) made further use of a Monfore Gauge to measure the relative humidity of concrete columns in an environment of 72 % average r.h. and in situ. The latter experienced a variable outdoor environment. Some of these results were presented as the time taken for the humidity to fall to 90 % r.h. at a given depth from the surface. At a depth of 100 mm, the laboratory beams required 40 to 45 days. At a depth of 200 mm, one set of columns required from 250 to 500 days and another set required 1900 days to reach the prescribed humidity. Thus, reductions in humidity in the interior of external members occurred very slowly.

The work referenced deals with relative humidity as this is conveniently measured. Of course, this is not the same as moisture content and the two are not linearly related. Pihlajavaara (79) suggests a relationship of the form indicated in figure 7. So_{∞} at a given relative humidity, the relative moisture content falls from unity until it reaches the value defined by the equilibrium curve or desorption isotherm. The remaining moisture content is then given by the vertical distance from beneath the isotherm.

3.5.5 Concluding Remarks

The migration of moisture in concrete is a complex process. It may occur as a result of drying to the ambient relative humidity or as a result of thermally induced pore pressure gradients.

Relative humidity is conveniently measured, but its relationship with actual moisture content is not straightforward. However, experimental evidence confirms the slow rate of drying of concrete structures.

3.6 The Creep of Concrete

3.6.1 Introduction

When a load is applied to a concrete specimen, there occurs an instantaneous elastic deflection and, if the load is maintained, further changes in deflection occur, the rate of which diminishes with time. In other words, the concrete creeps. Alternatively, if a deflection is imposed on a member, an instantaneous stress occurs which reduces with time. This other manifestation of the creep process is known as relaxation. However, the great majority of work on creep has dealt with deflection, so the following discussion will concentrate on creep deflections.

According to Troxell et al. (80), between 40 % and 70 % of the ultimate creep strain develops in the first 3 months from loading, although these workers detected changes in creep strain after 30 years under load. However, for practical purposes, it may be assumed that creep is complete after 5 years (81) and its limiting value is approximately twice the elastic deflection (82). This factor shows considerable variation and it is known to be greater under conditions of low relative humidity.

A typical creep curve is shown in figure 8. It shows that, following the application of the load, the rate of creep is relatively high, but the rate diminishes with time. The figure also indicates the response following the removal of the load. It may be seen that, when the load is removed, an instantaneous elastic recovery takes place. This is followed by a period of creep recovery, the ultimate magnitude of which is not as great as the original creep strain. Creep is not then a completely reversible process.

It is possible to consider creep as two separate components. Illston (84,85) terms the reversible component, delayed elastic strain and the non-recoverable component, flow. A further component is introduced to account for the increase in creep which results from the increase in temperature to a previously unattained temperature and this is known as transitional thermal creep. This particular categorisation of creep strains may be appropriate under conditions of varying stress and temperature, but it is known that the rate of creep is increased during drying. Therefore, an alternative approach is to divide creep into a basic component and a drying component (86,87,88).

This discussion of creep will deal firstly with the proposed mechanisms and then with the more important factors which affect creep. Only a small proportion of the literature on creep relates to tensile loading, but this will be discussed as it is an important consideration in the present study. The three popular methods of creep modelling will be described, followed by brief descriptions of some methods available for the prediction of creep in design.

3.6.2 Creep Mechanisms

As in the case of shrinkage, the aggregate is an effectively inert component, so the mechanisms described here are concerned with the cement matrix.

Despite the great amount of work which has been done on creep, the actual mechanism or combination of mechanisms has not yet been confirmed. Creep, like shrinkage, is a complex process and the two phenomena appear to be related, with the movement of moisture being a common influence.

Volume changes may be attributed to changes in the thickness of

layers of adsorbed water. At certain locations, the adsorption is hindered by insufficient space between gel particles and a disjoining pressure results (89). The proposition is that moisture moves from the regions of hindered adsoption to other locations, by means of molecular diffusion, and this is caused by the action of applied stress acting against the disjoining pressure. On removal of the load, the moisture may return to its original location, so that the process is reversible. Any movement which is not recovered is attributed to the formation of additional bonds during the period when the particles were in closer proximity to each other.

It is possible also that creep is facilitated by the sliding of gel particles (90). This process, which is affected by the Van der Waals forces between particles, is affected also by the disjoining pressures which were mentioned above. Therefore, moisture content is of importance to this mechanism.

In another model (52), the externally applied load is distributed between the solid and liquid phases of the specimen. Under load, the liquid diffuses from the regions of high pressure to regions of lower pressure, with an accompanying increase in the proportion of the load which is carried by the solid phase. In this model, the irreversible component is attributed to the removal of inter and intra-crystalline water.

The final mechanism which will be mentioned involves the movement of interlayer water (91). The applied load causes the moisture to diffuse out from between the layers, thus decreasing the layer spacing. The re-entry of this moisture increases the layer spacing, which allows for creep recovery. This model also allows for

the slippage between layers, but this too is affected by moisture content, as greater energy is required for slippage when the layer separation is reduced.

3.6.3 Factors Influencing Creep

3.6.3.1 The Influence of Stress and Strength

Neville (81) states that creep is directly proportional to the applied stress and inversely proportional to the strength of the specimen. Creep is thus proportional to the stress/strength ratio. This linearity holds to a certain ratio, in the range 0.4 to 0.6, beyond which creep increases at an increasing rate with the applied stress. The range of stress over which the linearity operates appears to be greater for mixes with a higher initial water/cement ratio (91).

The stress/strength ratio which marks the limit of the proportionality also coincides with the first occurrence of microcracking and it is to this effect that the increased creep is attributed (81).

At higher stresses still, a period of creep may be followed by complete failure of the specimen, even though the level of applied stress is maintained constant. For this to occur, stresses in the range 0.7 to 0.9 of the short-term strength are required (81,82).

3.6.3.2 The Influence of Moisture Content

This discussion on the influence of moisture content on creep will deal with specimens which are not exchanging moisture with the environment and are thus not experiencing drying creep.

There is widespread agreement that the rate of creep increases with moisture content, so that saturated specimens creep the most and dry specimens show little or no sign of creep. Indeed, Glucklich and

Ishai (52) observed little creep in specimens which had previously been dried to 7 % of their original evaporable moisture content at saturation, but, on rewetting of dried specimens, a recovery in creep potential was observed.

The influence of moisture content on creep appears to be greater at greater degrees of saturation. For instance, Glucklich and Ishai found a linear increase in the creep rate with moisture content up to 45 % of the evaporable moisture content at saturation, but beyond this the rate increased non-linearly. Also, Wittmann (93) found little change in the creep rate up to 60 % r.h., but a significant increase at higher humidities. A similar result was obtained earlier by the same author (90). In all cases, creep increased with moisture content.

3.6.3.3 The Influence of Drying

It is known that the creep of a drying specimen exceeds the creep of a similarly loaded sealed specimen, even after the strains have been corrected for shrinkage. It is therefore necessary to distinguish between basic creep, which relates to specimens which are not exchanging moisture with the environment, and drying creep, which is the additional component present during drying.

The rate of drying creep appears to be a function of the rate of shrinkage (86,88). In fact, it is not necessarily the case that the rate of drying creep is governed by the rate of shrinkage, but rather that the two share common causes. Gamble and Parrott (86) suggest the following relationship :

$$\varepsilon_{dc} = k.\sigma.\varepsilon_s$$

where ε_{dc} is the drying creep strain

σ is the applied stress

ϵ_s is the shrinkage strain

k is a constant

These authors also observed a sensibly linear relationship between the constant in the equation and the initial water/cement ratio.

It might be expected then that some of the factors which influence shrinkage influence drying creep also. Hanson and Mattock (94) observed reduced total creep in larger specimens and went on to conclude that, for very large members, the overall rate of creep approaches the rate of basic creep. Also, drying creep was found to increase in specimens which were stored in air at lower ambient relative humidities (92).

It is interesting to consider the effect of rewetting on creep. Gamble and Parrott (86) found that creep increased during rewetting also, although the nett movement was expansive due to swelling of the specimen. They termed this component of creep, wetting creep. In the same way as they observed the effectively linear relationship between drying creep and shrinkage, they also found linearity between wetting creep and swelling.

3.6.3.4 The Influence of Temperature

The influence of temperature on creep must be considered in two respects. Firstly, there is enhanced creep by virtue of a change in temperature and this effect will be described in the next section. This section will deal with the effect of constant temperature on the rate of creep.

Reutz (92) found that the 6 day creep strains of cement specimens increased with temperature in the range 20 ^{0}C to 60 ^{0}C. For a further increase in temperature, up to 80 ^{0}C, a slight reduction in

the creep rate was observed and this was attributed to the accelerated rate of hydration. Specimens which had previously been heated or dried exhibited enhanced creep up to 80 ^{0}C.

Illston (95) states that the creep of concrete at 80 ^{0}C is some two or three times greater than that at 20 ^{0}C. Fahmi et al. (96) use a time-shift principle to account for the effect, in which the specific creep curve is displaced along the time axis. However, a number of workers have found creep to be a linear function of temperature.

Arthanari and Yu (97) observed a sensibly linear relationship between creep and temperature in the range 20 ^{0}C to 80 ^{0}C. Linearity was also observed by Hannant (50) in the range 27 ^{0}C to 77 ^{0}C. Nasser and Neville (98) investigated the influence of temperature on the creep of 1 year old and 50 year old specimens. They too found a linear increase in creep with temperature up to 70 ^{0}C, but the enhancement at 96 ^{0}C was roughly the same as that at 46 ^{0}C.

The constant of the proportionality between creep and temperature varies between workers, but a simplifying assumption is to set the constant to unity (99). Here, it is convenient to define specific thermal creep as the specific creep divided by the temperature, so that :

$$\Delta\varepsilon_c = T.\sigma.\Delta c$$

where $\Delta\varepsilon_c$ is the creep strain

T is the temperature

σ is the applied stress

Δc is the change in specific thermal creep

Thus, for a specific thermal creep curve derived at 20 ^{0}C, an increase

in temperature to 40 ^{0}C results in a doubling of the creep strain. This approach is supported by some experimental findings. For instance, Hannant (50) found that the creep of specimens stored at 52 ^{0}C was between two and three times greater than that of specimens stored at 27 ^{0}C and Neville (81) reports a factor of 3.5 for storage at 71 ^{0}C compared to storage at 21 ^{0}C.

3.6.3.5 Transitional Thermal Creep

Hansen and Eriksson (100) investigated the influence of a temperature change on the deflection of cement and mortar beams. They found that, following the application of a load, an increase in temperature caused accelerated creep. When the beams were heated for a second time, the increase in creep was much less. Arthanari and Yu (97) compared the creep of concrete specimens, stored at 62 ^{0}C, with the creep of a specimen which was subjected to incremental increases in temperature up to 59 ^{0}C. The latter exhibited greater creep. There appears therefore to be a component of creep which emanates from a change in temperature and this component is greatest when a virgin temperature is attained. The component is known as transitional thermal creep.

According to Illston and Sanders (85), transitional thermal creep occurs during or immediately after an increase to a virgin temperature and it is irrecoverable. From their tests, it was concluded that the ultimate transitional thermal creep strain was independent of maturity, but maturity was found to reduce its rate of occurrence.

Parrott and Symmons (136) found evidence of a recovery process. Following a period of storage at a lower temperature, there appeared

to be a regeneration of transitional thermal creep potential. This feature is contrary to the definition of transitional thermal creep given by Illston and Sanders.

In a later work, Parrott (102) detected transitional thermal creep when specimens were subjected to elevated temperature on a second occasion, but its magnitude was not as great as for the first temperature increase. A further point is that, if the duration of heating is insufficient to permit the full development of transitional thermal creep, then the remaining potential may occur on subsequent heating (101).

It might be expected then that some enhancement in creep occurs whenever an increase in temperature takes place or when a member is subjected to thermal cycling. Indeed, Hanson and Eriksson (100) observed large changes in beam deflection whenever the temperature was increased, but they detected no such change in deflection when the temperature was decreased. Rainford and Timusk (103) concluded that temperature cycling increased the creep above that which occurred at the mean temperature. However, Hannant (50) observed no creep enhancement in a thermally cycled specimen and this is supported by results reported by Neville (81).

It appears then that the great majority of transitional thermal creep develops on first heating, although further diminished creep enhancement may occur on subsequent heating. This is all in addition to the increase in creep which occurs at higher constant temperatures.

3.6.3.6 The Influence of Aggregate

The aggregate content has a major effect on the creep of concrete. For example, Troxell et al. (80) found that the creep of

concrete containing sandstone aggregate was twice that of concrete containing limestone aggregate. Between these limits, the use of basalt, gravel, granite and quartz aggregates led to progressively reduced creep strains.

The influence of aggregate on creep response may be indirect. For example, the aggregate concentration may affect the required water/cement ratio, which in turn influences creep. Furthermore, if the aggregate is dry, the wet cement may lose moisture to the aggregate particles and thus undergo drying creep.

However, the primary influence of the aggregate is to restrain the creep of the cement and to reduce the concentration of material which is susceptible to creep (87,95). The influence is therefore similar to that for shrinkage. For this reason, Neville (81) proposes an equation to account for the influence of aggregate, which is similar in form to that advocated by Pickett (104) for shrinkage :

$$C=C_p.(1-g-u)^a$$

where C is the creep of concrete

C_p is the creep of the cement paste

g is the volume concentration of aggregate

u is the volume concentration of unhydrated cement

a is a constant which depends on the elastic moduli and Poissons ratios of the cement and aggregate

The equation assumes that the aggregate neither creeps nor shrinks and few aggregates exhibit appreciable shrinkage. However, rocks are known to creep at high levels of stress, but in the majority of cases the creep is very small when compared to that of cement (51).

3.6.3.7 The Influence of Age of Loading

With the exception of the first day or two from casting, the rate of creep decreases with the age at which the specimen is loaded and the influence of the age reduces with increased age (51,80). Gamble and Parrott (86) measured the 98 day basic creep of concrete specimens and found that the creep of specimens which were loaded at an age of 1 week exceeded that of 20 week specimens by a factor of 2.88. It is however suggested (51,86) that the influence of age at loading may be negligible beyond 1 month.

3.6.3.8 The Influence of Initial Water/Cement Ratio

The specific creep of cement and mortar specimens has been found to increase with the initial w/c ratio (81,92,105). For example, Davis et al. (105) compared the creep of concrete specimens with w/c ratios of 0.62 and 0.69. The higher ratio gave 50 % more creep after 1 year. It is suggested (82) that lower ratios cause reduced spacing of cement grains which in turn reduces the creep.

3.6.4 Creep in Tension

Only a small minority of the investigations into the creep of concrete have included tensile loading. This is due in part to the lack of demand for such data as, in the past, the tensile behaviour of concrete was largely ignored in design and much concrete is prestressed anyway. Experimentation itself presents serious difficulties. The applied loads are necessarily small, due to the low tensile strength of concrete, and the resulting creep strains may be overshadowed by drying shrinkage. Also, it is difficult to impose purely axial loads on specimens.

Davis et al. (105) conducted tests on sealed concrete cylinders

and found that the rate of creep in tension exceeded that in compression, the difference being greatest at early stages of loading. During the first 60 days under load, the tensile creep was more than twice as large as the creep in compression.

Glanville and Thomas (106) observed equal creep rates in tension and compression. Their specimens were unsealed and so a shrinkage correction was necessary, derived from a non-loaded companion specimen.

The results obtained by Hanson (107) are somewhat contadictory. The creep in compression was greatest for an age of loading of 28 days whilst, for an age of loading of 90 days, the tensile creep was greatest. The difference between tensile and compressive creep was greatest for the latter age of loading.

Unfortunately, Wajda and Holloway (108) did not compare tensile and compressive creep results. Their specimens were unsealed and, at a stress/strength ratio of 0.33, shrinkage exceeded the tensile creep by a factor of up to 5.

Illston (109) conducted a more extensive investigation and found that the characteristics of creep in tension were largely the same as in compression. He did find however that the initial rate of creep was higher in tension, although the difference between the two rates diminished with duration under load. For the first 60 days, the tensile creep factor, defined here as the specific creep in tension divided by that in compression, was approximately 2.5.

With such contradictory evidence, it is difficult to reach any conclusions regarding the creep of concrete in tension or a typical tensile creep factor, but it does appear that creep in tension is

greater than in compression. The difference in the tensile and compressive creep rates appears to diminish with time.

3.6.5 Methods of Modelling Creep

Three well known methods exist for the modelling of creep under variable stress. These are the effective modulus method, the rate of creep method, and the superposition method. Each of these will be described, with particular attention to the rate of creep and the associated relaxation methods, which were employed for the present study.

3.6.5.1 The Effective Modulus Method

In this method, creep strains and elastic strains are considered together in the evaluation of an effective modulus, given by :

$$E_{eff} = \frac{\sigma}{\varepsilon_e + \varepsilon_c}$$

where E_{eff} is the effective modulus

σ is the applied stress

ε_e is the elastic strain

ε_c is the creep strain

If it is then assumed that creep is a linear function of stress, then specific creep can be introduced to render a more convenient form of the expression :

$$E_{eff} = \frac{E}{1+cE}$$

where E is the elastic modulus

c is the specific creep

An important advantage of this approach is that the effective modulus may be substituted into a conventional elastic analysis, for

which commonly known solutions exist, but, under certain conditions, the approach results in serious inaccuracies. The method takes no account of the stress history of the specimen, but merely depends on the instantaneous magnitude of stress. Complete recovery is predicted on removal of the load, so that, under conditions of reducing stress, strains are underestimated. However, the method requires few material data and it is simple to apply.

3.6.5.2 The Rate of Creep Method

Here, the creep of concrete is given by :

$$\varepsilon_c = \int_0^t \sigma . \frac{dc}{dt} \, dt$$

where ε_c is the creep strain

σ is the applied stress

c is the specific creep

t is the time since loading

England (99) uses an incremental solution of this equation and introduces specific thermal creep to account for the influence of variations in temperature :

$$\Delta\varepsilon_c = \phi(T).\sigma.\Delta c$$

where $\Delta\varepsilon_c$ is the increment of creep strain

$\phi(T)$ is the function of temperature which relates the creep at any temperature to the specific thermal creep curve

Δc is the increment of specific thermal creep

The expression may be simplified by assuming that $\phi(T)=T$. Thus, with reference to figure 9, the change in strain which occurs during the increment of time, Δt, is obtained by multiplying the corresponding

increment of specific thermal creep, Δc, with the current values of temperature and applied stress.

Clearly, this method is an improvement over the effective modulus approach in that it takes some account of the stress and temperature history of the member, although it does suffer from inaccuracies. Unlike the previous approach, the rate of creep method predicts no creep recovery at all, but it is suggested (110) that the method could be modified to incorporate creep recovery.

An additional inaccuracy stems from the use of a single specific thermal creep curve. Strictly, since the creep is affected by the age of loading, a family of creep curves should be used, each corresponding to the time of a change in the applied load. This inaccuracy diminishes at more advanced ages, where the influence of age of loading on creep is less severe.

3.6.5.3 The Relaxation Method

In the case of the rate of creep method, strains were allowed to change during the increment of time, whilst stress remained constant. In this method, stress is allowed to relax according to the relaxation function :

$$\sigma=\sigma_i.e^{-E.\phi(T).c}$$

where σ is the relaxed stress

σ_i is the initial stress

E is the elastic modulus

$\phi(T)$ is the function of temperature as defined in the rate of creep method

c is the specific thermal creep

England (99) uses the incremental form of the equation, making the

approximation that $\phi(T)=T$, to give :

$$\Delta\sigma=\sigma_i.(1-e^{-E.T.\Delta c_i})$$

where $\Delta\sigma$ is the change in stress

Δc is the increment of specific thermal creep

It may be noted that, as the increment of time tends to zero, the solutions of the rate of creep method and the relaxation method tend to the same value. However, it is sensible to use the rate of creep method under imposed stress conditions and the relaxation method under conditions of known restraint (99).

3.6.5.4 The Superposition Method

It may be recalled that an inaccuracy of the rate of creep approach is that it fails to recognise the dependence of the age of loading on creep. The superposition method does not suffer from this deficiency, as it involves a separate creep curve for each increment of load. The creep strain is thus given by (95) :

$$\varepsilon_c=\Sigma\sigma_i.c_i$$

where ε_c is the total creep strain at time t

σ_i is an increment of stress

c_i is the specific creep at time t, for a particular age of loading

So, each time the load is changed, it is necessary to derive the specific creep curve for that particular age of loading.

3.6.5.5 Concluding Remarks

Of the main three methods mentioned here, superposition is potentially the most accurate, as it recognises the influence of age of loading on creep. It does however require a considerable amount of creep data under conditions of variable stress. The effective modulus

approach is the simplest method to apply and is therefore the most widely used, but it is the least accurate method, especially under conditions of decreasing stress (81,95). The rate of creep approach represents a compromise between these two methods. It takes account of the stress and temperature history of the member and only requires one creep curve. The related relaxation method is more suited to strain imposed problems.

3.6.6 The Prediction of Creep in Design

The design methods provide general guidance for the prediction of creep and they are relatively easy to use. They are not however intended as accurate methods of modelling.

3.6.6.1 The BS8110 Method

The current design document (111) adopts the method described by Parrott (129), where it is assumed that the ultimate creep strain is taken to be the elastic strain at the time of loading multiplied by a creep coefficient. This coefficient is deduced from a chart which takes account of the effects of ambient relative humidity, the age at loading and the effective thickness of the section. The strains at intermediate stages are estimated by assuming that 40 %, 60 %, and 80 % of the ultimate creep develops during the first month, 6 months and 30 months respectively.

For the calculation of creep recovery, it is stated that the final value, occurring after 1 year, is 0.3 times the elastic recovery, the latter being the stress reduction divided by the elastic modulus at the time of unloading.

3.6.6.2 The CEB-FIP Method

The method described in the Model Code (112) is considerably

more complicated than the foregoing approach, although under certain circumstances a simplified method may be used. As before, the elastic strain is multiplied by a creep coefficient, which in this case is given by :

$$\phi(t,t_0)=\beta(t_0)+\phi_d.\beta_d(t-t_0)+\phi_f.[\beta_f(t)-\beta_f(t_0)]$$

where $\phi(t,t_0)$ is the creep coefficient

t_0 is the age at loading

t is the age at the moment considered

The age is corrected to take account of the influence of ambient temperature on maturity and is thus given by :

$$t=(\alpha/30).\ \Sigma_0^{tm}[T(t_m)+10].\Delta t_m$$

where α is a constant which depends on the type of concrete

$T(t_m)$ is the temperature during the time increment

t_m is the time increment

A full explanation of the creep coefficient is rather complicated and not warranted here, but the significance of the three component terms is easily described. The first term relates to the irreversible creep which develops during the first few days after loading and the third term to the subsequent irreversible creep or flow. The second term relates to the recoverable component of creep.

Simplified expressions are suggested for certain conditions, such as where the variation in stress during the time increment does not exceed 30 % or where it is reasonable to assume a constant elastic modulus. Additional simplifications are permitted in consideration of creep at times in excess of 3 months.

3.6.6.3. The ACI Method

The ACI method (113) relies on a creep coefficient given by :

$$\phi(t,t_0) = \frac{(t-t_0)^{0.6}}{10+(t-t_0)^{0.6}} \cdot \phi_\infty(t_0)$$

where t_0 the age at loading

t is the age at the moment considered

$\phi_\infty(t_0)$ is the ultimate creep coefficient

Under standard conditions, the ultimate coefficient is 2.35, otherwise it must be multiplied by the appropriate factors. These factors allow for variations in the slump, the cement content, the fines content, the air content, the minimum thickness of the member, the loading age and the ambient relative humidity. The document gives guidance on the evaluation of these component factors.

3.7 The Shrinkage of Concrete

3.7.1 Introduction

Concrete may shrink for a number of reasons, but of primary concern in this work is shrinkage caused by loss of moisture to the environment.

There are three main types of shrinkage. These are carbonation shrinkage, plastic shrinkage and drying shrinkage. It may be noted that there are a number of additional chemical phemomena which result in shrinkage, but these are generally of less significance. A brief description of them is given by Wittmann (93).

Carbonation is a reaction between carbon dioxide, which is present in the atmosphere, and certain of the products of hydration. It occurs in the presence of moisture and is absent under saturated conditions (114). The actual mechanism by which carbonation leads to a volume reduction has not been confirmed, although a number of mechanisms have been proposed (115), which do not warrant discussion

here. This type of shrinkage may be characterised by small surface cracks, which give the member a crazed appearance. These cracks are of a superficial nature as carbonation penetrates only a few millimetres from the exposed surface (116). A further characteristic of carbonation shrinkage is that its rate of progress is very slow, so that crazing may not appear for a year or more from first exposure.

The loss of moisture from concrete is responsible for plastic shrinkage and ordinary drying shrinkage. The former occurs in the first few hours after casting, before the concrete has set. It is by far the most common cause of shrinkage induced cracking, with associated strains in the order of 1000 $\mu\epsilon$ to 2000 $\mu\epsilon$. These plastic shrinkage or pre-setting cracks may be found at the interface of precast and in situ concrete, for instance, or above reinforcement bars. They are easily prevented by prolonged curing and, if they are noticed early enough, they may be removed by re-vibration.

When fully-hardened-concrete loses moisture, it undergoes ordinary drying shrinkage. The ultimate drying shrinkage strain of concrete depends on the type of exposure, ambient relative humidity being a dominant factor. For indoor exposure, 600 $\mu\epsilon$ is a typical value (117), but outdoor exposure in the U.K. results in much smaller strains, in the region of 100 $\mu\epsilon$ to 200 $\mu\epsilon$. Indeed, from measurements on concrete bridges in England, a typical ultimate shrinkage strain of 200 $\mu\epsilon$ is suggested (118). Where such movements are partially or fully restrained, either by external or internally generated forces, cracking can result and, although this is less common than plastic cracking, instances of damage have been reported (eg 2,3).

The mechanisms of drying shrinkage are complex and these will be

discussed. Also, some of the factors which influence shrinkage will be discussed, with attention to the relationship between shrinkage and weight loss. The chapter will include a discussion of non-uniform shrinkage and its possible consequences.

3.7.2 Drying Shrinkage Mechanisms

This discussion will be limited to the mechanisms of the shrinkage of the cement matrix, since the aggregate is generally assumed to be an inert component, except for its restraining influence. The mechanisms described resemble those proposed for creep in section 3.6.2.

The drying shrinkage of cement is a complex process which is not entirely understood. However, several possible mechanisms have been proposed and these are listed by Soroka (116) as : capillary tension ; surface tension or surface energy ; swelling pressure ; and the movement of interlayer water. Only a brief description of these effects is warranted here, but the reader may refer elsewhere (90,93,116,119,120) for more extended explanations.

The capillary tension effect occurs when the gel pores become partially empty, allowing the formation of menisci between adjacent particles. These provide a capillary tension force, which is balanced by compression in the gel particles, resulting in shrinkage of the member.

The surface tension effect emanates from the forces within gel particles. The molecules which make up the outer layers of a particle experience a force, due to molecular attractions, whose nett direction is towards the centre of the particle. These have the effect of skin in tension around the particle. The molecular

attractions are affected by the presence of adsorbed water. Therefore, as water is removed, the attractions strengthen and the member shrinks.

The swelling pressure emanates from the layers of gel adsorbed water molecules. The thickness of such layers is governed by the ambient temperature and relative humidity, but, at certain locations, the layers are prevented from attaining their potential thickness due to insufficient space between gel particles. Here, a pressure exists which tends to force the gel particles apart. Removal of water reduces the pressure and thus causes the member to shrink.

Lastly, a proportion of the microstructure of cement exists in a layered arrangement and the spacing of these layers is affected by interlayer water. As the water is removed, the spacing reduces and the member shrinks.

The foregoing mechanisms may be reversible and so may be used to account for swelling, but it is known that there is an irreversible component of shrinkage for which additional mechanisms have been suggested (116). For instance, it is possible that, on shrinking, additional bonds form between particles due to their closer proximity and these bonds limit any subsequent expansion.

3.7.3 The Relationship Between Shrinkage and Weight Loss

A drying shrinkage with weight loss relationship, of the type indicated in figure 10, has been reported by a number of workers (119,121,122), for both cement and concrete specimens. The first phase of drying, characterised by a low rate of shrinkage with weight loss, may be attributed to the loss of capillary water and the second phase to the loss of gel pore water. This proposition is supported by

the results from tests on specimens which contained various concentrations of pulverised silica, as a means of controlling the unit capillary pore volume (119). It was found that, as the capillary pore volume reduced, the start of the second phase occurred at a lower weight loss and the gradient of the first phase increased. The specimen which was assumed to contain no or very little capillary space exhibited no bilinearity at all.

Maturity is known to reduce the capillary volume also as the pores become filled with the products of hydration, so it is to be expected that this too has an effect on the bilinearity of the shrinkage against weight loss curve. This effect is further discussed in section 3.7.4.5.

It may be noted also that on drying at elevated temperatures, a further two linear drying phases have been observed (121). Furthermore, at normal temperatures, a third non-linear phase has been identified and attributed to carbonation shrinkage (122). This was observed only in small specimens and is unlikely to be of any significance in structural elements, where carbonation is seen as a surface effect.

3.7.4 Factors Influencing Shrinkage

Shrinkage is affected by many factors. What follows is a description of the more important factors or those which are relevant to this project.

3.7.4.1 The Influence of Aggregate

The aggregate content substantially influences shrinkage behaviour of concrete. Most aggregates exhibit negligible shrinkage strains in comparison with cement, although several shrinking

aggregate types are known, such as the fine grained sandstones of Southern Africa (114).

If it is assumed that the aggregate does not shrink at all, then the amount of restraint offered to the shrinkage of the cement matrix depends on the aggregate concentration and the elastic properties of the materials. In a theoretical study, Pickett (123) deduced the following expression to account for the influence of the aggregate :

$$S=S_0.(1-g)^a$$

where S is the actual shrinkage

S_0 is the unrestrained matrix shrinkage

g is the aggregate concentration

a is a function of the elastic moduli and Poissons ratios of the cement and aggregate

The expression was found to be in good agreement with experimental results.

It is possible that the restraint caused by the aggregate particles leads to the formation of cracks at the cement/aggregate interface. This effect would then reduce the bulk shrinkage (116). It is also likely that interface stresses would be reduced by creep.

3.7.4.2 The Influence of Reinforcement

The shrinkage of concrete is partially restrained also by the reinforcement. The magnitude of this restraint is governed by the modular ratio and the amount of reinforcement present. For an uncracked and symmetrically reinforced member, the shrinkage is given by (117) :

$$S=S_0/[1+m\rho/(1-\rho)]$$

where S is the actual shrinkage

S_0 is the unrestrained shrinkage of the concrete

m is the modular ratio

ρ is the proportion of reinforcement present

In reality, the shrinkage induced stresses are reduced by creep, resulting in less shrinkage than predicted by the expression given. A creep reduction factor may be introduced to account for this effect (117,124).

Shrinkage may, for a number of reasons, cause warping of a member and one such reason is asymmetric reinforcement. Hobbs (125) examined a number of methods available for the prediction of these shrinkage induced curvatures, favouring the equivalent tensile force method. Here, the member is notionally allowed to shrink freely and uniformly. To maintain compatibility, the reinforcement is compressed. This compressive force is then released onto the transformed section to yield a longitudinal shortening and a curvature. Allowance for creep is made by the use of an effective elastic modulus.

3.7.4.3 The Influence of Size and Shape of Member

Hanson and Mattock (94) found that the rate of drying shrinkage of concrete specimens diminished with the size of the member and increased with the ratio of exposed surface area to volume. This is to be expected as the progress of drying depends on the average distance which moisture has to travel before escaping from the surface. This distance, termed the drying path, may be crudely approximated by assuming that it is equal to the volume to surface area ratio (122). It may then be assumed that drying shrinkage proceeds according to an equation of the form (117,122,124) :

$$S=fn[(1/d)^n.t]$$

where S is the drying shrinkage

d is the drying path

t is time

n is a constant between 1 and 2

More problematical is the influence of size and shape on the ultimate drying shrinkage. From their findings, Hansen and Mattock (94) concluded that ultimate shrinkage reduces with size and the volume to surface area ratio. However, Hobbs (122) observed that the 2 to 3 year shrinkage was approximately independent of specimen size. The issue is complicated by concurrent hydration, which is enhanced by the greater relative moisture retention of specimens with greater average drying paths. It is therefore suggested (122,124) that ultimate drying shrinkage is independent of size and shape per se.

3.7.4.4 The Influence of Relative Humidity

If a fresh concrete specimen is stored in very moist conditions, then it swells. This is certainly the case for curing in water. Shrinkage occurs when the relative humidity is below 90 % r.h. to 94 % r.h. (124).

The lower the ambient relative humidity, the more rapidly concrete shrinks and the greater the ultimate shrinkage. For instance, Troxell et al. (80) observed that shrinkage of concrete specimens at 50 % r.h. exceeded that at 70 % r.h. by a factor of approximately 1.4. Hobbs and Parrott (124) analysed the data from a number of sources and arrived at a similar result. However, from their observations, Evans and Kong (126) found that shrinkage increased at a rate of 2 % of the 70 % r.h. value for a decrease of

2 % r.h., in the range 70 % r.h. to 45 % r.h.

3.7.4.5 The Influence of Curing

The results of Verbeck and Helmuth (121) show that, for water/cement ratios of 0.5 and 0.7, increased curing leads to greater first drying shrinkage of concrete specimens. To account for this, it was suggested that as hydration proceeds, there is less cement clinker to offer restraint. On the other hand, Hobbs (117,122) found that drying shrinkage was essentially independent of the duration of curing. Powers (119) states also that curing time is relatively unimportant. From the results of a number of workers, Hobbs and Parrott (124) noticed that shrinkage decreases for curing times in excess of 1 month. Hanson (77) recorded reduced shrinkage in specimens cured for 28 days compared with those cured for 7 days. Evidently, the influence of curing on drying shrinkage is complex and the implication is that there is more than unhydrated cement restraint involved.

What appears to be clearer, is the influence of maturity on the bilinearity of the shrinkage against weight loss curve. The results collected by Verbeck and Helmuth (121) indicate that increased curing reduces the bilinearity effect. In other words, the extent of the first phase of drying reduces and its gradient increases. This behaviour is indicated in figure 10. The effect was more evident on concretes containing a higher water/cement ratio. Hanson's data (77) may be processed into a shrinkage against weight loss plot which confirms this behaviour.

The influence of capillary pore space on the relationship between shrinkage and weight loss was mentioned in section 3.7.3. The

behaviour described here is consistent with this, as capillary pore space reduces with continued hydration.

It is interesting to note that, from the results which have been referenced, the gradient of the second phase of drying is virtually independent of the duration of curing.

3.7.5 Differential Shrinkage Stresses

During drying, moisture content differences develop within a member and associated with these are variations in the notional unrestrained shrinkage with depth profile. Since the permeability of concrete is very low, the profile is severely non-linear. However, the free shrinkage is restrained by the cross-section of the member, resulting in a system of self-equilibrating stresses. These cause the fibres nearest the drying face to be in tension. The core and any reinforcement are accordingly placed in compression. In consideration of the forces required to restrain free shrinkage, tensile stresses of $-6\ N/mm^2$ (116) and $-10\ N/mm^2$ (51) have been estimated. Clearly, stresses of this magnitude cannot be carried by the concrete and so cracking takes place. Alternatively, since the stresses are slow to develop, it is possible that they are reduced by creep, perhaps to the point where cracking is avoided.

One way in which the free shrinkage profiles can be estimated is to assume that shrinkage is a feature which diffuses through a body in accordance with the simple diffusion equation (104,127,128), similar to that which models heat flow :

$$K_s \left[\frac{\partial^2 S}{\partial x^2} + \frac{\partial^2 S}{\partial y^2} + \frac{\partial^2 S}{\partial z^2} \right] = \frac{\partial S}{\partial t}$$

where S is the free drying shrinkage

K_s is the shrinkage diffusivity

x, y, z are the Cartesian coordinates

t is time

Other workers (70,71) employed an effectively identical method, where it was assumed that moisture migration obeys the simple diffusion equation and that shrinkage is a linear function of moisture loss. They obtained reasonable agreement with experimentally observed strains, using a suitable choice of diffusion coefficient.

A criticism of this type of analysis is that it assumes a constant shrinkage or moisture diffusion coefficient. It is known that the coefficient is not constant for moisture diffusion and is therefore unlikely to be constant for shrinkage diffusion. It was mentioned in section 3.5.2 that the coefficient is in fact a function of moisture concentration, but to incorporate this feature into the diffusion equation would render the equation non-linear and thus no longer open to solution by the methods used by the workers mentioned. Pickett (127) attempted to overcome the problem by allowing the coefficient to be a function of time and the dimensions of the member.

If it is accepted that moisture migration obeys the diffusion equation, then it necessary to consider the relationship between shrinkage and moisture loss. It was stated in section 3.7.3 that, except for very mature specimens or those with few capillary pores, the relationship is bilinear. No account of this is taken in the work reported.

If the analysis is extended to predict the self-equilibrating stresses which are induced by non-uniform shrinkage, then creep must be considered. Strictly, creep should be considered in the prediction

of strain, but this appears to be less critical (70,71) for unreinforced members.

Pickett (127) found evidence of this type of creep in relation to stress reversal in unreinforced prisms. These were allowed to dry in a laboratory and thus experienced tensile stresses which eventually caused surface cracks. Since the surfaces had elongated due to creep before cracking, drying of the core not only closed the cracks but placed the surface fibres into compression. In certain instances, the resulting tensile stresses in the core exceeded the tensile strength and so resulted in complete failure. In his subsequent analysis, Pickett used a reduced elastic modulus, derived from tests on the restraint of shrinkage-induced curvatures, to account for the influence of creep.

In their analysis, Zetlin et al. (128) allowed shrinkage stresses to reduce in accordance with a simple stress relaxation formula, but their treatment of tensile creep is not clearly described. This could be a critical factor as early tensile creep rates exceed compressive creep rates. This is dealt with in section 3.6.4.

3.7.6 The Prediction of Shrinkage in Design

The design methods give general guidance for the prediction of shrinkage. The methods described are the shrinkage counterparts of the creep prediction methods mentioned in section 3.6.6.

3.7.6.1 The BS8110 Method

The current design document (111) adopts the shrinkage chart given by Hobbs and Parrott (124), which takes account of the ambient relative humidity and the effective thickness of the section. From

this information, the chart provides estimates of shrinkage at 6 months and 30 years. Guidance is given in relationship to concretes with high or low initial w/c ratios and to the effects of reinforcement.

Seasonal fluctuations in moisture content are allowed for by superimposing plus or minus 0.4 times the ultimate shrinkage on the average value.

3.7.6.2 The CEB-FIP Method

In this method (112), shrinkage strains develop according to the expression :

$$\varepsilon_s(t,t_0)=\varepsilon_{so}.(\beta_s(t)-\beta_s(t_0))$$

where ε_{so} is the basic shrinkage coefficient, which depends on the environment and the notional thickness

β_s is a function related to the change in shrinkage with time

t is the corrected time, as defined for creep in section 3.6.6

t_0 is the age of first exposure

3.7.6.3 The ACI Method

The expression for the prediction of shrinkage recommended in the ACI document (113) is :

$$\varepsilon_t = \frac{t}{35+t}.\varepsilon_u$$

where ε_t is the shrinkage at any time after 7 days

t is the time of exposure

ε_u is the ultimate shrinkage

As with the accompanying expression for creep, a standard ultimate

shrinkage of 800 $\mu\epsilon$ is considered and this is modified by multiplication with a number of factors to account for variations in the slump, the cement content, the fines content, the air content, the minimum thickness of the member and the ambient relative humidity.

CHAPTER IV

COMPUTER PROGRAMS AND SENSITIVITY STUDY

4.1 Curve Fitting

The programs used in this work include curve fitting routines from the Numerical Algorithms Group library (130). These are used to fit smooth curves through experimentally observed data points, using a weighted least square polynomial approximation. The polynomial is represented in Chebyshev series form and routine E02ADF is used to obtain the series coefficients. The routine E02AEF is then used to evaluate the polynomial from the coefficients.

4.2 Description of SACRAK

The program SACRAK performs the section analysis which is described in section 2.4. Its main purpose is therefore to determine the curvature, axial strain and the self-equilibrating stresses of a simply supported reinforced concrete beam under a temperature profile. It also forms the basis of additional programs, to be described later, which deal with non-linear notional strain profiles caused by creep and shrinkage. For the description of the program which now follows, it may be useful to refer to the condensed flowchart in section 4.8.

The input data include the dimensions of the cross-section, the depth to the reinforcement and the area of reinforcement. A rectangular or T-section beam may be considered. The material properties include a coefficient of thermal expansion profile, which is a function of depth, and this is specified by three Chebyshev coefficients. The remaining information includes the magnitude of the applied bending moment and the temperature profile.

The temperature profile is specified at five depths, or nine for

the deep beams, in accordance with the experimental thermocouple locations, and a 4th order curve is then fitted to these points using the NAG routine.

The analysis proceeds by dividing the section into a number of horizontal layers of equal thickness. Initially, each layer is set to be uncracked and its depth to centre and width are then calculated. For the centre of each layer, the NAG routine is called to evaluate the temperature and the coefficient of thermal expansion. The product of these yields the notional free strain profile and further multiplication with the elastic modulus gives the free stress profile.

The flexural stiffness of the beam is based on the transformed section, which assumes an equivalent amount of concrete in place of the reinforcement. The evaluation of the free strains requires a separate consideration of the steel and concrete. Therefore, the concrete area and transformed area of each layer are calculated separately.

The force and moment contributions for each layer, due to the free stresses in the concrete, are summed to produce the total for the section. If any layer is set to be cracked, then its contribution is ignored. The contribution from the steel is then included.

The neutral axis depth and second moment of area of the section are calculated with regard for the presence of cracked layers.

From the total force provided by the free stresses, the average stress is determined and applied to each layer. The total moment of the average stress profile is then calculated.

At the next stage, moment equilibrium is restored to the section with the introduction of the bending moment stress profile. The free

stress, average stress and bending moment stress are summed for each layer to arrive at the self-equilibrating stress and, when necessary, the stress induced by the applied moment is included to arrive at the final stress distribution.

If the final stress in any layer exceeds the strength of concrete, then the concrete in that layer is set to be cracked. The number of cracked layers is counted and the analysis is repeated. Following this, the number of cracked layers is compared with the previous count and, if the two are not equal, the analysis is repeated until agreement is obtained.

Finally, the steel stresses are calculated from the transformed section values. The output data include the various component stress profiles, the axial strain and the curvature.

4.3 Calculation of Shrinkage Stresses Using SACRAK

The program may be used to estimate the effects of a non-linear free shrinkage distribution by setting the coefficient of thermal expansion to unity and inputting the free shrinkage profile in place of the temperature profile. A slight modification to the program is necessary so that the steel provides no free stress, as it does not shrink.

4.4 Description of CREEP

The program CREEP calculates the changes in creep curvature in a simply supported reinforced concrete beam. It is, in principle, the rate of creep approach described in section 3.6.5.2. A condensed flowchart for the program is shown in section 4.9.

The creep data are supplied to the program in the form of an experimentally determined specific thermal creep curve and the NAG

routine is used to determine the coefficients which define the curve. The actual creep curve used for this and subsequent analyses is presented in graph 74.

The analysis increments time, the length of each increment being one day, and, as before, the beam is divided into a number of horizontal layers. The program commences by reading in the SACRAK information, together with the five Chebyshev coefficients which define the specific thermal creep curve. The variation in the elastic modulus with time is similarly defined.

Next, all layers are set to be uncracked. The depth and width of each layer are determined and the NAG routine is called to evaluate the temperature for each layer.

The daily increments then commence. For the current day, the elastic modulus and the change in specific thermal creep are evaluated using the NAG routine and the section properties, including the neutral axis depth and second moment of area, are determined ready for the equilibrium calculation.

The stresses due to the applied bending moment are calculated and these are then multiplied by the temperature and change in specific thermal creep. The result is the free creep strain profile which, due to the presence of reinforcement and the non-linearity of the temperature profile, necessitates the use of an equilibrium calculation, of the type used in SACRAK, to produce the plane strain change. Like SACRAK, the program includes provision for adjusting the number of cracked layers.

The process is repeated for the next day with a new elastic modulus and increment of specific thermal creep. At the end of the

calculation period, the changes in creep curvature for each day are output.

4.5 Description of SCREEP

The program SCREEP calculates the relaxation of shrinkage induced stresses in a reinforced concrete beam. The initial creep free stresses are obtained from the modified version of SACRAK described above and SCREEP is then used to calculate the relaxation by the method described in section 3.6.5.3. For the description of the program which follows, it may be useful to refer to the flowchart in section 4.10.

The usual data specifying the details of the cross-section and the material properties are input, together with the specific thermal creep curve. The latter is specified, as before, by Chebyshev coefficients. The curve is fitted to the temperature data and the depth and temperature are determined for each layer. No provision is made in this program for variable member width as beams of only rectangular cross-section were tested in the accompanying experimental investigation.

The daily increment starts by evaluating the elastic modulus and the change in specific thermal creep for that day. The shrinkage stress profile is then read in. With a knowledge of the increment of specific thermal creep, the temperature and the stress in each layer, the relaxation can be calculated from the equation described in section 3.6.5.3. The effect of the free relaxation strain profile is determined from the SACRAK equilibrium calculation.

Once the calculations for the increment have been completed, the program returns to the start and proceeds, for the next day, with a

new elastic modulus, change in specific thermal creep and a new system of creep-free shrinkage stresses.

The main output data are the creep modified shrinkage stresses.

4.6 Description of TCREEP

This program is used to calculate the effects of the relaxation of thermally induced self-equilibrating stresses, during a daily thermal cycle. Due to the similarity between this and the shrinkage stress problem, the program SCREEP forms the basis of the analysis. The differences between the two programs are as follows.

The program increments on an hourly basis and, for each increment, a system of thermally induced stresses is input. This is derived from the unmodified SACRAK analysis. A constant elastic modulus and rate of specific thermal creep are used. The latter is determined from the master specific thermal creep curve for the day of interest. The output data are as for SCREEP.

4.7 Sensitivity Study Using SACRAK

The primary purpose of this study was to assess the influence of various parameters used in the analysis, which might affect the accuracy of the prediction of experimental response. For example, the elastic modulus varies with age and discrepancies might exist between the modulus derived from a companion specimen and that of a test beam. Similar discrepancies might be expected in relation to the coefficient of thermal expansion. Another possible source of error is the assumption regarding the extent of cracking. The study will be concluded by considering the effect of reinforcement content on the thermal response.

Variations were made on the standard cross-section, of the same

specification as the shallow test beams described in section 6.2.1, and, unless otherwise stated, a coefficient of thermal expansion of 11 $\mu\epsilon/^0C$ and an elastic modulus of 25 kN/mm^2 were assumed for the concrete. The temperature profile was typical of experimental observations, with a maximum positive temperature difference of 13.5 ^0C.

Emphasis is placed on thermal curvatures and axial strains, as these were used in comparison with the experimental results. The effects on self-equilibrating stresses are mentioned, although this study did not involve extreme stress conditions.

4.7.1 The Influence of Varying the Elastic Modulus

The effect of the magnitude of the modulus on thermal curvatures was negligible : an increase from 20 kN/mm^2 to 40 kN/mm^2 resulted in a curvature decrease of 1 %. The corresponding decrease in axial strain was also 1 %. However, the doubling of the modulus led to the maximum compressive and tensile stresses increasing from 0.31 N/mm^2 and -0.26 N/mm^2 to 0.65 N/mm^2 and -0.47 N/mm^2 respectively.

4.7.2 The Influence of Varying the Coefficient of Thermal Expansion

The coefficient of thermal expansion used in the analysis was varied between 10 $\mu\epsilon/^0C$ and 12 $\mu\epsilon/^0C$, in line with the 20 % increase suggested by Parrott (129) for the influence of moisture content. As well as uniform values, a parabolic distribution was considered, which assumed a coefficient of 12 $\mu\epsilon/^0C$ at the top and bottom surfaces, reducing to 10 $\mu\epsilon/^0C$ at the central plane of the beam. It was thought that such a condition could occur during drying.

The higher coefficient yielded a thermal curvature which was 14.8 % greater than that obtained from the lower coefficient and the

non-uniform distribution produced an 8.9 % increase. The increases in axial strains were 16.1 % for the higher coefficient and 5.6 % for the non-uniform distribution.

The influence on primary thermal stresses was somewhat greater. Compared with the maximum compressive stress of 0.38 N/mm^2 for the lower coefficient, that at the higher coefficient was 28.9 % greater and, for the non-uniform distribution, the increase was almost four-fold. The substantial increase of the latter is largely attributed to the fact that, in the upper fibres, the temperature and coefficient of thermal expansion increased non-linearly together. The influence on tensile stresses was less. The maximum values for the higher coefficient, the lower coefficient and the non-uniform distribution were -0.29 N/mm^2, -0.34 N/mm^2 and -0.53 N/mm^2 respectively.

4.7.3 The Influence of Cracking

The study was extended to investigate the influence of the depth of penetration of the crack from the soffit on the thermal strains of the standard section. Cracking led initially to increased thermal curvature, the increase being some 14.5 %. During this phase, the predominant effect was the reduction in internal section restraint. This was followed by a reduction in curvature, so that the final increase, at the fully cracked condition, was 8 %. The reduction resulted from the cracking of layers which had previously contributed a thermal force. The effect on axial strains was negligible, the maximum increase being less than 1 %.

4.7.4 The Influence of Reinforcement

A further source of discrepancy between theoretical and observed results was the inaccurate positioning of reinforcing bars in the test

beams. The position of the compression bars is of greatest significance, as these were nearest to the heated surface. The sensitivity study thus considered a movement of 5 mm in these bars.

For a distance to the centre of the bars of 25 mm, a 7.9 % increase in curvature was calculated and, for a distance 35 mm, a reduction of 1 % was calculated. The effect on axial strains was less than 1 % in both cases.

Also, the effect of the amount of reinforcement was considered. The results of this investigation are summarised as follows :

Area of Steel		Thermal Curvature	Maximum Stress	
Comp.	Tens.		Tens.	Comp.
0	0 mm^2	0.733×10^{-6} mm^{-1}	-0.25	0.43 N/mm^2
0	226	0.713	-0.27	0.47
226	226	0.748	-0.31	0.40
226	452	0.734	-0.33	0.34
452	452	0.758	-0.37	0.37

Thus, the effect of increasing the tensile steel was to reduce the thermal curvature by means of increased section restraint. An increase in the compression steel increased the curvature by providing more thermal force to the section.

4.7.5 Concluding Remarks

The study demonstrates that the major possible sources of error in the prediction of thermal curvature are the assumptions regarding the extent of cracking and the coefficient of thermal expansion. The prediction of axial strains is also sensitive to changes in the thermal coefficient, although the extent of cracking is of negligible importance. The choice of the elastic modulus is of less significance

to strains, but it has a considerable effect on primary thermal stresses and, through its effect on flexural stiffness, on secondary stresses also.

4.8 Flowchart for SACRAK

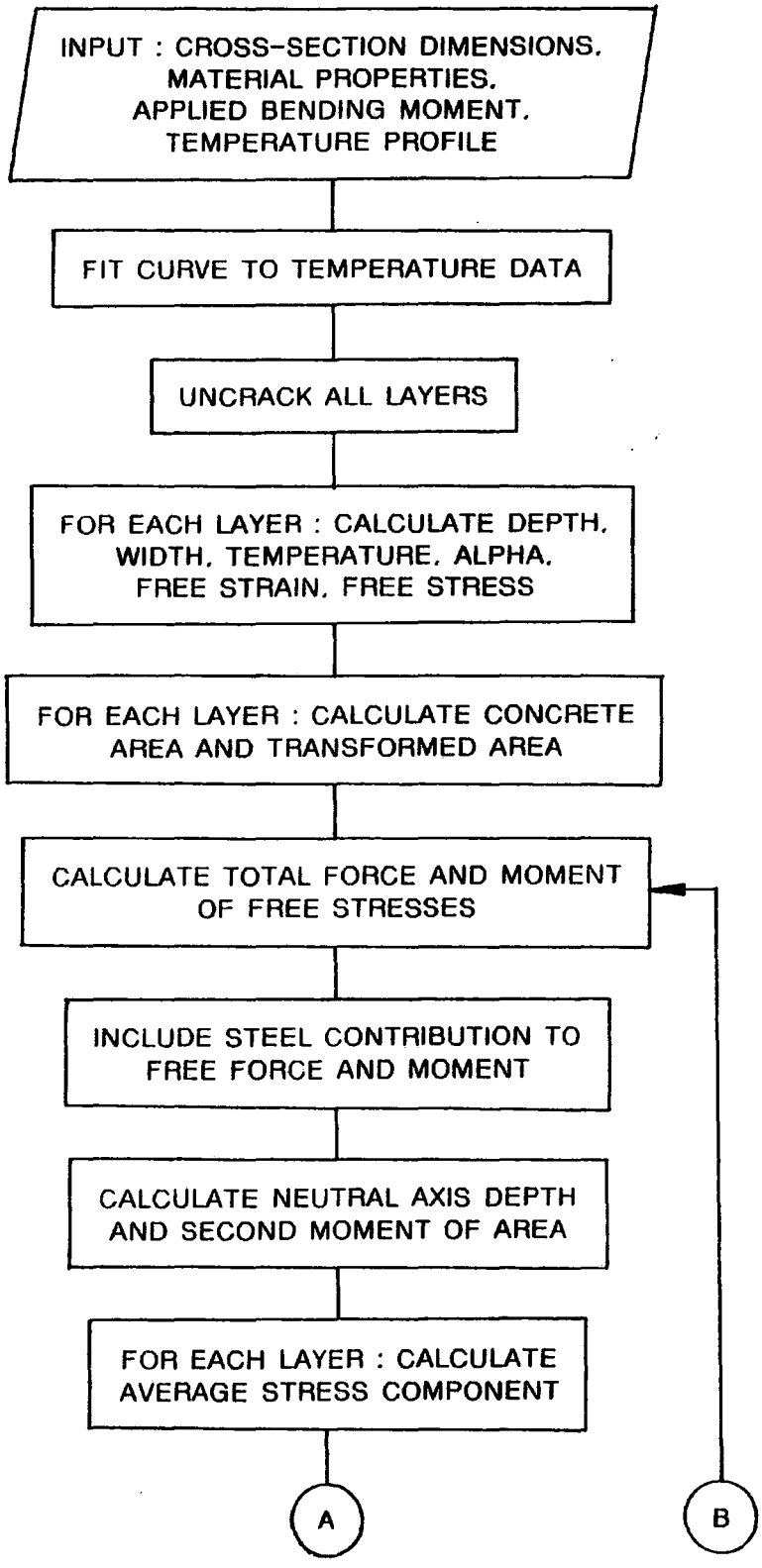

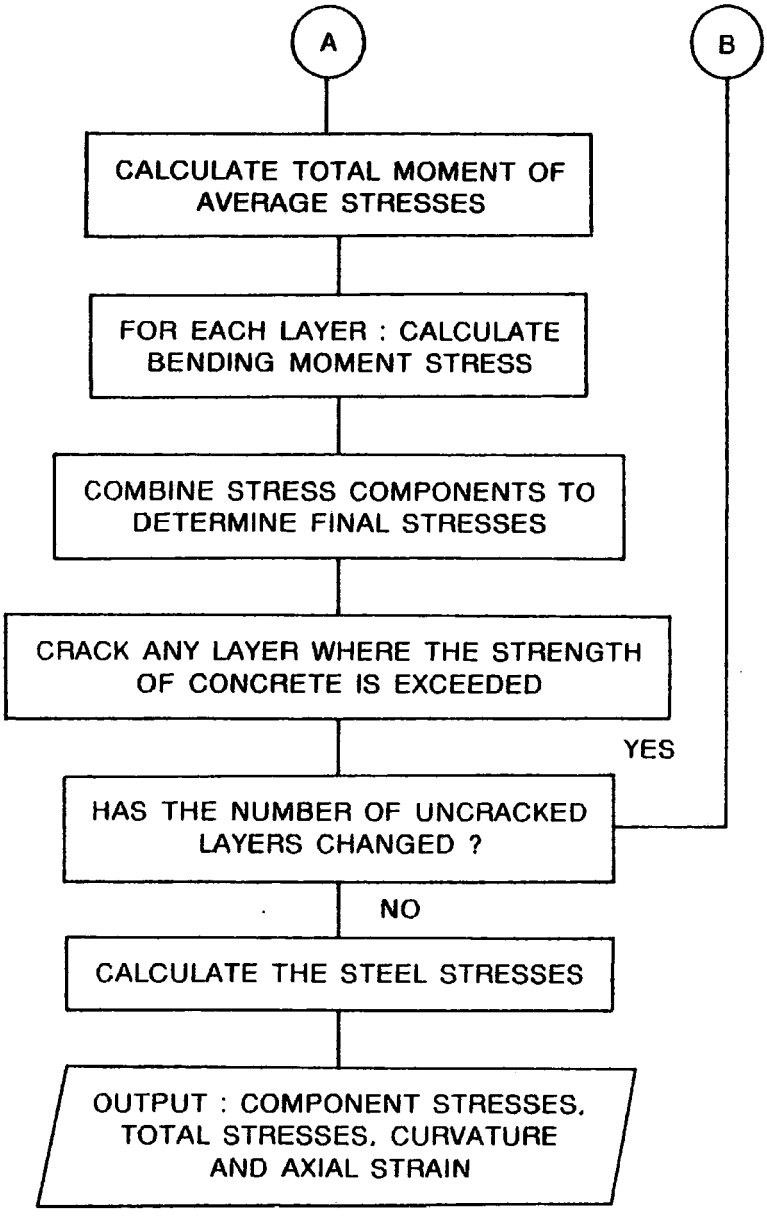
A
B
CALCULATE TOTAL MOMENT OF AVERAGE STRESSES
FOR EACH LAYER : CALCULATE BENDING MOMENT STRESS
COMBINE STRESS COMPONENTS TO DETERMINE FINAL STRESSES
CRACK ANY LAYER WHERE THE STRENGTH OF CONCRETE IS EXCEEDED
YES
HAS THE NUMBER OF UNCRACKED LAYERS CHANGED ?
NO
CALCULATE THE STEEL STRESSES
OUTPUT : COMPONENT STRESSES, TOTAL STRESSES, CURVATURE AND AXIAL STRAIN

4.9 Flowchart for CREEP

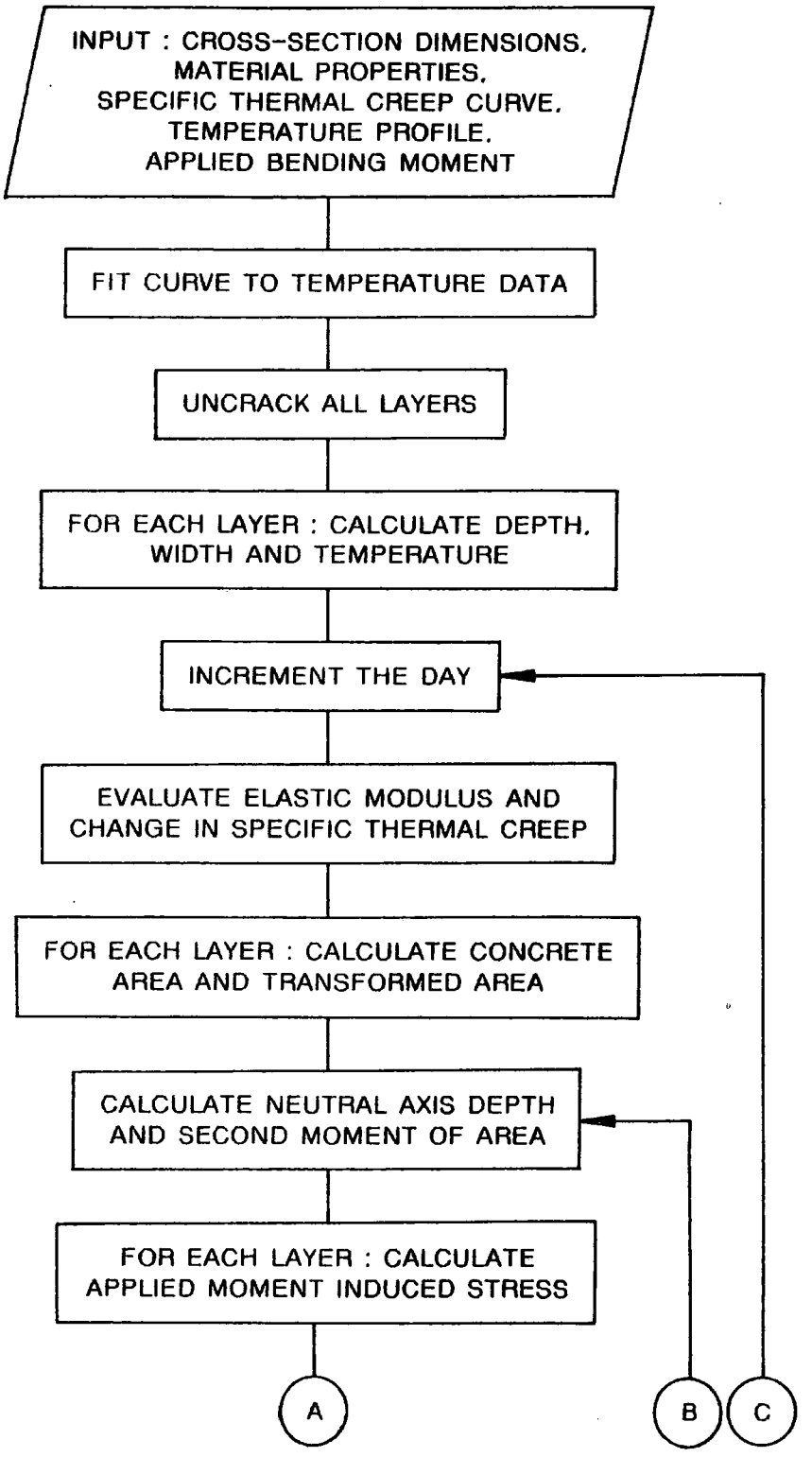

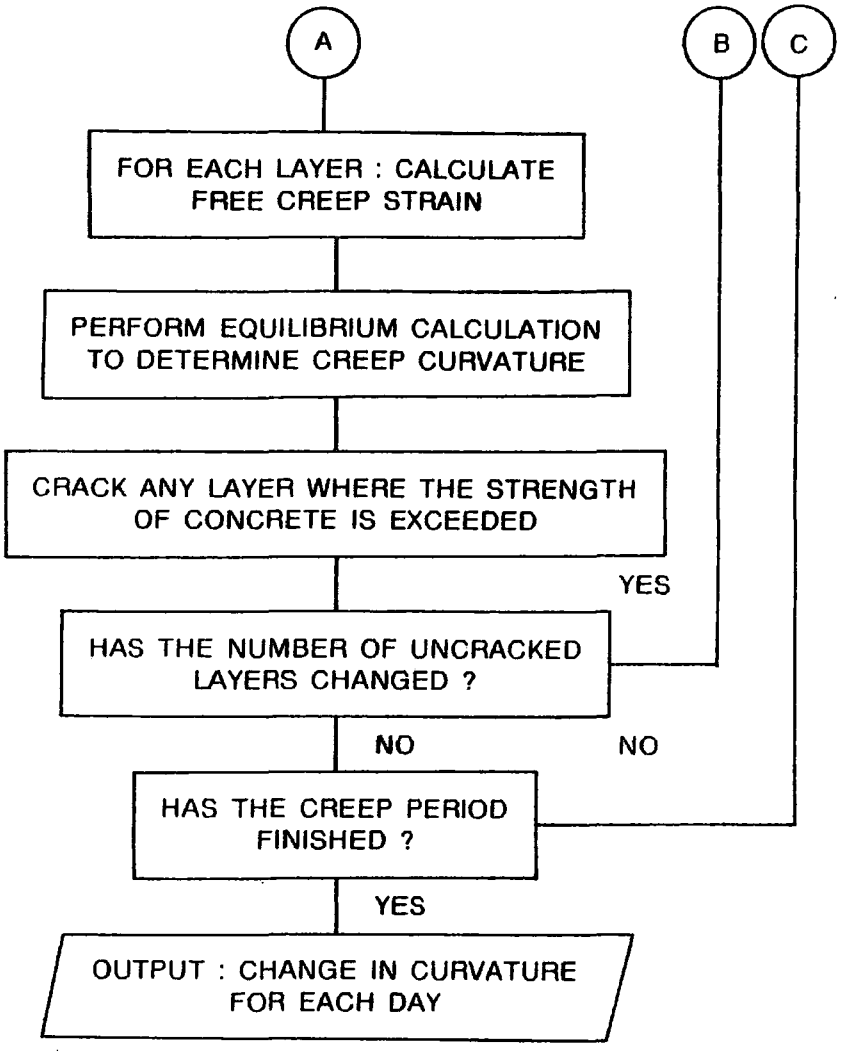
A
B
C
FOR EACH LAYER : CALCULATE FREE CREEP STRAIN
PERFORM EQUILIBRIUM CALCULATION TO DETERMINE CREEP CURVATURE
CRACK ANY LAYER WHERE THE STRENGTH OF CONCRETE IS EXCEEDED
YES
HAS THE NUMBER OF UNCRACKED LAYERS CHANGED ?
NO
NO
HAS THE CREEP PERIOD FINISHED ?
YES
OUTPUT : CHANGE IN CURVATURE FOR EACH DAY

4.10 Flowchart for SCREEP

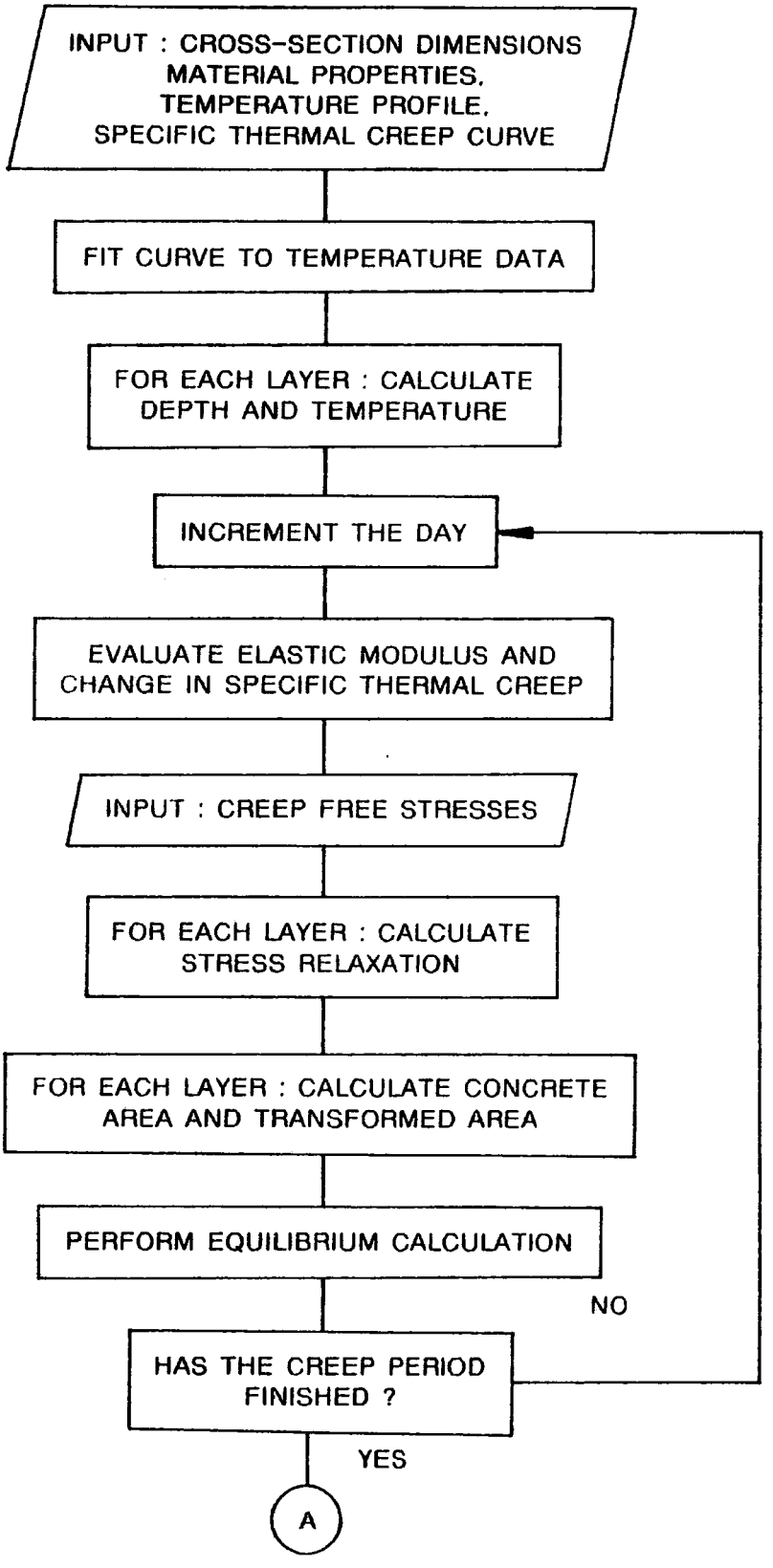

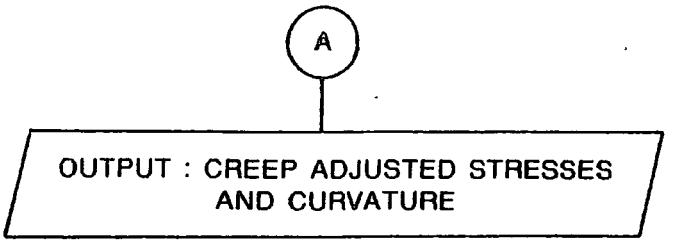
A
OUTPUT : CREEP ADJUSTED STRESSES
AND CURVATURE

CHAPTER V

VARIATIONS IN MOISTURE CONTENT IN MEMBERS

5.1 Introduction

During the course of drying, non-uniform moisture content profiles develop in concrete members. This chapter will describe a method for measuring these profiles.

The work stemmed from certain aspects of the behaviour of the main test beams. These tests will be described in later chapters. Of interest were shrinkage-induced curvatures and stresses, and increases in the coefficient of thermal expansion. These three aspects will now be introduced in turn.

Over a period of several weeks, changes in curvature of non-loaded beams were recorded. These were in addition to the daily fluctuations caused by the temperature profiles. Curvatures reached values of approximately 0.4×10^{-6} mm^{-1} to 0.6×10^{-6} mm^{-1}, depending on whether the beams had been thermally cycled or not. The main beams (Chapter VI) were sealed on all faces except their soffits. It is well known that shrinkage curvatures are induced in members which contain asymmetric reinforcement, but all of the test beams were symmetrically reinforced. Changes in curvature were therefore attributed to non-uniform free shrinkage in beams, resulting from non-uniform moisture content profiles.

Such effects would be expected also to cause stresses in beams. The moisture content profiles would be highly non-linear, as the migration of moisture through concrete is slow. Assuming that shrinkage is approximately proportional to moisture loss, then the resulting free shrinkage profiles would themselves be non-linear. It

is possible to imagine these free shrinkage profiles in the same manner as the free strains resulting from non-linear temperature profiles. In the presence of internal restraint between adjacent fibres of the beams, the notional free strains cannot be fully realised and so there results a system of self-equilibrating stresses. Initial estimates of these stresses showed them to be rather high, exceeding the tensile strength of concrete under certain circumstances. No evidence of shrinkage induced cracking was found from the main test beams and it was suspected that the development of stresses was slow enough for creep relaxation to be an important factor.

Finally, the daily thermal strain results from the main test beams indicated that the coefficient of thermal expansion of concrete was increasing over the several weeks of testing. The suspected cause of the increase was the reduction in moisture content in members. Since non-uniform moisture content profiles were expected, variations in the coefficient of thermal expansion within members were expected also.

The objectives of the work were as follows :

i The measurement of moisture content profiles in members.

ii The prediction of shrinkage-induced curvatures and stresses, resulting from the moisture content profiles.

iii The measurement of coefficient of thermal expansion profiles in members.

5.2 Approach

The approach towards the first of the stated objectives was to expose concrete companion specimens to the same drying conditions as

the main test beams. The companion specimens were therefore of the same cross-sectional dimensions as the main test beams and they were sealed on all surfaces except their soffits. The method of sealing was by application of epoxy resin, as described in section 6.5.2. Several of the specimens were thermally cycled in the same manner as the main test beams, with temperature profiles comparable to that shown in graph 22.

The important feature of the companion specimens was that they contained crack initiators, so that, after given periods of exposure, the specimens could be segmented into several prisms. The moisture content of each prism was determined by recording the weight loss after oven drying. In this way, variations in moisture content could be identified.

The drawback of such a method is that it is destructive and therefore requires a number of specimens in order to determine time dependent trends. However, no elaborate equipment is required and the measurement of moisture content is direct.

In order to fulfil the second stated objective, it was necessary to determine the relationship between weight loss and shrinkage. A number of additional specimens were tested for this purpose.

Thus, the moisture content profiles were measured and then translated into free shrinkage strain profiles, using the empirically derived relationship between weight loss and free shrinkage. The effect of free shrinkage profiles was estimated using a modified version of the thermal analysis program SACRAK. The similarity between the shrinkage and thermal stress problems has been mentioned. Further calculations, using SCREEP, were necessary to account for the

influence of creep relaxation of stresses. The end results were estimates of shrinkage induced curvatures, axial strains and self-equilibrating stresses.

The third aim was to measure variations in the coefficient of thermal expansion. The approach was to use the same segmentation specimens as were used for moisture content measurements. The specimens were subjected to the same heating cycles as the main test beams and sealed in the same way. Following periods of thermal cycling, the specimens were segmented and the coefficient of thermal expansion was determined for each segment.

5.3 Cylinder Specimens

Preliminary tests involved the measurement of moisture content in small cylinder specimens.

5.3.1 Experimental Procedure

Early tests were performed on cylindrical specimens, 200 mm deep and 60 mm in diameter, which were cast in lengths of plastic pipe. Fourteen such specimens were cast at the same time. After a period of 10 days curing in water, they were sealed at one end with epoxy resin and allowed to remain in their moulds which then acted as seals to the curved surfaces. All specimens were then resaturated and, at an age of 14 days, testing commenced. Seven specimens were allowed to stand in the laboratory with their lower unsealed surfaces raised clear of the bench top to allow free loss of moisture. A further seven specimens were similarly placed but were also laterally insulated with expanded polystyrene, and heating tape was applied to their upper sealed surfaces. A pair of thermocouples was inserted into one of the specimens and all seven were then subjected to thermal

cycles of the same type as experienced by the main beams.

At regular intervals throughout the test, including the first day, one specimen was taken from each set and then extruded from its plastic mould. It was segmented perpendicularly to the axis to produce five pieces of approximately the same size. A hammer and chisel was used for this task in the interest of speed and to avoid the liquid lubricant and heat of the saw which would have affected the moisture levels. The segments were placed on metal trays and quickly weighed before placing in an oven at 105 ^{0}C for 24 hours. They were reweighed at the end of this time and, from the weight loss, the nominal evaporable moisture content could be calculated.

5.3.2 Results and Discussion

The moisture content results, presented in graphs 1 and 2, indicate a decrease in moisture content over the the 6 week period. There is however a considerable amount of scatter. This might be expected from the difficulty in ensuring consistency between separate specimens, in terms of initial composition and testing conditions. Nevertheless, the results show increased drying in the lower segments of cylinders compared to inner segments and this is to be expected from their proximity to the exposed surface. A further region of increased drying is indicated from the moisture contents of the upper segments of the heated cylinders and this is due to their closer proximity to the heated surface. In addition, the heated cylinder results show greater overall moisture loss.

The results suggest three possible sources of error. Firstly, the moisture contents from, for instance, week 2 of the non-heated test were reduced below what might be expected from the general trend,

implying a difference in original composition of the cylinder. Although the cylinders were cast at the same mix, differences in compaction might have occurred and, for such small specimens, there may have been differences in mix proportions between individual cylinders.

Secondly, where one particular point appears to be out of place, it could be due to differences in composition between segments of one cylinder. This seems possible as the maximum aggregate size was quite large compared with the size of segments, and the porosity of the aggregate can differ markedly from cement.

Finally, the erratic results from the upper segments of the heated cylinders could have been attributable partially to differences in applied heat as the cylinder temperatures were not monitored and controlled individually .

5.4 Segmentation Block Tests

5.4.1 The Development of Segmentation Blocks

These specimens were developed originally for measurements of profiles of the coefficient of thermal expansion, but they also found use in moisture content tests and it is convenient to describe them in this context. The segmentation blocks were used to overcome some of the inaccuracies experienced with the cylinders, especially relating to the size of prisms compared with the maximum aggregate size.

The blocks were of the same cross-section as the main beams, 100 mm x 200 mm, and were 260 mm in length. Due to their size, it was necessary to introduce crack initiators to enable an effective segmentation. Each block contained three crack initiators allowing segmentation into four prisms of equal size. Photograph 7 shows two

segmentation blocks, one before and one after segmentation.

During the casting operation, the moulds were filled initially to a depth of 50 mm and vibrated, and this was followed by the placement of a crack initiator, which covered the entire top suface. Three further layers were similarly applied, with a crack initiator separating each layer. In this way, all moulds were filled and vibrated together.

Since the crack initiators occupied the entire horizontal plane of the blocks, it was necessary to ensure that they would not obstruct the migration of moisture and, for the first test, hessian was selected as a suitable material. The sheets were fixed into place by pinning them to the sides of the mould, a process which proved to be time consuming and awkward. These were replaced in the second test by sheets of hessian attached to rectangular wire frames which could be dropped into place. So, during casting, the moulds were filled to the level of sets of nails, which protruded through the sides of shutters, and these nails then located the crack initiators.

The hessian sheets worked reasonably well as crack initiators, but it was feared that they might also have acted as a moisture reservoir and, as mentioned, they were difficult to use. Therefore, various types of metal mesh were evaluated, but none of these produced clean cracks. Further tests were conducted using sheets of Netlon, a low density polyethylene mesh commonly used for the stabilisation of soil banks. These proved to be successful, so all subsequent batches of blocks contained sheets of Netlon CE111 attached to rectangular wire frames and located, as before, by nails passing though the shutters. An example of a Netlon crack initiator is shown in

photograph 7.

The grade of Netlon selected had a mesh size of approximately 8 mm, with the spaces occupying approximately 50 % of the area of the sheet. With such a high area interference, it was suspected that a significant restriction would be posed to the migration of moisture and this would be unrepresentative of conditions within a main test beam. An experiment was therefore undertaken to assess the extent of this restriction.

Twelve concrete cubes were cast, six of them each containing two parallel sheets of Netlon attached to a wire frame. After curing under water for 2 weeks, the cubes were sealed with the resin on five faces, the exposed face being parallel to the Netlon sheets, to ensure a nett movement of moisture in a direction perpendicular to the sheets. All twelve cubes were placed in an oven at 60 ^{0}C and, during the course of drying, were periodically removed, weighed and replaced in the oven. Both sets of cubes followed effectively the same weight loss curve, indicating no measurable obstruction to moisture movement by the crack initiators.

It was considered impractical to remove the resin seal before moisture content determination of segmented prisms, so it was necessary to discover whether the resin itself would lose weight during oven drying. The seal was applied to a sheet of aluminium of the same surface area as the prisms and, 2 weeks later, it was placed in the oven for 2 days. A weight loss of approximately 1 % was recorded which, when applied to the much heavier concrete prisms, was insignificant.

5.4.2 Test Program and Procedure

A set of eighteen segmentation blocks was produced, containing Nelon crack initiators as described above. At an age of 2 weeks, testing commenced under similar conditions to the cylinders : all blocks stood on a raised frame to allow free moisture loss from the lower surfaces and half of the batch was laterally insulated, with heating cycles applied to the upper surfaces.

Segmentation took place at weekly intervals over an 8 week period and the resulting prisms were placed in trays to retain any loose particles during the moisture content determination. The prisms were oven dried for 96 hours at a temperature of 105 ^{0}C. Weighing took place before and after oven drying, to determine the nominal evaporable moisture content.

5.4.3 Results and Discussion

The moisture contents of the various segmented prisms, at weekly intervals, are represented by the points on graphs 3 and 4, for the unheated and heated specimens respectively. These results are an improvement on the previous cylinder results as they do not suffer from such erratic variations. Presumably, this is due to the fact that the moulds were filled together in layers, reducing the likelihood of differences between specimens. Also, since the blocks produced much larger segments than the cylinders, there was less of an influence from individual aggregate particles.

From the results, it is clear that significant moisture content differences did not exist at the beginning of the test period and the initial moisture content, expressed as a percentage of the dry weight, was in the order of 6.5 %. This figure then corresponds to the

saturated condition. Thereafter, the prisms proceeded to lose moisture, the amount lost being dependent on the conditions of the test and the location of the prism within the segmentation specimen. Although a trend emerges from the results, there is scatter, probably due to differences in the initial composition of the supposedly identical segmentation blocks.

Smooth curves were fitted to the data, so that the moisture content profiles could be plotted for various drying times. For this purpose, a uniform moisture content was assumed for the beginning of the test, equal to the average for the four prisms, and then a quadratic was fitted to this and the remaining results. For instances such as the lower prism of the heated block, the initial curves had to be modified since they implied a small increase in the moisture content towards the end of the test period. This was physically not the case and so a progressively decreasing curve was fitted instead.

The next stage was to translate the moisture content curves into profiles of moisture loss. So for each day, a third order polynomial was fitted to the four moisture content points to obtain a moisture loss profile through the depth of the member. The polynomial was evaluated at five points for the purpose of the subsequent shrinkage stress analysis and the results so obtained are shown in graph 5 and graph 6 Again, a modification to some of the curves was necessary. As a result of the diminished moisture loss gradient in, for example, the 55 day heated specimen, the raw curve implied an increase in moisture content in the extreme fibres. To overcome this, it was assumed that once the moisture content at a given level had reduced, it did not subsequently increase. Thus, the moisture losses for the

extremities of the heated blocks were pinned to the maximum value from day 25 onwards.

The data smoothing techniques were necessary for the subsequent predictions of shrinkage induced stresses, but the smoothed data are not markedly different from the raw data. For the 55 day results, for instance, the maximum differences between smoothed and raw data are 0.3 % and 0.2 % of the dry weight, for the non-heated and heated blocks respectively.

The results obtained from the heated specimens are much as anticipated, with two drying regions clearly identifiable : one in the upper fibres due to the elevated temperatures and the other in the lower fibres due to the loss of moisture from the exposed surface. The specimens which were not heated exhibited the accelerated drying in the lower fibres, but the results also appear to show a smaller accelerated drying region in the upper fibres which was not expected. Initially, it was suspected that this was due to some free moisture being retained in the upper prism during oven drying as a result of its increased sealant coverage. Following segmentation of a block, the upper prism had one horizontal unsealed surface only whereas the remaining three prisms each had two unsealed surfaces. This explanation is contradicted by the fact that neither of the two specimens which were segmented at the beginning of the test show any sign of the effect. Furthermore, several sets of prisms were oven dried for an additional period, to confirm that negligible additional weight loss occurred.

Differences between the initial composition of the prisms within a single block were ruled out as a possible cause since, as already

stated, the effect did not occur in the first blocks and, although a variation in compaction might have resulted from the incremental filling of the moulds, any segregation would have been obstructed by the crack initiators.

Another possible cause of the unexpected drying is the escape of moisture through the sealant. If this did occur, the upper prism would be affected most due to its larger surface area to volume ratio and increased temperature prior to segmentation. Tests at 50 ^{0}C over 2 days confirmed the effectiveness of the seal, but the action of elevated temperatures over several weeks may have led to a reduction in effectiveness. It must be said however that no conclusive explanation for the reduced moisture levels in the upper fibres of the non-heated blocks can be given.

The moisture loss profiles, which are shown in graph 5 and graph 6, may be unrepresentative of conditions in close proximity to the drying surfaces of the blocks, where the microstructure of the cement differs from elsewhere (131). Also, long-term results collected from unsealed specimen tests suggest an ultimate weight loss of between 2.6 % and 3.1 %, which one might expect to apply to the drying surface of members at 55 days. Although the heated block results show an ultimate weight loss of this magnitude, the non-heated block results do not. These surface effects could be critical as shrinkage induced cracks would be expected to initiate at the surface.

A further point to note is the effect of self-desiccation on the moisture content values. Since hydration was not complete after 2 weeks, some of the loss of evaporable water recorded in the tests can be attributed to self-desiccation rather than evaporation to the

environment. Experiments to quantify this effect were beyond the scope of the present project, but it is interesting to consider the results of Copeland and Bragg (132). Using their figures, it is possible to arrive at a moisture loss of around 0.4 % of the dry weight, in consideration of the period between 14 days and 55 days from casting. Clearly, this effect is not insignificant in light of a 1.5 % moisture loss from the interior of the non-heated specimens.

It is interesting to compare the present results with those obtained by other investigators. Unfortunately, comparisons cannot be made in respect of heated beam results as no reports involving similarly tested specimens have been found, but measurements of relative humidity have been made elsewhere.

The present results indicate a reduction in moisture content of some 1.5 % of the dry weight, after 55 days, within the interior of specimens which were not heated. It is necessary to convert this value into a relative humidity in order to make a comparison with the humidity results reported elsewhere. For this purpose, it is necessary to refer to a desorption isotherm, as mentioned in section 3.5.4. The derivation of an isotherm was beyond the scope of the present project, so that derived by Pihlajavaara (79) was used to provide a rough estimate. This indicates an equilibrium humidity of 85 % r.h. to 90 % r.h., corresponding to a weight loss of 1.5 %.

Thus, attention is drawn to the times reported for the relative humidity in members to drop to 90 % r.h. For example, Arumugasaamy and Swamy (69) reported 40 days to 45 days, for a distance to the exposed surface of 100 mm. It must be noted however that these tests were performed at 72 % average r.h. and at a temperature of between

6 ^{0}C and 16 ^{0}C, so that slower drying than for the present tests would be expected. Hanson's (77) testing environment was comparable to that of the present tests and a drying time of 30 days was reported, for distance of 75 mm from the drying surface.

5.5 Shrinkage Specimens

Having obtained the moisture loss profiles, the next step was to translate them into free shrinkage profiles and to do this the relationship between moisture loss and shrinkage had to be found. This was achieved from tests on small cylinders, whose weight and shrinkage strain were monitored during slow drying. It is recognised that shrinkage stresses would occur also in such specimens. However, these would not be of primary importance to the overall axial strains.

5.5.1 Experimental Procedure

5.5.1.1 First Batch

A series of six cylinders, 200 mm in length and 60 mm diameter, were cast together in plastic pipe and cured in water. At an age of 10 days they were removed from the water, extruded from their moulds and allowed to surface dry. Demec studs were fixed to the cylinders to give three equally spaced axial gauge lengths of 150 mm. The specimens were resaturated and, at an age of 14 days, testing commenced.

On removal from the tank, following resaturation, the surface water was removed and the weights and Demec readings recorded. The cylinders were then placed in the laboratory, where their weights and strains could be measured during drying. This was continued until no further weight loss was observed.

5.5.1.2 Second Batch

A second batch of fifteen cylinders was prepared in the same manner as the previous set. However, these were cured for different durations, so that, for the first group of five, measurements commenced at an age of 7 days ; for the second group, measurements commenced at an age of 14 days ; and for the remaining group, measurements commenced at an age of 21 days. In common with the first set, the cylinders remained in water prior to testing, except for the period when Demec studs were attached.

5.5.2 Results and Discussion

5.5.2.1 First Batch

The results from the first batch of cylinders are given in graph 7. It can be seen that the drying proceeded in two distinct phases, as anticipated. The first phase involved a shrinkage rate of 92 $\mu\varepsilon$/% dry wt. and the second phase occurred at a rate of 226 $\mu\varepsilon$/% dry wt., with the intersection at 97 $\mu\varepsilon$. The end point of the plot approximates to the stage at which the cylinder reached hygral equilibrium with the environment.

5.5.2.2 Second Batch

These results, presented in graph 8, are similar in form to the first set with the bilinear relationship. However, it can be seen that the intersection points and the gradients of the initial phase both appear to be functions of maturity. This is consistent with the explanation of drying shrinkage which has been suggested earlier in section 3.7.3. The results are summarised in the following table :

Curing Time	7 Days	14 Days	21 Days
Gradient of the First Phase	58	124	124 $\mu\varepsilon$/% dry wt.
Gradient of the Second Phase	257	220	296
Intersection Point	66	100	93 $\mu\varepsilon$

5.6 The Estimation of Shrinkage-Induced Stresses

The non-linear moisture loss profiles, indicated in graphs 5 and 6, cause notional non-linear free strain profiles, similar to those caused by temperature profiles. In this case, the free strains were deduced from the moisture measurements, with the aid of the relationship between shrinkage and weight loss. The 14 day relationship, from graph 8, was used, appropriate to the age of first exposure of the test specimens.

The stresses induced by the free shrinkage strains were calculated using the modified version of SACRAK, described in section 4.3. The stresses are presented, with respect to time, in graphs 9 and 10. Graph 9 relates to the blocks which were not heated and graph 10 to those which were. In both cases, maximum tensile stresses occurred at the soffits.

The program SCREEP was then used to estimate the effects of creep relaxation on the shrinkage stresses. So, two creep modified stress curves are shown on the each of graphs 9 and 10. One of these is based of the assumption that creep in tension and in compression are equal, while the other assumes that creep in tension exceeds creep in compression by a factor of 2.5. Two factors were considered as the author could find no general agreement, in the literature, on the relative magnitude of tensile creep. This is discussed in section 3.6.4. However, it was stated in that section that the factor

exceeds unity, at least in the early stages of loading.

5.6.1 Discussion of Results

Considering first the non-heated member calculations, the maximum tensile stress, in the absence of creep, is -4.7 N/mm^2. The value may be compared with the splitting strength results, derived from companion specimens, which are shown also on the graphs. Clearly, the implication is that slight cracking is possible. However, the creep modified results fall below the tensile strength limit.

The heated member results show much higher stresses as a result of more severely non-linear free shrinkage profiles, due to the presence of two drying regions. With a maximum tensile stress of approximately -8 N/mm^2, cracking seems likely. Even when creep is considered, with a tensile creep factor of 1.0, the tensile strength is significantly exceeded. When the higher factor is considered, cracking seems less likely.

5.7 The Measurement of the Coefficient of Thermal Expansion

5.7.1 Introduction

The early measurements of the coefficient of thermal expansion were conducted on small sealed cylindrical specimens, equipped with Demec studs. The application of the values so obtained to the computer analysis SACRAK was not very successful, due, in part, to the experimental inaccuracy in the determination of the coefficient of thermal expansion. It was suspected also that the coefficients of the test beams and the companion specimens were different. A basis for this might have been small differences in initial composition, compaction or the moisture condition of specimens.

Various assumed values of the coefficient were tried in the prediction, in an attempt to reach better agreement with the observed strains. Although an improvement over the experimentally determined coefficient could be achieved, it was usually found that a good agreement could not be achieved for axial strains and curvatures simultaneously. A probable explanation for the inconsistency was the existence of variations in the coefficient of thermal expansion within members, as a result of moisture content variations.

The aim of this investigation was to perform measurements of the coefficient of thermal expansion in specimens subjected to the same drying conditions as the test beams and, more importantly, to identify variations in the coefficient within members. To achieve this, it was necessary to employ a technique whereby specimens could be segmented, so that the coefficient could be determined for each segment.

The segmentation blocks were identical in size and method of preparation to those used in the moisture content determinations, described in section 5.4. They were therefore of the same type as shown in photograph 7. A preliminary test involved the use of hessian crack initiators, pinned to the sides of the moulds during casting. As mentioned earlier, this process proved to be very time consuming, so subsequent crack initiators were attached to rectangular wire frames, which could be dropped into place during casting.

5.7.2 Experimental Procedure

5.7.2.1 First Batch

Five segmentation blocks were cast containing hessian crack initiators attached to wire frames. The casting, curing and sealing procedures were as already described in section 5.4. The blocks were

laterally insulated with expanded polystyrene sheet and heating tape was applied to their upper surfaces. They were all stored in a raised position so that their soffit surfaces could experience similar conditions to the main beams. Heating cycles commenced when the blocks were 14 days old. The temperature profiles were accordingly similar to those applied to the test beams.

At times throughout the test period, a block was removed and segmented, using a hammer and chisel, to produce four prisms of approximately the same size. Any residual hessian was scraped away from the surfaces of the prisms before they were fully sealed with the resin. This was all performed quickly, to minimise moisture loss. The seal was necessary in order to prevent any drying shrinkage, which would have reduced the apparent coefficient of thermal expansion. On the following day, a 5 mm diameter hole was drilled into each prism and a thermocouple then inserted. Epoxy resin was injected into the hole to fix the thermocouple and restore the seal. One prism from the first block was equipped with a set of six thermocouples, at locations ranging from the centre of the prism to a distance of 10 mm from what was previously the vertical surface of the block. This was done to determine whether the prisms reached a sensibly uniform temperature in the oven.

On the same day, Demec studs were attached to the prisms, on opposite vertical faces, to allow two readings to be taken from each prism. A 200 mm gauge length was used for this purpose.

Two days later, the determination of the coefficient of thermal expansion was made. The temperature and Demec readings were recorded for each prism and they were then placed in the oven at 60 ^{0}C for 6

hours. At the end of this time, they were removed individually and temperature and Demec readings were recorded. The prisms were placed on expanded polystyrene to minimise heat loss whilst measurements were being taken.

Further sets of readings were taken on the following day, when the prisms had cooled down to room temperature.

5.7.2.2 Second Batch

A total of seven blocks was cast in the second batch. They were cast, cured, sealed and tested in the same manner as the first set except for the fact that Netlon, instead of hessian, was attached to the wire frames to form the crack initiators.

5.7.3 Results

5.7.3.1 First Batch

The prism which was equipped with thermocouples at six locations assumed a sensibly uniform temperature by the end of the heating period. In fact, the maximum temperature difference was 0.2 ^{0}C, some 0.5 % of the total temperature rise.

As far as the accuracy of the strain measurements was concerned, the one-division sensitivity of the Demec equipment represents a maximum error of around 5 % for each determination of the coefficient. This figure may be an overestimate, as two gauge lengths were used on each prism, but this does not necessarily imply a two-fold increase in accuracy, as non-uniform expansion of prisms occurred. In fact, the maximum indicated difference between the strain changes of the two sides of a prism was two dial gauge divisions. A further improvement in accuracy might be expected from the fact that each result was the average of two thermal changes, namely heating and cooling.

The main results for the test are shown in graphs 11 and 12. Each of the points on these graphs is, as stated, the average of the heating and cooling values. The two are not presented separately as neither of them was found to be systematically greater than the other. If any actual differences were present, then they were beyond the resolution of this experiment. This would not have been the case if the specimens had remained unsealed, as drying shrinkage would have affected the results.

Graph 11 indicates an increase in the coefficient over the period of the test, from an average of 10.1 $\mu\varepsilon/^0C$, at the start, to 12.3 $\mu\varepsilon/^0C$, at 56 days. The variations within specimens are more apparent in graph 12, where the results suggest reasonably uniform values at the start and finish of the test and non-linear variations for the three intermediate blocks.

5.7.3.2 Second Batch

Graph 13 indicates also an increase in the coefficient of thermal expansion over the duration of the test, but the rate of increase is less than indicated in the previous test. After 56 days, an 11.5 % average increase was observed, which may be compared with the 21.8 % from the previous batch of specimens.

The coefficient profiles are shown in graph 14 and, as before, a sensibly uniform value is indicated for the start of the test. Also apparent are the subsequent non-uniform profiles, with the increased values in the upper and lower segments.

5.7.4 Discussion

The overall trend was an increase in the coefficient of thermal expansion in specimens and it is suggested that the increase was

caused largely by the loss of moisture from the concrete. It may be recalled, from section 3.4.1.2, that, as a specimen dries from the saturated condition, its coefficient increases to a maximum value and this increase may be in the order of 20 % (57). The maximum occurs at an intermediate stage of drying, beyond which a reduction in the coefficient occurs. The experimental results show no clear evidence of such a reduction.

The second point to note is the non-uniformity of the coefficients measured in specimens. Some of this must be attributed to experimental inaccuracy, but it is suggested that the major cause is also seated in the loss of moisture. The determinations of moisture content within members showed up two drying regions, which would develop also in the present specimens for the measurement of the thermal coefficient. Thus, the coefficient profiles are a reflection of the moisture content profiles.

Many of the possible causes of inaccuracy of the present method are the same as for the moisture content determinations on segmentation blocks. Firstly, there is the extrapolation of the curves to the top and bottom surfaces of the specimens. It is known that microstructural differences exist near to the surface of drying members (131) and these would be expected to affect thermal expansion. Secondly, it is possible that the value of the coefficient levels out in the surface fibres as ultimate moisture loss is attained. Indeed, small reductions in the value of the coefficient might occur if the relative humidity in the fibres were to fall below that corresponding to the peak coefficient, although no such effect is apparent from the results presented.

A further difficulty exists in attempting to identify time-dependent trends from a series of individual specimens. Although the results do show a trend, they do not form smooth curves. Possible reasons for the discrepancies are the same as for the moisture content determinations, such as small differences in initial composition, drying conditions and applied temperature profiles. As well as these effects, the estimated errors in measurement were greater in this test compared with the moisture content tests.

5.8 Concluding Remarks

Variations in moisture content were detected within concrete blocks. These variations are attributed to evaporation from the exposed surface and to the existence of thermal gradients within members.

Moisture loss measurements have been included in a theoretical consideration of shrinkage induced stresses and it has been shown that otherwise high tensile stresses are greatly relaxed by creep, possibly to the point where cracking is avoided.

Variations in moisture content affect material properties and measurements have shown that non-uniform profiles of the coefficient of thermal expansion occur within members. Moreover, the overall coefficient has been found to increase with the progress of drying.

CHAPTER VI

EXPERIMENTAL PROCEDURE AND EQUIPMENT FOR MAIN TESTS

6.1 Purpose of the Tests on Beams

The overall objectives of this project were defined in the first chapter. This section will deal with the tests on beams in a more detailed manner.

A series of eight tests was performed to investigate the influence of cyclic variations in temperature on the behaviour of loaded and non-loaded reinforced concrete beams. Of interest were the curvatures of simply supported beams and the changes in the support reactions of continuous beams during a daily thermal cycle. Also of interest was the effect of creep and shrinkage on induced stress and overall beam deflection during the first 6 to 8 weeks after casting.

The applied temperatures were based on the those suggested by Emerson et al., relating to the unsurfaced condition. It may be recalled, from the earlier discussion, in Chapter II, that this condition is approximately representative of 50 mm of black top surfacing.

The program by Jones (28) was implemented on the departmental computer with input data pertaining to extreme environmental conditions for positive temperature profiles. The maximum temperature differences so obtained were 13.5 ^{0}C and 16.1 ^{0}C for 200 mm deep beams and 400 mm deep beams respectively.

The computed results for the shallow beam did not show soffit temperatures in excess of those in the concrete above. However, for the deep beam, soffit temperatures were shown to exceed the minimum bridge temperature by up to 2.5 ^{0}C.

With the exception of the T-section beam test, the experiments attempted to simulate the conditions within a bridge deck, where it is assumed that the diffusion of heat and moisture have no transverse components. Beams were therefore sealed against moisture loss on all vertical surfaces. They were sealed also on one horizontal surface to be representative of the waterproof membrane which is applied to the top surfaces of bridge decks. The soffit remained exposed to permit the loss of moisture to the environment.

Thermal insulation was applied to all sealed surfaces in order to ensure that the diffusion of heat was one-dimensional also. The analysis of thermally induced stresses and strains is simplified considerably if it can be assumed that temperatures within the horizontal plane are constant.

It is recognised that conditions such as these do not relate to the extremities of a member, where the diffusion of both heat and moisture in a horizontal sense may predominate.

The T-section beam was a departure from the others in that transverse heat and moisture diffusion were allowed, as would be the case in practice. The beam was however sealed and insulated on the top and vertical surfaces of the flange, to be representative of a surfaced component member of a bridge deck. Furthermore, this was effectively a model test, as handling and testing facilities prevented the use of a realistically sized member.

The aims of the individual tests will now be described.

6.1.1 First Single Span Beam Test

The main purpose of this test, as far as short-term response was concerned, was to collect measurements of thermally induced elongation

and curvature, which could be compared with predicted values, and to assess the influence of creep on these strains. The beams were tested at two levels of loading, to observe the influence of cracking on thermal strains and to test the proposition that mechanically and thermally induced effects can be simply superimposed at these levels of stress. Thus, in the second phase of loading, the cracking moment was exceeded.

The long-term observations were conducted to investigate the influence of thermal cycling on creep and shrinkage deflections. Thus, of the two loaded beams, one was heated and the other was not.

6.1.2 Second Single Span Beam Test

An additional objective of this and subsequent tests was to observe the shrinkage effects separately. To do this, the tests also included a pair of short non-loaded beams, which were subjected to the same environmental conditions as the loaded beams. In addition, they provided a direct comparison of cracked and non-cracked beam thermal response.

The main beams of this test were subjected to a higher initial loading than the beams from the first test. Also, after the first phase of the test, involving heating of the upper surface, the soffit was heated. This was done in order to assess the effect of the heating of a cracked surface on thermal response. It might be expected that, during a thermal cycle, the opening and closing of cracks diminish the overall changes in curvature and longitudinal strain. Such an effect would be at its greatest during heating of the cracked surface.

6.1.3 Third Single Span Beam Test

This test was performed to confirm the findings of the previous single span tests, but with a greater loading. The main reason for doing this was to further investigate the influence of the extent of cracking on changes in beam curvature during a thermal cycle. Also, the frequency of thermal cycling was increased to five, rather than three, cycles per week.

6.1.4 Deep Beam Test

The objectives of this test were the same as for the previous tests, but deep beams were used because they exhibit more severely non-linear temperature profiles compared to similarly heated shallow beams. They therefore experience greater thermal stresses. Consequently, there is more opportunity for creep to influence thermal strains and so reduce the accuracy of prediction method.

6.1.5 T-Section Beam Test

An upright T-section beam has a relatively large surface to which heat can be applied and there is more material at the level where the greatest temperature occurs. It follows from this that there is a greater thermally induced force on the section, compared to the rectangular section beams. The objective of this test was therefore to determine whether the conclusions which had been drawn from the tests on rectangular section beams were applicable also to a T-section beam.

The long-term deflections of the beam were of less significance, as the moisture migration pattern did not conform to other beam tests and the work on segmentation blocks, which is described in Chapter V. For instance, in the case of the T-section beam, an increased

proportion of moisture is lost from the upper fibres of the member, resulting from the reduction in sealed surface area. There is also the existence of transverse moisture migration. It follows therefore that the curvatures induced by non-uniform shrinkage are different, and creep curvatures are likely to be affected by the different moisture distribution also.

A further purpose of the test was to investigate the behaviour of a crack during a thermal cycle and, for this reason, a crack gauge was built which was mounted on the beam following loading.

6.1.6 First and Second Two Span Beam Tests

Whereas the previous tests were concerned mainly with the measurement and prediction of thermally induced strains, the purpose of the two span tests was to investigate the changes in support reaction due to the restraint of thermal curvature. The first test was performed with a small load so that the cracking moment was not exceeded. Unfortunately, the test had to be abandoned after one week of thermal cycling, due to unforeseen circumstances. The second two span test was therefore a repeat of the first.

6.1.7 Third Two Span Test

The aim of this test was to assess the influence of cracking on thermally induced restraint force, so an increased moment was applied to the beams.

6.2 Description of Beams

The geometries of the test beams are shown in figure 11, where the Demec stud locations are indicated also.

6.2.1 Single Span Beams

The beams for use in the loading rig were 2800 mm long, 200 deep

and 100 wide.

They were symmetrically reinforced with two ϕ 12 mm bars in each face : the first set of beams contained mild steel plain bar and all other beams contained high yield deformed bar. In all cases, the cover to the bars was 25 mm. Nominal links of 6 mm diameter were included. They were located away from the section of the beams where strain measurements were to be taken.

Free standing beams were used also. These were 1000 mm long and of the same cross-section as the loaded beams.

6.2.2 Deep Beams

The loaded beams were 400 mm deep and 100 wide in the central 1400 mm, and 200 mm deep and 100 wide over the remaining length, the overall length being 2800 mm. The reduction in depth was necessary in order to avoid substantial modifications to the loading rig and due to the weight limitations of the handling facilities. Also, as the level of the end-supports was higher than the soffit level of the deep section, the arrangement benefited from improved stability.

The central section was also symmetrically reinforced with Y 12 high yield deformed bar, with 25 mm cover. Again, only nominal links were required. The tension bars were bent up at 45^0 and continued into the shallow section to provide sufficient anchorage. A pair of links, inclined at 45^0, was included to relieve the stress at the inside corner of the step. The moment which could be applied to the central section of the beam was limited by the load capacity of the 200 mm deep section. This was increased by including a third tension bar in this section.

The free standing beams were 1000 mm long and of 400 mm deep x

100 wide cross-section over their entire lengths. They also were symmetrically reinforced with two Y 12 high yield deformed bars in each face.

6.2.3 T-Section Beam

The T-section beam was 2800 mm in length, with an overall depth of 200 mm. The flange was 300 mm in width and 70 deep, and the web was 100 mm wide.

Only tension reinforcement was included, which was provided by a pair of Y 12 high yield deformed bars, with a cover of 25 mm.

6.2.4 Two Span Beams

The two span beams were of 200 mm deep x 100 wide cross-section, symmetrically reinforced with pair of Y 12 high yield deformed bars in each face. They therefore had the same cross-sectional properties as the single span beams, but they were 4000 mm in length.

The free standing beams were 1000 mm in length and of the same cross-section as the loaded beams.

6.3 The Measurement of Surface Strains

6.3.1 Demountable Mechanical Strain Gauge

The surface strains of concrete specimens were measured using demountable mechanical (Demec) strain gauges, which are commonly used for this purpose. This method was selected for a number of reasons. Firstly, there is no need for temperature calibration, as the gauge itself can be stored at a constant temperature between readings. Electrical resistance strain gauges, although intrinsically more accurate, are susceptible to temperature change effects. These can constitute a serious problem where the mechanical strains are small, as is the case here. Secondly, the Demec gauge lengths are relatively

long, so that averaged strain readings are automatically produced. More localised methods are affected by cracks and possibly the presence of large aggregate particles. The method selected thus negates the necessity to use a large number of gauges. Lastly, the method is simple and robust.

The method of taking measurements was to apply the gauge to the locating studs twice. If the consecutive readings were more than one division out, the reading was repeated until satisfactory agreement was obtained.

The gauge lengths used were 150 mm and 200 mm. Assuming a sensitivity of plus or minus one dial gauge division, the corresponding strain accuracies are 10.7 $\mu\varepsilon$ and 8.1 $\mu\varepsilon$ for the short and long gauges respectively.

The locating studs were mounted on both sides of the beams to identify any transverse warping. Their positions are shown in figure 11.

6.3.2 Crack Gauge

In a preliminary investigation, a surface microscope was used to measure crack widths. By this method, it was not possible to detect any changes in crack width during a thermal cycle. However, a better knowledge of the behaviour of a crack, during heating, was sought. For this purpose, a crack gauge was developed for use in the T-section beam test.

The gauge, which is shown in photograph 6, comprised of a strip of high tensile strength steel, 0.5 mm thick and 5 mm wide. This was spot welded to steel pads, whose purpose was to lift the strip 3 mm clear of the concrete surface to allow the attachment of two

electrical resistance strain gauges to the underside. Four strain gauges, of type FLA311, were attached to the strip in total. Two of these, mounted on the inactive arm of the strip, acted as dummy gauges for temperature compensation. The other two were mounted in the active section, between the pads and on either side of the strip to reduce bending effects. They were connected to a 'Peekel' strain gauge meter in full bridge configuration.

Before attachment to the beam, the thermal sensitivity of the crack gauge was checked by placing it on some heating tape. A maximum shift of 3 $\mu\varepsilon$ was observed for a temperature change of 10 ^{0}C.

It was appreciated that the crack gauge would make a contribution to the flexural stiffness of the beam at the section where it was attached, but, from calculation based on the fully cracked section, the increase would be no greater than 1.4 %.

6.4 The Measurement of Temperature

Temperatures were measured in concrete members by embedded thermocouples, which were generally cast into the member. On occasion it was necessary to drill holes in members, into which the thermocouples could be inserted. Copper/constantan thermocouples were used in all tests.

For the beam tests, the thermocouples were attached to wooden spars, which were of 4 mm square cross-section. These spars were of sufficient length to run the entire depth of the beams, enabling temperature measurement at the top surface, the soffit and at locations inbetween. Notches, 50 mm apart, were cut into the spars to locate the thermocouples. The bared thermocouple wires were wrapped around the spars at the notches and then glued in place. They were

thus positioned to within 2 mm of their prescribed depths.

For the first two tests, the thermocouples were connected through a switching box to a `Comark' electronic cold junction. This was then connected to a digital voltmeter, giving readings to the nearest 0.25 $^{0}$C. A `Comark' thermocouple meter, with its own built-in cold junction, was used in the remaining tests and this arrangement gave readings to the nearest 0.1 ^{0}C.

Accuracy was checked by wrapping a thermocouple around the bulb of a precision mercury thermometer which was placed in a water bath. The water temperature was increased from 20 ^{0}C to 50 ^{0}C, with a maximum discrepancy between thermometer and thermocouple readings of 0.4 ^{0}C. It is likely that part of this discrepancy is attributable to small actual temperature differences.

6.5 Preparation of Beams

6.5.1 Concrete Specification

The concrete mix was designed following the procedures of `Design of Normal Concrete Mixes' (133), to provide a characteristic strength of 40 N/mm^{2} and a slump of 10 mm to 30 mm. The mix proportions were 1 : 2.1 : 2.9, with a water to cement ratio of 0.42. For most mixes, additional water was necessary to achieve a required slump of approximately 20 mm, due to the drying of the aggregate during indoor storage.

Blue Circle O.P.C. was used throughout the tests. The coarse aggregate was Scorton River Gravel, which contained a number of rock types. The larger particles were composed of sandstones and fossiliferous limestone. The smaller particles included Old Red Sandstone, dolerite and siltstones. The grading was within the limits

for a graded coarse aggregate as specified by BS882 (134). The grading of the sand was within Zone 2 of BS882.

6.5.2 General Procedure

All of the beams tested, except for the first set and the T-section beam, were prepared in the same manner, thus attempting to ensure consistency between tests.

They were cast in wooden moulds which were treated with demoulding oil. Small spacing blocks, made from cement mortar, were placed into the moulds, following application of the oil. The reinforcement cages were lowered into place, to rest on the spacing blocks, and were then secured with wire attached to the blocks. The moulds were then lifted onto the vibrating bed to await casting.

The concrete was prepared in a mechanical pan mixer. Between three and five separate mixes were required for each cast. The moulds were filled in four layers, with vibration after each layer. The thermocouple spars were inserted after the moulds had been filled, by driving a hole into the freshly placed concrete with a steel rod. The spars were inserted into the resulting holes and the moulds were vibrated again in order to close the holes.

The beams were cured under damp hessian for a period of approximately 10 days before demoulding. At first, only the side shutters were removed to maintain a moisture seal at the soffit. The beams were allowed to stand for 1 hour, in order to surface dry, before the sealant primer was applied to all exposed surfaces. The top-coat was applied on the following day : one coat was applied in the morning and another was applied 8 hours later. The sealing agents were `Colebrand' CXL 121 primer and CXL 141 top-coat.

The Demec studs were attached to the beams on the 12th day by firstly scraping away small areas of the seal at the required locations. The studs could then be fixed to the bare concrete using epoxy resin, held in place temporarily by strips of adhesive tape. A Demec locating bar was used to obtain the required gauge length.

On the 13th day, the strips of adhesive tape were removed from the Demec studs and the beams were lifted clear of the soffit moulds, thus breaking the seal.

The only difference in procedure for the first set of beams was that they were moist cured for an additional 2 weeks due to a delay in sealant supply.

With each set of beams, various control specimens were cast and cured in water. These included 102 mm cubes to enable the determination of the 28 day cube strength. In addition, each set included a cylinder, 300 mm in length and 150 mm in diameter, for compressive elastic modulus tests. These cylinders were fully sealed with the resin and three sets of axially aligned Demec studs were attached. Also, cylinders were cast and cured in water for determination of the 14 day indirect tensile strength. Three such cylinders, 150 mm in length and 150 mm in diameter, were produced per test.

The first two tests each included a concrete cylinder, 60 mm in diameter and 200 mm long, for coefficient of thermal expansion measurements. These cylinders were sealed with the resin and equipped with Demec locating studs. When the limitations of the method were appreciated, it was decided to employ a more elaborate procedure to determine the value of the thermal coefficient, under conditions more

representative of the main beam tests. This investigation is described in Chapter V.

6.5.3 Heating and Insulation

Once the beams had been placed in the laboratory, either in the loading rig or simply supported, the heating tape and thermal insulation were applied. The heating tape, manufactured by 'Electrothermal', was a braided fine iron wire enclosed in a knitted glass fibre sleeve. It was applied to the upper surfaces of one loaded beam and one non-loaded beam, and secured in place with heat-resisting adhesive tape. Four strands of the tape were used per 100 mm width of the beam. They were connected to a 'Variac' variable resistance box to enable the regulation of temperature. The tape was covered over with aluminium foil to improve the thermal efficiency and to protect the insulation from elevated temperatures.

Expanded polystyrene, 20 mm thick, was attached to the vertical surfaces and the top surface of the heated beams. It was secured in position with adhesive tape. In the sections where access to the Demec studs was required, removable panels of the insulation were used.

The ambient temperature of the laboratory was 20 ^{0}C and the average humidity was 50 % r.h. It was possible to record higher humidities, up to 65 % r.h., when the laboratory was being used by a large number of people. The minimum humidity recorded was 38 % r.h., but these extreme conditions did not prevail for long durations.

6.5.4 T-Section Beam Preparation

This beam differed from the rest in that the vertical faces of the web and the underside of the flange were not sealed against

moisture loss nor were they thermally insulated.

The casting procedure was identical to that for the other beams. However, during the initial stage of demoulding, only the vertical faces of the flange and the top surface were exposed and then sealed with the resin. All other surfaces remained unsealed and uninsulated throughout the test. Thus, the nett direction of moisture migration and heat flow was no longer perpendicular to the heated surface.

Since transverse temperature gradients were expected in this beam, especially in the uninsulated web, it was considered necessary to measure temperatures at various locations within the cross-section. The actual locations of the additional thermocouples are shown in figure 12.

The additional thermocouples in the flange were positioned using thin wooden spars, attached originally to the mould. This method was not thought to be sufficiently robust for the accurate location of the thermocouples in the web. Instead, 6 mm diameter holes were drilled into the beam to the required depth, following demoulding. The thermocouple wires were inserted into lengths of stiff plastic tubing and then glued in place. Epoxy resin was injected into the drilled holes to displace any air and the thermocouple tubes were then inserted.

6.6 The Loading Rig

A rig was built to provide sensibly constant loading to a pair of test beams, using a lever arm mechanism. The actual loading arrangements for the various tests are shown in figure 13.

6.6.1 Single Span Tests

Initially, the rig was used to apply a four point loading to a pair of beams which were installed in the rig in a back-to-back arrangement. Four point loading was employed to give a region of sensibly constant bending moment. The loads were applied by means of a pair of loadings arms, whose action was to prise the beams apart, thus causing a hogging moment in the upper beam and a sagging moment in the lower beam. The forces from the arms were transmitted to the beams by means of saddle bearings. These are shown in figure 14.

The beams were supported at their extremities by end-support stands which, by using vertical steel plates, provided an effectively knife-edge end reaction. The inclination of these plates could be altered to accommodate any initial twist in the beams which might have resulted from warped moulds. A bearing was included between the plates and the surfaces of the beam to eliminate the possibility of frictional restraint to thermal expansion of beams. These comprised of a layer of 1.5 mm thick P.T.F.E. sandwiched between two small stainless steel plates.

The loading arm arrangement was selected primarily due to the fact that the applied bending moments could be easily maintained at a sensibly constant value throughout the duration of the test. Any vertical deflection of the beams could be accommodated by rotations of the arms from the horizontal. Provided that such rotations were small, the effect on the loading geometry was negligible. However, large beam deflections occurred during loading. Also, under large applied moments, substantial deflections occurred as a result of creep. It was therefore necessary to re-level the loading arms by

tightening the adjustment bolts which transmitted the load from the loading arm to the saddle bearing on the lower beam.

For the first two tests, saddle bearings were used on both upper and lower beams and, as already mentioned, the load was transmitted via the adjustment bolts to the lower beams. In the case of the upper beams, the end plates of the loading arms bore directly onto the saddle bearings. This arrangement was modified for subsequent tests to reduce the possibility of restraint to longitudinal thermal response. This modified arrangement is shown also in figure 14. With the existing set-up, the expansion of the constant moment section of the lower beam might have been resisted by the non-expanding constant moment section of the upper beam. Any such restraint would have been transmitted via the loading arms and bearings. To avoid this possibility, portal frames were fabricated which were bolted to the ends of the loading arms. These carried hangers which then supported the upper beam. By this means, any differences in the expansion of the two beams would cause flexure of the hanger bars which could offer very little restraint.

6.6.2 Deep Beam Test

No modifications to the existing rig were necessary for this test. However, consideration had to be given to the beam geometry to permit installation. The rig, complete with the deep beams, is shown in photograph 1.

6.6.3 T-Section Beam Test

In this test, only one T-section beam was used, but it was placed in the rig together with a reaction beam from a previous single span test to complete the loading arrangement. This is shown in

photograph 2.

The rig remained essentially unaltered from the configuration used for the other single span tests, but it was necessary to redesign the loading bearings for the lower beam. The increased width of the T-section beam could not be accommodated in the existing saddle bearings, so they were replaced with a rectangular section steel bar, drilled and tapped to accept the adjustment bolts.

6.6.4 Two Span Tests

Again, no fundamental modifications were necessary to the end-support stands and loading arms, but, in addition to the existing equipment, a device was required to provide restraint to the vertical deflection at the centre of the beams. The resulting rig is shown in photograph 3.

6.6.4.1 Central Restraint

The design of the central restraint had to meet three criteria : adequate overall strength ; sufficient rigidity to limit deflections ; sensitivity to enable the measurement of small changes in reaction due to restrained thermal curvature.

After considering a number of alternative methods, it was decided to use a block-and-strap arrangement, where the central deflections of the lower beam could be restrained by the upper beam and by the connection to the ground support. The device is shown in figure 15. Electrical resistance strain gauges were selected as a means of measuring the reaction force.

In the arrangement used, the vertical forces were carried by lengths of M20 high yield strength studding. A pair of these provided the restraint between the beams and a third connected the restraint

assembly to the ground support. The beams were clamped in place between steel cross-members through which the studding passed. The third bar passed from the lower cross-member to a length of inverted channel-section girder which rested on the ground. Concrete kentledge beams were placed on the ground support to prevent the lifting of the restraint during application of a positive temperature profile.

Each of the three restraint bars contained a section which was necked to 7 mm, in order to provide the necessary sensitivity for the strain gauge measurements. These can be seen, for two of the bars, in photograph 4. Since this section was relatively short, it was of negligible significance to overall rigidity. Three strain gauges of type FLA311 were mounted on each bar, equally spaced around the circumference of the necked section and axially aligned with the bar.

The load cells were in close proximity to the heating tape, so it was necessary to use dummy gauges for temperature compensation. The first set of dummy gauges was attached directly to the bars and, as there was insufficient space on the 7 mm section, they had to be mounted on the section of reducing diameter. Their effectiveness was assessed by placing the bars in an oven at 60 ^{0}C, which proved that the compensation was unsatisfactory. This was probably due to the unusual surface geometry. The problem was rectified by mounting three gauges on the flats of a nut which was later screwed onto the bar, to be in close proximity to the necked section. Three such nuts were used so that each active gauge had a dummy. These are shown also in photograph 4.

The gauges were connected to a 'Peekel' switching box. The box contained internal resistances, thus providing a full bridge

configuration at the output, which was then connected to a `Peekel' strain gauge meter.

Before tests on the beams commenced, the load cells were calibrated in a `Denison' testing machine. Their average sensitivity was 8.1 N/$\mu\varepsilon$

6.6.4.2 End Support Load Cell

For the second two span test, it was decided to incorporate a load cell in one of the end supports of the lower beam. This is shown in photograph 5. The cell consisted of a hollow steel cylinder, 8 mm in length and 15 mm mean diameter, sandwiched between two steel plates. The wall thickness, where the strain gauges were mounted, was 1.5 mm. This increased to 2.5 mm at the ends to provide a larger surface to glue onto the steel plates. Three gauges were used, equally spaced around the cell and axially aligned. They were connected to a `Peekel' strain gauge meter in quarter bridge configuration. Dummy gauges were not used as significant temperature changes were not anticipated.

To accommodate the load cell, a rectangular slot was removed from the vertical support plate, allowing the cell to stand slightly proud of the top of the plate. A bevelled edge was machined onto the bottom edge of the slot, to allow unrestrained tilting of the cell.

The load cell was calibrated under compression in a `Denison' testing machine and was found to have a sensitivity of 12.1 N/$\mu\varepsilon$. Unlike the restraint bar load cell, this load cell would not operate linearly unless all three gauges were under compression. It was therefore necessary to reposition the cell in the rig several times to achieve all-round compression.

6.7 Beam Loading

As regards the beams which were tested in single span arrangement, and this includes the deep beams and T-section beam, the constant moment sections were of prime interest. The bending moments in these sections were as follows :

			Upper Beam	Lower Beam
Single Span Test	-Set 1	-Phase 1	3.03	2.98 kNm
		-Phase 2	6.06	5.76
	-Set 2		6.06	5.76
	-Set 3		6.13	6.60
Deep Beam Test			10.60	11.00
T-Section Beam Test			-	7.80

As regards the two span tests, the bending moments along the entire lengths of the beams were of interest and are shown in figure 16. However, the maximum values were as follows :

		Upper Beam	Lower Beam
Two Span Test	-Set 1	1.95	2.16 kNm
	-Set 2	1.95	2.16
	-Set 3	5.78	6.10

With the exception of the first set of beams and the T-section beam, shorter companion beams were produced which were not loaded.

6.8 Test Procedure

6.8.1 First Single Span Test

The beams were loaded and then thermally cycled following 4 weeks of moist curing. The cycles were applied on alternate week days so that there were three cycles per week. At 15 days, the loading was increased to its Phase Two value and then thermal cycling continued as

before, for a further 22 days.

For the heated beam, Demec readings and temperatures were recorded every 2 hours over the 8 hour heating period. For the beam which was not heated, the Demec readings were recorded at the beginning of each day of testing.

6.8.2 Second Single Span Test

These beams were incrementally loaded and then thermally cycled after 2 weeks moist curing. As before, three cycles were applied per week.

After 16 days from the beginning of the test, the heating tape was removed from the upper surface of the beams and applied to the soffit surface. As before, the tape was held in place with heat resisting adhesive tape, covered with aluminium foil and insulated with expanded polystyrene sheet. Thermal cycling then continued, still with maximum temperature differences of approximately 13.5 ^{0}C, but with the maximum temperature occurring at the soffit. The duration of the test was 4 weeks.

Demec readings and temperatures were recorded every 2 hours during the heating phase.

6.8.3 Third Single Span Test

These beams were loaded and thermally cycled after 2 weeks moist curing. The loading operation was performed incrementally, with Demec readings being recorded after the application of each hanger weight. Thermal cycling continued for just over 6 weeks. For this, and the remaining tests, the heating was applied on each week day.

Demec readings and temperatures were recorded every 2 hours during the heating period.

6.8.4 Deep Beam Test

These beams were tested in the same manner as the third single span set of beams, with the exception that heating was also applied to the soffits of beams. The latter was done to provide the 'tail' of the temperature profile, which occurs in deep beams.

6.8.5 T-Section Beam Test

As already mentioned, only one T-section beam was produced and this was thermally cycled initially with no applied bending moment.

Following 2 weeks moist curing, the beam was placed in the end-support stands, with no loading arms or upper beam present. Thermal cycling commenced on the day after loading and continued for 18 days. At the end of this initial period, the loading gear and upper beam were installed. The upper beam was left over from a previous single span test and was present only to complete the loading arrangement. Loading was performed incrementally. With the full load applied, a major crack was identified and the crack gauge attached. The pads of the gauge were fixed to the surface of the soffit, on either side of the crack, using epoxy resin. Thermal cycling recommenced on the 20th day.

6.8.6 First Two Span Test

These beams were loaded after 2 weeks moist curing. Loading was performed incrementally, with central restraint load cell readings being taken after each increment of load. Heating commenced on the following day, but the test had to be abandoned after a week due to unforeseen circumstances.

6.8.7 Second Two Span Test

This was a repeat of the previous test which was prematurely

abandoned.

6.8.8 Third Two Span Test

These beams were tested in the same manner as the previous two span beams, but with greater applied moments.

6.9 Creep Tests

It was necessary to derive the specific thermal creep curve for use in the computer analysis, described in Chapter IV. Two separate tests were performed for this purpose, both of which involved compression testing.

6.9.1 First Test

A test was performed on a concrete cylinder which was of 100 mm diameter, 300 mm in length and of the same composition as the test beams. A thermocouple was cast into the specimen. Following curing in water for 10 days, the cylinder was allowed to surface dry before sealing with the epoxy resin. Three sets of Demec studs were attached axially and the specimen was loaded at an age of 14 days.

The loading rig comprised of three parallel tension bars, between a pair of end plates. The end plates thus applied a compressive force to the concrete cylinder and a steel cylinder in series. The latter was equipped with Demec studs in order to act as a load cell.

A stress of 7.9 N/mm^2 was applied to the cylinder by tightening nuts on the tension bars. These required adjustment throughout the test, due to the creep-induced length reduction of the specimen.

6.9.2 Second Test

The second test was performed to assess the relative magnitudes of drying and basic creep. Three cylinders were used, each of 60 mm

diameter and 200 mm in length. All three were cast at the same time and one was sealed. They were equipped with thermocouples and Demec studs.

For this test, a pair of weights-and-levers creep rigs were used. One sealed cylinder and one unsealed cylinder were loaded. The applied stress was 8.1 N/mm^2. The third unsealed cylinder was not loaded and was thus used to observe shrinkage.

CHAPTER VII

RESULTS AND DISCUSSION OF SHORT-TERM BEAM RESPONSE

7.1 Introduction

This chapter will deal with the response of beams to daily thermal cycles, during the main tests, involving both single span and two span beams. The single span beams were tested with a number of objectives in mind. The first objective was to investigate the effect of load, and thus the extent of cracking, on daily thermal strains. Tests included the measurement of changes in crack width during heating. A second objective was to determine whether creep affected the thermal response, despite the relatively short time scales involved. Creep arises from the externally applied load, the internally generated thermal stresses and, in the two span tests, from secondary thermal stresses. The intention was then to assess the suitability of a linear elastic analysis for the prediction of thermal strains. Investigations were extended to tests on two span beams, where support reactions were measured during daily heating cycles. The effect of different loads was also observed, with regard to the presence of cracking.

The chapter will begin with a brief discussion of the loading up of the beams, prior to thermal testing. Thermally induced strains will then be examined, first with reference to some typical observations taken from beams during a heating cycle. Typical results of thermally induced changes in support reaction in two span beams will be examined also. Daily thermal strains were compared with predictions, based on the SACRAK analysis, described in Chapter IV. For two span beams, measured changes in support reactions, during

heating, were compared with predicted values. Lastly, the ratios of experimental to calculated results are presented and discussed. The presentation of results as ratios permitted direct comparison of strains or changes in support reactions in beams under different temperature profiles.

7.2 Initial Beam Loading

The single span beams were loaded incrementally and Demec readings were taken after each increment of load. These loads were chosen to represent self-weight plus imposed loading. In total, the beams carried up to 56 % of the CP110 ultimate moment. The loading curves are shown in graphs 15 to 18. The presence of cracking is apparent from the non-linearily in the curves for all tests, this being most severe for the T-section beam. The initial loading curve for the first single span test was not derived, since only a light load was applied.

For the two span tests, the changes in support reactions which occurred during incremental loading are shown in graphs 19 to 21. The theoretical response is indicated also on these graphs. Clearly, the measured support reactions were smaller than the predicted values and this was caused by some differential movement of supports, during the initial load increment. The reductions in reaction correspond to differential support movements of less than 1 mm. So, the self-weight of the loading arms was an effective holding load, which was sufficient to settle any minor differential movements. When subsequent increments of load were applied, the rate of increase of support reaction with applied load was as predicted by simple slope deflection analysis.

7.3 Typical Results of Thermal Response

During each day of testing, temperature profiles and strains were measured. For the two span tests, changes in support reaction were measured. These results cannot be presented individually as there are too many for inclusion. They were however all used in the determinations of observed to computed ratio results which will be discussed later. Some example results will first be presented.

In addition to the observed strains, predicted strains will be presented. These were obtained, using the program SACRAK, taking the measured temperature profiles as input data. The predictions were based on analysis of the uncracked section. For the two span tests, predicted changes in support reactions will be plotted with the observed values. The predicted values were obtained by calculating the free thermal curvature, as for the single span tests, and then calculating the reaction required to restrain the resulting vertical deflection at the central support. These results also were derived from an uncracked section analysis. It is emphasised that these are example results and the more general conclusions will be drawn from the ratio results which follow in section 7.4.

7.3.1 Single Span Tests

Graphs 22 and 23 show daily results from the non-loaded beam of the third single span test. Graph 23 indicates a relatively rapid development of thermally induced curvature and a slower axial expansion. It can be seen also that an initial small compression strain occurred in the lower fibres. Both effects were caused by early thermal force in the top surface zone only. From the results presented, the maximum thermal curvature, occurring after

approximately 4 hours, was 0.76×10^{-6} mm^{-1}. The maximum axial expansion was 134 $\mu\varepsilon$.

Results from a loaded beam of the same test are presented in graphs 24 and 25. It can be seen that, although the beam was cracked, its thermal response was similar to that of the non-loaded beam. In fact, as will be demonstrated in section 8.4, thermal response of all loaded beams was similar to that of non-loaded beams, except for the first few days after loading.

A typical set of results from the 400 mm deep beam tests is shown in graphs 26 and 27. These results were taken from a non-loaded beam, but they are representative of loaded beam results. The increase in soffit temperatures is shown and it is clear that the temperature profiles show a greater degree of non-linearity than those from the shallow beams, in agreement with the results of Emerson. The thermal curvature increased throughout the period of heating. The maximum value indicated on the graph is 0.40×10^{-6} mm^{-1}, concurrent with the maximum axial expansion of 116 $\mu\varepsilon$.

A typical set of results from the T-section beam test is shown in graphs 28 and 29. The maximum thermal curvature shown is 0.84×10^{-6} mm^{-1} and the maximum axial expansion is 161 $\mu\varepsilon$. It can be seen that the temperature profile after 8 hours of heating closely resembled the 8 hour profile from the 200 mm deep, rectangular section beam test, shown in graph 22. However, the T-section beam produced a greater thermal curvature and axial strain. This was due, in part, to the fact that the upper fibres of the T-section beam were able to contribute a greater thermal force, for a given temperature rise, as a result of the increased member width. Also, the overall temperature

rise in the web of the T-section beam was less than that in the rectangular section beam, due to the absence of thermal insulation to the web, resulting in larger thermal curvatures.

A two-dimensional temperature variation occurred in the T-section beam because of variable member width and the absence of thermal insulation from the flange soffit and the web sides. The pattern of temperature increase was monitored by means of additional thermocouples. The locations of the thermocouples are shown in figure 12.

The transverse temperature differences measured in the web were not large. At a height of 10 mm from the soffit, the temperature difference after 2 hours was 0.2 ^{0}C, rising to 0.4 ^{0}C after 4 hours. At 100 mm from the soffit, the differences were 0.3 ^{0}C and 0.5 ^{0}C.
The thermocouples referred to were at distances of between 10 mm and 50 mm from the vertical surface of the web. It is likely that a more severe transverse temperature gradient existed within the 10 mm from the surface.

Larger differences were measured in the flange, at a vertical distance of 10 mm from the flange soffit. The thermocouples were located at distances of 0 mm, 50 mm and 140 mm from the centre of the beam. Typical temperature differences were as follows.

	Temperature / ^{0}C		
Time	(0 mm)	(50 mm)	(140 mm)
2 Hours	11.6	10.1	9.8
4 Hours	13.5	12.1	11.6

Thus, transverse temperature differences of up to 2 ^{0}C occurred in the flange.

The predicted T-section beam strains, indicated by the broken lines on the graph 29, show good agreement with the observed values. This is despite the fact that the analysis assumed that temperature was constant in the horizontal plane. Further strain predictions, to be presented later, confirmed that it was reasonable to rely upon the uniform transverse temperature assumption. Of greatest influence to strains were the temperature increases near the top of the flange. Here, the transverse temperature differences would not have been large.

7.3.2 Crack Gauge Results

The crack gauge was attached to the soffit of the T-section beam, across a crack which had been initiated by the mechanically imposed loading. Readings from the gauge were taken, at the same time as Demec readings, during the daily heating cycles. Results from a week of testing are presented below.

Duration of heating	4 Hours		8 Hours	
Test Day	ε_{CG}	ε_{D}	ε_{CG}	ε_{D}
41	2	28 $\mu\varepsilon$	22	53 $\mu\varepsilon$
42	2	24	28	69
43	24	22	53	61
44	30	37	47	49
45	26	16	55	61

ε_{CG} - Crack Gauge Strain ; ε_{D} - Demec Gauge Strain

On occasions when a crack gauge reading was taken after 1 hour of heating, compressive strains of up to -20 $\mu\varepsilon$ were recorded.

Considering the small strains involved, the crack gauge and Demec strains are comparable. The measured strains are also

comparable with the typical results, presented in graph 29. This indicates that the presence of a crack did not substantially affect thermal strains. It can be seen however that, on most occasions, the crack gauge strains were not as large as the Demec gauge strains. It is difficult to generalise about the effect of cracking on strains at the soffit. Although increased cracking may increase the thermally induced axial strains, the effect on soffit strains is countered by larger thermal curvatures. The relative magnitudes of these two effects depend on the particular temperature profile considered and the member geometry. Most of the results presented suggest that the increased curvature effect predominated.

The crack gauge could not be used to obtain results during the initial loading of the beam, as the gauge could be attached only after the identification of a crack. However, an assessment of the performance of the gauge was possible at the end of the testing period. This involved taking measurements during the incremental unloading and reloading of the beam. The results are shown in graph 30. In addition to the crack gauge results, Demec gauge results are shown also. These were taken from the Demec gauge lengths which straddled the crack gauge. Also shown are the theoretical results for the uncracked and fully cracked sections. Whilst the Demec results show closest agreement with the uncracked prediction, the crack gauge results are in very close agreement with the fully cracked prediction. These results indicate that the crack gauge was operating satisfactorily.

The strain changes from crack gauge taken during the unloading of the beam may be contrasted with the results from the gauge during a

heating cycle. The maximum change in the crack gauge strain, occurring during the heating cycle, was 55 $\mu\epsilon$. Extrapolation of the unloading results to zero load produces a crack gauge strain change of approximately 1200 $\mu\epsilon$, which corresponds to a crack width of approximately 0.025 mm.

It may be concluded then that heating resulted in only minor changes in crack width. The maximum change observed was less than 5 %.

7.3.3 Two Span Tests

An example of the daily thermal response, taken from the loaded beam of the second two span test, is shown in graphs 31 and 32. Similar results were observed in the first test. Results from the third test are shown in graphs 33 and 34.

The plots of temperature are similar to those derived from the single span tests. The measured central support reactions show a relatively rapid decrease during the first 2 hours of heating, with little change after 4 hours. The results from the second test show the greatest initial rate of decrease in the central support reaction. This was due, in part, to a slightly greater rate of top surface temperature increase, as is apparent from the temperature plots.

For both sets of results, the temperature difference profiles after 8 hours are similar, the maximum difference between upper and soffit surfaces being approximately 14 ^{0}C. However, the change in support reaction in the second test is some 14 % greater than that observed in the third test. Both temperature profiles give rise to similar free curvatures, so a difference in the flexural stiffnesses of the beams is implied. A companion specimen in the second test

produced an elastic modulus result of 25.0 kN/mm^2, whereas a value of 27.5 kN/mm^2 was measured for the third test. However, in the third test, the theoretical cracking moment was deliberately exceeded, over certain sections of the beam, thus reducing the overall flexural stiffness of the beam. A reduction in flexural stiffness leads to reduced restraint reaction for a given temperature profile.

The theoretical response of the beams is indicated also on the graphs. It is clear that the level of agreement is best for the results from the second two span test. The beam from the third test was cracked and therefore did not provide the change in reaction predicted by the uncracked analysis. An improved analysis will be described later.

The effect of the heating was to increase the total reactions at the end supports and decrease those at the centre support. For the first and second tests, the maximum thermally induced changes in the central reaction were around 2.5 kN, as indicated by graph 32. This corresponds to a 37 % reduction in the central reaction. The third set of beams, which carried a greater mechanical load, were of reduced overall flexural stiffness, due to the presence of cracking. Here, the imposition of temperature profiles caused a reduction in the central support reaction of around 10 %. As stated, the end support reactions increased during heating. The increase was some 64 % in the case of the first and second tests and 19 % in the case of the third test. The latter carried the highest mechanical load.

These changes in the support reactions, during heating, led to bending moment changes, the maximum changes occurring at the central restraint. For the first and second tests, the change was

approximately 2.46 kNm, around 20 % of the CP110 ultimate moment. This value slightly exceeded the mechanically induced moment, which was in the opposite sense. Thus, an initial central hogging curvature became a slightly sagging curvature, upon heating. For the third set of beams, where the loading was higher, the initial hogging curvature was reduced by approximately 36 %, during heating.

Since, at the central support, thermal moments were in the opposite sense to applied load moments, heating reduced the stresses in the beam. The thermally induced moment of 2.46 kNm, mentioned above, corresponds to a change in the soffit stress of $-2.9\ N/mm^2$, but the stress resulting from the applied mechanical load was $2.5\ N/mm^2$. At 580 mm from the centre of the beam, where the applied load induced moment was zero, a thermally induced stress of $-1.7\ N/mm^2$ occurred at the soffit. These stresses are considerably larger than the self-equilibrating stresses which will be discussed in section 8.5.

7.4 Ratios of Measured to Predicted Thermal Response

The results from the daily thermal cycles are presented as ratios of experimentally observed curvatures and axial strains to those predicted by the computer program SACRAK. Thus, in cases where the prediction and observation agreed, the ratio is one. The ratios are plotted against a time axis in order to identify long-term variations.

The experimental axial strains and curvatures presented are the average values for the gauged sections of the beams. The temperatures, which were measured at the same time as the strains, were supplied to SACRAK to arrive at the predicted strains. Thus, each point on the plots relies on a minimum of five temperature

readings and eight Demec readings.

The elastic moduli used in the predictions were those obtained from the compression tests on companion specimens. The coefficients of thermal expansion measured on cylindrical companion specimens were unreliable, so a value of 11 $\mu\varepsilon/^{0}C$ was assumed throughout.

For tests in which the cracking moment was exceeded, graphs of curvature ratios are presented for both the uncracked and fully cracked section computer analyses. The sensitivity study, mentioned in Chapter IV, demonstrated that cracking had a negligible influence on axial strains. Therefore, axial strain ratios for the fully cracked section analysis are not presented. The cracked section analyses were not performed for the period during which the soffit of the second single span test beam was heated. Since the fully cracked section analysis assumed no concrete in the tension zone, there was, in theory, no surface to heat. Also, a very poor level of agreement with experimental results was obtained by considering the temperatures in the compression zone of the beam only.

Shown on the graphs are least squares fit regression lines. It is not suggested that the ratios are in fact a linear function of time, but the lines do give an indication of long-term variations in the ratios. Also, with the amount of scatter present in the results, more sophisticated curve fitting was not warranted. There were however certain results for which the regression lines were not appropriate. These will be discussed later.

An indication of the amount of scatter is given by the two parallel lines which lie on either side of the regression line. These are one unit of standard deviation above and below the regression line

and thus contain approximately two thirds of the points, assuming normal distribution.

7.4.1 Non-Loaded Beams

An inspection of both the axial strain and curvature ratio plots for the non-loaded beams, in graphs 35 to 46, indicates that the computer predictions yielded reasonable agreement with the observed values.

Ideally, the regression lines should lie on the lines of unity ratio on the plots. However, it is clear that the intercepts of the regression lines do not generally occur at unity and the lines are not horizontal. Possible explanations of these two features will be discussed. Attention is drawn to the sensitivity study described in Chapter IV, where it was shown that the strains predicted by the program SACRAK were particularly sensitive to the assumed value of the coefficient of thermal expansion of concrete.

Consider first the regression line intercepts for the axial strain results from the non-loaded beams, shown in graphs 35 to 40. These are dependent on the values of the coefficient of thermal expansion for concrete assumed in the analysis. In most instances, the intercepts lie below unity, but consideration of a slightly decreased coefficient in the analysis would cause the intercepts to occur at unity. This adjustment was not made as it was not acceptable to use the observed results as a means of calculating the predictions.

Consider next the gradients of the regression lines. Since these are non-zero and generally positive, a variation in material properties, during the course of the testing period, is implied. The sensitivity study demonstrated that variations in the coefficient of

thermal expansion had an appreciable effect on the predicted axial strains. Take, for example, the axial strain ratios from the non-loaded beam of the second single span test. The regression line suggests an increase in the ratio of some 13 %, over the course of the 47 day testing period. This may be explained in terms of a 15.5 % increase in the coefficient of thermal expansion of concrete.

It appears then that the coefficient of thermal expansion of concrete increased during the test period. It was mentioned, in section 3.4.1.4, that no conclusive evidence regarding the effect of age on the coefficient had been found. However, it is known that moisture content influences the value of the coefficient. When a saturated specimen loses moisture, the coefficient increases and reaches a maximum value at some intermediate stage of drying. It may be recalled that an increase of some 20 %, occurring at a humidity of 70 % r.h., was observed by one worker. It is suggested therefore that the beams involved in the present tests experienced increases in their thermal coefficients as a consequence of reduced internal humidities.

Evidence that moisture loss was causing the increase in the coefficient is provided by the gradient of the regression line from the deep beam axial strain results. It may be seen that the gradient of this line is smaller than the others, implying a reduced rate of increase in the coefficient of thermal expansion. This would follow from the increased average drying path length of the beam. It may be seen also that the results from the non-loaded T-section beam provided the largest gradient. This beam had the shortest average drying path length.

Now consider the curvature ratio results from the non-loaded

beams. These are shown in graphs 41 to 46. The intercepts from these results are in line with those derived from the axial strain ratios. Furthermore, the regression lines have positive gradients, indicating increases in the coefficients of thermal expansion over the test periods. However, the gradients do not compare well with those from the axial strain ratios. It is probable that non-uniform drying is the cause of this discrepancy.

Consider, for example, an initially saturated, partially sealed beam within which there exists a uniform coefficient of thermal expansion. The soffit surface is exposed and so a moisture content profile develops. This, in turn, leads to a variation in the thermal coefficient within the member, such that the coefficient increases with depth. Now consider the effect of a positive temperature profile on the beam. Compare the thermally induced axial strains and curvatures of the partially dry beam with those of the saturated beam. Since the overall coefficient of thermal expansion has increased, the thermally induced axial strains are larger than before. However, the thermally induced curvatures do not increase to the same degree and may even decrease. This follows from the fact that, as temperature decreases with depth, the thermal coefficient increases. The effect of this is to reduce the overall gradient of the free thermal strain profile.

The response of the actual test beams was further complicated by the fact that two drying regions developed. However, it can be said that whenever an asymmetric thermal coefficient profile develops, the rate of increase of thermally induced axial strains is not the same as the rate of increase of thermal curvatures.

With the exception of the non-loaded beams from the second two span test, the regression lines for the shallow beam results show shallower gradients for the curvature ratios than for the axial strain ratios. The implication is then that non-uniform coefficient of thermal expansion profiles developed, with the lower fibres experiencing the greatest increases in the coefficient. The basis for this was a moisture content profile, where the greatest moisture loss was from the lower fibres. The non-loaded deep beams deviate from this behaviour and so does the T-section beam. However, in the case of the latter, the deviation is to be expected. The flange surface was heated and the flange soffit was exposed, thus permitting appreciable moisture loss from the upper fibres of the beam. An accompanying increase in the coefficient of thermal expansion in these fibres would thus occur.

So to conclude, an accurate knowledge of the coefficient of thermal expansion is required in order to predict thermal response of beams. The value of the coefficient varies, according to moisture content, so the use of an upper value is safest for the purposes of design.

7.4.2 Loaded Single Span Beams

7.4.2.1 Axial Strain Ratios

As with the non-loaded beams, the predicted and observed results are in fair agreement. The regression lines through the ratios, presented in graphs 47 to 50, show positive slopes, as was seen with the axial strain ratios from the non-loaded beams. A positive slope is shown also for the loaded phase of the T-section beam test, presented in graph 38. Although there are differences in detail

between the non-loaded and loaded beam results, there are common features. For instance, the regression line from the deep beam results has the smallest gradient and the loaded phase of the T-section beam test continued to produce a relatively high rate of increase of the ratios.

The loaded beam results from the third single span test produced the regression line with the steepest gradient, which was not expected. The proposed explanation of the upward trend is, as already described, the increase in the coefficient of thermal expansion of concrete as a result of moisture loss. It follows then that the steepest gradient would have been expected from the T-section beam, with its shorter average drying path length. The reason for this inconsistency is not clear, but it may have been due to differences in initial w/c ratios or ambient relative humidities.

Finally, attention is drawn to the fact that, part way through the first single span test and the T-section beam test, the applied load was increased, in order to compare uncracked with cracked beam response. The axial strain ratios, presented on graphs 47 and 38, show no clear deviation from the general trend as a result of these load increases. Firstly, this suggests that the rig was offering no restraint to thermal expansion, as any such restraint might have been expected to have increased under the heavier loading. Secondly, is it possible to compare the axial strain results before the cracking moment was exceeded with those after. The results show that the extent of cracking had no appreciable effect on thermally induced axial strains. This confirms the findings of the sensitivity study, described in section 4.7.3, where cracking was also found to have had

a negligible effect on axial strains.

7.4.2.2 Curvature Ratios

In consideration of curvature ratios, two sets of results are plotted. In the first set, the analysis assumes an uncracked section, whilst a fully cracked section is assumed in the second. In fact, it is clear, from the results presented in graphs 51 to 59, that the uncracked analysis was the most successful, producing ratios nearer to unity. Therefore, the discussion will concentrate initially on the results from the uncracked analyses.

Unlike the results from the non-loaded beams, these results were affected by creep. Whilst the beams were undergoing diurnal thermally induced hogging curvatures, creep was causing sagging. Thus, the observed beam curvatures were, to some extent, reduced. The feature is apparent in the curvature ratios from the T-section beam test, presented in graph 44. The plot shows a reduction in the ratios, immediately following the application of the load. The reduction affects the 8 hour results the most, as these allowed the greatest time for the development of creep. Reduced ratios are evident also in the results from the third single span test, presented in graph 53. Both graphs indicate that creep ceased to have any significant influence on ratios beyond the first week of loading.

The curvature ratios from the first single span test do not show these reductions, which is not surprising. The initial loading was light and was not applied until 4 weeks after casting. The second load increment was applied at an even greater age. It is surprising though that the deep beam did not show greater curvature reductions. Only on the first day of cycling were there any reductions and these

were relatively small.

It is possible to compare the reduced ratios with the reductions implied by the long-term results. For this purpose, the total changes in curvature, occurring during the first day of heating, were taken from the long-term results. These long-term results will be discussed in greater detail in the next chapter. As a first approximation, the results were multiplied by one third to arrive at an estimate for the end of the 8 hour period. These curvatures are presented in the table below, expressed as a percentage of the average thermally induced curvatures. They are therefore estimates of the percentage reductions in the curvature ratios. The values in brackets are the percentage reductions taken from the graphs. They represent the differences between the mean ratio, as defined by the regression line, and the measured 8 hour ratio for the first day of heating.

Percentage Reduction in Curvature Ratio :

First Single Span Test	5 %	(0) %
Second Single Span Test	18	(25)
Third Single Span Test	33	(14)
Deep Beam Test	22	(12)
T-Section Beam Test	21	(36)

The level of agreement between the two sets of results is poor, but they are of the same order. It must be borne in mind that the plotted ratio results show appreciable scatter, the average standard deviation being some 8.4 % of the mean. The conclusion is that early age daily curvature reductions can be ascribed to primary creep.

Besides these variations in the early curvature ratios resulting from primary creep, most of the remaining results produced regression

lines with positive gradients. These upward trends may have been due, in part, to the declining influence of creep. However, the feature is attributed primarily to an increase in the coefficient of thermal expansion, caused by the drying of concrete. The exception is the first single span test where the gradient is small but negative. A possible explanation for a negative gradient was described in section 7.4.1. It may be recalled that this involved an asymmetric coefficient of thermal expansion profile.

Graph 52 shows the curvature ratios for the second single span test. After the first two weeks of heating, the heating tape was transferred to the soffit of the beam and heating was continued. With the cracked surface heated, no reduction in the accuracy of the prediction method occurred. The prediction assumed an uncracked section.

The most important fact to have emerged from the results is that the uncracked analysis adequately predicted the thermal curvatures of both the uncracked and moderately cracked beams. The fully cracked analysis provided overestimates of curvatures. As with the non-loaded beam results, the regression lines, derived from the uncracked analysis, did not quite pass through the curvature ratio of one, but this is attributed to the choice of the coefficient of thermal expansion of concrete used in the analysis. However, the prediction cannot be relied upon during the first few days after loading when primary creep affects the results.

7.4.3 Loaded Two Span Beams

As before, ratios of observed to calculated axial strains are presented. These are plotted in graphs 60 and 61, and show the same

trends as were seen with the other axial strain ratio results. However, the most important results are the ratios of observed to calculated changes in the central support reaction, during the thermal cycle.

The calculated reactions were arrived at by first estimating the free thermal curvatures of the beams, in the absence of the central restraint, and then calculating the reactions necessary to prevent the resulting central deflections. The free thermal curvatures were computed from the measured temperature profiles, using the program SACRAK. It was shown earlier that the uncracked thermal analysis produced satisfactory estimates of strains for both uncracked and cracked beams. Thus, the uncracked analysis was used to predict free thermal curvatures for all two span tests. The restraint reactions were calculated also, in the first instance, by assuming uncracked section flexural stiffness.

The thermally induced changes in central support reactions were compared with the changes in reaction at the end support. Ideally, the ratio of these reactions should have been 2.0, because of symmetry.

7.4.3.1 Ratios of Measured to Predicted Support Reactions

The ratios of measured to predicted changes in the central support reaction are shown in graphs 62 and 63. Testing of the first two span beam was maintained for one week only and the results for this test are tabulated in Appendix II.

The results from the first and second two span tests show reasonable agreement between predictions and observations. In both cases, the 8 hour ratios for the first day of heating were reduced.

These reductions were the result of primary creep relaxation of thermally induced secondary stresses. The ratios from the third, partially cracked beam test are consistently lower and this will be discussed later, but again the ratios for the first day are reduced in comparison with later values. This is attributed also to creep relaxation.

The regression lines for the tests have positive gradients and this may be attributed to the increase in the coefficient of thermal expansion. However, the declining influence of creep relaxation may also have had a contributory effect. Additionally, the elastic modulus increased with age, so that similar thermal curvatures caused increased restraint reaction changes. For both the second and third two span tests, the increase in the modulus, taken from companion specimens, suggests an increase in beam flexural stiffness of approximately 5.5 %, over the course of testing. This increase cannot account fully for the increase in the reaction ratios, especially in the case of the third test where the increase was some 18 %. Thus, the increase in the coefficient of thermal expansion was of importance also.

The most important feature of the results from the third two span test is that the reaction ratios are consistently low, with the intercept occurring at a ratio of 0.742. This arises from the fact that the cracking moment was exceeded over certain sections of the beam. Therefore, the uncracked section assumed in the analysis overestimated the flexural stiffness of the test beam. Although it was demonstrated that the uncracked thermal analysis yielded acceptable predictions of strains in single span tests, the uncracked

section was not appropriate for the prediction of restraint reactions.

In order to improve the prediction method, the analysis for the third two span beam was repeated for a partially cracked beam. For the lengths of the beam where the cracking moment was not exceeded, the uncracked flexural stiffness was assumed. For the remainder of the beam, a partially cracked stiffness was calculated using the method described by Clark and Spiers (135). The restraint reactions were then determined, for a beam of varying flexural stiffness, using the area-moment method.

It was not necessary to recalculate the ratios individually, as each was increased by the same factor. The effect was a shift of the regression line to the new position, as indicated on graph 63. Clearly, this gives improved agreement over the previous method of analysis, but the result is an underestimate of reactions. The implication is that the prediction assumed too small a value for the cracked flexural stiffness. The value taken was $11x10^{11}$ Nmm^2, whereas a value of $12x10^{11}$ Nmm^2 would have been required to have caused the intercept to occur at a ratio of one. The values for the uncracked and fully cracked sections are $20x10^{11}$ Nmm^2 and $8x10^{11}$ Nmm^2 respectively.

7.4.3.2 Ratios of Central Support to End Support Reactions

Graphs 64 and 65 show the ratios of measured central to end support reactions. Ideally, the ratio should have been two, but most of the ratios plotted are slightly in excess of two. It is possible that axial expansion of the beams caused the discrepancy. This seems likely in view of the results from the third two span test, where the 8 hour ratios are greater than the 4 hour ratios. The additional

axial expansion at the 8 hour stage may have affected the results by the application of shear force to the end support. There are a number of other possible explanations, such as warping of the beams or the absence of temperature compensation to the end support load cell. However, the discrepancies resulted in an average error of only 10 %.

7.5 Self-Equilibrating Stresses

Self-equilibrating stresses cannot be measured directly, so the computer program SACRAK was used to provide estimates. A uniform coefficient of thermal expansion, of 11 $\mu\varepsilon/^0C$, was assumed. For all uncracked, 200 mm deep beams, maximum compressive self-equilibrating stresses were approximately 0.45 N/mm^2. They occurred at the top surfaces of beams. Maximum tensile self-equilibrating stresses were approximately -0.35 N/mm^2. Larger stresses were present in the deep beams as a result of an increased degree of non-linearity in the temperature profiles. Maximum compressive and tensile stresses were around 1.59 N/mm^2 and -0.44 N/mm^2 respectively. Reduced stresses were calculated in cracked beams, due to the reduction in internal restraint, although the reductions in tensile stresses were slight.

The program TCREEP was used to assess the influence of creep relaxation on thermally induced self-equilibrating stresses. It may be recalled that TCREEP uses the average rate of development of specific thermal creep for the day under consideration. Calculations were performed for the first day of testing and for 30 days from the beginning of the test.

In all cases, the creep relaxation of self-equilibrating stresses was found to have a very small influence on strains. For the first day of a shallow beam test, for example, the change in axial

strain due to creep was 0.3 $\mu\varepsilon$ and the change in curvature was 0.6×10^{-9} mm^{-1}. The effect on stresses was also very small. The maximum stress relaxation was less than 2 % for both tensile and compressive stresses.

These results confirmed that the influence of creep was very small because of the relatively short time-scale involved. Peak stresses existed for a few hours only, allowing little time for the development of creep. This was not the case for the constant, and much greater, applied load induced stresses. It is recognised however that greater than predicted creep relaxation could have occurred during the first day of heating, under the influence of transitional thermal creep.

To conclude, predictions of self-equilibrating stresses were small and, since peak stresses did not exist for long, creep relaxation of self-equilibrating stresses was negligible.

7.6 Concluding Remarks

7.6.1 Single Span Beams

The assumption of an uncracked section provided the closest predictions of thermal curvatures for the single span beams. The fully cracked section analysis provided consistent overestimates of curvatures.

It may appear preferable to consider some form of partially cracked section, but there are a number of arguments against it. The sensitivity study demonstrated that the difference between thermal curvatures of the uncracked and fully cracked sections was only 8 %. Consideration of a partially cracked section, under moderate load, would therefore produce results which were not greatly different from

the uncracked analysis. Also, a difficulty exists in the formulation of a partially cracked section for thermal response. For the restraint of mechanical loads, cracking influences the flexural stiffness. For thermal response, the extent of cracking not only influences the amount of internal restraint, but it also affects the amount of concrete which is able to contribute a thermal force. Thus, conventional methods of tension stiffening, such as that developed by Clark and Spiers, are not appropriate.

Consideration of anything other than an uncracked section becomes problematical when the tension surface is heated. The fully cracked section, for instance, assumes no concrete below the plane of the neutral axis. There is then, in theory, no surface to heat and no concrete through which to transmit the heat in the tension region. Also, as mentioned, thermal calculations, based on the compression zone only, provide very large errors.

The ratios of observed to predicted axial strains and curvatures show up a number of features. Firstly, the curvature predictions gave large errors, during the early stages of mechanical loading, due to the influence of creep. In the majority of single span tests, sagging creep curvatures operated in the opposite sense to thermal curvature. Heating of the soffit provided the exception. The influence of creep varied between tests, but it did not substantially affect the results beyond the first few days from loading.

The axial strain and curvature ratios of both non-loaded and loaded beams increased during the test period. This is attributed to the increases in the coefficient of thermal expansion, as a result of moisture loss. Further evidence of this effect was seen in the

results from the segmentation blocks. It may be recalled that an upward trend in the coefficient was observed, together with non-uniform values within a member. It was hoped originally to use the segmentation block results in order to achieve better predictions of beam response, using the program SACRAK. No significant improvement was achieved. Inconsistencies existed between the tests, probably as a result of differences in initial water content, compaction and the rate of drying.

Predictions of self-equilibrating stresses in beams were small and the calculated creep relaxation of such stresses was negligible.

7.6.2 Two Span Beams

In the two span tests, an apparent contradiction arises in the prediction of thermally induced changes in support reaction. The free thermal curvatures were predicted, assuming an uncracked section. The tests on loaded single span beams showed this to be a reasonable assumption. For the first and second two span beams, where the cracking moment was not exceeded, the predictions of restraint reaction were based on the uncracked flexural stiffness. However, in the case of the third two span test, where cracking was present, it was necessary to consider a partially cracked flexural stiffness, to calculate the restraint reactions. This is contradictory in that the same beam was assumed to be uncracked and then partially cracked. It is suggested however that this is a reasonable approach. It must be remembered that cracking does not influence thermal curvatures in the same way as it does flexural stiffness. Also, cracking is of much greater importance to flexural stiffness than it is to thermal curvature. In the previous section it was remarked that the thermal

curvature of a fully cracked 200 mm deep beam was only 8 % greater than that of an uncracked beam. However, an uncracked beam is some 2.5 times flexurally stiffer than a fully cracked beam.

The method of calculating reactions described above is reasonably straightforward. Free thermal curvatures are calculated assuming an uncracked section, whilst restraint forces are based, where appropriate, on a partially cracked section. What might appear at first sight to be a further simplification is the consideration of a partially cracked section throughout the analysis. This appears to have the additional advantage that cracking increases thermal curvatures and thus provides a more conservative estimate of the resulting restraint reactions. However, the approach yields further complications. In a continuous structure, heating will be applied to a tensile surface, which may well be cracked. As already stated, this situation is difficult to analyse since, for instance, there may be no theoretical tension surface to heat. In any event, the extent of cracking has a large effect on the value of flexural stiffness. The conservative approach is then to assume an uncracked section at all stages in the analysis.

The measured changes in reaction at the end of the first day of heating were smaller than predicted. This effect resulted from the creep relaxation of secondary thermal stresses.

Estimates of secondary thermal stresses were rather larger than self-equilibrating stresses, although they did not cause the cracking moment to be exceeded. Maximum secondary thermal stresses occurred at the central support, where maximum stresses of the opposite sign were induced by the mechanical load.

The reaction ratios increased during the course of testing. This is attributed to three possible factors. Firstly, the coefficient of thermal expansion increased, as a result of drying. Secondly, the elastic modulus increased during testing, thus increasing the flexural stiffness of the beam. Lastly, creep relaxation of reactions decreased with age. It is suggested that the latter effect was not of importance beyond the first few days of testing.

CHAPTER VIII

RESULTS AND DISCUSSION OF LONG-TERM BEAM RESPONSE

8.1 Introduction

The primary objectives of the project were concerned with the response of beams during a daily heating cycle. However, for a number of reasons, it was necessary to continue testing over a period of several weeks. As well as the daily results, this continued testing provided information on the early age creep and shrinkage response of beams.

The results which will be discussed in this chapter were recorded at the start of each day of testing, before the application of the heating. They were used to identify the long-term movements of the beams, excluding the strains resulting directly from the heating cycles.

Two factors were of primary interest. The first of these was the effect of heating on creep curvatures of beams and the second was the effect of heating on non-uniform shrinkage induced curvatures.

The chapter will begin with a discussion of the axial strains and will then go on to discuss curvatures. Where appropriate, the experimental results will be compared with predictions from codes and the results from the program CREEP.

8.2 Axial Strains

8.2.1 Results of Axial Strains

A typical plot of the long-term shrinkage strains of test beams is presented in graph 66. These results were taken from the four beams of the third single span test. It can be seen that, as expected, the heated beams experienced greater axial shrinkage than

did the non-heated beams. One might have expected also to find similar shrinkage curves for beams tested under similar thermal conditions. Indeed, the heated beam results are almost coincident. However, a significant discrepancy exists between the results from the beams which were not heated and such discrepancies were found throughout the entire series of tests.

A comparison of the 30 day axial shrinkage results of all the beams tested is presented in Appendix III. The results show considerable variations, although the increased shrinkage of heated beams is evident.

The results are condensed in the table which is shown below. This gives the average axial shrinkage strains of all the beams tested. Shown also are predicted values. These will be discussed in sections 8.2.2 and 8.2.3.

30 Day Average Axial Strains :

	Experimental	ACI	CEB-FIP	BS8110 (6 months)	Computed
Shallow Beams	88/101 $\mu\varepsilon$	111	21	45	94/146
Deep Beams	26/29	20	11		
T-Section Beam	-/202	167	69	189	

(Non-heated/Heated)

The axial shrinkages from the first single span test were smaller than those of the other beams of similar cross-section. It may be recalled however that these beams were cured for a longer period before testing commenced. The reduced shrinkage rate is therefore attributed to a reduction in the moisture diffusion coefficient with time, as a consequence of increased hydration. The

test which was described in section 5.5.1.2, involving shrinkage of specimens cured for different periods, confirmed this effect.

The remaining discrepancies among the 200 mm deep beam results were caused by environmental and intrinsic factors. Variations in humidity and temperature were recorded in the laboratory. For example, humidities in the range 38 % r.h. to 65 % r.h. were measured and, according to Evans and Kong (126), a decrease of 1 % r.h can cause a 2 % increase in shrinkage. Furthermore, the laboratory temperature could fall as low as 16 ^{0}C. However, significant variations in ambient conditions did not prevail for long and so their effects would have been diminished.

As far as intrinsic factors were concerned, small differences in initial moisture content, resulting from variability in aggregate saturation, would have affected the diffusion of moisture and thus shrinkage, as was mentioned in section 3.5.2, with higher w/c ratios resulting in more rapid shrinkage. Also, the aggregate used was not from a single batch and so minor variations in quality and grading would have occurred also. As was mentioned in section 3.7.4.1, reduced aggregate stiffness leads to greater shrinkage.

Considering next the deep beam and T-section beam results, the influence of the drying path lengths on the progress of shrinkage is evident. In the case of the non-loaded deep beams, the non-heated beam appears to have undergone slightly greater shrinkage than the heated beam. For these beams, relatively large temperature corrections were necessary, which might have reduced the experimental accuracy. This will be mentioned again in the context of observed curvatures.

In all of the tests undertaken, the shrinkage strains at the end of the test periods were far below the estimated ultimate values. An earlier test, described in section 5.5, provided an ultimate concrete shrinkage of 600 $\mu\epsilon$. This result was obtained from small specimens and so a slightly reduced value would be expected for the larger test beams. The influence of size and shape on ultimate shrinkage was described in section 3.7.4.3. However, taking the 600 $\mu\epsilon$ and allowing for the restraining effect of the reinforcement, ultimate beam shrinkages of around 375 $\mu\epsilon$ would be expected for the shallow beams and slightly greater shrinkages for the deep beams and T-section beam. This is clearly in excess of the 30 day values observed in the test beams.

8.2.2 Comparison with Predictions from Codes

The three prediction methods mentioned in section 3.7.6 were used in a comparison with the experimental data. For the ACI and CEB-FIP methods, the 30 days shrinkage strains were calculated, but BS8110 provided only a 6 month and a 30 year estimate. Thus, the BS8110 estimates quoted are the 6 month values. Also, BS8110 does not allow for effective thicknesses in excess of 600 mm, so that an estimate for the deep beam was not possible.

The CEB-FIP code permits the consideration of elevated temperatures, with the use of a corrected age. This had the effect of an additional 3 days shrinkage, in comparison with the non-heated beam estimate, at 30 days. However, the effect on calculated strains was negligible.

The calculated concrete strains were adjusted for the restraining influence of the reinforcement, in accordance with Hobbs

and Parrott (124), by multiplication by the factor $1/(1+25\rho)$, where ρ is the reinforcement proportion. These results are given in Appendix III.

Considering the shallow beams, the discrepancies among the three prediction methods are enormous. Clearly, the ACI approach yields the closest agreement with the observed shrinkage results. This method also predicts an ultimate concrete shrinkage strain of 640 $\mu\varepsilon$, which is in good agreement with the ultimate strains observed on companion specimens. Attention is drawn to the ultimate shrinkage indicated in graph 8. It is evident also that the ACI approach produced the closest predictions of shrinkage for the deep beams and the T-section beam.

8.2.3 Comparison with the Computer Prediction

The method of analysis described in section 5.6 also produced estimates of shrinkage strains. It may be recalled that this method was based on the moisture loss results obtained from the tests on segmentation blocks and the experimentally derived relationship between moisture loss and free shrinkage. This information was taken from 200 mm deep rectangular section specimens, so that the results obtained from the analysis were applicable only to the beams of similar cross-section, namely the shallow beams.

The 30 day shrinkage predictions are presented also in Appendix III. Three figures are shown ; the first takes no account of creep, the second assumes a tensile creep factor 1.0 and the third assumes a factor of 2.5. Clearly, the choice of the tensile creep factor is of importance, as much of the concrete was in tension.

As expected, the predicted heated beam result shows the greatest

shrinkage, although the difference between this and the non-heated beam result is greater than was seen in the actual tests. Also, the shrinkage predictions are generally greater than observations, especially in the case of the heated beam results. This overestimation could have been caused by a number of factors, such as an actual tensile creep factor in excess of the 2.5 used or differences in drying rates between test beams and the segmentation specimens.

8.3 Curvatures of Non-Loaded Beams

8.3.1 Results of Curvatures

The non-heated test beams experienced changes in curvature as a result of shrinkage. The loaded beams also experienced shrinkage curvatures, although these were not seen in isolation, as they were accompanied by creep deflections. Therefore, the discussion will concentrate initially on the non-loaded beam results.

Consider first the long-term results for the non-loaded companion beams from the second and third single span tests, which are presented in graphs 68 and 69. For all four beams, hogging curvatures were observed, with the non-heated beams undergoing the greatest changes in curvature. At 30 days, the curvatures of the non-heated beams were in the range 0.5 to 0.6×10^{-6} mm^{-1}, whereas the heated beam curvatures were in the range 0.3 to 0.4×10^{-6} mm^{-1}. The similarly tested non-loaded beams from the two span tests showed the same trends.

These particular beams were symmetrically reinforced, but curvatures were induced by non-uniform shrinkage. This effect was explained in Chapter V. To recapitulate, the non-heated beams

experienced increased drying in the lower fibres, as a result of their closer proximity to the exposed surfaces. This asymmetric shrinkage induced a hogging curvature. However, in the case of the heated beams, a second drying region developed in the upper fibres, thus reducing the curvature.

The shrinkage curvatures experienced by the deep beams were considerably less than those reported above. At 30 days, the curvature of both beams was 0.14×10^{-6} mm^{-1}. Again, with such small curvatures, reduced accuracy of observation was expected. This was compounded, as corrections to the results were necessary, to compensate for small temperature gradients at the time when the strains were being measured. The corrections were typically of the same order of magnitude as the final results.

Only one T-section beam was tested, but this was not loaded until the 19th day of the test. Thus, the long-term curvatures which were recorded before that time were induced solely by shrinkage. Unlike the other beams tested, the T-section beam experienced a sagging shrinkage curvature of approximately 0.4×10^{-6} mm^{-1}. The opposite sense of this curvature was as a result of two features. Firstly, the beam included only tension reinforcement, so that the shrinkage of the lower fibres was restrained, and, secondly, the moisture loss pattern was different to the other tests. A considerable moisture loss was permitted from the flange soffit, which was not fully sealed, and this effect would have been enhanced by the heating of the upper surface.

8.3.2 Comparison with the Computer Prediction

The shrinkage curvatures of the non-loaded beams may be compared

with the results predicted from the moisture profiles deduced from the segmentation blocks. The analysis of shrinkage induced stresses, described in section 5.6, provided estimates of the resulting curvatures. Unlike the estimates of axial strains, mentioned in section 8.2.3, the results were sensibly independent of creep.

Taking first the non-heated block calculations, the predicted curvature was 0.62×10^{-6} mm^{-1} at 30 days and this compares well with the beam observations. However, by 50 days the prediction was reduced to 0.48×10^{-6} mm^{-1}, as a result of the reduction in the non-uniformity of free shrinkage in the member. No evidence of such a reduction is apparent in the beam results, presented in graphs 68 and 69.

Also, the moisture loss profiles deduced from the heated segmentation blocks were almost symmetrical about the mid-height, as is clear from graph 6, so that the resulting curvature estimates were negligible. However, as stated, curvatures of approximately 0.3×10^{-6} mm^{-1} were observed in the actual test beams.

In conclusion, the segmentation block technique and the subsequent computer analysis did not fulfil one of the intended objectives, which was the prediction of beam curvatures. It is suggested that the experimental technique lacked the accuracy for this purpose. Consider, for a example, a hypothetical linear moisture content variation in a member, where the maximum moisture content difference is 0.3 % of the dry weight. In fact, according to the analysis, this difference is sufficient to induce a curvature of 0.3×10^{-6} mm^{-1}, which is similar to that recorded for heated test beams. It is not suggested that such a moisture content profile existed, but the exercise does demonstrate that apparently small

moisture loss gradients can cause curvatures in the order of those seen in beam results. The identification of these small moisture loss gradients may have been beyond the accuracy of the segmentation technique.

8.4 Curvatures of Loaded Beams

8.4.1 Results of Curvatures

The long-term changes in curvature of the beams which were subjected to four point loading are shown in graphs 67 to 71. Firstly, the senses of these curvatures require some explanation. In all cases, the non-loaded beams exhibited hogging curvatures and the heated, loaded beams experienced sagging curvatures. The non-heated, loaded beams experienced upward curvatures, but it may be recalled, from the description of the rig, that the loading was upward also. Therefore, to be consistent with the other beams tested, in terms of the sealing and thus moisture movement, the beams were considered to have undergone sagging curvatures, with respect to load direction.

The deflection coefficients of the the beams tested are given in Appendix III. The deflection coefficient is defined here as the long-term change in curvature divided by the initial curvature and is thus a non-dimensional value. For reasons which will be made apparent, this coefficient is not necessarily equal to the creep coefficient. For the purpose of comparison, the 30 day values will be considered in detail. For the first test, two coefficients are given. The first of these relates to the initial phase of loading and the second to the phase of increased loading. The figure presented for the T-section beam relates to the 45th day, corresponding to the 26 days under load.

For a consistent definition of beam curvatures, two sets of

30 day coefficients are given. The first set was calculated from the raw data, whilst the second set includes a correction to account for the shrinkage-induced curvatures which were mentioned in section 8.3.1. The method of correction was to subtract the curvature of the non-loaded beam from that of the similarly heated loaded beam, with due regard for sign. This was done in order to provide an estimate of the change in curvature due to creep alone. This can only be an approximation as creep and shrinkage are not mutually independent. In the case of the first test, no shrinkage control beams were included and so the curvature corrections were obtained from the second, similar test. Also, no control beam was included in the T-section beam test, so that shrinkage correction was not possible. With this exception, the discussion will deal with the corrected results.

The results are presented in a condensed form in the table below. This gives the average deflection coefficients of all the beams tested. The experimental values are shrinkage curvature corrected. The predicted values will be discussed in sections 8.4.2 and 8.4.3.

30 Average Deflection Coefficients :

	Experimental	ACI	CEB-FIP	BS8110	Computed
Shallow Beams	0.48/0.54	0.46	0.57	0.58	0.56/0.64
Deep Beams	0.48/0.51	0.45	0.62	0.66	0.59/0.73
T-Section Beam	-/0.50	0.71	0.83	1.10	-/0.68

(Non-heated/Heated)

In all cases, the heated beams experienced greater changes in the deflection coefficients than the non-heated beams. This was expected, as creep increases with temperature. There was also the

likelihood of transitional thermal creep, as thermal cycling commenced following the application of the load. The T-section beam test was an exception in this respect, as loading followed heating.

It may be noted however that the corrected coefficients for the first test are probably less accurate than the rest, for two reasons. Firstly, the creep deflections were small during the initial phase of moderate loading and it is during this phase that the rate of change of shrinkage curvature would have been greatest. As a first estimate, shrinkage could have accounted for roughly half of the measured curvature change. Secondly, since the corrections were derived from the subsequent test, they were not truly representative of the moisture conditions in the first test.

The heated beams of the first and second tests produced deflection coefficients which were 10 % in excess of those produced by the non-heated beams. In the third test, the increase was 15 %. The greater increase in the latter test was expected as the beams were heated on five occasions each week, compared with three for the previous beams.

It is interesting to make the rather simplistic comparison between these results and the average temperatures of the test beams. For this purpose, the temperatures were averaged through the depths of the beams and with respect to time. For the first and second tests, the average temperatures of the heated beams were some 11 % in excess of the non-heated beams and, for the third test, the increase was some 18 %. These figures are broadly in line with the proposition that the increase in creep is proportional to the increase in temperature. However, this takes no account of transitional thermal creep. A

reduced dependence on temperature for conventional creep would allow scope for transitional thermal creep in the results. In the absence of the relevant data from companion experiments, these effects cannot be properly quantified.

8.4.2 Comparison with Predictions from Codes

The three code predictions, mentioned in section 3.6.6, were used in a comparison with the experimental data. For the majority of tests, the creep coefficients at 30 days were calculated, except for the case of the T-section beam test. For this test, the period of loading considered was from 19 days to 45 days from the beginning of the test, in line with the testing procedure.

The creep coefficients were then used to calculate effective moduli which, in turn, were used to calculate the effective flexural stiffnesses of the beams. Thus, the predicted creep deflection coefficients were the changes in the effective flexural stiffness divided by the initial flexural stiffness.

The calculations were performed for both the uncracked and, where appropriate, the cracked sections. In all cases, the estimates of the coefficients from the fully cracked analyses were smaller than those from the uncracked analyses. The reason for this feature is that a cracked section is composed of a smaller proportion of 'creepable' material than an uncracked section.

As with the shrinkage predictions, only the CEB-FIP method permitted a consideration of the temperature of the member, with the inclusion of a corrected age. In fact, the corrections were small, the heated beam predictions being not more than 2.5 % in excess of the non-heated beam predictions. This increase is clearly much less

than was observed in the test beams.

The BS8110 method had the deficiency that, in the case of the T-section beam, the effective thickness was outside the range of the design chart. It was therefore necessary to extrapolate to obtain a prediction. The deep beam was also outside the range, so an approximation was taken by assuming that the beam was fully sealed.

For the purposes of comparison, it is appropriate to consider the the shrinkage corrected results. In most cases, these lie between the cracked and the uncracked section predictions. Of the two approaches, the uncracked analyses provided the closest agreement and this might reasonably be expected as the extent of cracking of the beams was slight to moderate. Ideally, consideration of a partially cracked section would have been preferable, but, considering the variability of the experimental results and the other possible inaccuracies of the prediction, such a refinement was not warranted.

8.4.3 Comparison with the Computer Prediction

The program CREEP was used to provide predictions of the creep deflections of the simply supported beams. For this purpose, the time averaged temperature profile was used.

The analyses were performed for the uncracked and, where appropriate, the fully cracked sections. The specific thermal creep curve used was that shown in graph 74. In fact, with all other parameters held constant, the cracked analyses yielded lower deflection coefficients than the uncracked analyses. The reasons for this were stated in the previous section. These results are given in Appendix III.

In order to make a comparison, it is necessary to consider the

deflection coefficients which include the correction for curvatures resulting from non-uniform shrinkage. The present analysis was for creep alone.

For the cracked beams, the observed curvatures lie between the uncracked and cracked predictions, with a greater tendency towards the uncracked response. The second phase of the first test is an exception to this latter point, but this could have been attributable to factors other than the extent of cracking. Again, with the variability of the experimental results, there is little to be gained from an analysis of a partially cracked section.

A criticism of the approach was the use of a single specific thermal creep curve. As already stated, the accurate control of initial moisture content of the beams was a problem and this factor is of central importance to creep. It would therefore have been preferable to produce separate creep curves for each test.

However, of greater importance than the test variability was the problem that the consideration of a single curve failed to take proper account of the combinations of temperature and moisture conditions which existed within the test beams.

Finally, a further deficiency of the method was its neglect of transitional thermal creep. This would have been of relevance to the heated beam predictions, except in the case of the T-section beam test. In the latter test, the load was applied after several cycles of heating, during which the maximum temperature was attained. In view of the experimental results, the heating did not appear to increase the extent of creep beyond that which might be expected from the increase in average temperature. This is not to say that

transitional thermal creep did not occur. However, the lack of more extensive test data on creep does not permit a quantitive assessment of the effect.

8.5 Two Span Beams

Changes in the support reactions of the continuous beams were measured. These were the result of both temperature gradient and shrinkage effects. Before looking at the experimental results and comparing them with predictions, the mechanisms will be considered.

In the two span arrangement considered, creep resulting from the imposition of the applied mechanical load alone would not lead to a modification of support reactions. Changes would however occur if the cracking pattern altered.

Changes in support reactions would be expected from the effects of non-uniform shrinkage. The two span beams were of the same cross-section as the other shallow beams tested. The hogging shrinkage-induced curvatures which were observed in these other tests would be restrained at the mid-point in a two span test. The result would then be a decrease in the central support reactions of loaded beams and increases at the end supports. These changes in reactions would themselves be reduced by creep.

Lastly, long-term changes in support reaction would be expected in relation to the daily fluctuations in temperature. This effect is rather complicated, but a simplified explanation can be given with reference to figure 17.

Suppose that a two span beam is subjected to periodic applications of a positive temperature profile. The argument is simplified by assuming that the indicated temperature profile is

instantaneously assumed or lost by the beam. Thus, the first temperature cycle is applied and, as a result of the change in free thermal curvature, a reaction P is induced at the central support. As the temperature profile is maintained, the magnitude of the reaction diminishes as stresses in the beam are relaxed by creep. After some time, the thermal gradient is removed and, assuming a constant flexural stiffness, the magnitude of the resulting decrease in support reaction is numerically equal to P. There remains therefore a reversed support reaction which is itself reduced under the action of creep. The heating cycles are repeated and the changes in support reaction are as indicated in the figure. In this way, the support reaction, immediately before heating is applied, decreases with time, although the rate of decrease diminishes with time.

Of course, the effect is complicated considerably by the fact that the temperature fluctuations are continuous. Also, the elastic modulus and possibly the extent of cracking vary with time.

Thus, the long-term changes in support reaction emanate from non-uniform shrinkage and relaxation of thermal stresses.

8.5.1 Results of Changes in Support Reaction

The observed changes in support reactions are presented in graphs 72 and 73. It may be seen that, as anticipated, reductions occurred in the central support reactions, with increases at the end supports.

Points to note are that the changes in reactions were greatest for the non-heated beams and that the second test produced greater changes than the third. The cause of the greater changes in the non-heated beams was the greater free non-uniform, shrinkage-induced

curvatures which had to be restrained. Additionally, the heated beams experienced a component of reaction resulting from the temperature gradient induced creep. This operated in the opposite sense to the shrinkage curvature effect.

The restraint force is proportional to the flexural stiffness of the beam. Primarily for this reason, the third test produced smaller changes in reactions as a result of the beams being moderately cracked.

The experimental results from the second test indicate a rather erratic long-term response. There are a number of possible explanations for this. It was found, for instance, that any slight disturbance of the strain gauge wires could affect the meter readings. Also, small residual temperature differences existed in the beams when the measurements were taken. It is suggested however that the primary reason was differential movement at the supports. It may be noted that a change in the central support reaction of 0.1 kN corresponds to a differential movement of the end support of less than 0.1 mm.

The results from the third test show a considerably less erratic behaviour than those from the second and this may be attributed to the greater loading which the rig carried. It is suggested that the this caused a greater degree of 'bedding in' of the rig, thus affording less opportunity for movement of the supports.

8.5.2 Estimates of Changes in Reaction

Estimates of the changes in the central support reaction, at 30 days from the beginning of test, may be found in Appendix III. The method of estimation will be described.

The changes in reaction resulting from non-uniform shrinkage

were calculated from the long-term curvatures of the non-loaded beams. It was assumed that the free shrinkage curvatures of the loaded beams were of the same magnitude as these. So, from these figures, the reactions required to fully restrain the central deflections of the loaded beams were calculated. This was done in consideration of the uncracked and the partially cracked sections. The latter was based on the method of tension stiffening described in section 7.4.3.1. The uncracked analysis was performed in relation to the second two span test and the partially cracked to the third.

These changes in reaction were then modified for the effects of creep using the program CREEP. The analysis was performed incrementally, to take account of the increase in reaction over the test period.

A simplified approach was adopted for the estimation of the changes in support reaction resulting from the temperature gradient induced creep. Here, the average temperature profile was considered and was assumed to remain constant. This enabled use of the program CREEP to perform the analysis. Incorporation of the temperature fluctuations would have required an analysis of considerably greater complexity.

According to the estimates, non-uniform shrinkage accounted for the majority of the change in support reactions. In the case of the heated beams, this change was reduced by the temperature gradient induced creep component.

8.6 Concluding Remarks

All of the beams tested exhibited axial shrinkage strains, these being greatest in the heated beams. However, variability was evident

between the results of the various tests and this was caused, at least in part, by differences in initial moisture content of the beams. Variations in ambient conditions would have been of influence also. The observed shrinkage strains in the shallow beams after 30 days corresponded to movements of no greater than 0.5 mm in a 4000 mm span, with an estimated ultimate movement of 1.6 mm. With proper provision of bearings, such movements would cause no structural problems.

Results from non-loaded beams provided clear evidence of curvatures as a consequence of non-uniform shrinkage within members. These were smallest in the heated beams, in the presence of two opposing drying regions. Such curvatures were significant in relation to creep curvatures and therefore warranted consideration in the prediction of long-term beam response.

Results from the loaded beams showed increased creep in beams which were heated. This increase was greatest in beams which were heated on five, rather than three, occasions each week. The results obtained did not supply any clear evidence of transitional thermal creep, although, for most beams tested, the effect would have occurred to some extent.

Applying the normalised transitional thermal creep measured by Parrott and Symmons (136) to the test beams, a change in the deflection coefficient of 0.13 is obtained. However, this estimate is excessive in consideration of the results from the test beams.

The long-term support reactions of the two span tests changed during the test period. Estimates showed the restraint of non-uniform shrinkage-induced curvatures to be the dominant effect. This led to a reduction in central support reactions, the reductions being greatest

in the non-heated beams. The heated beams experienced smaller free shrinkage curvatures and they experienced smaller changes in support reactions as a result of the creep relaxation of temperature gradient induced stresses.

The erratic nature of the results is attributed largely to the movement of supports. The central restraining device, incorporating the load cells, was designed to limit the deflections at the centre of the beams. It is therefore more likely that the movement occurred at the end supports. In this respect, it would have been preferable to have constructed a rig of greater rigidity. However, the performance of the rig in relation to the daily response was satisfactory and the equipment was designed primarily to investigate this latter aspect of beam response.

The restraint reactions which have been mentioned above give rise to tensile stresses in the concrete, which are greatest at the soffits in the vicinity of the central supports. The results from the non-heated beam of the second test provide a stress of -1 N/mm^2. Such tensile stresses add to those which arise from the non-linearity of the free shrinkage profiles. It may be recalled that estimates of these latter stresses were in the region of the tensile strength of concrete, so that any further contribution would increase the likelihood of cracking. However, in the beams tested, the externally applied loads ensured that the concrete remained in compression in these critical sections of the beams. In the sections of maximum sag moment, the additional tensile stress caused by these long-term effects would have been approximately -0.5 N/mm^2.

CHAPTER IX

CONCLUSIONS AND SUGGESTIONS FOR FURTHER WORK

9.1 Conclusions

Positive temperature profiles, based on extreme environmental conditions, were applied to a number of concrete specimens. These included non-loaded beams, single span beams and two span beams. In addition, similar positive temperature profiles were applied to segmentation specimens. From these tests, the following conclusions were drawn.

9.1.1 Short-Term Beam Response

9.1.1.1 Non-Loaded and Single Span Beams

Temperatures and strains were measured during the daily cyclic heating of beams. Measured temperatures were used in an incremental computer prediction of thermal strains. Linear elastic behaviour was assumed. Analysis based on the assumption of an uncracked section provided reasonable predictions of thermal strains for both uncracked and cracked beams. Fully cracked analysis overestimated strains.

The response of beams during the first few days of loading was affected by the presence of creep curvatures, induced by the mechanical load, operating in the opposite sense to thermal curvatures. For this reason, the observed changes in beam curvatures, during heating, were less than predicted in the computer analysis. The effect was insignificant beyond the first week of heating.

During the several weeks of each test, the thermally induced strains increased steadily. The effect is attributed to increases in the coefficient of thermal expansion as a result of moisture loss, except for in the first few days of loading. For the latter, the

increase is attributed largely to the diminishing magnitude of changes in creep curvature.

The behaviour of a crack, during a heating cycle, was examined with the aid of a crack gauge. Negligible changes in crack width were recorded during heating. Thermally induced soffit strains in the locality of the crack were not significantly different to the overall soffit strains.

Estimates of self-equilibrating stresses were small. Based on measured temperature profiles, maximum tensile stresses of approximately -0.5 N/mm^2 were calculated. It is appreciated that larger self-equilibrating stresses are induced in deeper beams.

9.1.1.2 Two Span Beams

Thermal effects are of greater importance for two span beams, where temperature profiles cause large changes in support reactions. Decreases in central support reactions and increases in end support reactions were recorded during daily heating cycles. These were greatest in uncracked beams.

Thermally induced changes in support reactions were predicted in the following way. Measured temperature profiles were used as input data, in the linear elastic computer analysis, to predict free thermal curvatures. For this purpose, an uncracked section was assumed. The restraint of the associated central deflections was calculated, for a beam of varying flexural stiffness, using an area-moment analysis. For sections of the beams where the cracking moment was exceeded, a partially cracked flexural stiffness was assumed. Elsewhere, uncracked stiffness was assumed. A conservative approach is to assume an uncracked section throughout.

9.1.2 Long-Term Beam Response

As anticipated, heated beams experienced more rapid axial shrinkage than non-heated beams. Also, the shrinkage rate was greater for beams with higher exposed surface to volume ratios. At the end of test periods, axial shrinkages of beams were well below ultimate values.

Beams experienced curvatures which were induced by non-uniform shrinkage. The non-uniform shrinkage was caused by asymmetric sealing and heating of beams. The beams of rectangular cross-section experienced hogging curvatures. These were greatest for non-heated beams, due to the existence of only one drying region, in the soffit zone. In heated beams, the presence of the additional upper drying region led to reduced curvatures. The T-section beam experienced a sagging curvature. This was due to asymmetric reinforcement and to additional moisture loss from the partly sealed flange.

Creep curvatures of beams were evaluated by subtracting the shrinkage induced curvatures of non-loaded companion beams from loaded beam curvatures. Resulting curvatures were greatest in heated beams, the increases being roughly in proportion to time-averaged temperature increases.

An incremental rate of creep analysis was employed to predict creep curvatures of beams. This used an empirically derived specific thermal creep curve. Predictions overestimated beam curvatures. It is suggested that a single specific thermal creep curve cannot be used to accurately model the creep of a partly sealed drying member, under cyclic temperatures.

In two span tests, small changes in support reactions were

observed. They were caused primarily by restraint of curvatures induced by non-uniform shrinkage. They were affected, to a lesser extent, by creep relaxation of secondary thermal stresses.

9.1.3 Segmentation Specimens

Non-uniform moisture content profiles were measured in concrete specimens, using a segmentation technique. In non-heated beams, measured moisture contents were lowest in the lower segments, as a result of the loss of moisture from the unsealed soffit surfaces. In heated beams, low moisture contents were measured in the upper segments also, as a result of positive temperature gradients.

Measured moisture content profiles, together with the empirically derived relationship between free shrinkage and weight loss, were used in an evaluation of shrinkage-induced stresses. Peak tensile stresses of approximately -8 N/mm^2 were estimated for heated beams. However, consideration of creep relaxation resulted in large reductions in estimated stresses. Final stress predictions suggested very slight or no shrinkage-induced cracking.

A similar segmentation technique was employed to measure variations in the coefficient of thermal expansion within beams. Highest values were measured in the upper and lower segments, where moisture contents were lowest. The overall coefficient for specimens increased with age.

9.2 Suggestions for Further Work

The degree of non-linearity of the temperature profile increases with member depth, and so therefore do the self-equilibrating stresses. Further tests could be performed on deeper members, say 1000 mm in depth, where self-equilibrating stresses are of greater

importance.

The present study concentrated on positive temperature profiles. There are circumstances in which negative profiles could be of interest. A negative profile induces tensile self-equilibrating stresses at the surfaces of a member. These could be considered in conjunction with, for instance, pre-stress. Under highly eccentric pre-stress loads, tensile stresses are induced at the surface at transfer. The combination of these two effects may be sufficient to induce cracking.

This project has been concerned with thermal effects in a plane stress consideration. Tests could be extended to include the thermal response of slabs, where transverse effects are of importance. A modified analysis would be necessary, taking account of Poisson ratio effects. Transverse effects are also of importance in box sections, under non-linear temperature profiles, due to differential transverse thermal expansion of deck and soffit slabs. This problem could be investigated theoretically.

There may be a need to consider further the way in which thermal effects are combined with other categories of loading in design. One study (35) recommends the use of different partial safety factors to the ones which are presently in use.

There is considerable scope for more tests on segmentation specimens, to measure moisture content variations in members. Further tests could involve longer drying periods, thicker specimens or different initial w/c ratios. In fact, since the completion of this project, the experimental technique has been further refined and tests are currently underway in the department. Interim results are in

line with results presented here.

Finally, it would be useful to take measurements of both temperatures and thermal strains from an actual structure in service. This would involve casting thermocouples into the structure, to measure temperature profiles, and the installation of a strain measurement system.

REFERENCES

1 CLARKE, J.L., Thermal Stresses in Concrete Gravity Platforms, C&CA, Mar 79.

2 DE SERIO J.N., Thermal and Shrinkage Stresses : They Damage Structures, ACI, SP27, pp 43-49, 1971

3 EVANS, E.P. and HUGHES, B.P., Shrinkage and Thermal Cracking in a Reinforced Concrete Retaining Wall, ICE Proceedings, Vol. 39, pp 111-125, 1968.

4 WILLIAMS, A. and CLEMENTS, S.W., Thermal Movements in the Upper Floor of a Multi-Storey Car Park, Technical Report 539, C&CA, Oct 80.

5 HIRST, M.J.S., Thermal Loading of Concrete Roofs, Proc. 8th Australasian Conf. on the Mechanics of Structures and Materials, Aug 82.

6 PRIESTLEY, M.J.N., Ambient Thermal Stresses in Circular Prestressed Concrete Tanks, ACI Journal, pp 553-560, Oct 76.

7 BRITISH STANDARDS INSTITUTION, BS153, Part 3A, 1972.

8 EMERSON, M., Extreme Values of Bridge Temperatures for Design Purposes, Laboratory Report 744, TRRL, 1976.

9 EMERSON, M., Temperature Differences in Bridges : Basis of Design Requirements, Laboratory Report 765, TRRL, 1977.

10 PRIESTLEY, M.J.N., Linear Heat Flow and Thermal Stress Analysis of Concrete Bridge Decks, Research Report 76/3, University of Canterbury, New Zealand, Feb 76.

11 DEPARTMENT OF THE ENVIRONMENT, Technical Memorandum BE5/73, 1973.

12 WHITE, I.G., Non-Linear Differential Temperature Distributions in Concrete Bridge Structures : A Review of the Current Literature, Technical Report 525, C&CA, May 79.

13 CLARK, L.A., Concrete Bridge Design to BS5400, Construction Press

14 BLYTHE, D.W.R. and LUNNISS, R.C., Temperature Difference Effects in Concrete Bridges, Supplementary Report 442, TRRL, pp 68-80, 1978.

15 CHURCH, J.G., The Diurnal Thermal Loading of Cracked Reinforced Concrete Bridges, PhD Thesis, University of Birmingham, 1983.

16 EMERSON, M., The Calculation of the Distribution of

Temperature in Bridges. Laboratory Report 561. TRRL. 1973.

17 CEB. Thermal Effects in Concrete Structures. Bulletin D'Information 167. Jan 85.

18 CEB. Structural Analysis. Vol. 2. Bulletin D'Information 154. Apr 82.

19 EMERSON. M.. Thermal Movements of Concrete Bridges : Field Measurements and Methods of Prediction. Supplementary Report 747. TRRL. 1982.

20 EMERSON. M.. Bridge Temperatures and Movements in the British Isles. Laboratory Report 228. TRRL. 1968.

21 EMERSON. M.. Bridge Temperatures Estimated from the Shade Temperature. Laboratory Report 696. TRRL 1976.

22 PRIESTLEY. M.J.N.. Design Thermal Gradients for Concrete Bridges. New Zealand Engineering. pp 213-219. Sept 76.

23 REYNOLDS. J. C. and EMANUEL. J. H.. Thermal Stresses and Movements in Bridges. Journal of the Structural Division. ACSE. pp 63-78. Jan 74.

24 Institution of Heating and Ventilation Engineers. Guide Book A. London. 1970

25 BILLINGTON. N.S.. The Thermal Properties of Buildings. Cleave Hume Press. 1952.

26 WOOD. J.H.. In-situ Thermal Measurements. Bridge Seminar 1978. Vol.2. Road Research Unit. New Zealand. 1979.

27 BUCKLE. I.G. and LANIGAN. A.G.. Transient Thermal Response of Box Girder Bridge Decks. Proc. Third Australasian Conf. on the Mechanics of Structures and Materials. University of Aukland. Aug 71.

28 JONES. M.R.. Bridge Temperatures Calculated by a Computer Program. Laboratory Report 702. TRRL. 1976.

29 HUNT. B. and COOKE. N.. Thermal Calculations for Bridge Design. Journal of the Structural Division. ASCE. pp 1763-1781. Sept 75.

30 HAMBLY. E.C.. Temperature Distributions and Stresses in Concrete Bridges. The Structural Engineer. Vol. 56A. No.5. pp 143-148. May 78.

31 PRIESTLEY. M.J.N.. Design of Concrete Bridges for Temperature Gradients. ACI Journal. Vol. 75. Part 5. pp 209-217. May 78.

32 TIMOSHENKO. S.P. and GOODIER. J.N.. Theory of Elasticity.

Chapter 13, McGraw-Hill, 1970.

33 PRIESTLEY, M.J.N., Thermal Gradients in Bridges : Some Design Considerations, New Zealand Engineering, pp 228-233, July 72.

34 HAMBLY, E.C., Bridge Deck Behaviour, Chapman and Hall.

35 CHURCH, J.G. and CLARK, L.A., Combination of Highway Loads and Temperature Difference Loading on Bridges, The Structural Engineer, Vol. 62A, No. 6, pp 177-181, Jun 84.

36 RADOLLI, M. and GREEN, R., Thermal Stresses in Concrete Bridge Superstructures Under Summer Conditions, Transportation Research Record, No. 547, pp 23-36, 1975.

37 PRIESTLEY, M.J.N. and BUCKLE, I.G., Ambient Thermal Response of Concrete Bridges, Bridge Seminar 1978, Vol.2, Road Research Unit, New Zealand, 1979.

38 THURSTON, S.J., PRIESTLEY, M.J.N. and COOKE, N., Thermal Analysis of Thick Concrete Sections, ACI Journal, Vol. 77, No. 5, pp 347-357, Sept/Oct 80.

39 CLARKE, J.L., Monitoring Multi-Storey Car Parks, C&CA, May 83.

40 THURSTON, S.J., PRIESTLEY, M.J.N. and COOKE, N., Influence of Cracking on Thermal Response of Reinforced Concrete Bridges, Concrete International, pp 36-43, Aug 84.

41 BRITISH STANDARDS INSTITUTION, BS5400, 1978.

42 PIHLAJAVAARA, S.E., An Analysis of Factors Exerting Effect on Strength and Other Properties of Concrete at Elevated Temperatures, ACI, SP 34, Vol. 1, pp 347-354, 1972.

43 ABRAMS, M.S., Compressive Strength of Concrete at Temperatures to 1600 ^{0}F, ACI, SP 25, pp 33-58, 1971.

44 LANKARD, D.R., BIRKIMER, D.L., FONDRIEST, F. and SNYDER, M.J., Effects of Moisture Content on the Structural Properties of Portland Cement Concrete Exposed at Temperatures up to 500 ^{0}F, ACI, SP 25, pp 59-102, 1971.

45 SULLIVAN, P.J.E. and POUCHER, M.P., The Influence of Temperature on the Physical Properties of Concrete and Mortar in the Range 20 ^{0}C to 400 ^{0}C, ACI, SP 25, pp 103-136, 1971.

46 MEARS, A.P., Long-Term Tests on the Effect of Moderate Heating on the Compressive Strength and Dynamic Modulus of Elasticity of Concrete, ACI, SP 34, Vol. 1, pp 355-376, 1972.

47 HARADA, T., TAKEDA, T., YAMANE, S. and FURUMURA, F., Strength, Elasticity and Thermal Properties of Concrete

Subjected to Elevated Temperatures, ACI, SP 34, Vol. 1, pp 377-406, 1972.

48 NASSER, K.W., Creep of Concrete at Low Stress/Strength Ratios and Elevated Temperatures, ACI, SP 25, pp 137-148, 1971.

49 KAPLAN, M.F. and ROUX, F.J.P., Effects of Elevated Temperatures on the Properties of Concrete for the Containment and Shielding of Nuclear Reactors, ACI, SP 34, Vol. 1, pp 437-442, 1972.

50 HANNANT, D.J., Strain Behaviour of Concrete up to 95 ^{0}C Under Compresssive Stresses, Conf. on Prestressed Concrete Pressure Vessels, London, Part 17, pp 177-191, 1967.

51 NEVILLE, A.M., Properties of Concrete, Third Edition, Pitman, 1981.

52 GLUCKLICH, J. and ISHAI, O., Creep Mechanism in Cement Mortar, ACI Journal, Vol. 59, Part 7, pp 923-948, Jul 62.

53 ZOLDNERS, N.G., Thermal Properties of Concrete Under Sustained Elevated Temperatures, ACI, SP 25.1., pp 1-30, 1971.

54 MARSHALL, A.L., The Thermal Properties of Concrete, Building Science, pp 167-174, 1972.

55 SULLIVAN, P.J.E., The Effects of Temperature on Concrete, Developments in Concrete Technology 1, Edited by LYDON, F.D., Applied Science Publishers Ltd., 1979.

56 WALKER, S., BLOEM, D.L. and MULLEN, W.G., Effects of Temperature Changes on Concrete as Influenced by Aggregates, ACI Journal, Vol. 48, pp 661-679, Apr 52.

57 BROWNE, R.D., Thermal Movement of Concrete, Concrete, pp 51-53, Nov 72.

58 MEYERS, S.L., How Temperature and Moisture Changes May Affect the Durability of Concrete, Rock Products, pp 153-178, Aug 51.

59 BONNELL, D.G.R. and HARPER, F.C., The Thermal Expansion of Concrete, National Building Studies, Building Research Station, Technical Paper No.7, 1951.

60 LOUBSER, P.J., and BRYDEN, J.G., An Apparatus for Determining the Coefficient of Thermal Expansion of Rocks, Mortars and Concretes, Magazine of Concrete Research, Vol. 24, No. 79, pp 97-100, June 72.

61 POWERS, T. C., Structure and Physical Properties of Hardened Portland Cement Paste, ACI Journal, Vol. 41, No. 1, pp 1-6.

Jan 58.

62 BAZANT, Z.P., Delayed Thermal Dilations of Cement Paste and Concrete Due to Mass Transport, Nuclear Engineering and Design, Vol. 14, pp 308-318, June 70.

63 WITTMAN, F. and LUKAS, J., Experimental Study of Thermal Expansion of Hardened Cement Paste, Materiaux et Constructions, Vol. 7, No. 40, pp 247-252, 1974.

64 MARECHAL, J.C., Thermal Conductivity and Thermal Expansion Coefficients of Concrete as a Function of Temperature and Humidity, ACI, SP34, 1972

65 BERWANGER C. and SARKAR, A.F., Thermal Expansion of Concrete and Reinforced Concrete, ACI Journal, pp 618-621, Nov 76.

66 BROWNE, R.D. and BAKER, A.F., The Performance of Structural Concrete in a Marine Environment, Developments in Concrete Technology 1, Edited by LYDON, F.D., Applied Science Publishers Ltd., 1979.

67 POWERS, T.C., COPELAND, L.E. and HAYES, J.C., Permeability of Hardened Cement Paste, ACI Journal, Vol. 51, Part 3, pp 285-298, Nov 54.

68 HUGHES, B.P., LOWE, I.R.G., and WALKER, J., The Diffusion of Water in Concrete at Temperatures Between 50 ^{0}C and 95 ^{0}C. British Journal of Applied Physics, Vol. 17, pp 1545-1552, 1966.

69 ARUMUGASAAMY, P. and SWAMY, R.N., Moisture Movement in Reinforced Concrete Columns, Il Cemento, Vol. 75, pp 121-128, July/Sept 78.

70 BECKER, N.K. and MACINNIS, C., A Theoretical Method for Predicting the Shrinkage of Concrete, ACI Journal, Vol. 70, Part 9, pp 652-657, Sept 73.

71 CARLSON, R.W., Drying Shrinkage of Large Concrete Members, ACI Journal, Vol. 33, pp 327-336, 1937.

72 LOWE, I.R.G., HUGHES, B.P. and WALKER, J., The Diffusion of Water in Concrete at 30 ^{0}C, Cement and Concrete Research, Vol. 1, pp 547-557, 1971.

73 CHAPMAN, D.A., and ENGLAND, G.L., Effects of Moisture Migration on Shrinkage, Pore Pressure and Other Concrete Properties, Conf. on SMIRT, Part H4/d, Aug 77.

74 ENGLAND, G.L. and ROSS, A.D., Shrinkage, Moisture and Pore Pressures in Concrete, ACI, SP34, Vol. 2, pp 883-907, 1972.

75 ENGLAND, G.L. and SHARP, T.J., Migration of Moisture and Pore

Pressures in Heated Concrete.

76 ROSS, A.D. and PARKINSON, J.D., Shrinkage in Concrete Pressure Vessels, Nuclear Engineering and Design, Vol. 5, pp 150-160, 1967.

77 HANSON, J.A., Effects of Curing and Drying Environments on Splitting Tensile Strength of Concrete, ACI Journal, pp 535-543, July 68.

78 MONFORE, G.E., A Small Probe-Type Gage for Measuring Relative Humidity, PCA Journal, pp 41-47, May 63.

79 PIHLAJAVAARA, S.E., Estimation of Drying of Concrete at Different Relative Humidities and Temperatures of Ambient Air with Special Discussion about Fundamental Features of Drying and Shrinkage, Creep and Shrinkage in Concrete Structures, Edited by BAZANT, Z.P., John Wiley and Sons Ltd., 1982.

80 TROXELL, G.E., RAPHAEL, J.M. and DAVIS, R.W., Long-Time Creep and Shrinkage Tests of Plain and Reinforced Concrete, ASTM Proceedings, Vol. 58, pp 1-20, 1958.

81 NEVILLE, A.M., Creep of Concrete : Plain Reinforced and Prestressed, North Holland Publishing Company, Amsterdam, 1970.

82 CONCRETE SOCIETY, The Creep of Structural Concrete, Concrete Society Technical Paper No. 101, Jan 73.

83 ILLSTON, J.M. and ENGLAND, G.L., Creep and Shrinkage of Concrete and Their Infleunce on Structural Behaviour : A Review of Methods of Analysis, The Structural Engineer, Vol. 48, No. pp 283-292, July 70.

84 ILLSTON, J.M., The Components of Strain in Concrete Under Sustained Compressive Stress, Magazine of Concrete Research Vol. 17, No. 50, pp 21-28, Mar 65.

85 ILLSTON, J.M. and SANDERS, P.D., Creep of a Saturated Mortar Under Variable Temperature, Magazine of Concrete Research, Vol. 26, Part 88, pp 169-179, Sept 74.

86 GAMBLE, B.R. and PARROTT, L.J., Creep of Concrete in Compression During Drying and Wetting, Magazine of Concrete Research, Vol. 30, No. 104, pp 129-138, Sept 78.

87 ILLSTON, J.M., The Creep of Concrete in Terms of its Developing Structure and Moisture Condition, Structure, Solid Mechanics and Engineering Design, John Wiley and Sons Ltd., 1969.

88 PARROTT, L.J., Basic Creep, Drying Creep and Shrinkage of a Mature Cement Paste After a Heat Cycle, Cement and Concrete

Research, Vol. 7, pp 597-604, 1977.

89 POWERS, T.C., Mechanisms of Shrinkage and Reversible Creep of Hardened Cement Paste, Proc. of an International Conf. on the Structure of Concrete, London, 1965.

90 WITTMAN, F.H., Interaction of Hardened Cement Paste and Water, ACS Journal, Vol. 56, pp 409-415, Aug 73.

91 ISHAI, O., The Time-Dependent Deformational Behaviour of Cement Paste, Mortar and Concrete, Proc. of an International Conf. on the Structure of Concrete, London, 1965.

92 REUTZ, W., A Hypothesis for the Creep of Hardened Cement Paste and the Influence of Simultaneous Shrinkage, Proc. of an International Conf. on the Structure of Concrete, London, Sept 65.

93 WITTMAN, F.H., Creep and Shrinkage Mechanisms, Creep and Shrinkage in Concrete Structures, Chapter 2, John Wiley and Sons Ltd., 1982

94 HANSEN, T.C. and MATTOCK, A.H., Influence of Size and Shape of Member on the Shrinkage and Creep of Concrete, ACI Journal, Vol. 63, Part 2, pp 267-289, Feb 66.

95 ILLSTON, J.M., Creep : Part 1 and Part 2, Concrete, pp 37-41, May 76.

96 FAHMI, H.M., BRESLER, B. and POLIVKA, M., Prediction of Creep of Concrete at Variable Temperatures, ACI Journal, pp 709-713, Oct 73.

97 ARTHANARI, S. and YU, C.W., Creep of Concrete Under Uniaxial and Biaxial Stresses at Elevated Temperatures, Magazine of Concrete Research, Vol. 19, No. 60, pp 149-156, Sept. 67.

98 NASSER, K.W. and NEVILLE, A.M., Creep of Old Concrete at Normal and Elevated Temperatures, ACI Journal, pp 97-103, Feb 67.

99 ENGLAND, G.L., Numerical Creep Analysis Applied to Concrete Structures, ACI Journal, pp 301-310, June 67.

100 HANSEN, T.C. and ERIKSSON, L., Temperature Change Effect on Behaviour of Cement Paste, Mortar and Concrete Under Load, ACI Journal, Vol. 63, Part 4, pp 489-504, Apr 66.

101 CLARKE, J.L. and SYMMONS, R.M., Effects of Temperature Gradients on Walls of Oil Storage Structures, C&CA, Mar 78.

102 PARROTT, L.J., A Study of Transitional Thermal Creep in Hardened Cement Paste, Magazine of Concrete Research, Vol 31, No. 107, Jun 79.

103 RAINFORD, E.C. and TIMUSK, J., Creep of Hardened Portland Cement Paste Under Cyclic Temperature, ACS Journal, Vol. 61, pp 380-388, Sept/Oct 78.

104 PICKETT, G., Shrinkage Stresses in Concrete : Part 1, ACI Journal, Vol. 17, No. 3, pp 165-195, Jan 46.

105 DAVIS, R.E., DAVIS, H.E. and BROWN, E.H., Plastic Flow and Volume Changes of Concrete, ASTM Proc., Vol. 327, Part 2, pp 317-331, 1937.

106 GLANVILLE, W.H. and THOMAS, F.G., Further Investigations on Creep or Flow of Concrete Under Load, Building Research Technical Paper No. 21, London, 1939.

107 HANSON, J.A., A Ten Year Study of Creep Properties of Concrete, United States Department of the Interior, Bureau of Reclamation, Laboratory Report SP38, July 53.

108 WAJDA, R.L. and HOLLOWAY, L., Creep Behaviour of Concrete in Tension, Engineering, pp 209, Aug 64.

109 ILLSTON, J.M., The Creep of Concrete Under Uniaxial Tension, Magazine of Concrete Research, Vol. 17, No. 51, pp 77-84, June 65.

110 ENGLAND, G.L., The Direct Calculation of Stresses in Creeping Concrete and Concrete Structures, Structure, Solid Mechanics and Engineering Design, John Wiley and Sons Ltd., pp 1269-1276, 1969.

111 BRITISH STANDARDS INSTITUTION, BS8110, Part 2, 1985.

112 CEB-FIP Model Code for Concrete Structures, 1978.

113 ACI, Prediction of Creep Shrinkage and Temperature Effects in Concrete Structures, Commitee 209, SP27/3, 1971.

114 LEA, F.M., The Chemistry of Cement and Concrete, Third Edition, Edward Arnold Ltd., 1970.

115 RAMACHANDRAN, V.S., FELDMAN, R.F. and BEAUDOIN, J.J., Concrete Science, Heyden and Sons Ltd., 1981.

116 SOROKA, I., Portland Cement Paste and Concrete, The Macmillan Press Ltd., 1979.

117 HOBBS, D.W., Drying Shrinkage and Movement of Reinforced Concrete, C&CA, Technical Report, Apr 78.

118 TYLER, R.G., Creep, Shrinkage and Elastic Strain in Concrete Bridges in the United Kingdom, 1963-71, Magazine of Concrete Research, Vol. 28, No. 95, pp 55-84, June 76.

119 POWERS, T.C., Causes and Control of Volume Change, PCA Journal, Vol. 1, Part 1, pp 29-39, Jan 59.

120 FELDMAN, R.F. and SEREDA, P.J., A New Model for Hydrated Portland Cement and its Practical Implications, Engineering Journal, Vol.53, pp 53-59, Aug/Sept 70.

121 VERBECK, G.V. and HELMUTH, R.H., Structures and Physical Properties of Cement Paste, Proceedings of a Symposium on the Structure and Physical Properties of Cement Paste, Tokyo, Vol. 3, pp 1-32, 1968.

122 HOBBS, D.W., Influence of Specimen Geometry Upon Weight Change and Shrinkage of Air-Dried Concrete Specimens, Magazine of Concrete Research, Vol. 29, Part 99, pp 70-80, June 77.

123 PICKETT, G., Effect of Aggregate on Shrinkage of Concrete and a Hypothesis Concerning Shrinkage, ACI Journal, Vol. 52, pp 581-590, Jan 56.

124 HOBBS, D.W. and PARROTT, L.J., Prediction of Drying Shrinkage, Concrete, Vol. 13, Part 2, pp 19-24, Feb 79.

125 HOBBS, D.W., Shrinkage Induced Curvature of Reinforced Concrete Members, C&CA, Development Report 4, Nov 79.

126 EVANS, R.H. and KONG, F.K., Estimation of Shrinkage of Concrete in Reinforced and Prestressed Concrete Design, Civil Engineering and Public Works Review, Part 730, pp 559-561, May 62.

127 PICKETT, G., Shrinkage Stresses in Concrete : Part 2, ACI Journal, Vol. 17, No. 4, pp 361-398, Feb 46.

128 ZETLIN, L., THORNTON, C.H. and LEW, I.P., Design of Concrete Structures for Creep, Shrinkage and Temperature Changes, Symposium on Design of Concrete Structures, Final Report, Vol. 5, 1970.

129 PARROTT, L.J., Simplified Methods of Predicting the Deformation of Structural Concrete, C&CA, Development Report 3, Oct 79.

130 National Algorithms Group, NAG Mark 10, 1983.

131 Patel, R.G., Parrott, L.J., Martin, J.A. and Killoh, D.C., Gradients of Microstructure and Diffusion Properties in Cement Paste Caused by Drying, Cement and Concrete Research, Vol. 15, pp 343-356, 1985.

132 Copeland, L.E. and Bragg, R.H., Self-Desiccation in Portland Cement Pastes, ASTM Bulletin, pp 34-39, Feb 55.

133 Teychenne, D.C., Franklin, R.E. and Erntroy, H.C., Design of Normal Concrete Mixes, TRRL, 1975.

134 British Standards Institution, BS882, 1973

135 Clark, L.A. and Spiers, D.M., Tension Stiffening in Reinforced Concrete Beams and Slabs Under Short-Term Load, C&CA Technical Report, Jul 78.

136 Parrott, L.J. and Symmons, R.M., Deformation Properties of an Oil Strorage Vessel, C&CA, Dec 77.

APPENDIX I

RESULTS FROM COMPANION SPECIMENS

I.1 Elastic Modulus Results

Week	1	2	3	4	5	6	8
	Elastic Modulus ... kN/mm^2						
First Single Span Test	25.1	25.5	26.0	26.1	26.5	26.6	26.5
Second Single Span Test	21.8	22.5	23.9	24.2	25.2	25.8	26.6
Third Single Span Test	22.6	23.9	25.0	25.2	25.9		
Deep Beam Test	22.4	23.9	24.2	25.2	25.8	25.9	26.1
T-Section Beam Test	23.1	24.3	24.6	25.9	26.4	26.9	27.5
First Two Span Test	19.6	20.5					
Second Two Span Test	19.5	19.9	21.1	20.5	21.5	21.3	21.5
Third Two Span Test	24.1	24.9	25.6	26.8	25.5	27.4	27.0

I.2 28 Day Strength Results

	Cube Strength N/mm^2	Tensile Strength N/mm^2
First Single Span Test	48.6	4.0
Second Single Span Test	50.8	3.2
Third Single Span Test	43.4	3.2
Deep Beam Test	44.1	3.9
T-Section Beam Test	47.7	3.7
First Two Span Test	44.2	
Second Two Span Test	49.0	
Third Two Span Test	43.2	3.8

(Tensile Strength from Brazilian Test)

I.3 Creep Results

The results collected from the first creep test produced the

specific thermal creep curve which is presented in graph 74. It can be seen that the specific thermal creep after 60 days under load was 2.36 $\mu\varepsilon/(N/mm^2)/^0C$.

The raw strain data from the second creep test are shown in graph 75. These results indicate a drying creep component which was some 30 % as great as the basic creep. The specific thermal creep after 60 days. based on the results from the sealed specimen. was 2.60 $\mu\varepsilon/(N/mm^2)/^0C$. comparable with the result from the first test. The increase over the value obtained in the first test may be due to a slightly greater initial water content.

The relative magnitudes of drying and basic creep components. found here. relate only to the particular drying rate of the cylinder specimens used. Although the fibres in close proximity to drying surfaces of the main beams may approximate to this condition. the overall magnitude of drying creep in the beams would be smaller than found here.

The specific thermal creep curve. presented in graph 74. was used for all of the computer creep predictions.

APPENDIX II

DAILY RESPONSE OF FIRST TWO SPAN TEST

The results which are presented below are from the first week of testing of the first set of two span beams. They relate to the reductions which occurred in the central support reaction, during the daily heating cycles.

Day	Hour	Reduction in Reaction		Obs./Comp.
		Computed	Observed	
1	2	1.91 kN	1.93 kN	1.01
	4	2.61	2.74	1.05
	6	2.73	2.02	0.84
	8	2.79	2.06	0.74
2	2	2.42	2.03	0.84
	4	2.50	2.15	0.86
	6	2.73	2.76	1.01
	8	2.91	2.91	1.00
3	2	1.82	1.91	1.05
	4	2.30	2.19	0.95
	6	2.55	2.40	0.94
	8	2.69	2.80	1.04
4	2	1.64	1.57	0.96
	4	2.05	2.17	1.06
	6	2.38	2.33	0.98
	8	2.66	2.58	0.97
5	2	1.95	1.91	0.98
	4	2.34	2.39	1.02
	6	2.50	2.60	1.04

8	2.65	2.78	1.05

APPENDIX III

LONG-TERM RESULTS FROM BEAMS

III.1 30 Day Axial Shrinkage

Experimental Results

First Single Span Beam Test

Loaded	Non-heated	64 $\mu\varepsilon$
Non-loaded	Heated	69

Second Single Span Beam Test

Non-loaded	Non-heated	87 $\mu\varepsilon$
Non-loaded	Heated	87
Loaded	Non-heated	93
Loaded	Heated	104

Third Single Span Beam Test

Non-loaded	Non-heated	83 $\mu\varepsilon$
Non-loaded	Heated	121
Loaded	Non-heated	105
Loaded	Heated	125

Deep Beam Test

Non-loaded	Non-heated	30 $\mu\varepsilon$
Non-loaded	Heated	29
Loaded	Non-heated	21
Loaded	Heated	29

Second Two Span Beam Test

Non-loaded	Non-heated	109 $\mu\varepsilon$
Non-loaded	Heated	121
Loaded	Non-heated	105
Loaded	heated	107

Third Two Span Beam Test

Non-loaded	Non-heated	72 $\mu\varepsilon$
Non-loaded	Heated	86
Loaded	Non-Heated	76
Loaded	Heated	92

T-Section Beam Test 202 $\mu\varepsilon$

Predictions From Codes

Shallow Beams (200 mm deep, rectangular section)

ACI	111 $\mu\varepsilon$
CEB-FIP	21
BS8110 (6 months)	45

Deep Beams

ACI	20 $\mu\varepsilon$
CEB-FIP	11

T-Section Beam

ACI	167 $\mu\varepsilon$
CEB-FIP	69
BS8110 (6 months)	189

Predictions From Segmentation Block Results

Non-heated	No Creep	116 $\mu\varepsilon$
Non-heated	TCF=1.0	110
Non-heated	TCF=2.5	94
Heated	No Creep	187
Heated	TCF=1.0	175
Heated	TCF=2.5	146

TCF = specific creep in tension / specific creep in compression

III.2 30 Day Deflection Coefficients

Experimental Results - Not Corrected for Shrinkage

	Non-heated	Heated
First Single Span Test (0-15 Days)	0.15	0.20
(15-30 Days)	0.08	0.13
Total	0.23	0.33
Second Single Span Test	0.29	0.39
Third Single Span Test	0.44	0.58
Deep Beam Test	0.34	0.36
T-Section Beam Test (19-45 Days)		0.50

Experimental Results - Corrected for Shrinkage

First Single Span Test (0-15 Days)	0.38	0.40
(15-30 Days)	0.11	0.14
Total	0.49	0.54
Second Single Span Test	0.42	0.46
Third Single Span Test	0.54	0.62
Deep Beam Test	0.48	0.51

Predictions From Codes

ACI/CEB-FIP/BS8110	Uncracked	Cracked
First Single Span Test (0-15 Days)	0.35/0.34/-	
(15-30 Days)	0.10/0.10/-	0.03/0.03/-
Total	0.45/0.44/0.52	0.38/0.37/-
Second and Third Single Span Tests	0.47/0.63/0.61	0.12/0.16/0.15
Deep Beam Test	0.45/0.62/0.66	0.13/0.18/0.19
T-Section Beam Test (19-45 Days)	0.71/0.83/1.10	0.09/0.12/0.12

Predictions From Program CREEP

Non-heated/Heated	Uncracked	Cracked
First Single Span Test (0-15 Days)	0.38/0.42	
(15-30 Days)	0.18/0.22	0.06/0.07
Total	0.56/0.64	0.44/0.49
Second Single Span Test	0.56/0.62	0.18/0.20
Third Single Span Test	0.56/0.66	0.18/0.21
Deep Beam Test	0.59/0.73	0.25/0.33
T-Section Beam Test (19-45 Days)	-/0.68	-/0.11

III.3 30 Day Predictions of Support Reaction Changes

	Heated	Non-heated
Uncracked Analysis		
Temperature Gradient Effect	262 N	- N
Shrinkage Effect	-523	-959
Total	-261	-959

Partially Cracked Analysis

Temperature Gradient Effect	148 N	- N
Shrinkage Effect	-287	-562
Total	-139	-562

FIGURES

FIGURE 1. ENVIRONMENTAL FACTORS AFFECTING BRIDGE TEMPERATURES (REF 17)

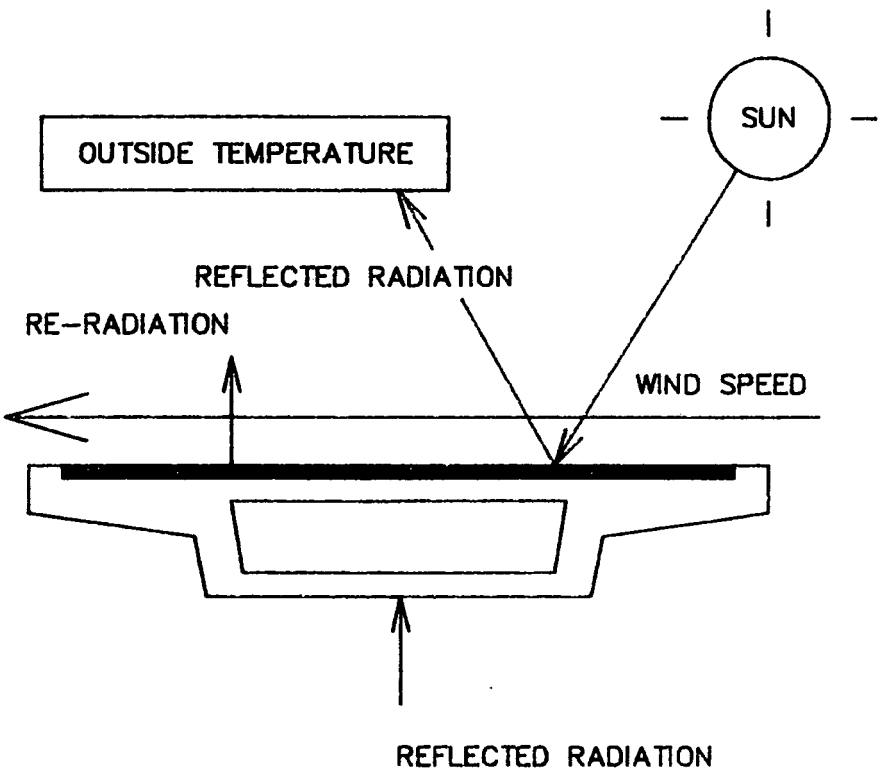

FIGURE 2. THERMAL STRESSES AND STRAINS

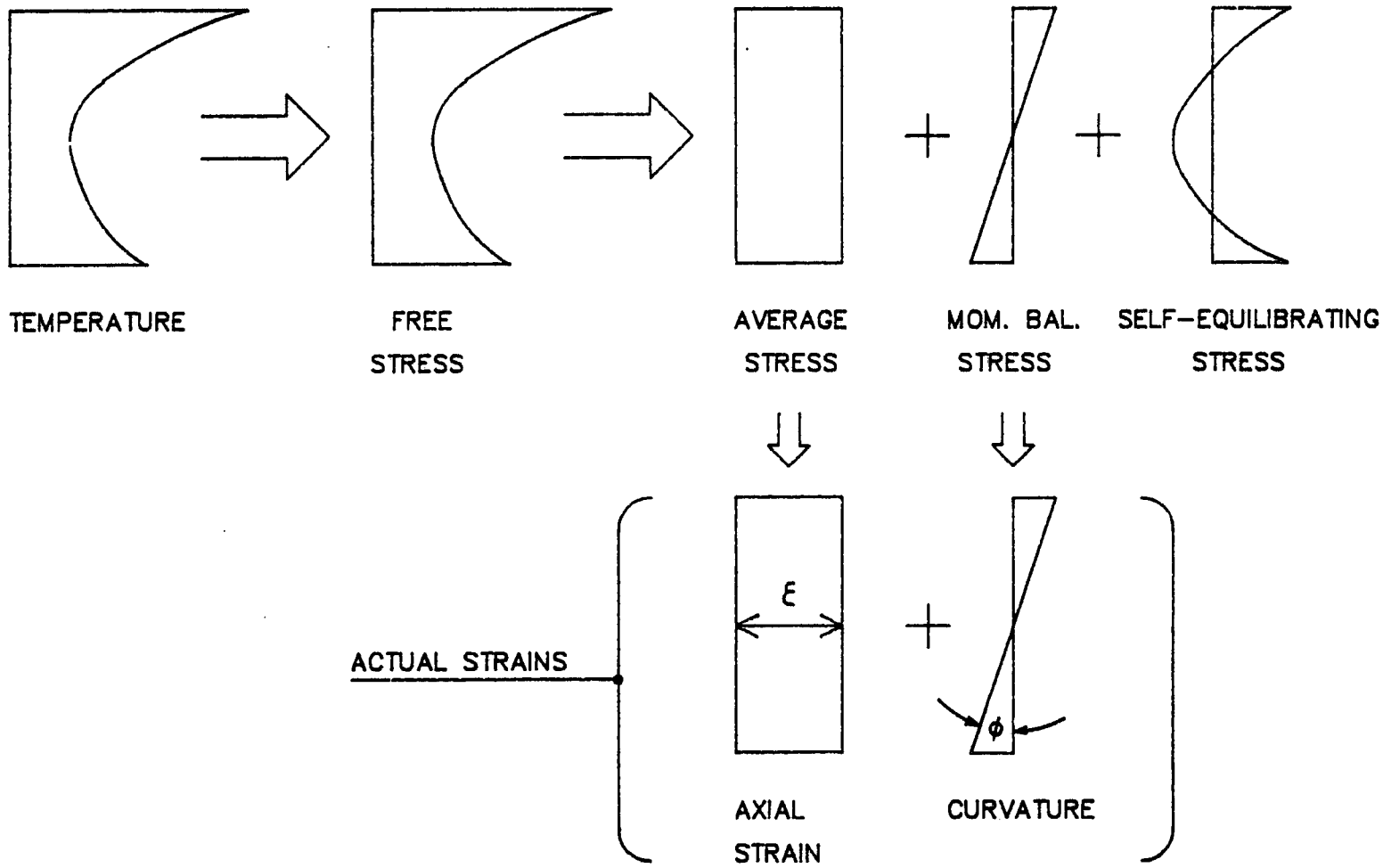

FIGURE 3. EXAMPLE DESIGN TEMPERATURE PROFILES

a) POSITIVE TEMPERATURE DIFFERENCES

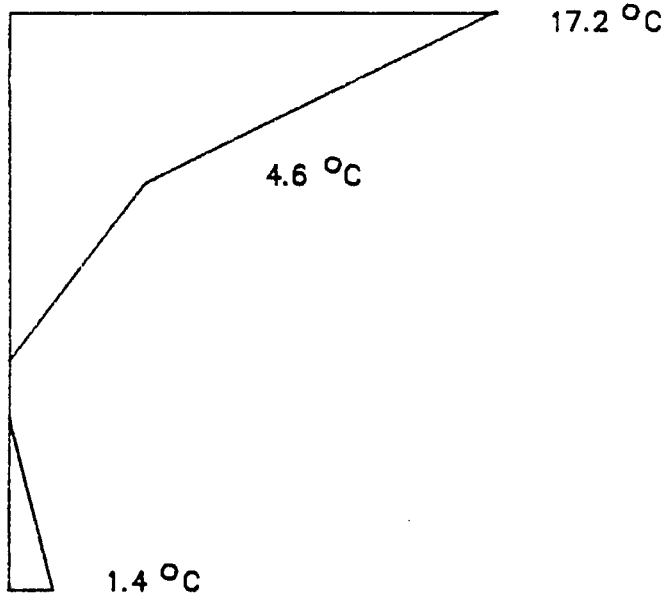

b) REVERSED TEMPERATURE DIFFERENCES

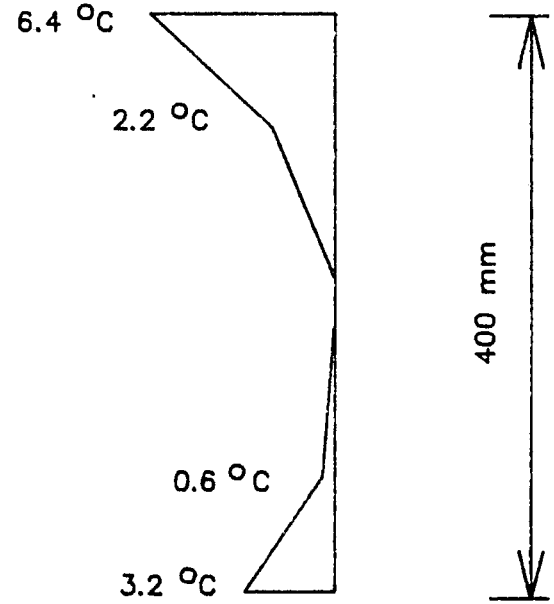

DEPTH OF SURFACING = 50 mm

FIGURE 4. ALPHA V. MOISTURE CONTENT (REF 58)

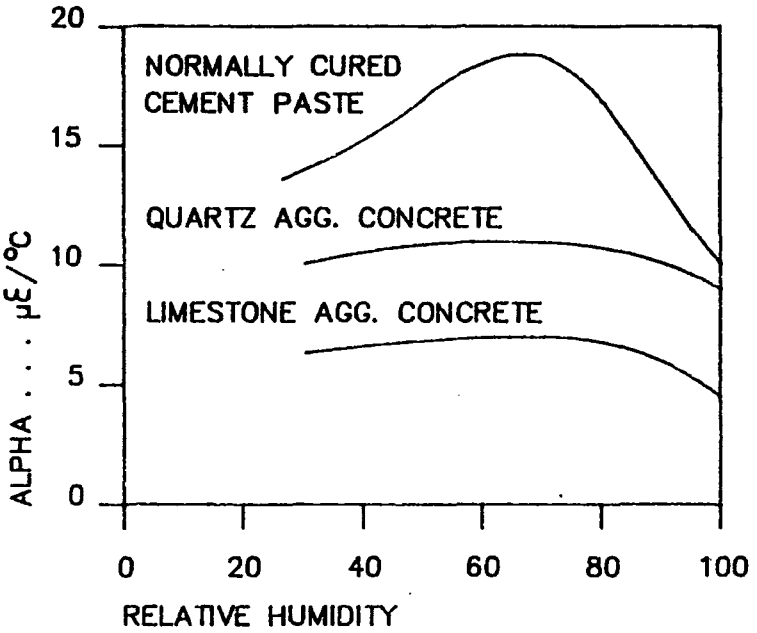

FIGURE 5. PERMEABILITY V. CAPILLARY POROSITY (REF 61)

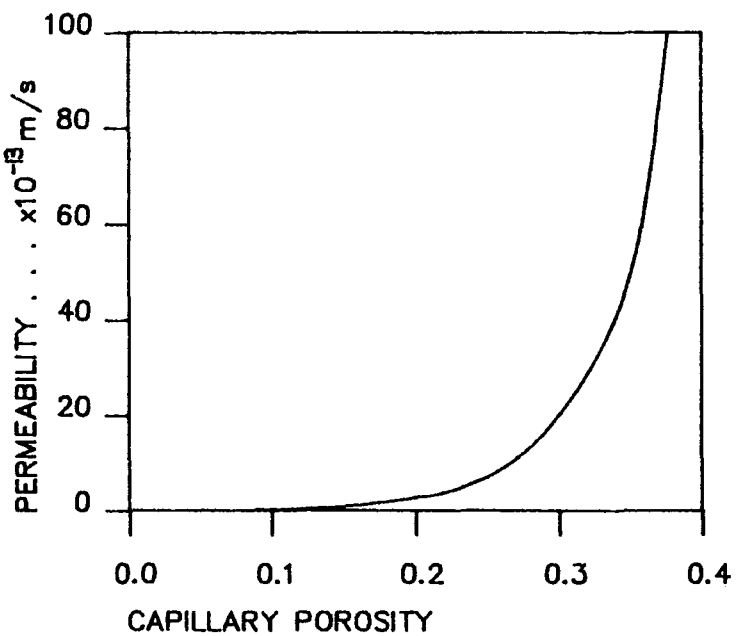

FIGURE 6. RATE–OF–DRYING CURVE (REF 68)

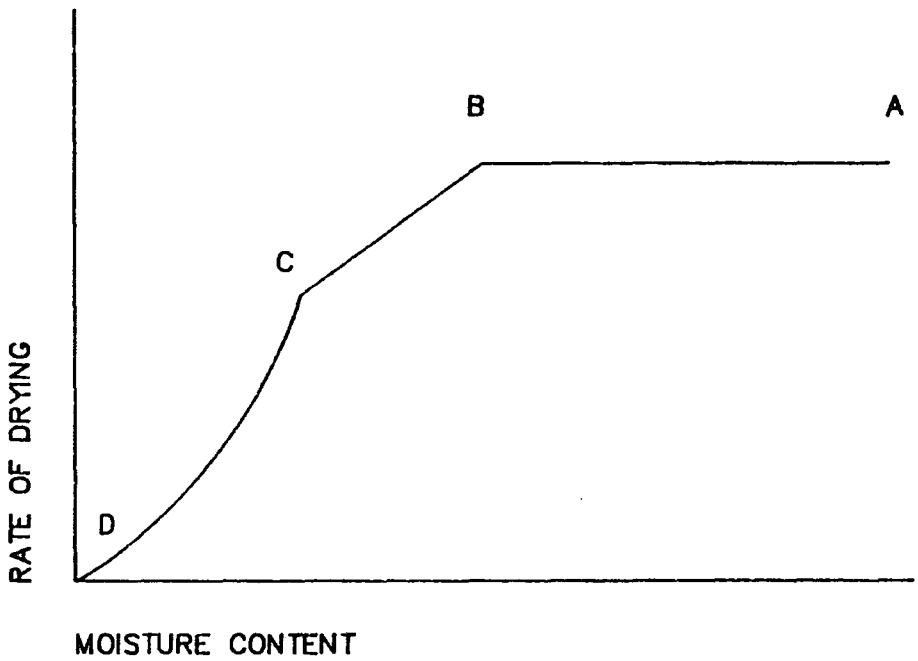

FIGURE 7. MOISTURE CONTENT V. RELATIVE HUMIDITY (REF 79)

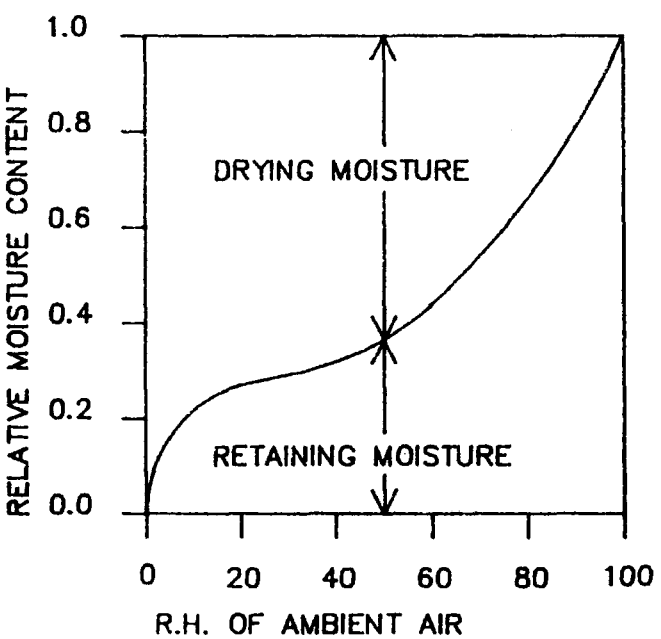

FIGURE 8. TYPICAL CREEP CURVE

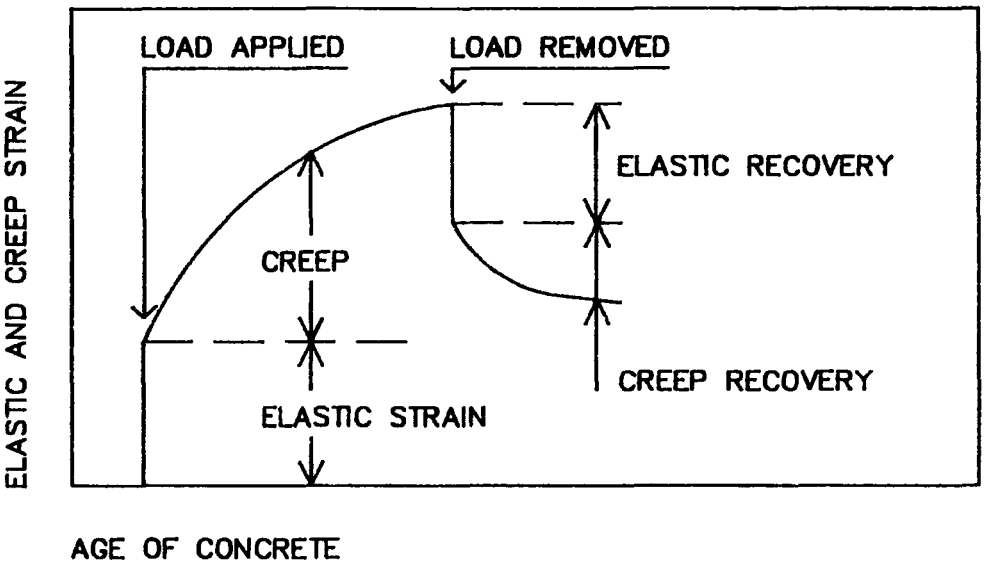

FIGURE 9. SPECIFIC THERMAL CREEP CURVE

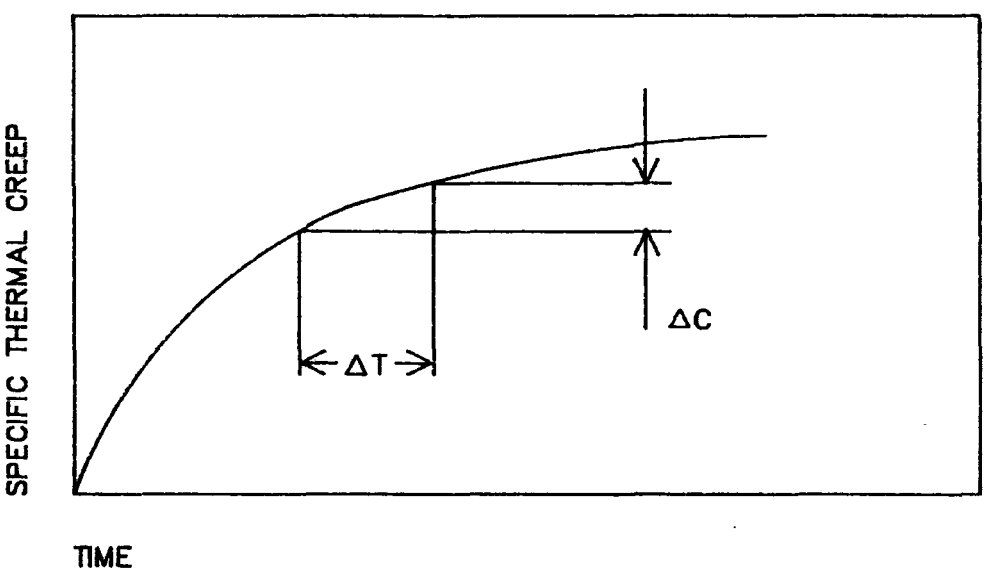

FIGURE 10. SHRINKAGE V. WEIGHT LOSS (REF 122)

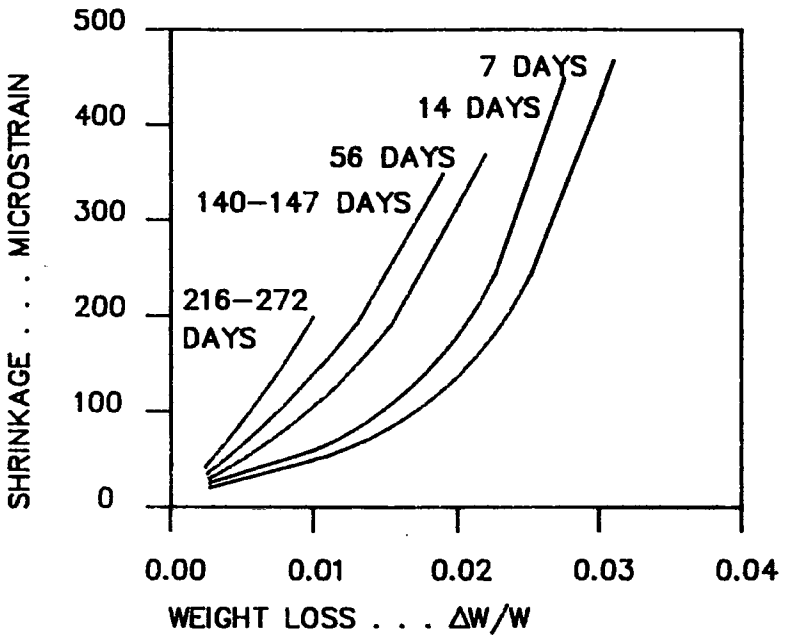

FIGURE 11. BEAM GEOMETRIES AND DEMEC STUD LOCATIONS

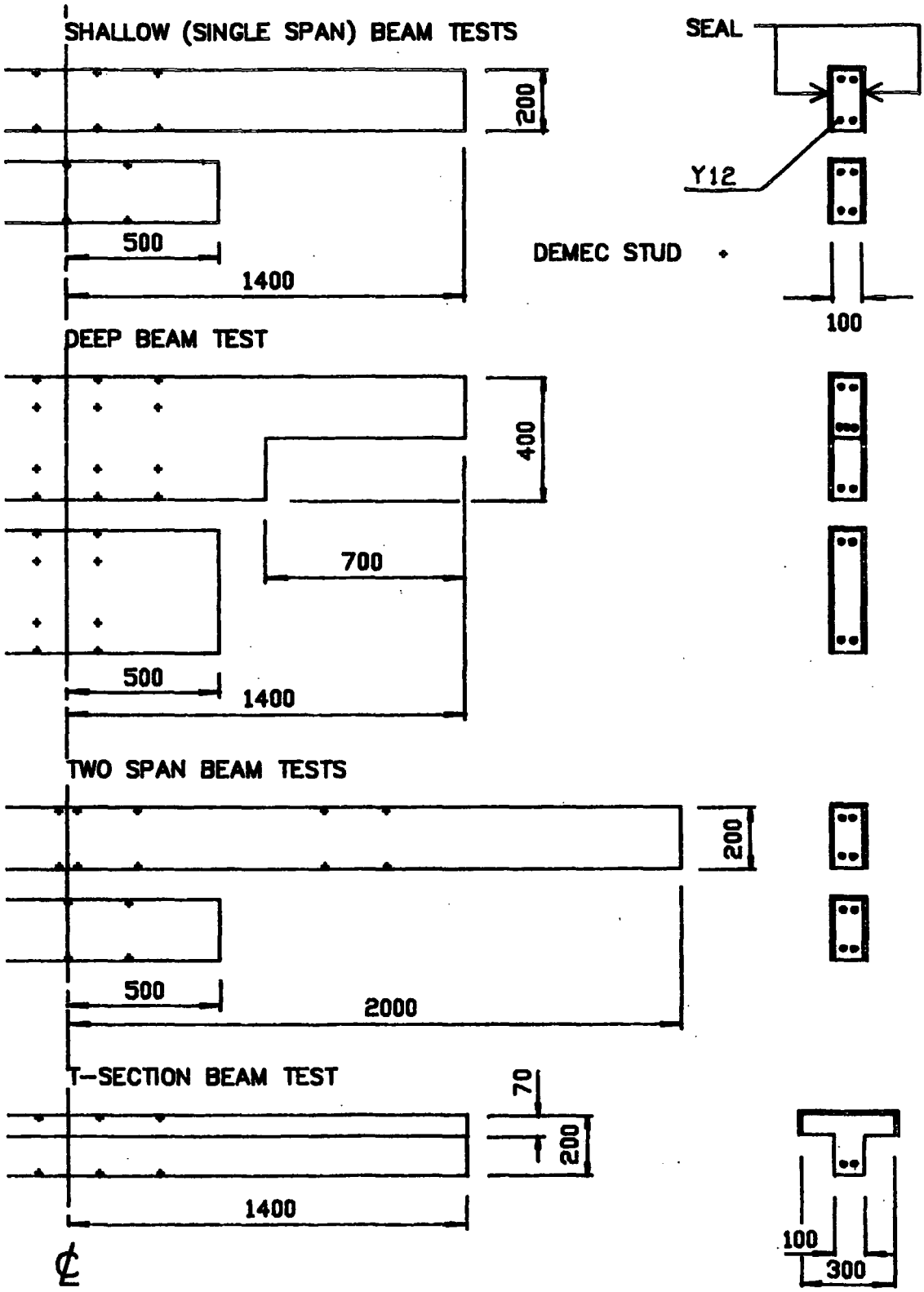

FIGURE 12. T-SECTION BEAM THERMOCOUPLE LOCATIONS

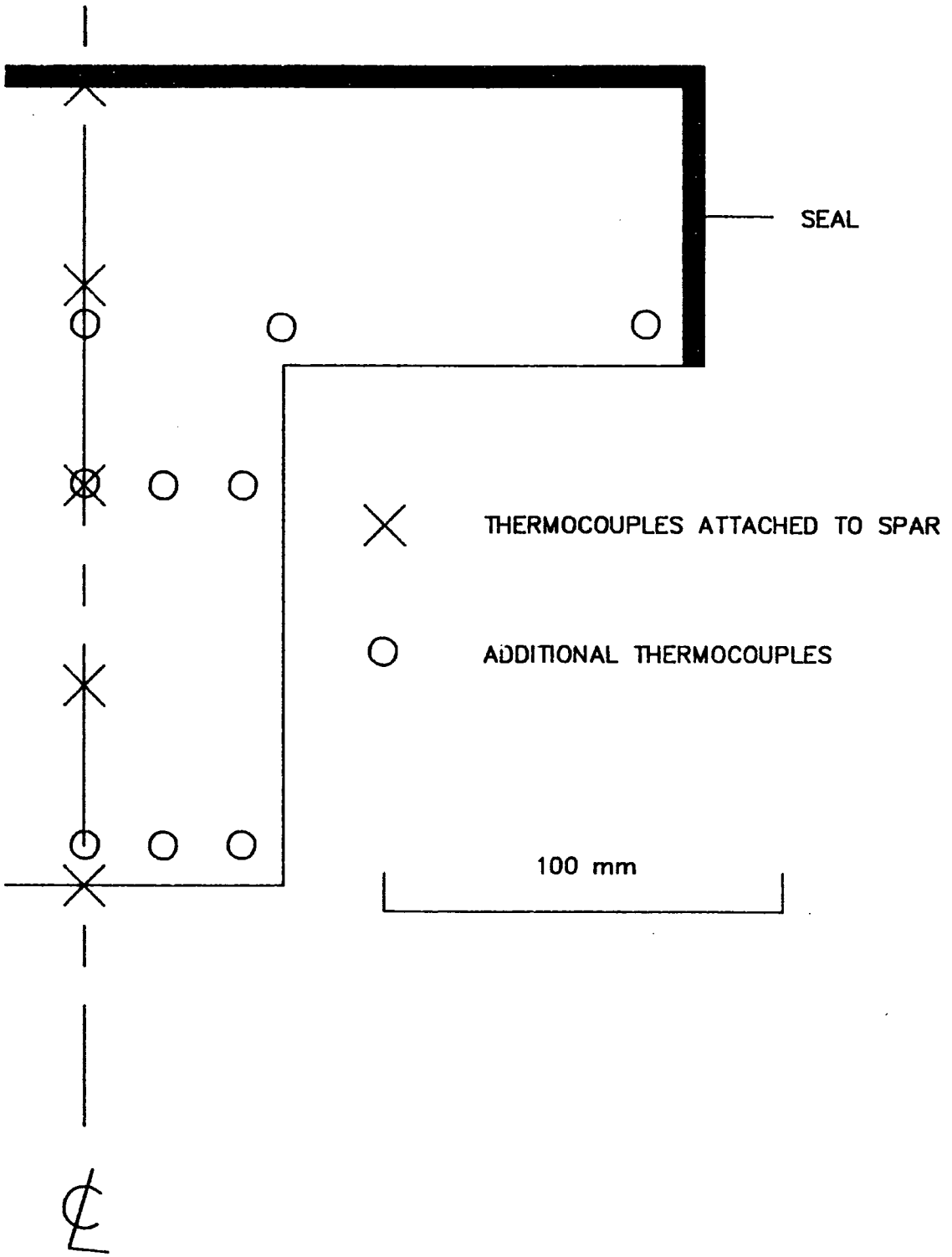

FIGURE 13. BEAM LOADING ARRANGEMENTS

SINGLE SPAN ARRANGEMENT

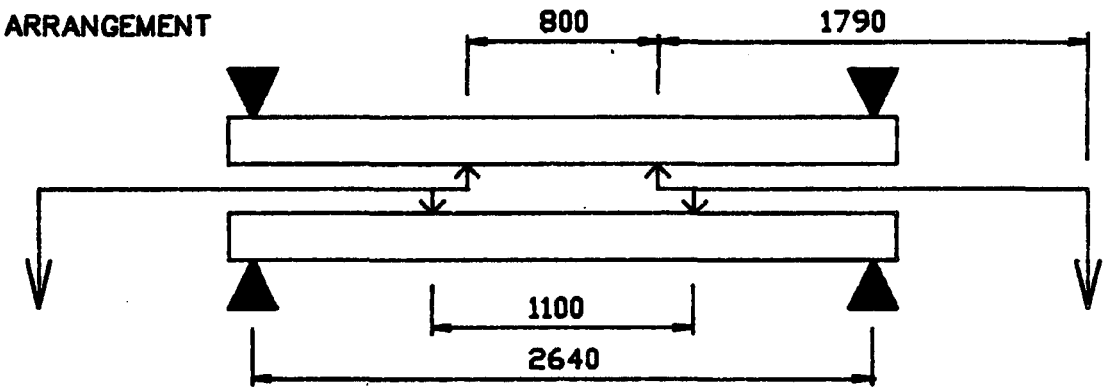

TWO SPAN ARRANGEMENT

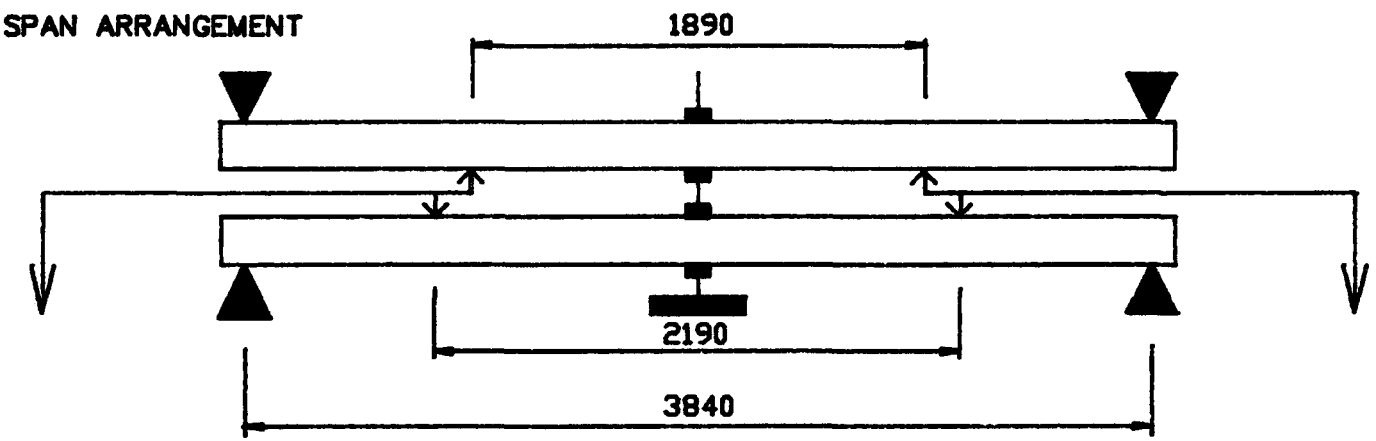

FIGURE 14. BEAM LOADING BEARINGS

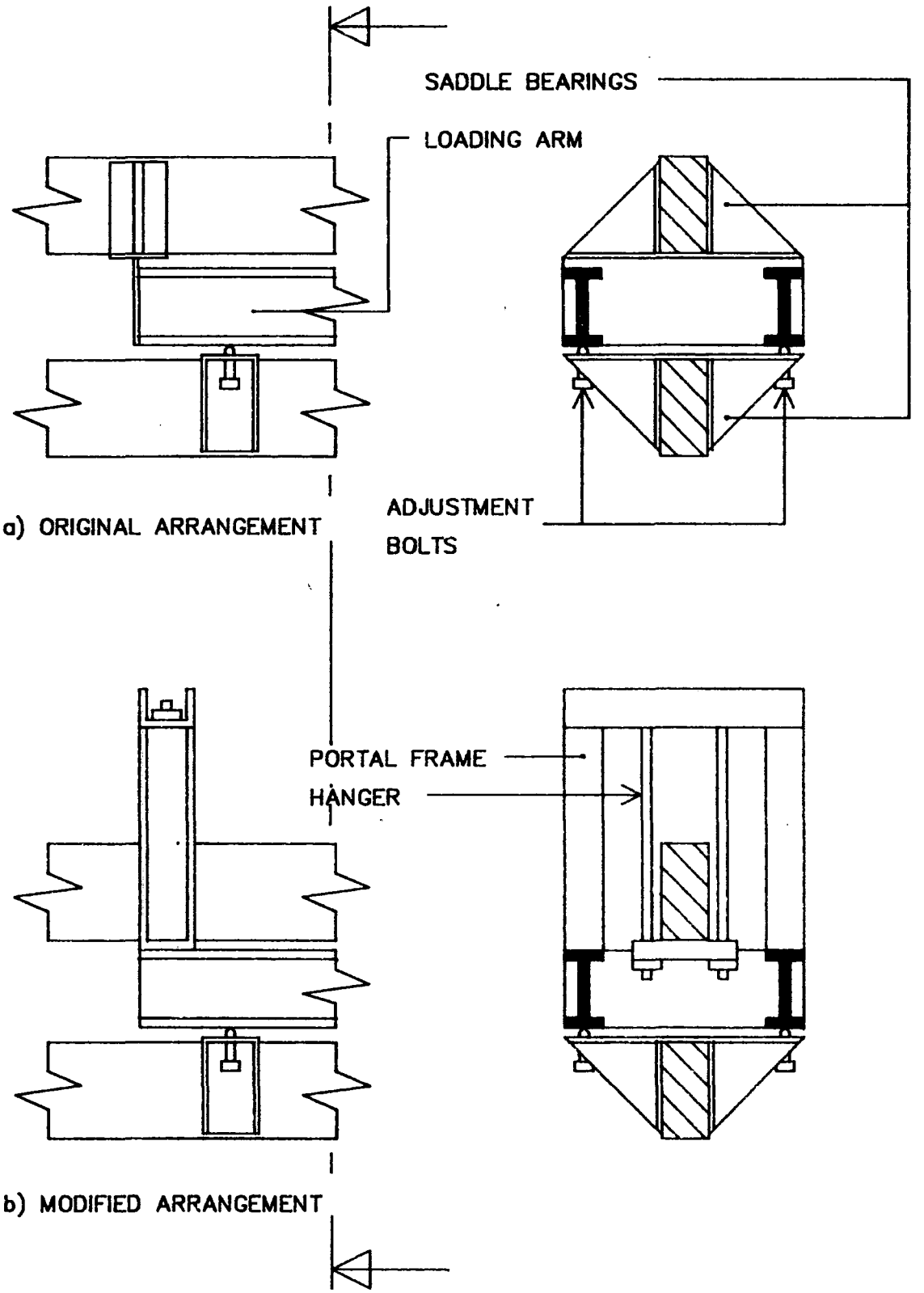

FIGURE 15. CENTRAL RESTRAINT ARRANGEMENT

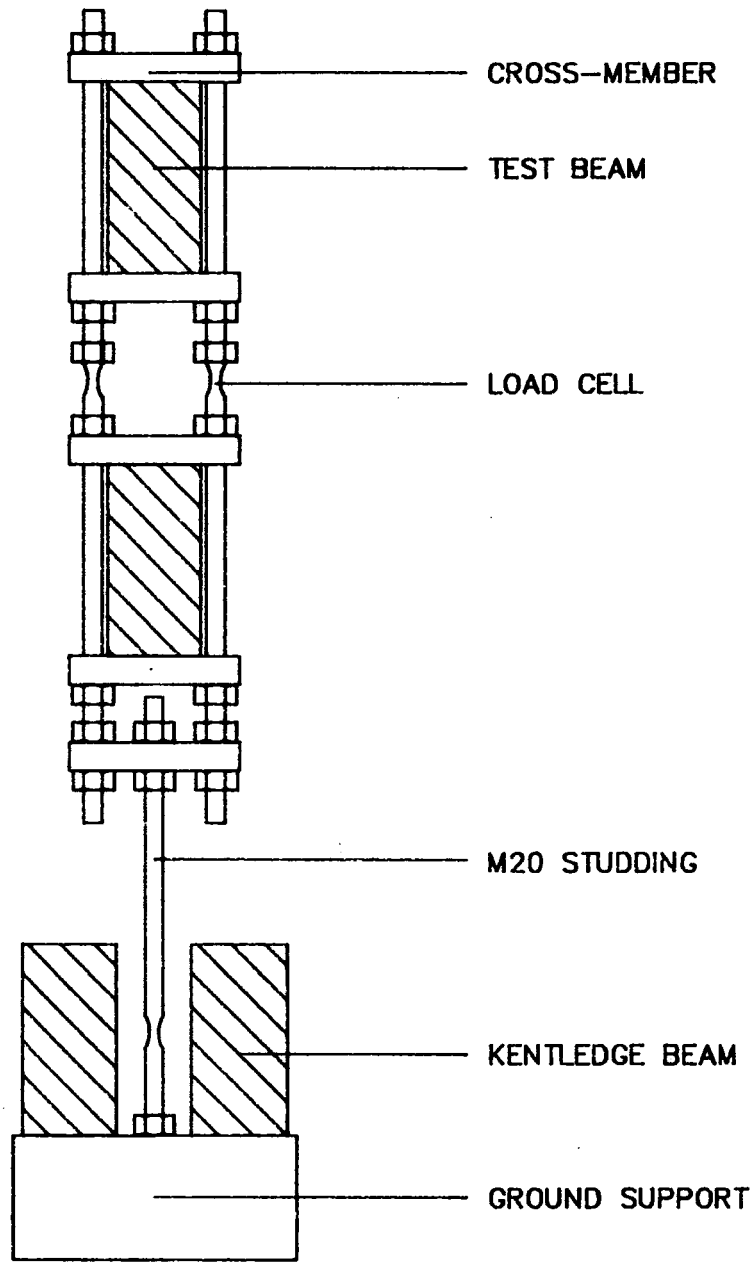

FIGURE 16. TWO SPAN BENDING MOMENT DIAGRAMS

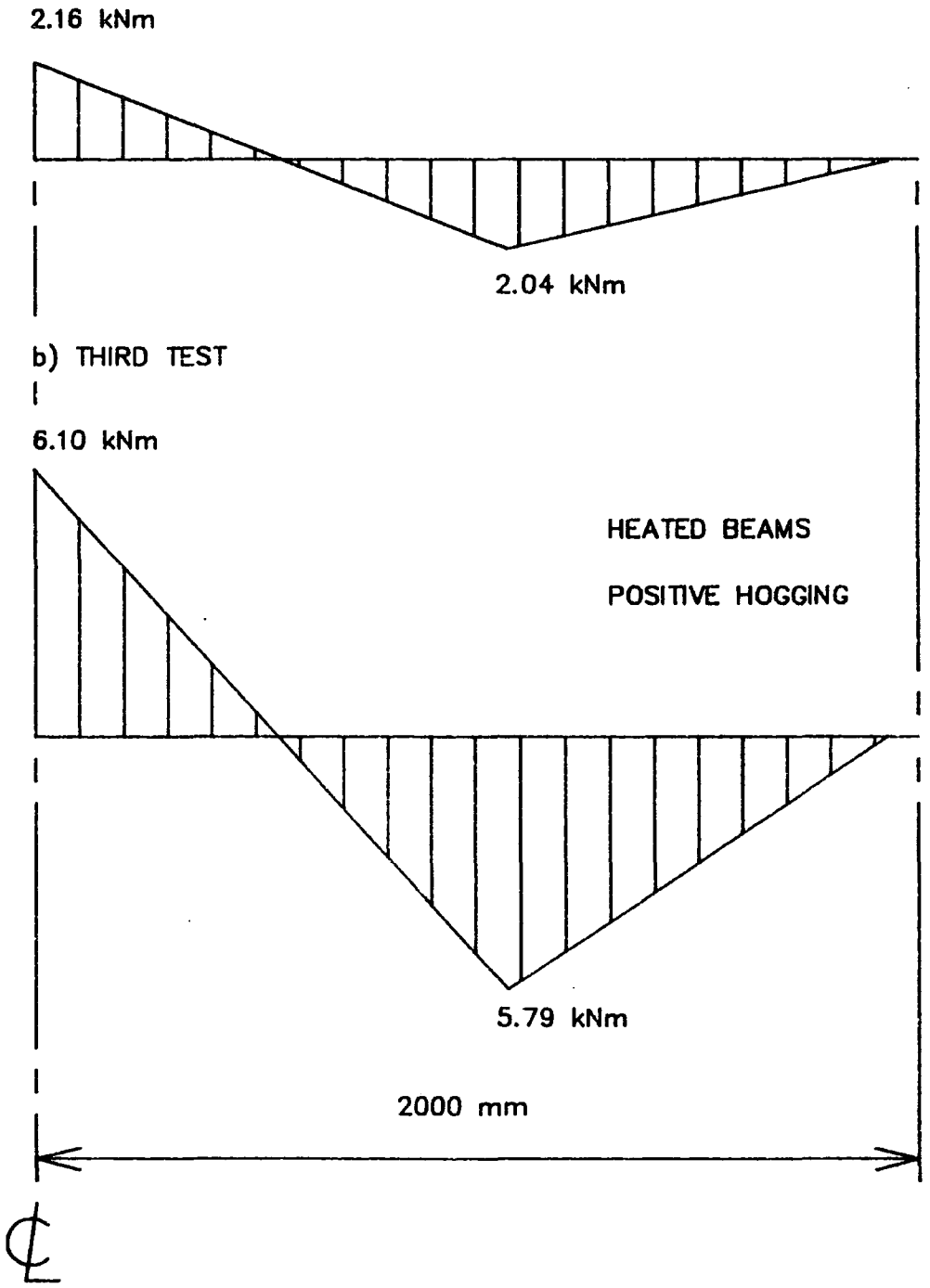

FIGURE 17. THERMAL RESPONSE OF A TWO SPAN BEAM

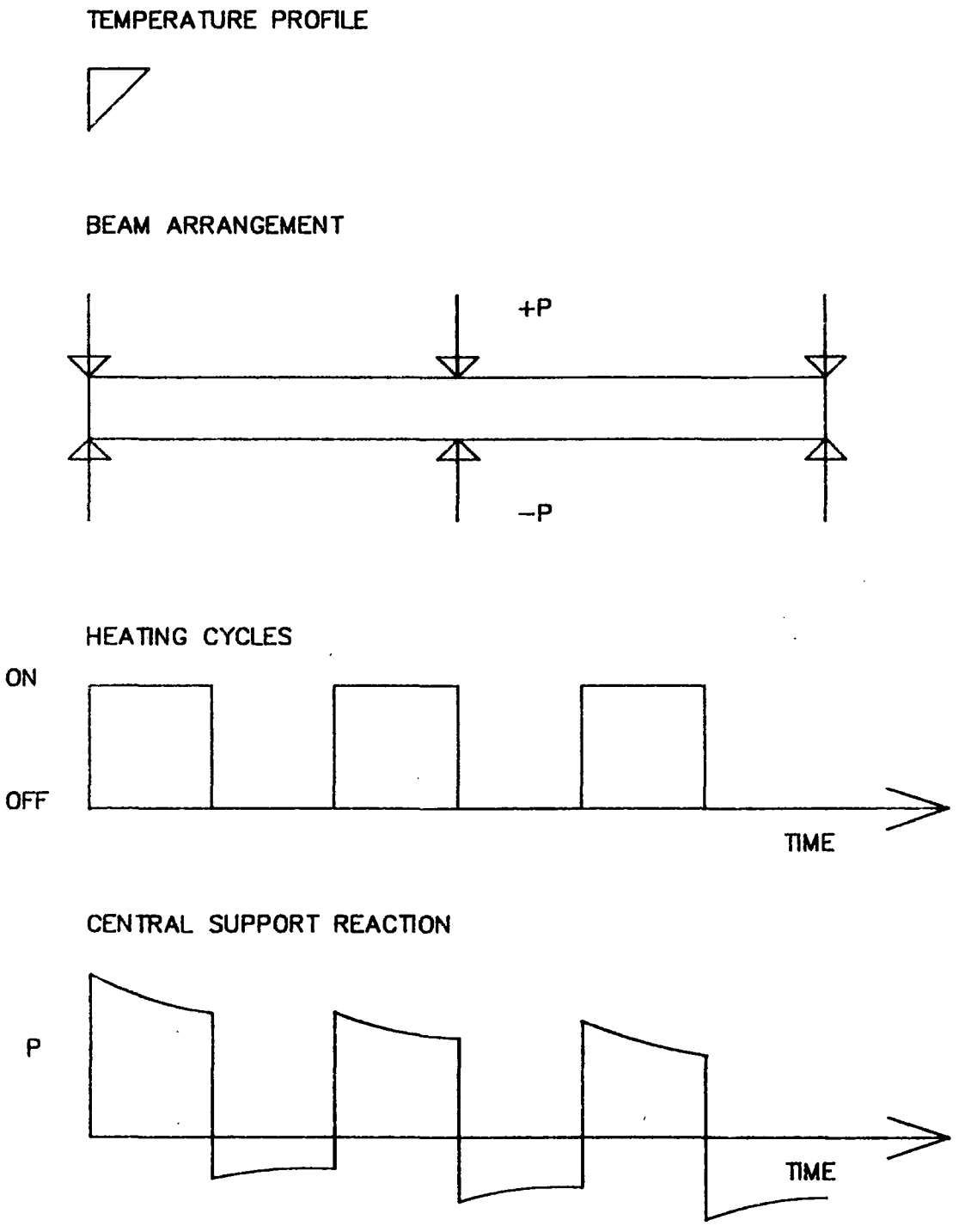

PHOTOGRAPHS

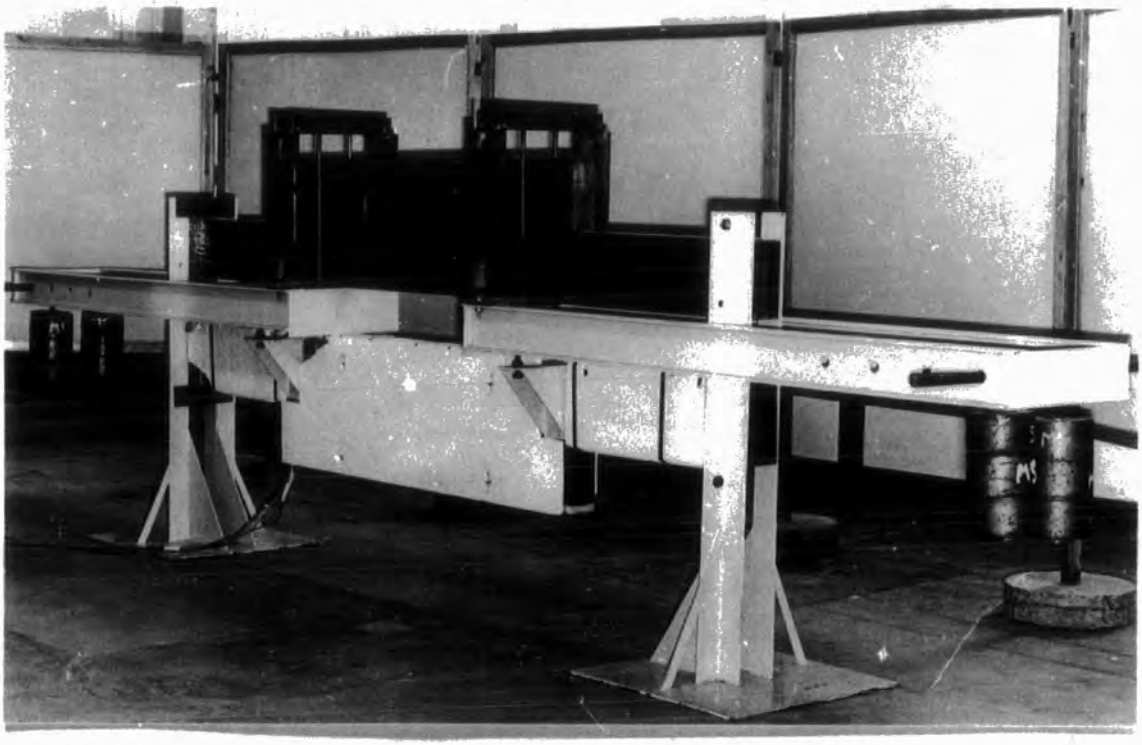

PHOTOGRAPH 1. DEEP BEAM TEST

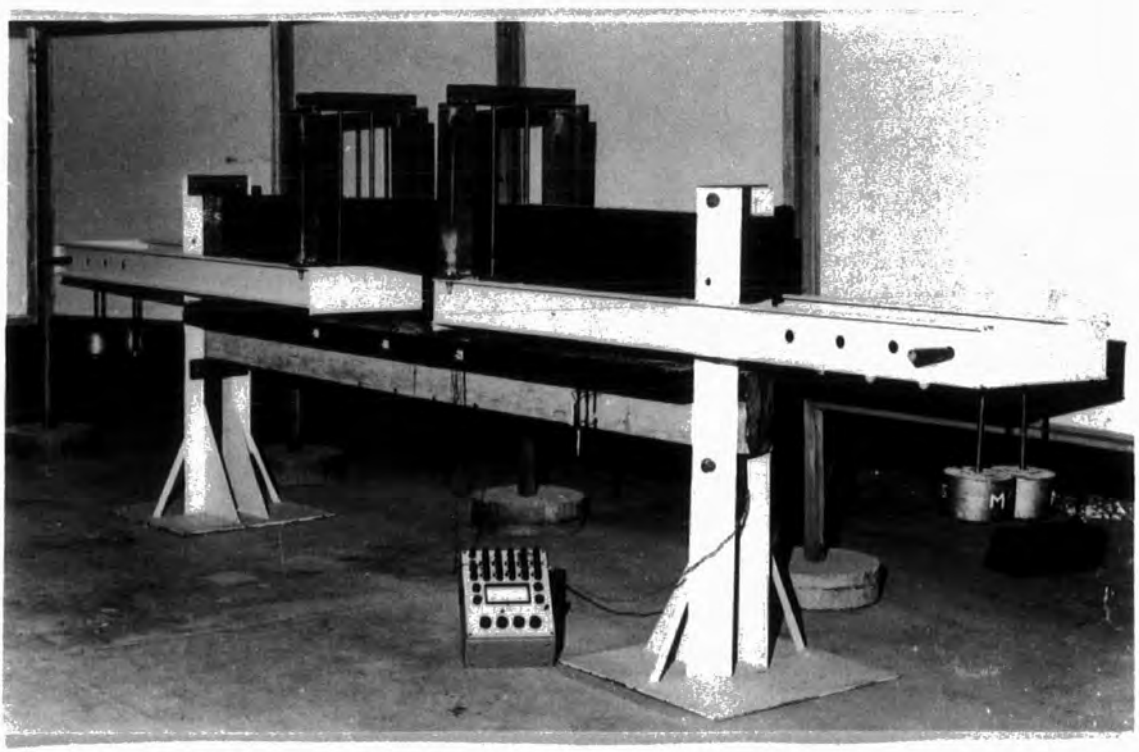

PHOTOGRAPH 2. T-SECTION BEAM TEST

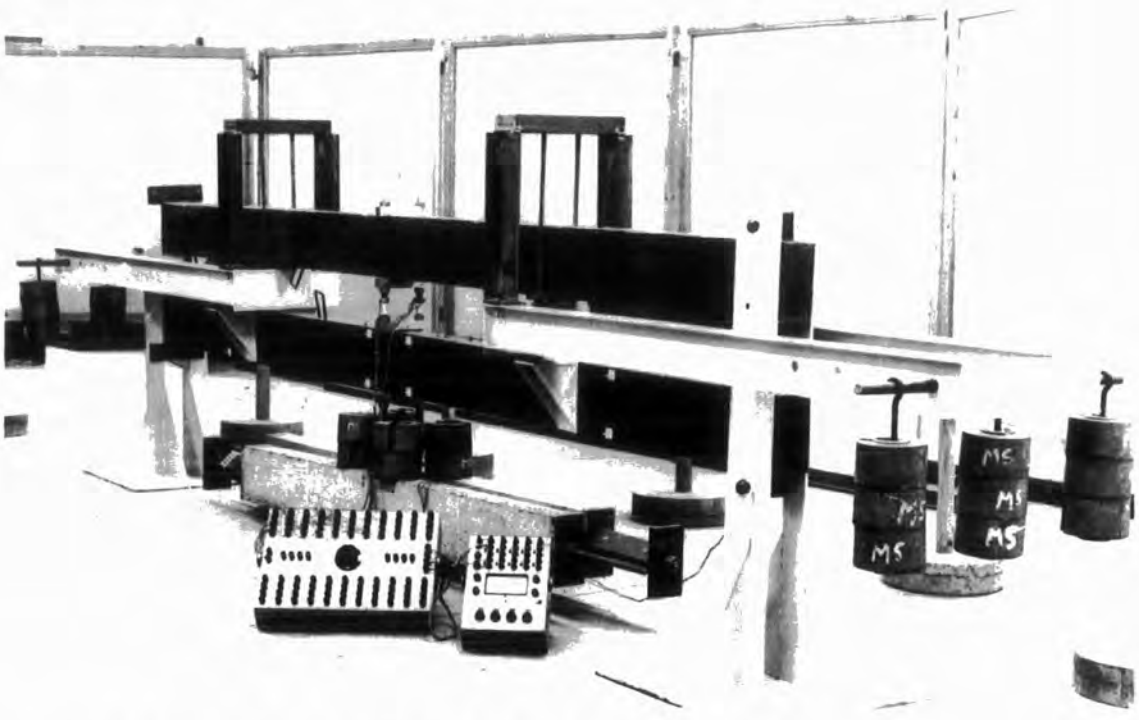

PHOTOGRAPH 3. TWO SPAN BEAM TEST

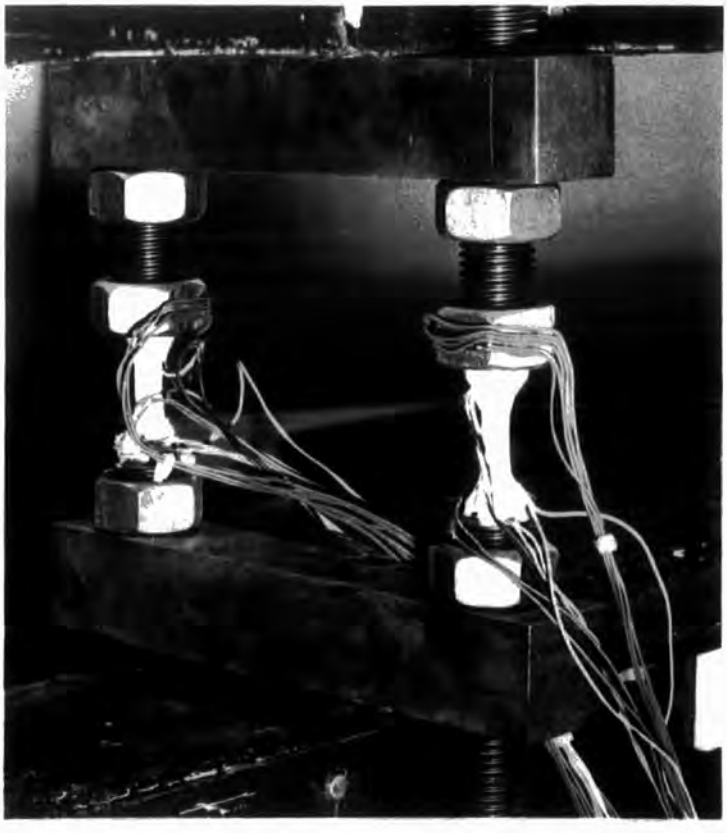

PHOTOGRAPH 4. CENTRAL RESTRAINT DETAIL

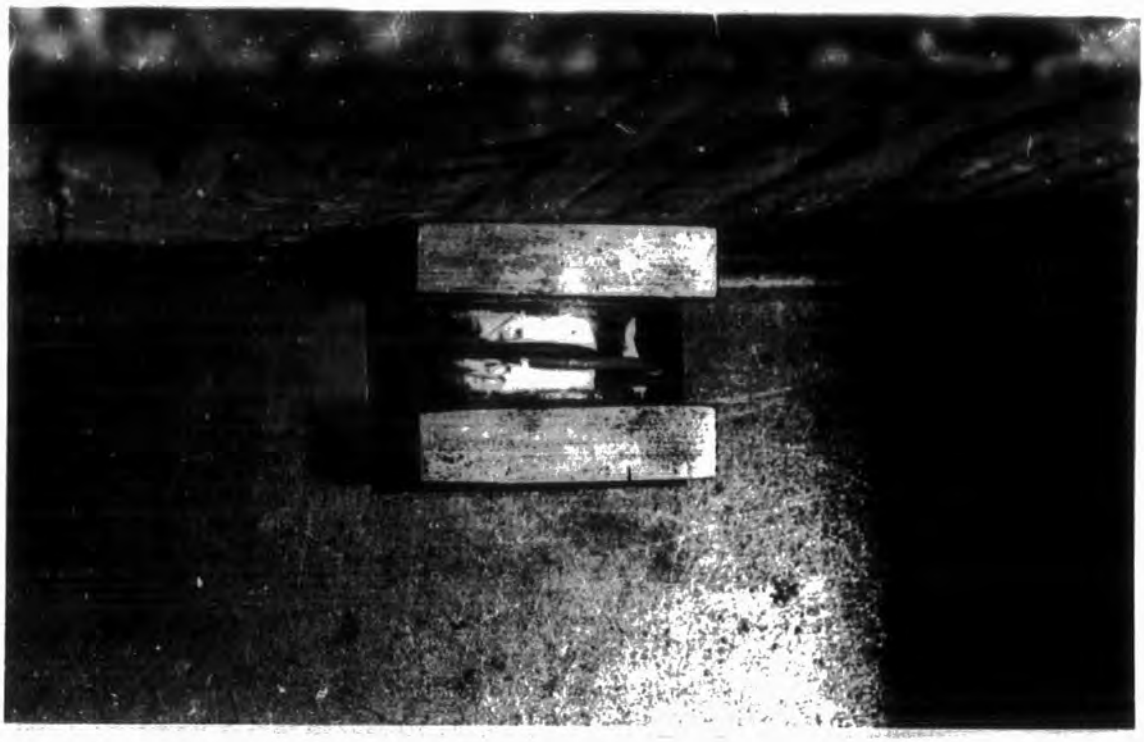

PHOTOGRAPH 5. END SUPPORT LOAD CELL

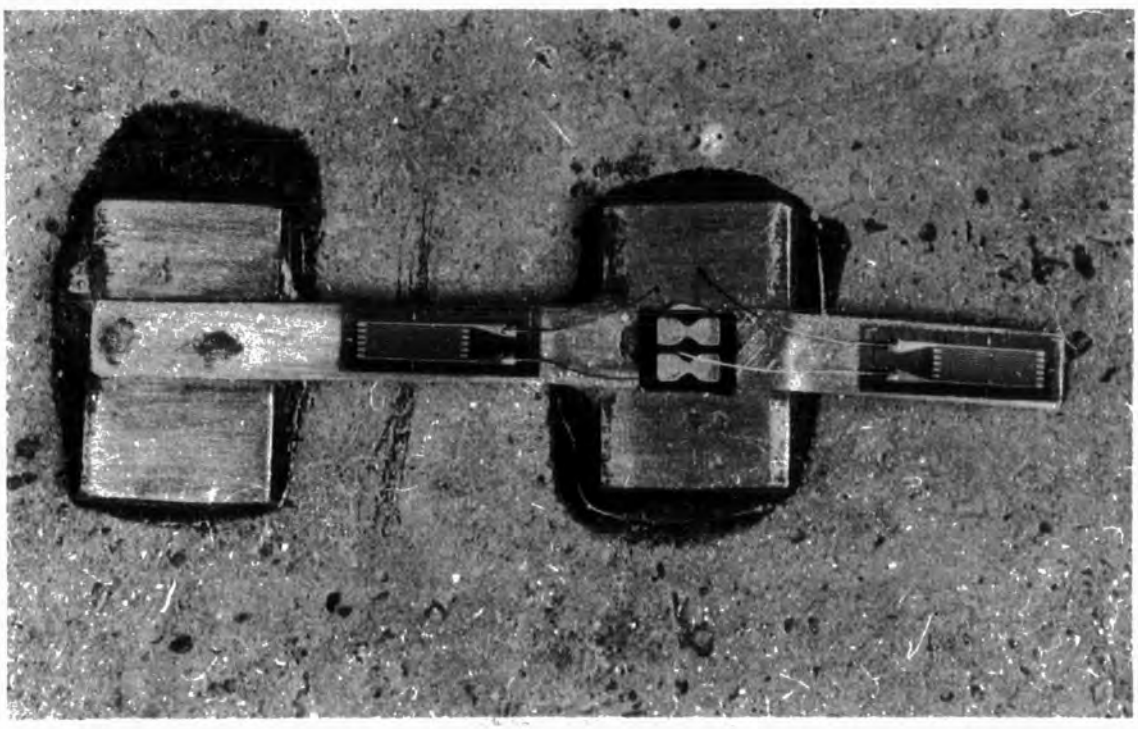

PHOTOGRAPH 6. CRACK GAUGE

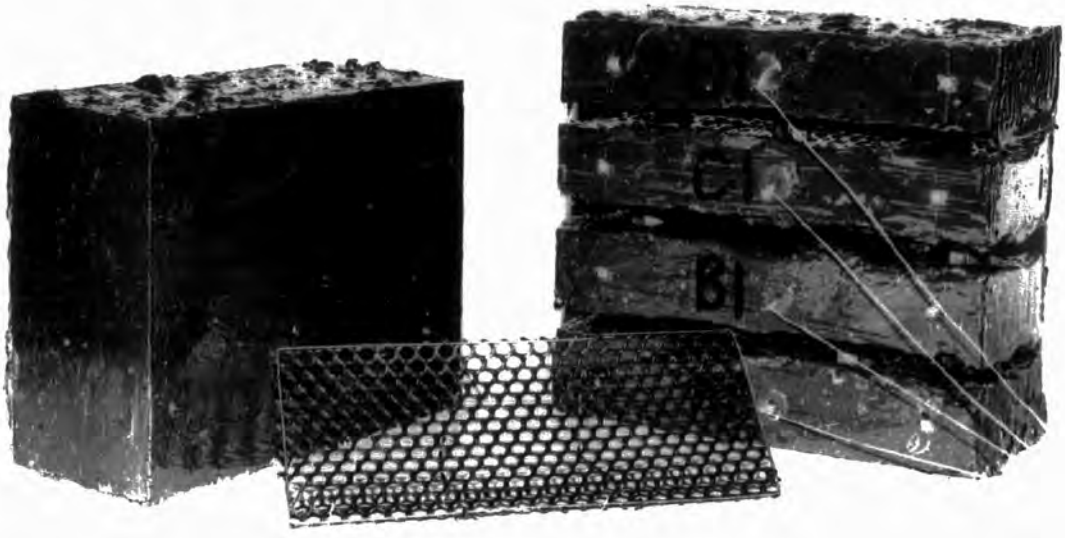

PHOTOGRAPH 7. SEGMENTATION BLOCK

GRAPHS OF EXPERIMENTAL RESULTS

KEY FOR RATIO RESULTS:

(GRAPHS 35 TO 65)

FIRST SET OF READINGS	△
SECOND SET OF READINGS	×
THIRD SET OF READINGS	+
FOURTH SET OF READINGS	Y

GRAPH 1. MOISTURE CONTENT IN CYLINDERS
CYLINDERS NOT HEATED

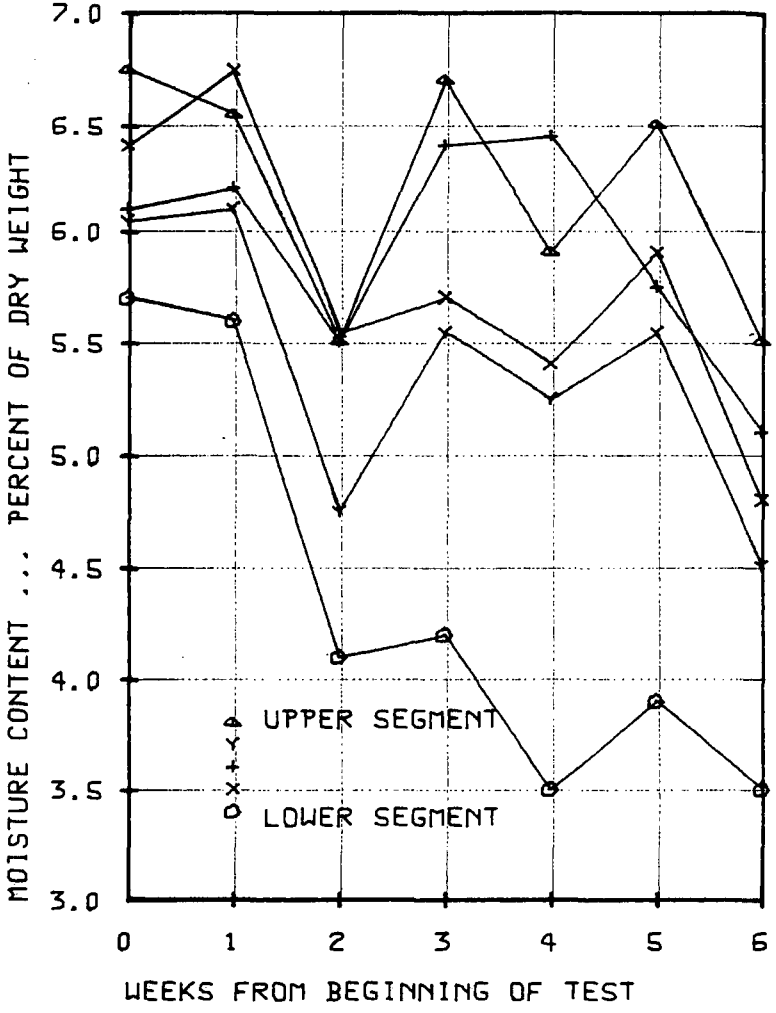

GRAPH 2. MOISTURE CONTENT IN CYLINDERS
CYLINDERS HEATED

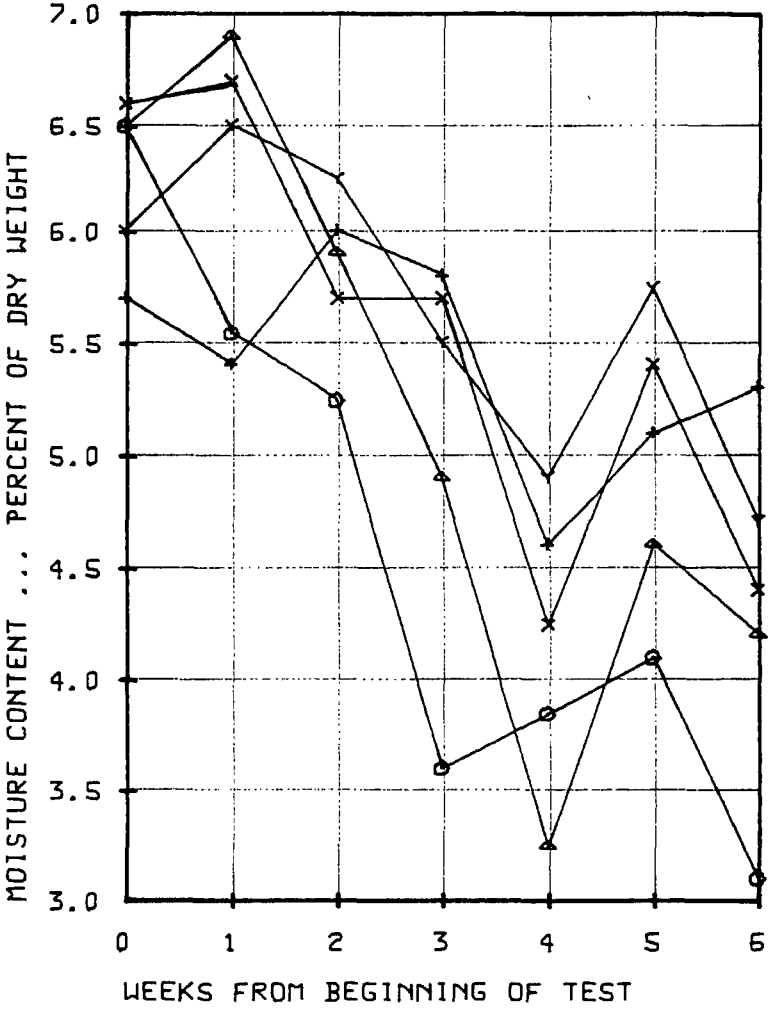

GRAPH 3. MOISTURE CONTENT IN SEGMENTATION BLOCKS BLOCKS NOT HEATED

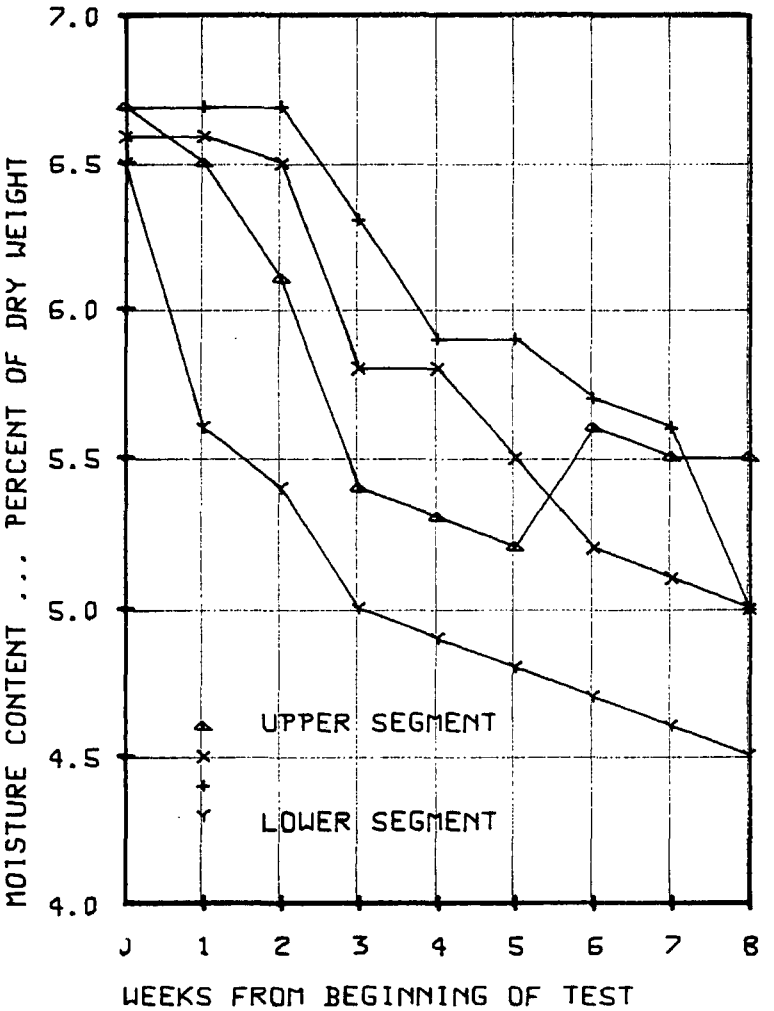

GRAPH 4. MOISTURE CONTENT IN SEGMENTATION BLOCKS BLOCKS HEATED

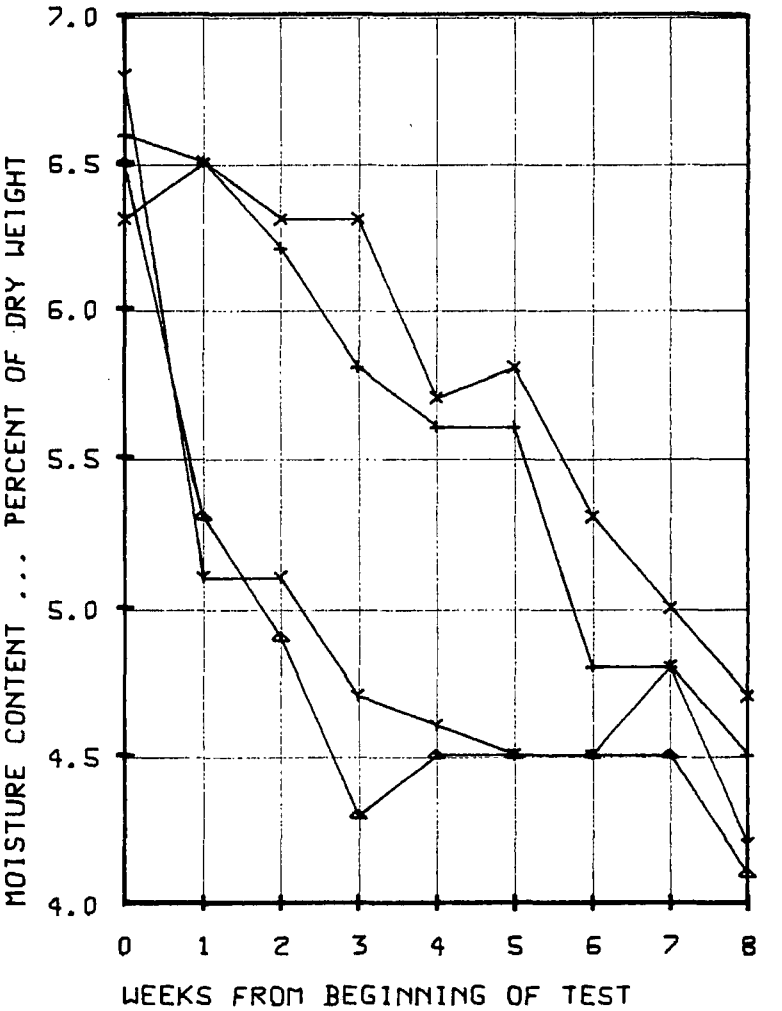

GRAPH 5. MOISTURE LOSS PROFILES
BLOCKS NOT HEATED

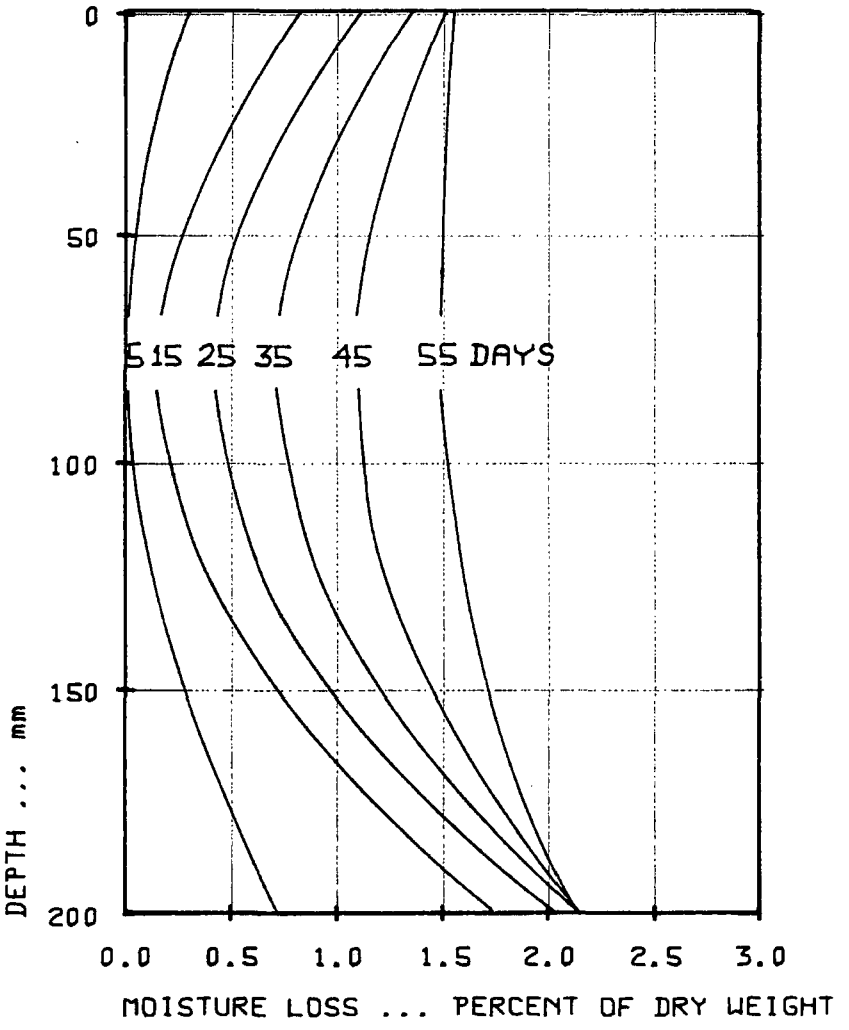

GRAPH 6. MOISTURE LOSS PROFILES
BLOCKS HEATED

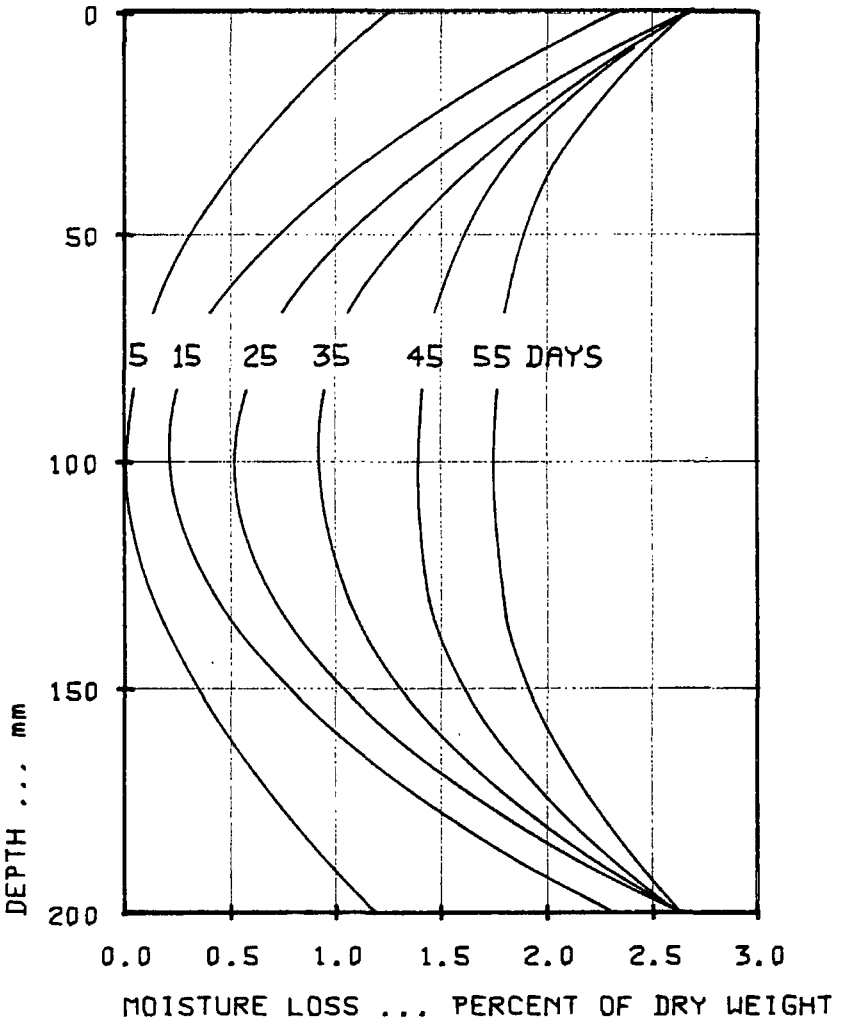

GRAPH 7. SHRINKAGE V. WEIGHT LOSS
FIRST BATCH

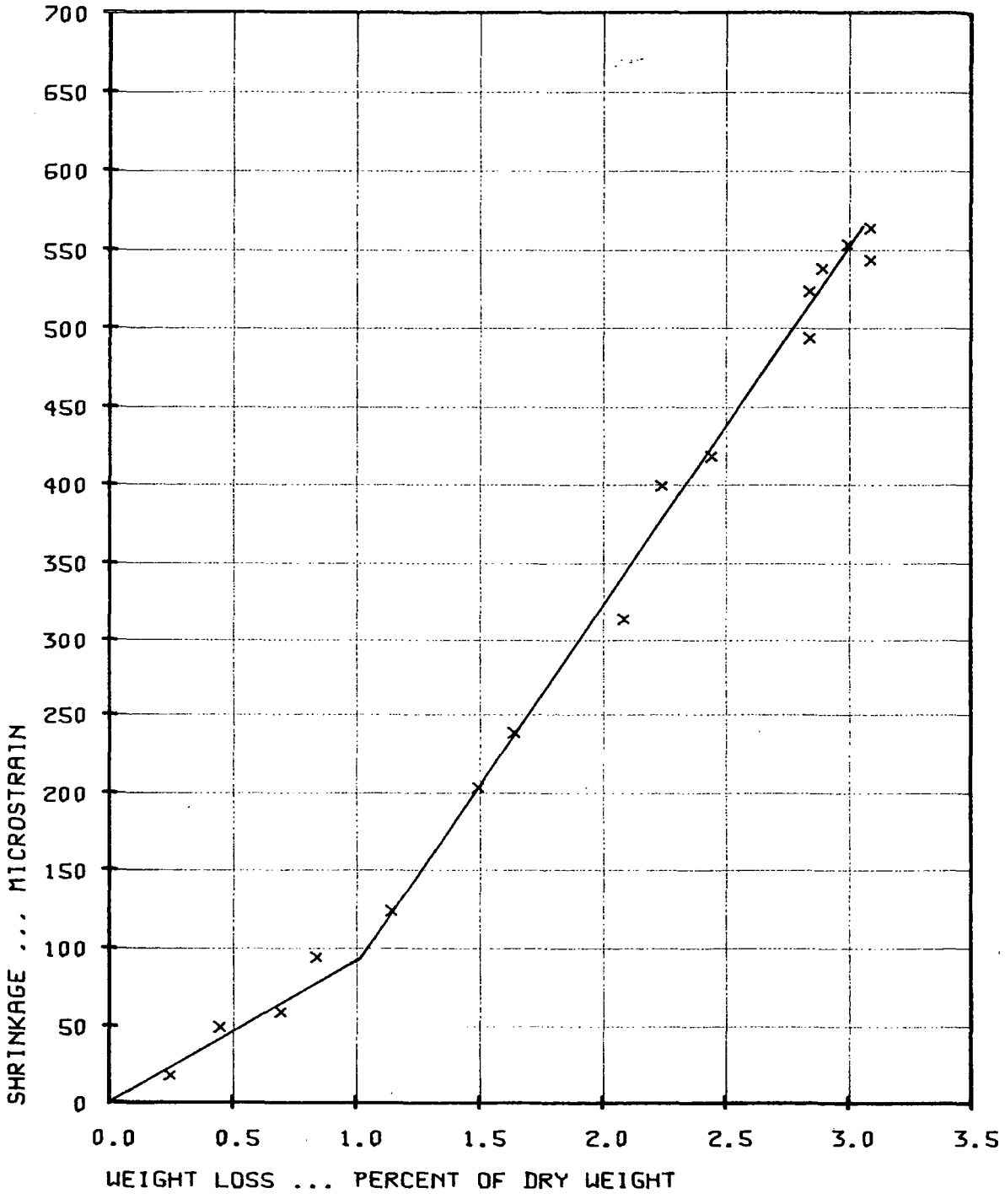

GRAPH 8. SHRINKAGE V. WEIGHT LOSS
SECOND BATCH

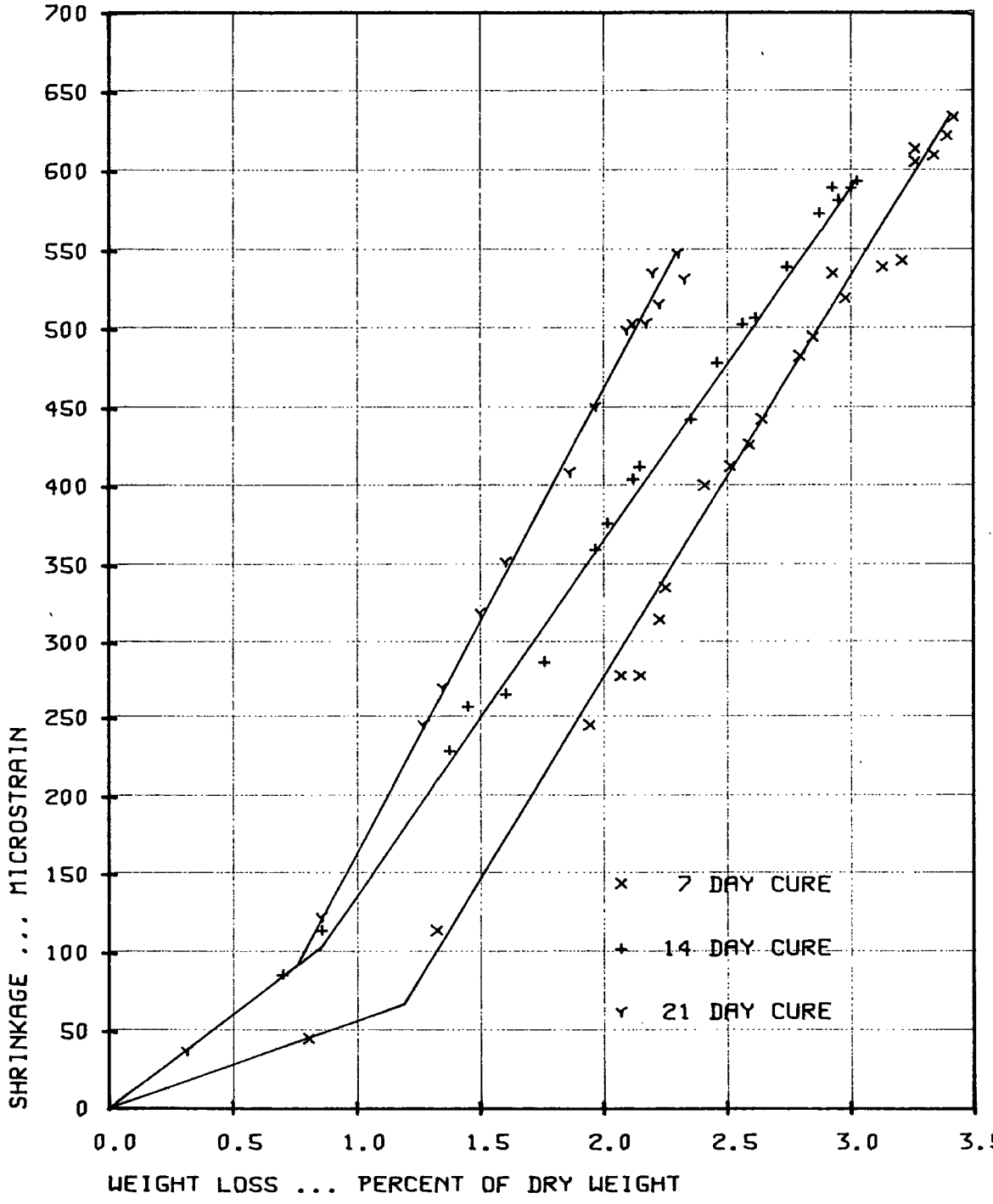

GRAPH 9. MAXIMUM TENSILE SHRINKAGE STRESSES
BLOCKS NOT HEATED

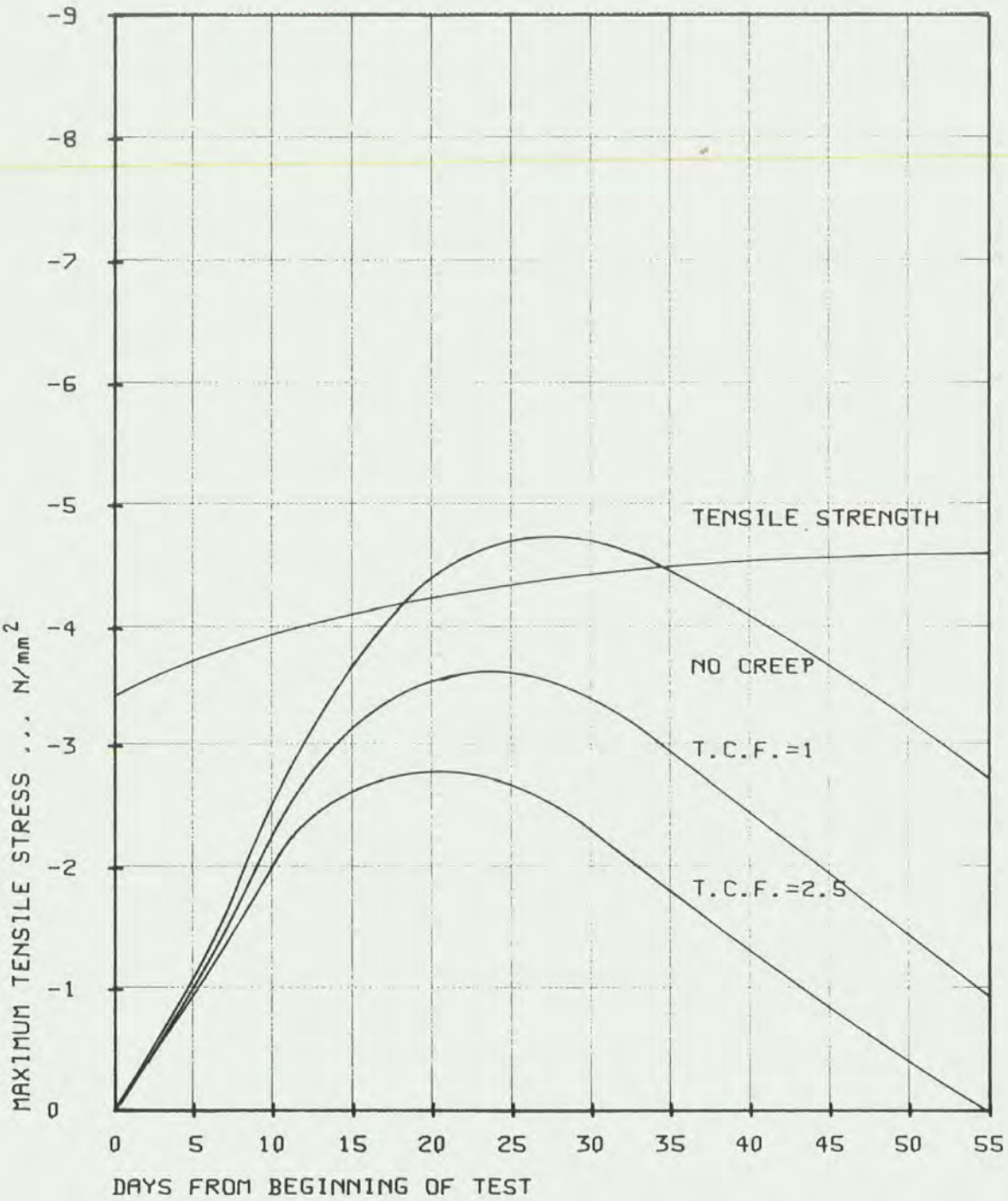

GRAPH 10. MAXIMUM TENSILE SHRINKAGE STRESSES
BLOCKS HEATED

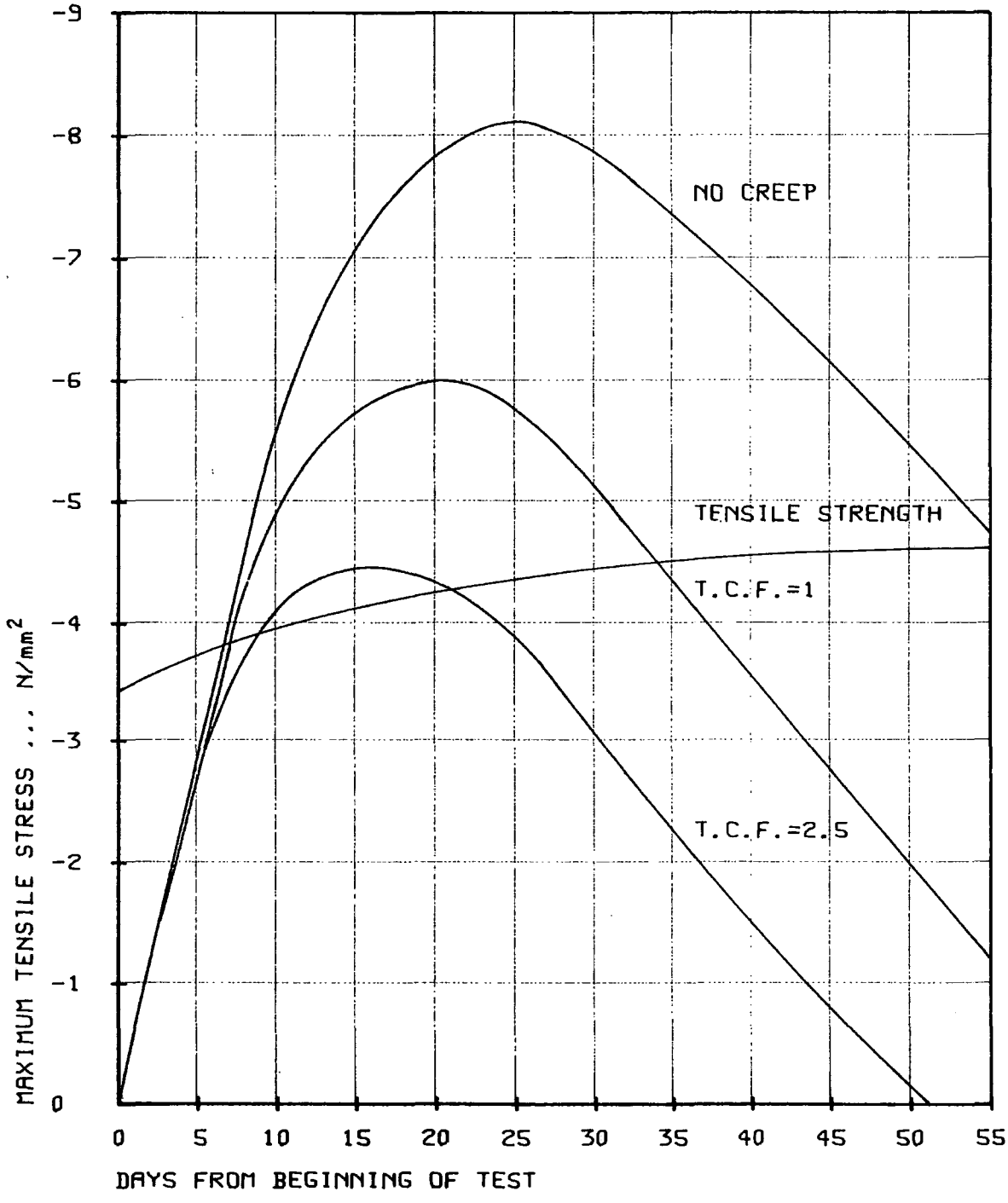

GRAPH 11. ALPHA V. TIME
FIRST BATCH

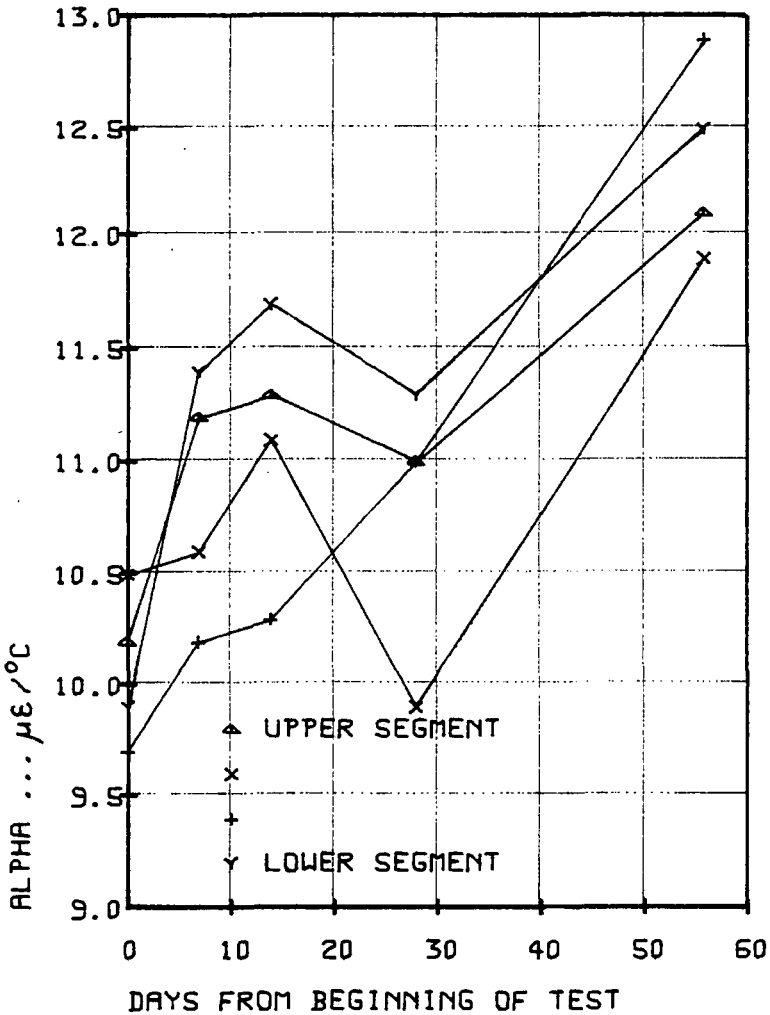

GRAPH 12. ALPHA PROFILES
FIRST BATCH

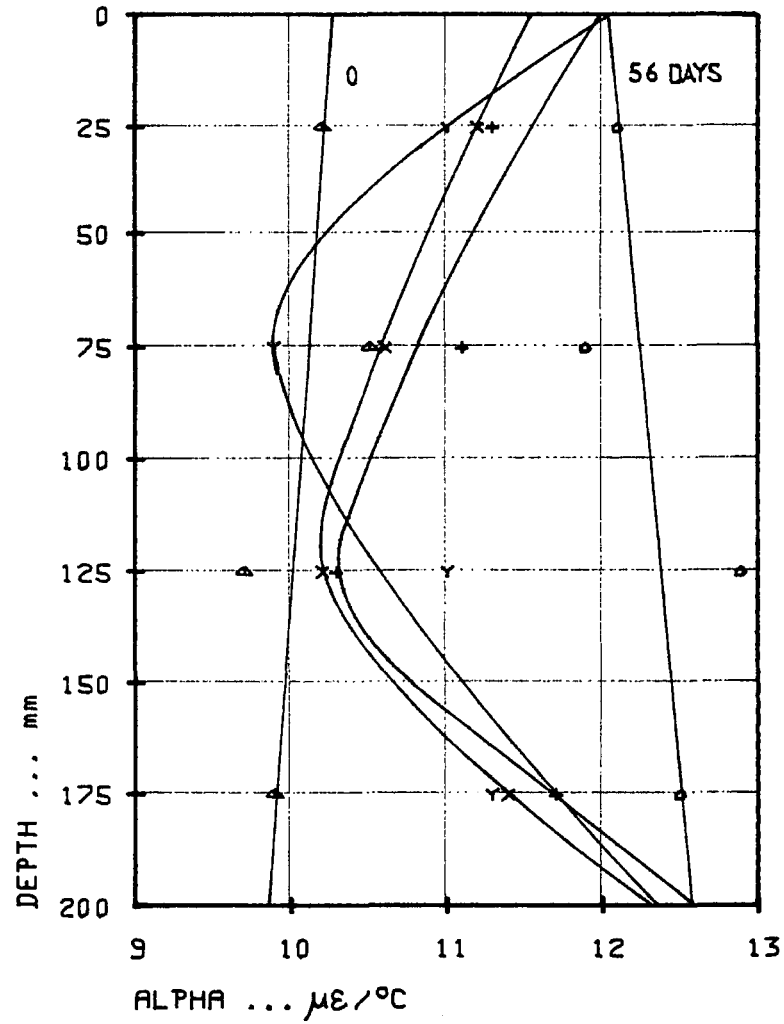

GRAPH 13. ALPHA V. TIME
SECOND BATCH

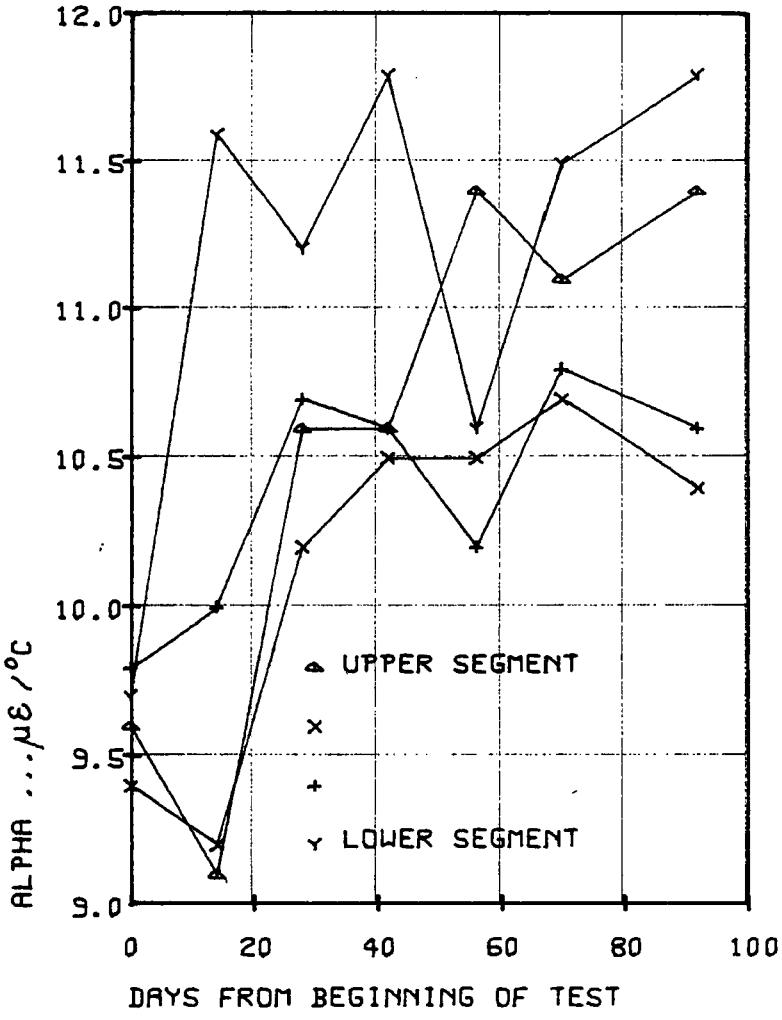

GRAPH 14. ALPHA PROFILES
SECOND BATCH

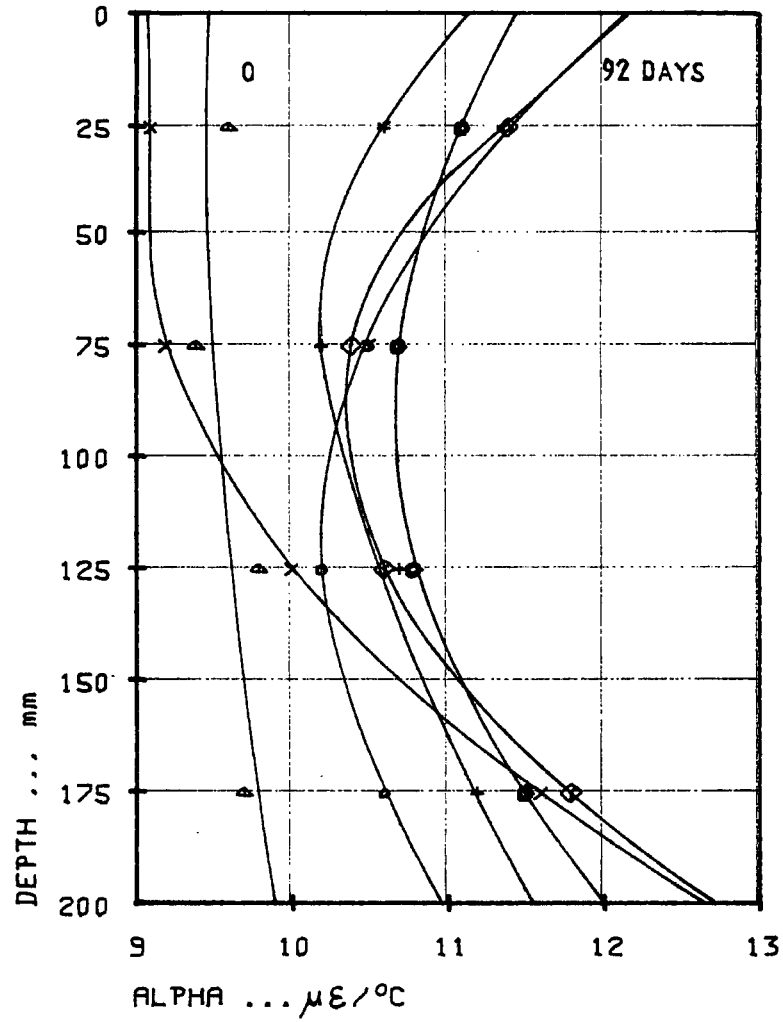

GRAPH 15. LOADING CURVE
SECOND SINGLE SPAN TEST

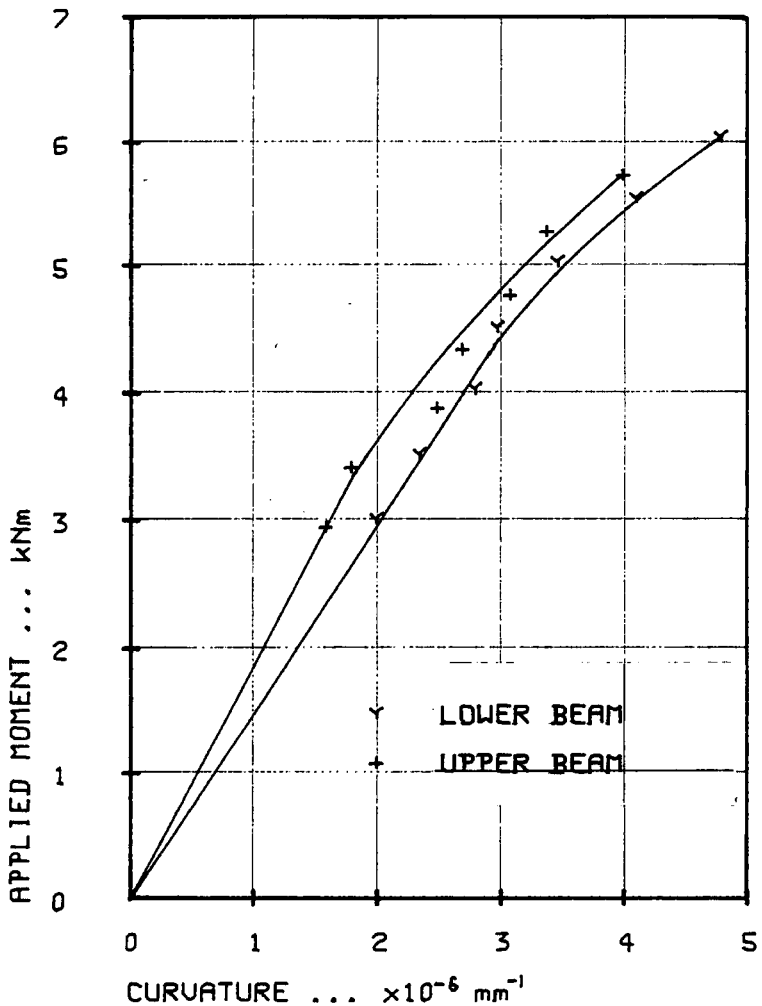

GRAPH 16. LOADING CURVE
THIRD SINGLE SPAN TEST

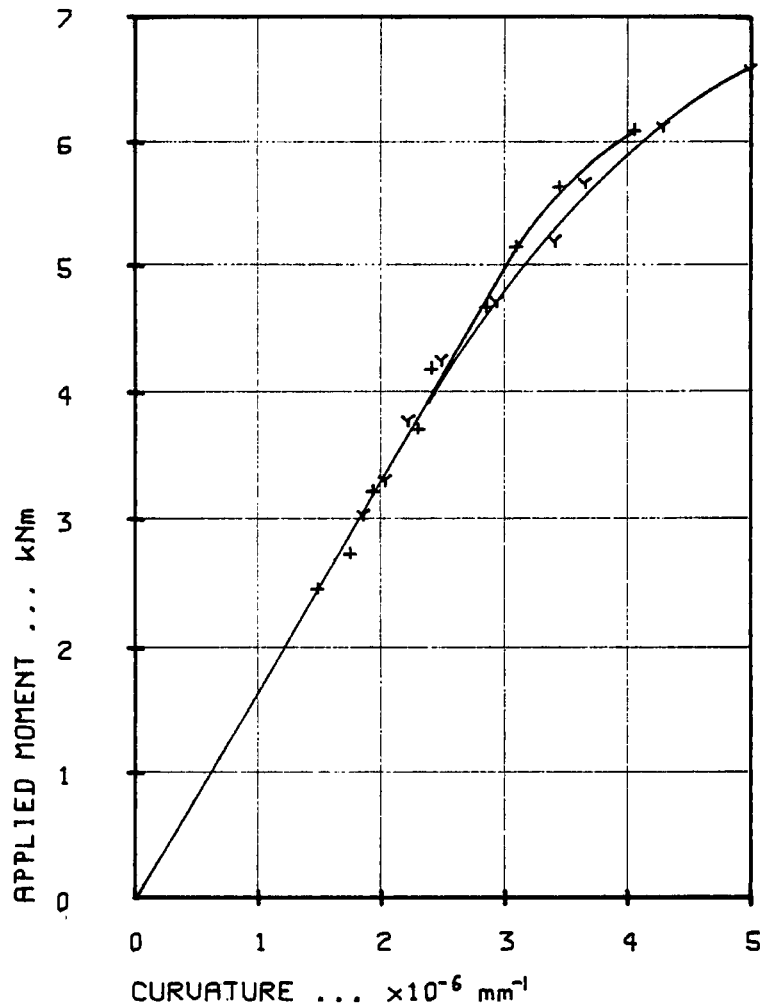

GRAPH 17. LOADING CURVE
DEEP BEAM TEST

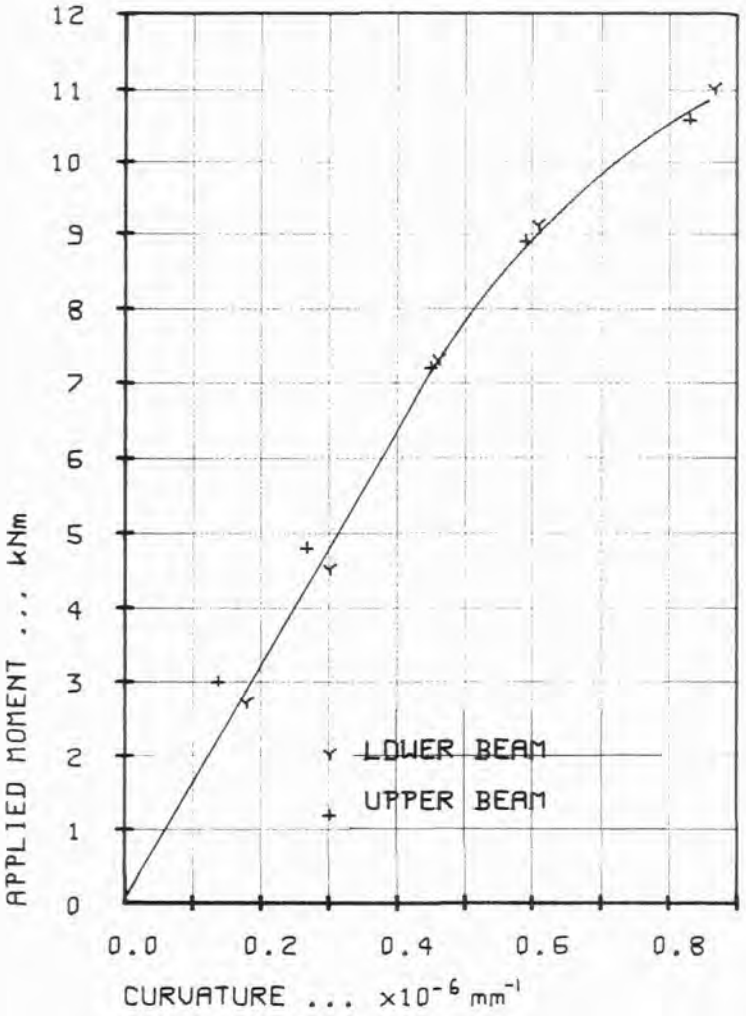

GRAPH 18. LOADING CURVE
T-SECTION BEAM TEST

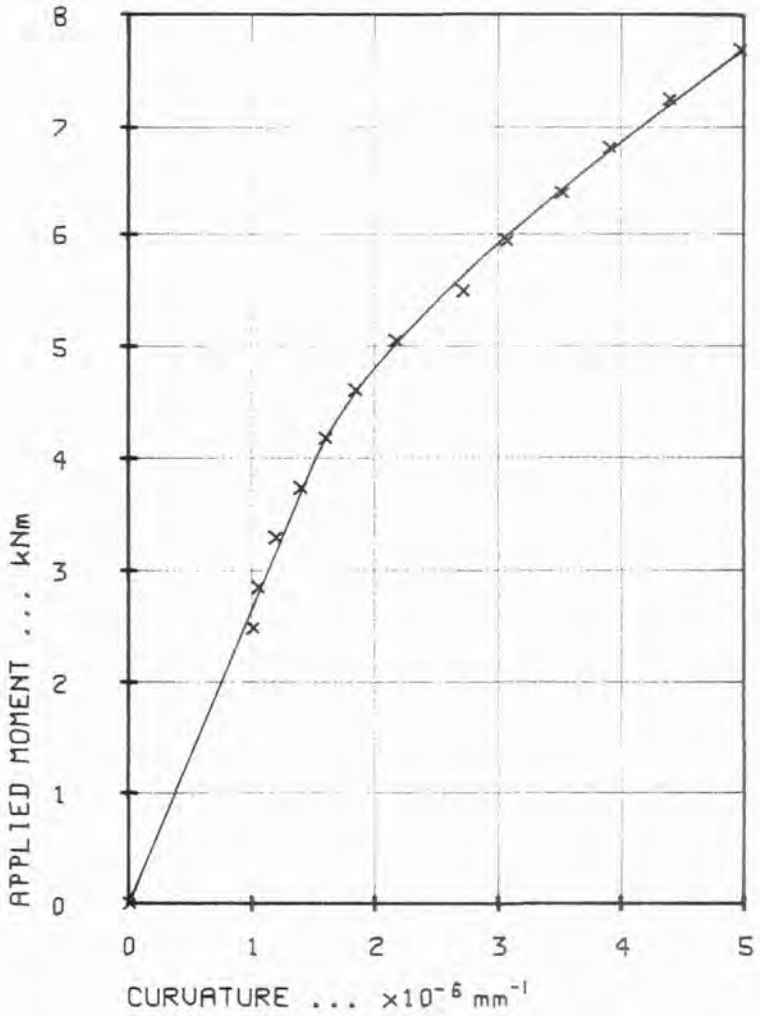

GRAPH 19. LOADING RESULTS
FIRST TWO SPAN TEST

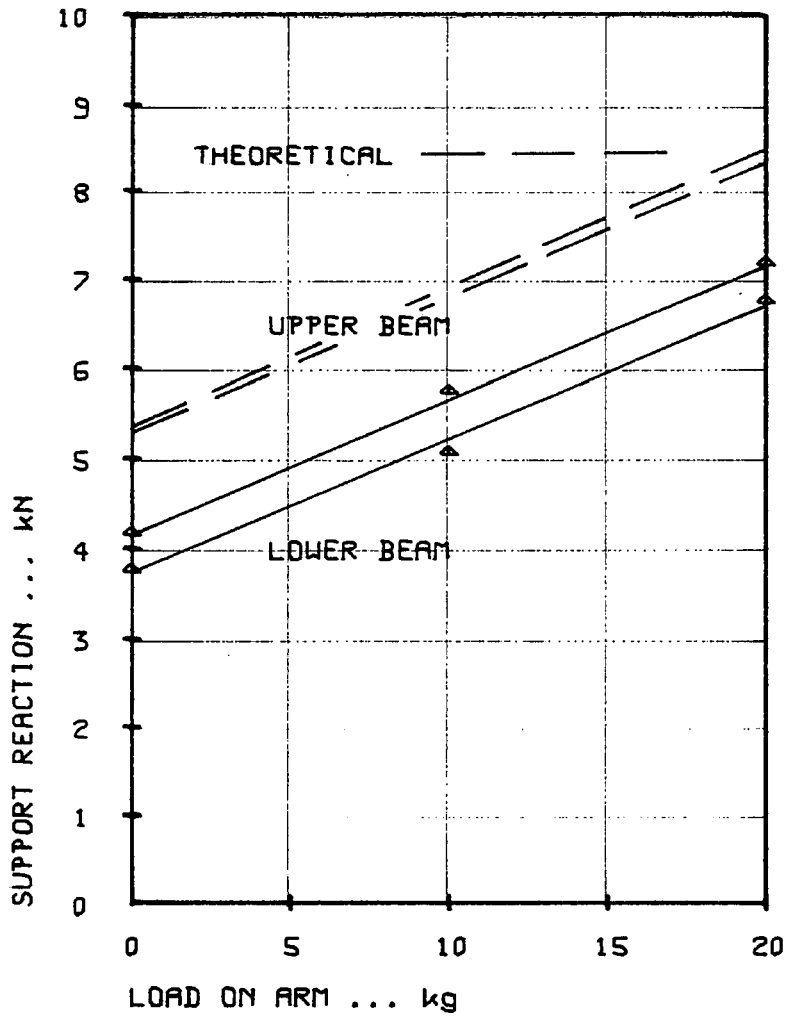

GRAPH 20. LOADING RESULTS
SECOND TWO SPAN TEST

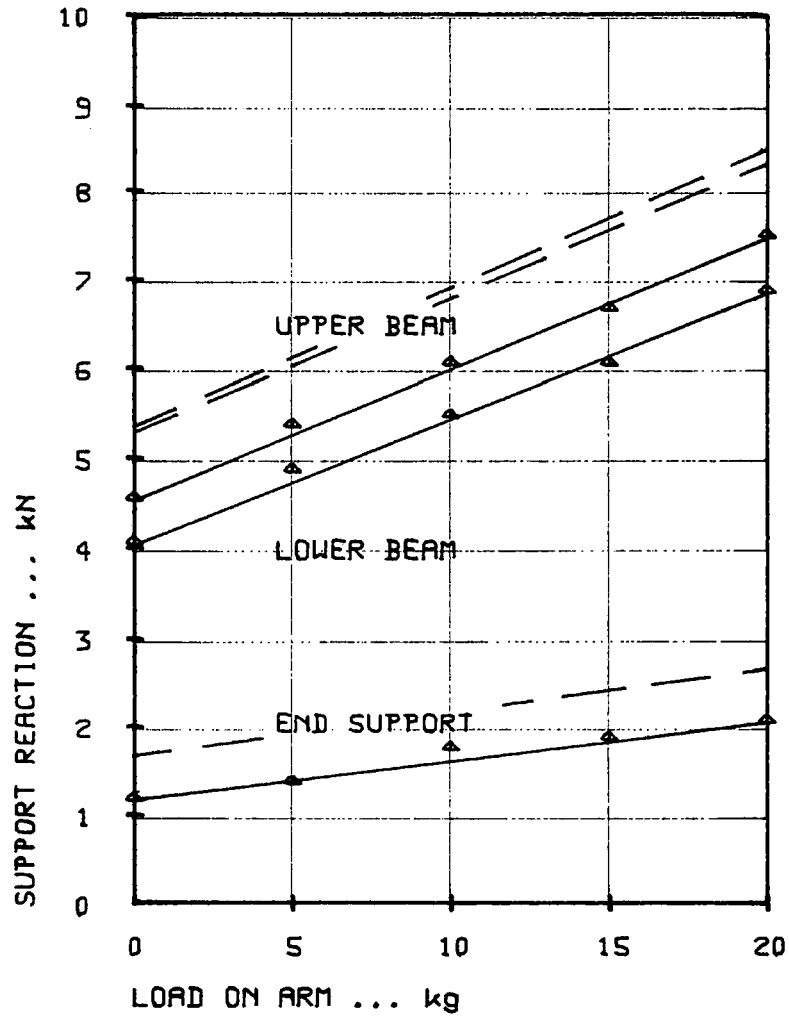

GRAPH 21. LOADING RESULTS
THIRD TWO SPAN TEST

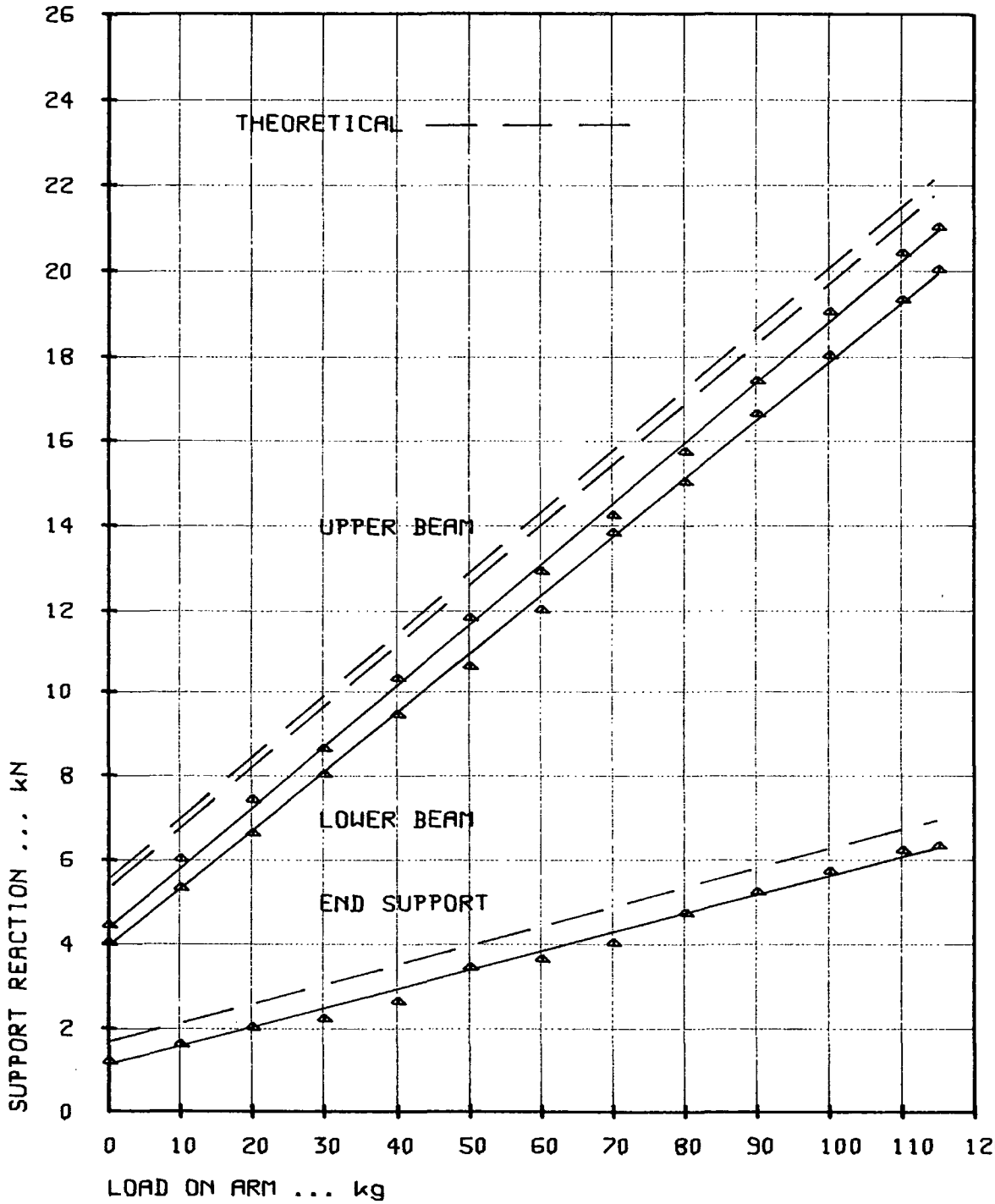

GRAPH 22. TEMPERATURE PROFILES
THIRD SINGLE SPAN TEST
BEAM NOT LOADED

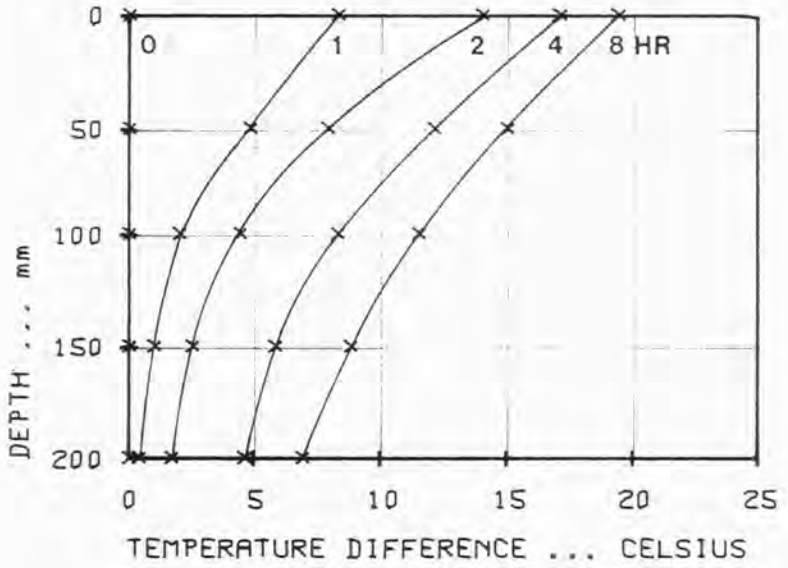

GRAPH 23. STRAINS
-DURING HEATING
THIRD SINGLE SPAN TEST

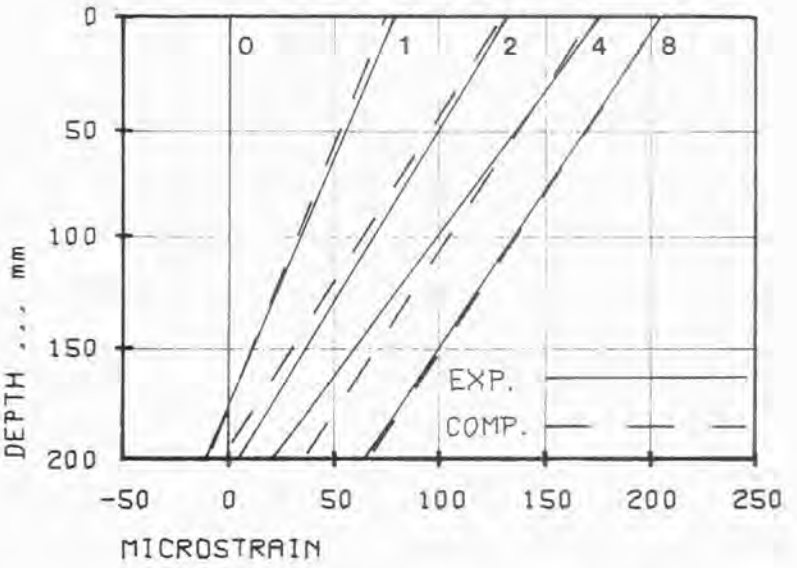

GRAPH 24. TEMPERATURE PROFILES
THIRD SINGLE SPAN TEST
BEAM LOADED

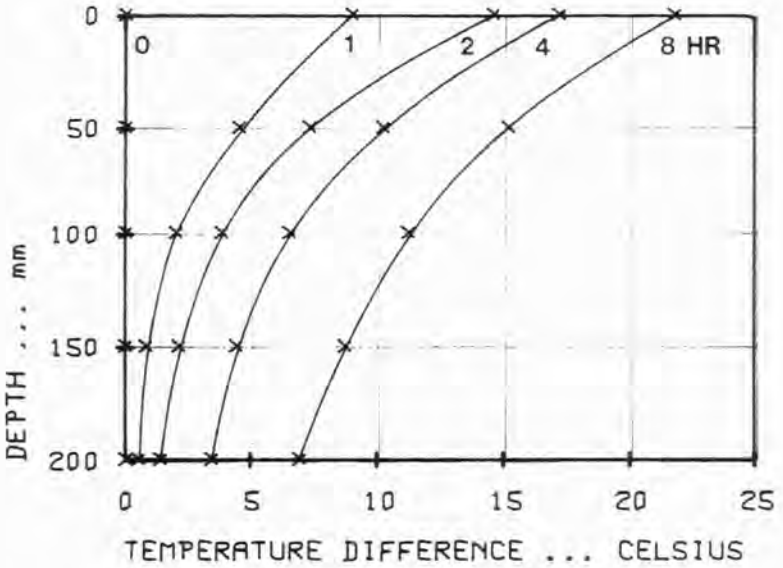

GRAPH 25. STRAINS
-DURING HEATING
THIRD SINGLE SPAN TEST

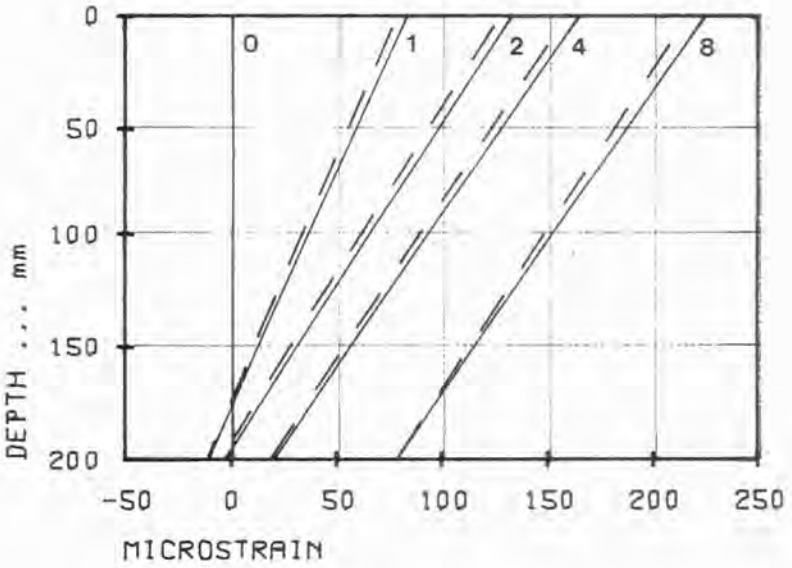

GRAPH 26. TEMPERATURE PROFILES
DEEP BEAM TEST

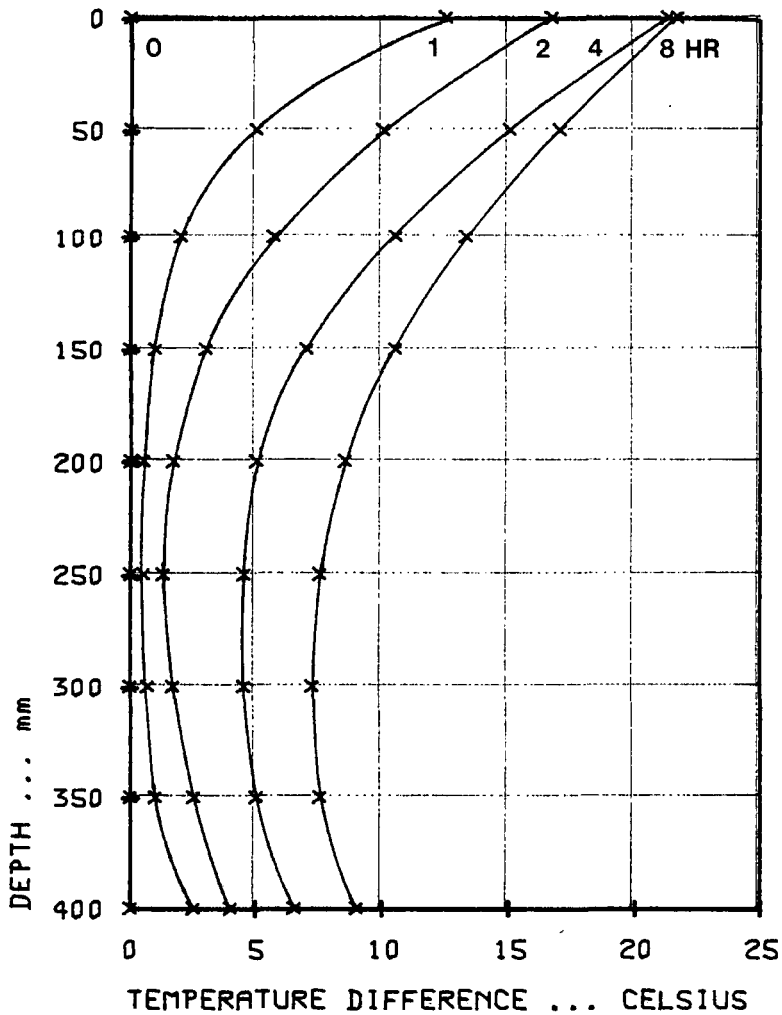

GRAPH 27. STRAINS
-DURING HEATING
DEEP BEAM TEST

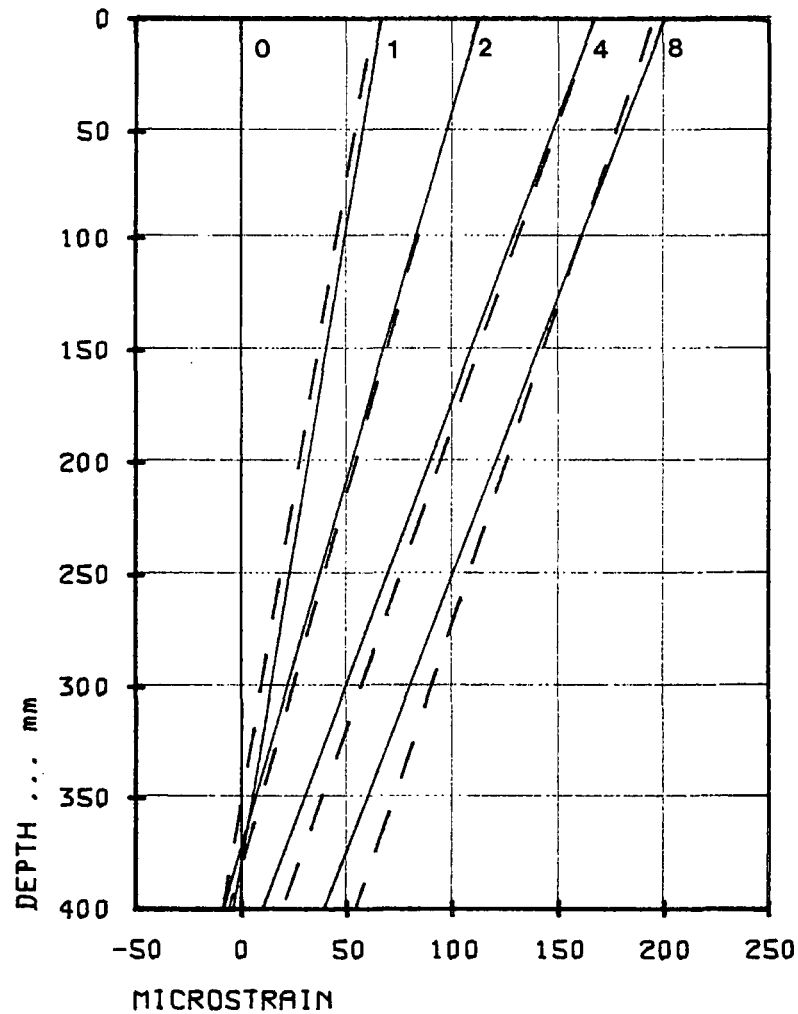

GRAPH 28. TEMPERATURE PROFILES
T-SECTION BEAM TEST

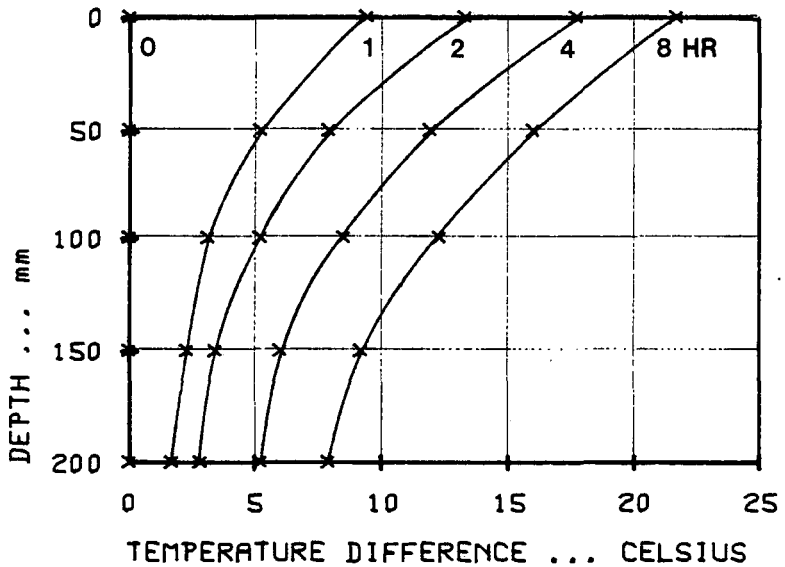

GRAPH 29. STRAINS
-DURING HEATING
T-SECTION BEAM TEST

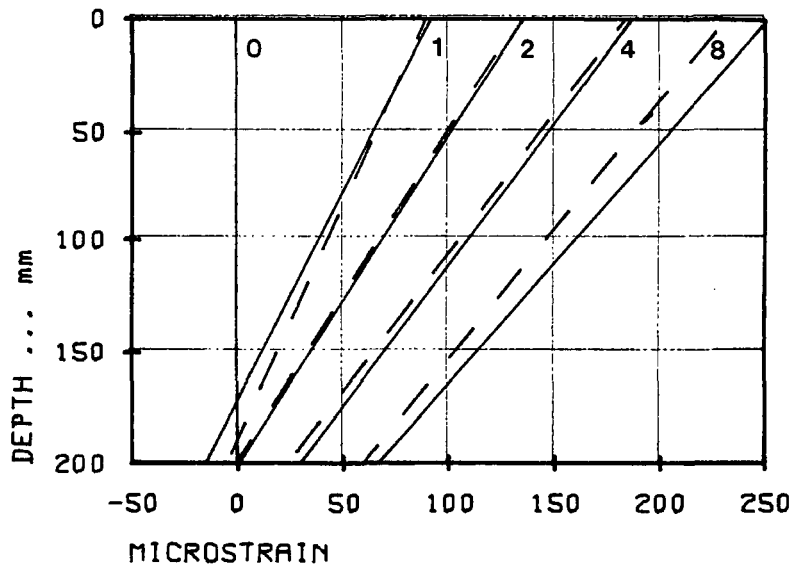

GRAPH 30. SOFFIT STRAIN RESULTS
UNLOADING AND RELOADING
T-SECTION BEAM TEST

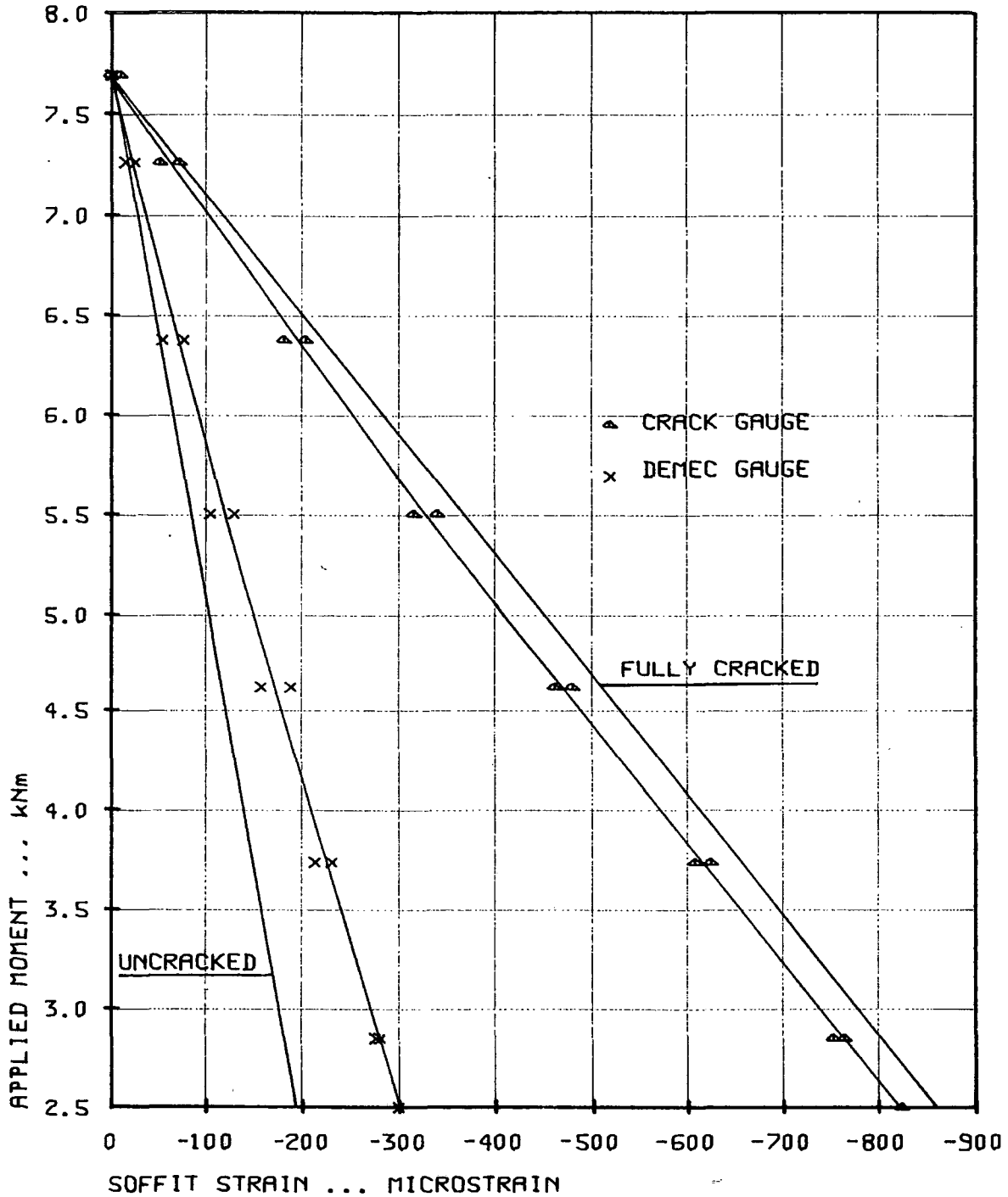

GRAPH 31. TEMPERATURE PROFILES
SECOND TWO SPAN TEST

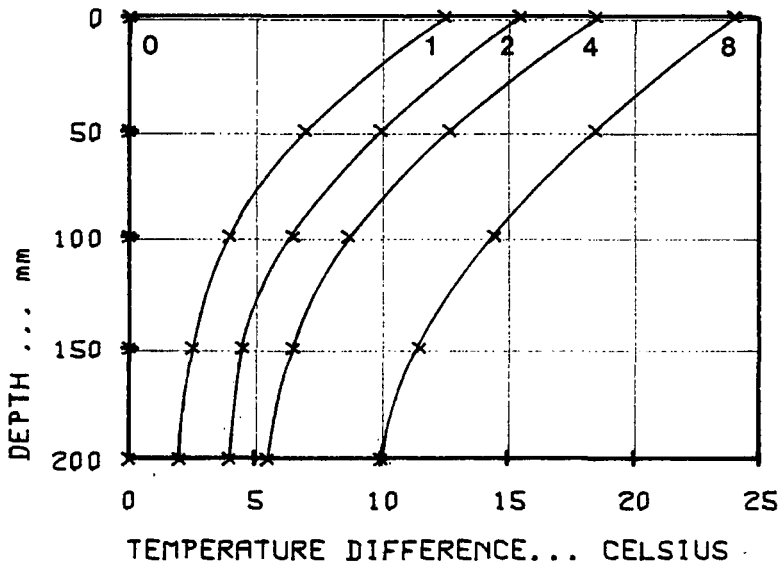

GRAPH 32. CENTRAL SUPPORT REACTION
-DECREASE DURING HEATING
SECOND TWO SPAN TEST

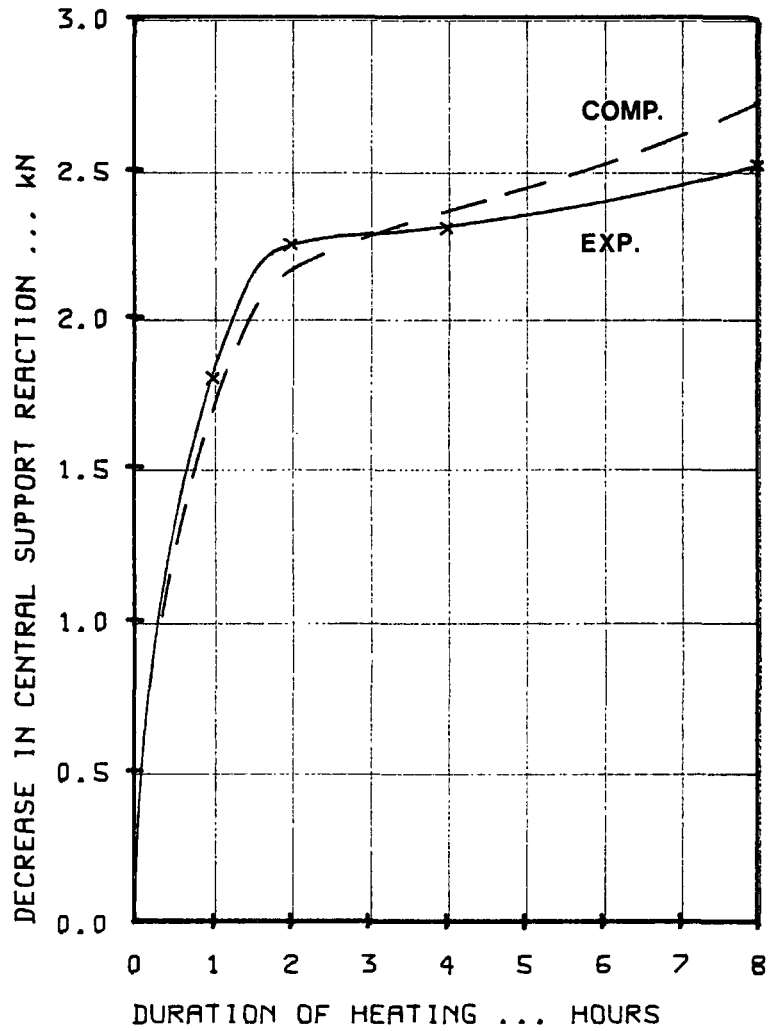

GRAPH 33. TEMPERATURE PROFILES
THIRD TWO SPAN TEST

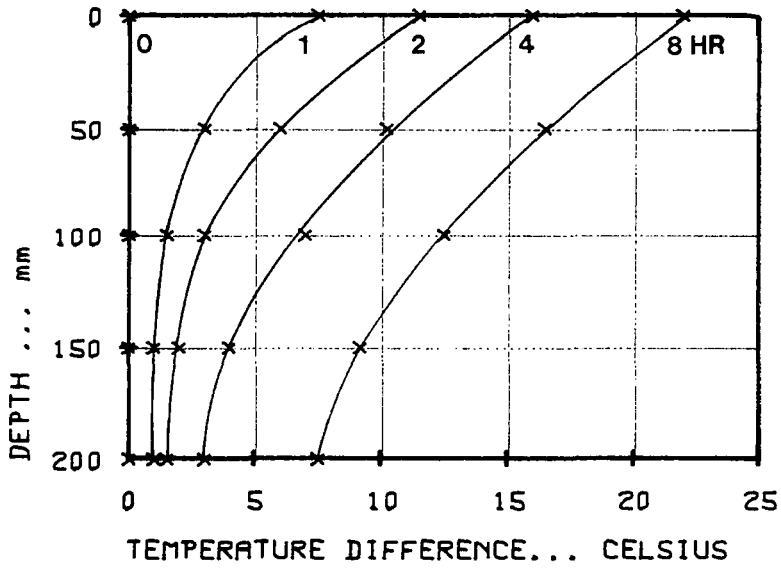

GRAPH 34. CENTRAL SUPPORT REACTION
-DECREASE DURING HEATING
THIRD TWO SPAN TEST

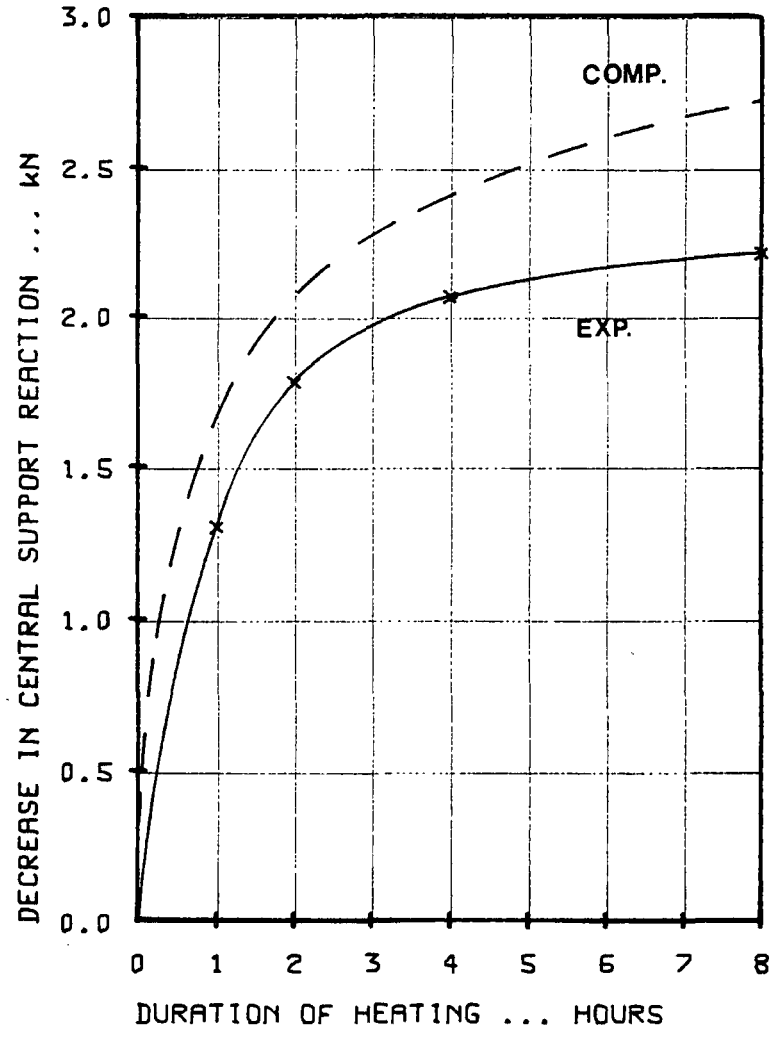

GRAPH 35. RATIOS OF OBSERVED TO CALCULATED AXIAL STRAIN
SECOND SINGLE SPAN TEST
BEAM NOT LOADED

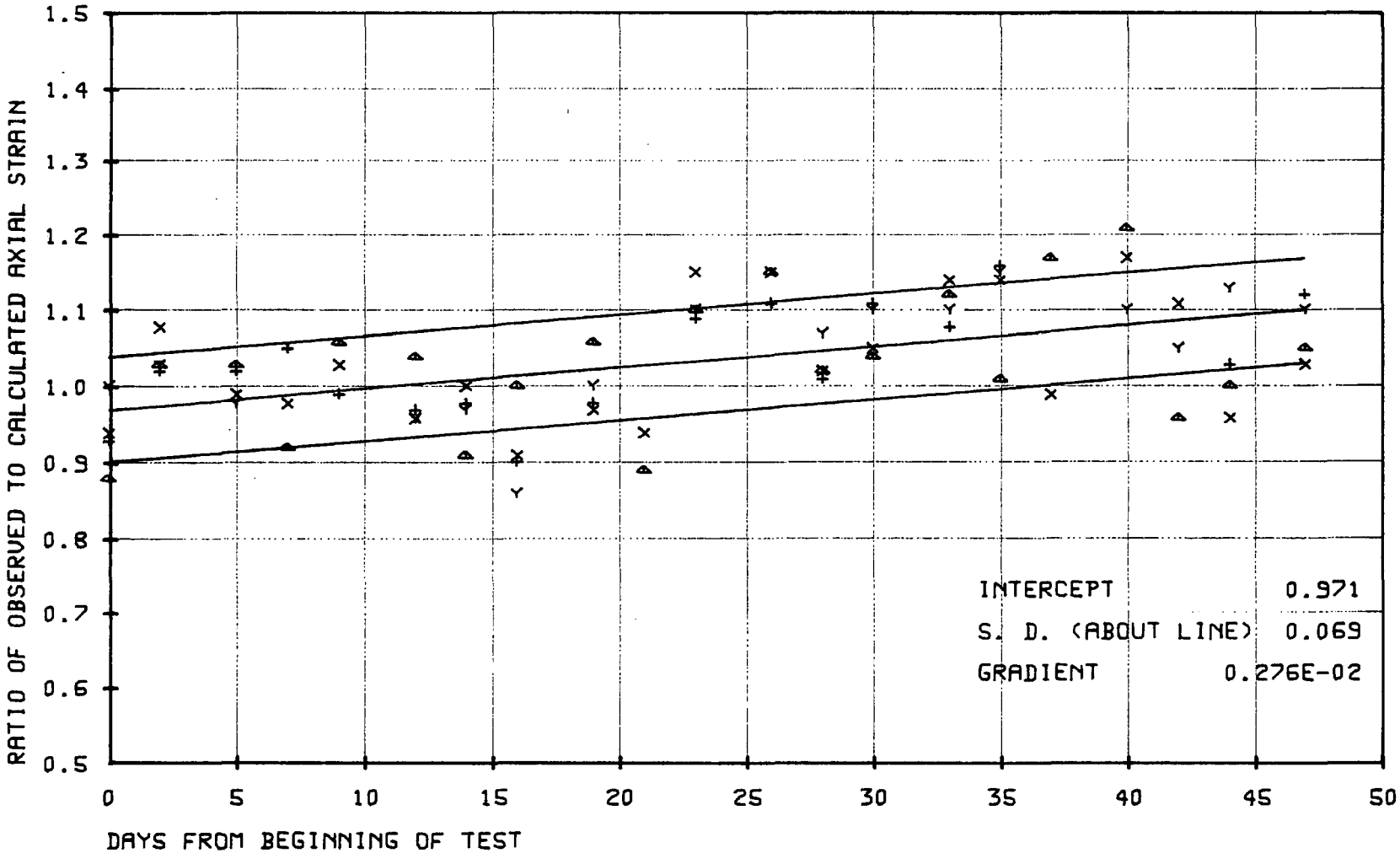

GRAPH 36. RATIOS OF OBSERVED TO CALCULATED AXIAL STRAIN
THIRD SINGLE SPAN TEST
BEAM NOT LOADED

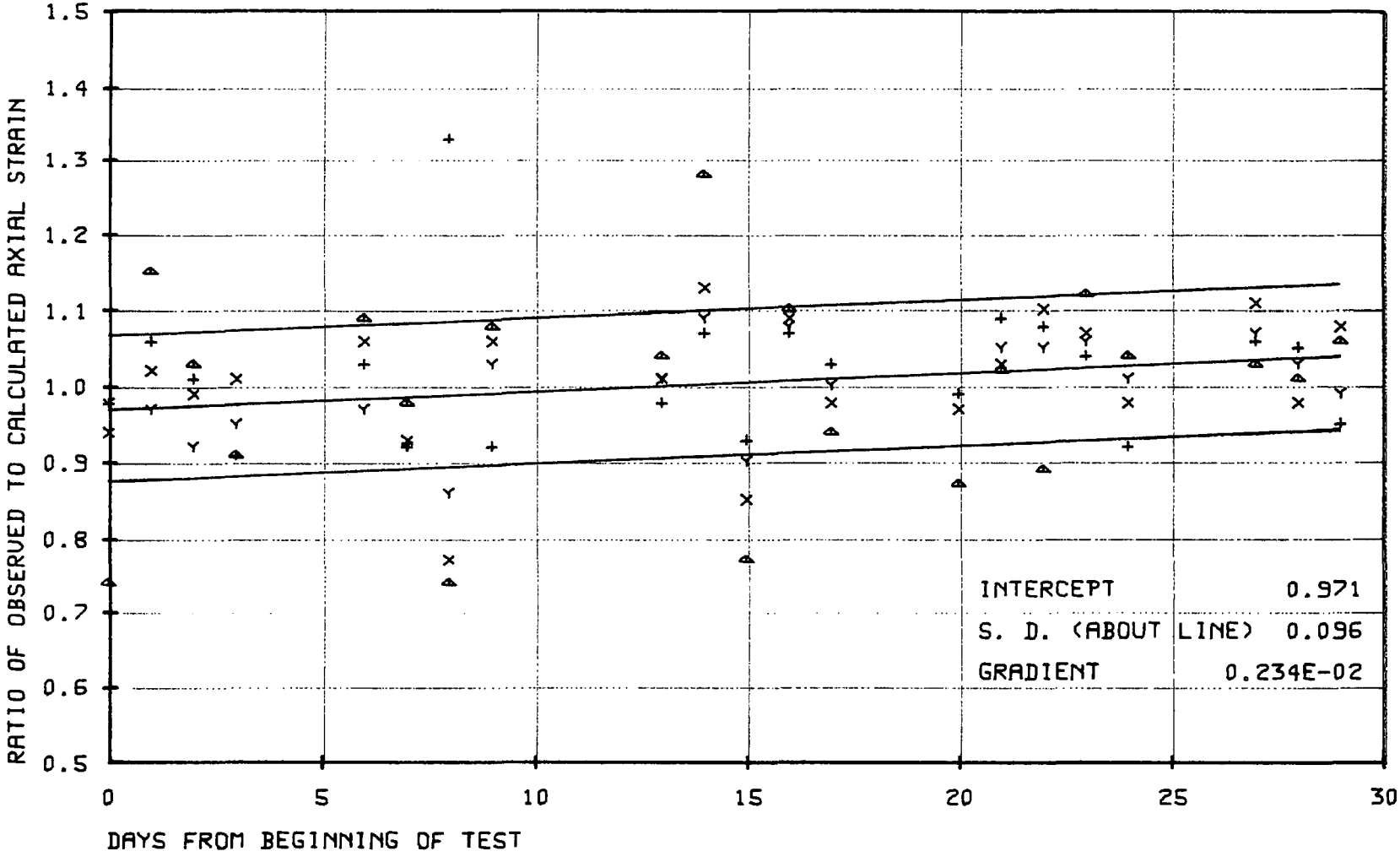

GRAPH 37. RATIOS OF OBSERVED TO CALCULATED AXIAL STRAIN

DEEP BEAM TEST

BEAM NOT LOADED

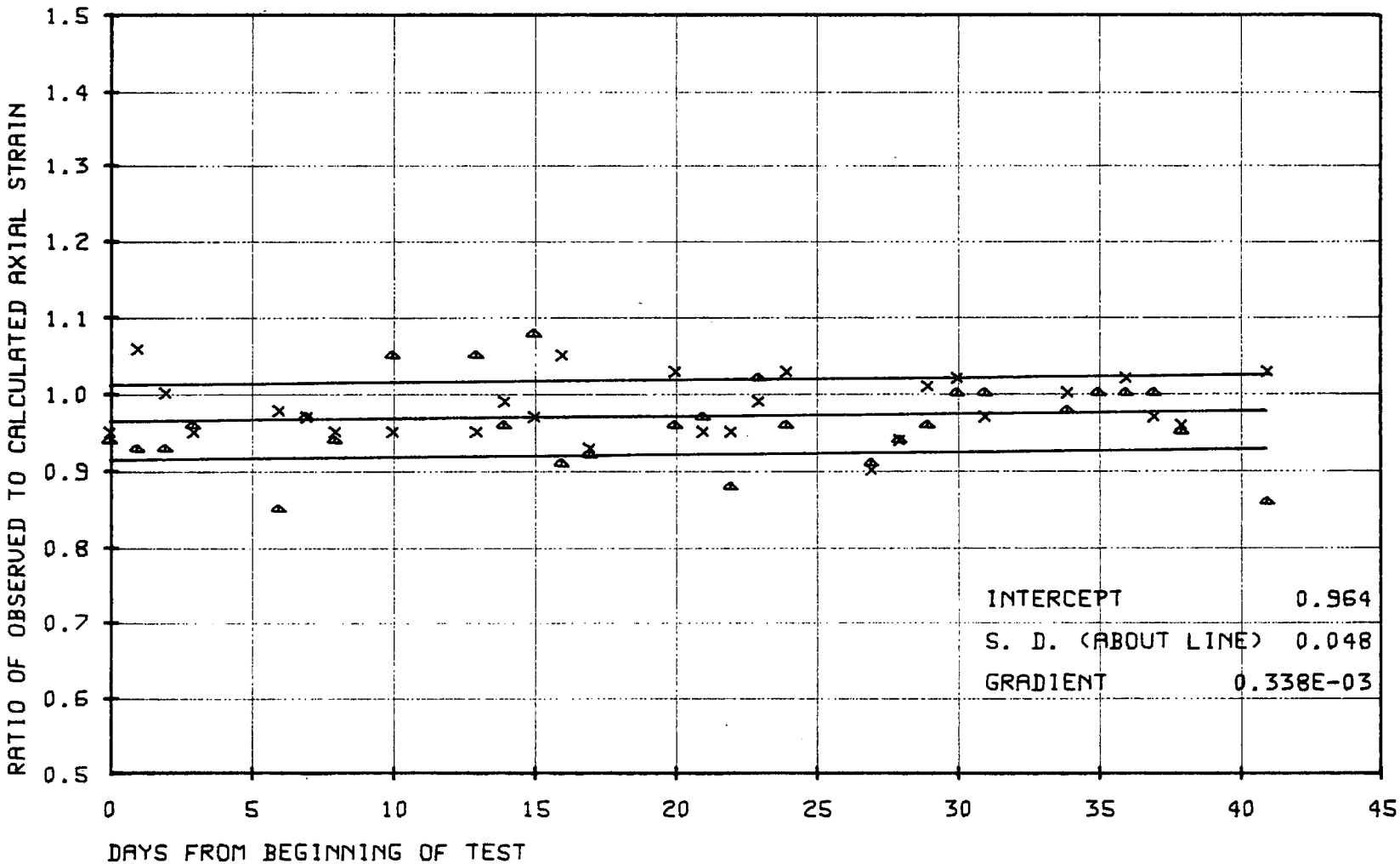

GRAPH 38. RATIOS OF OBSERVED TO CALCULATED AXIAL STRAIN
T-SECTION BEAM TEST
BEAM LOADED ON DAY 19

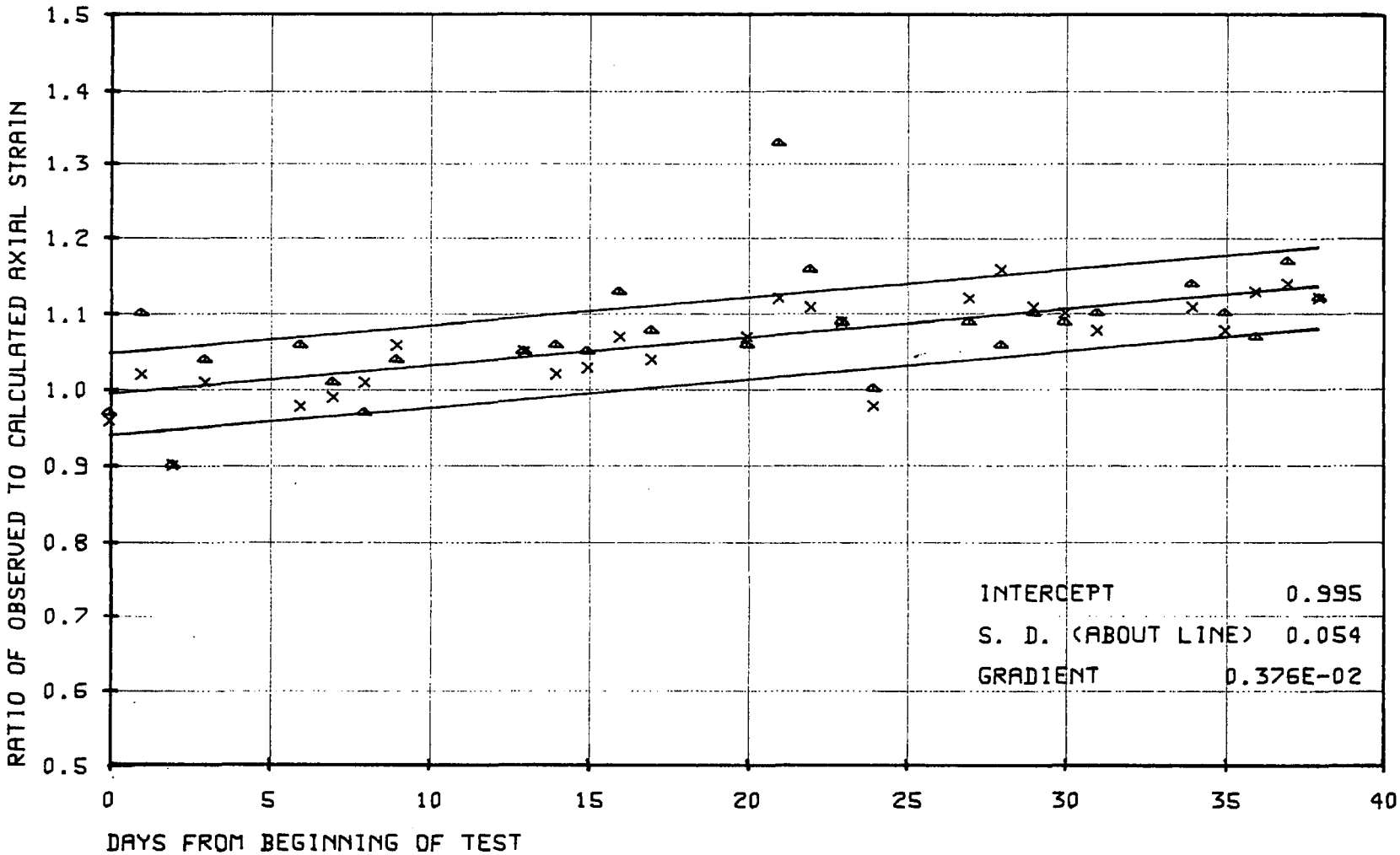

GRAPH 39. RATIOS OF OBSERVED TO CALCULATED AXIAL STRAIN
SECOND TWO SPAN TEST
BEAM NOT LOADED

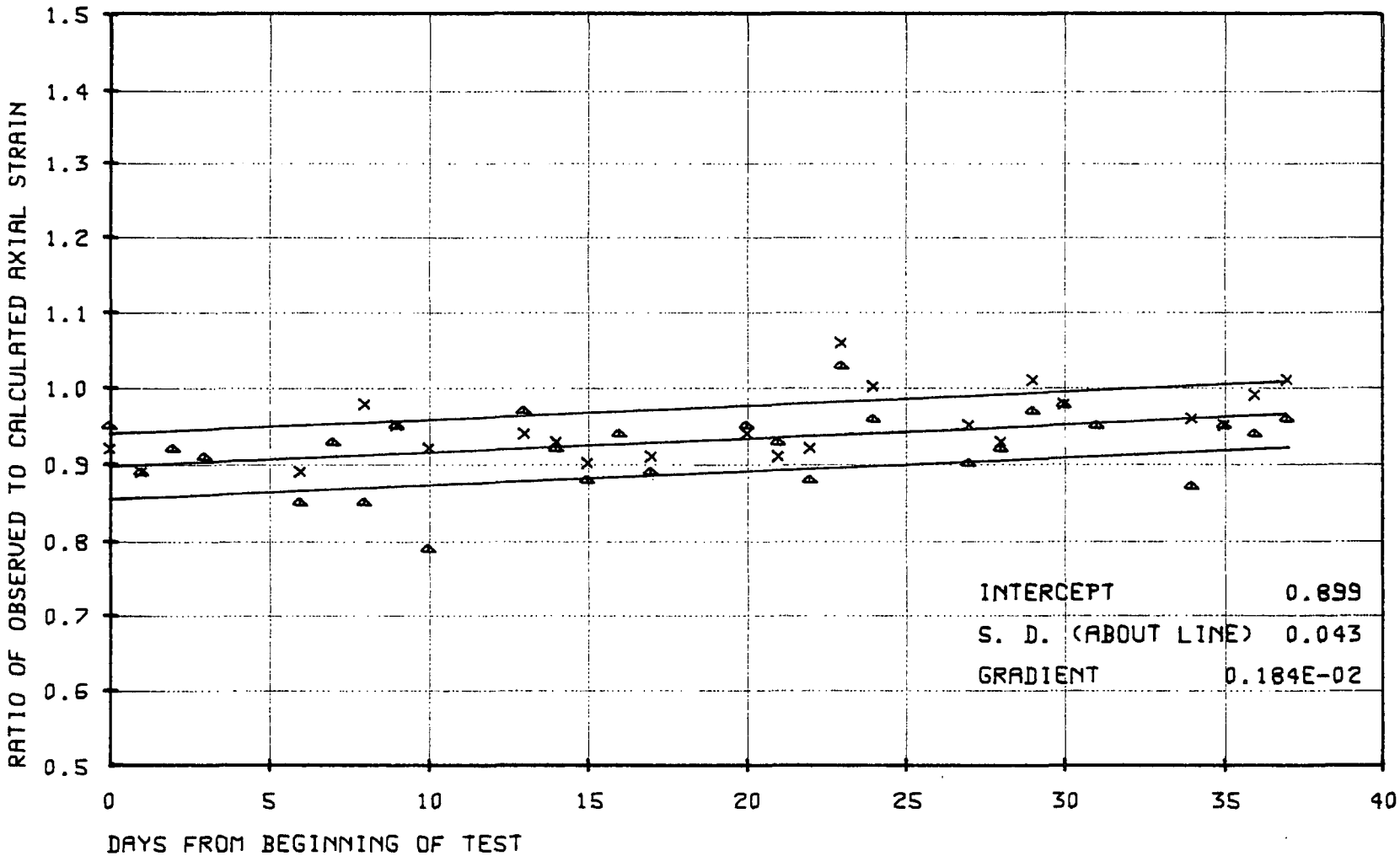

GRAPH 40. RATIOS OF OBSERVED TO CALCULATED AXIAL STRAIN
THIRD TWO SPAN TEST
BEAM NOT LOADED

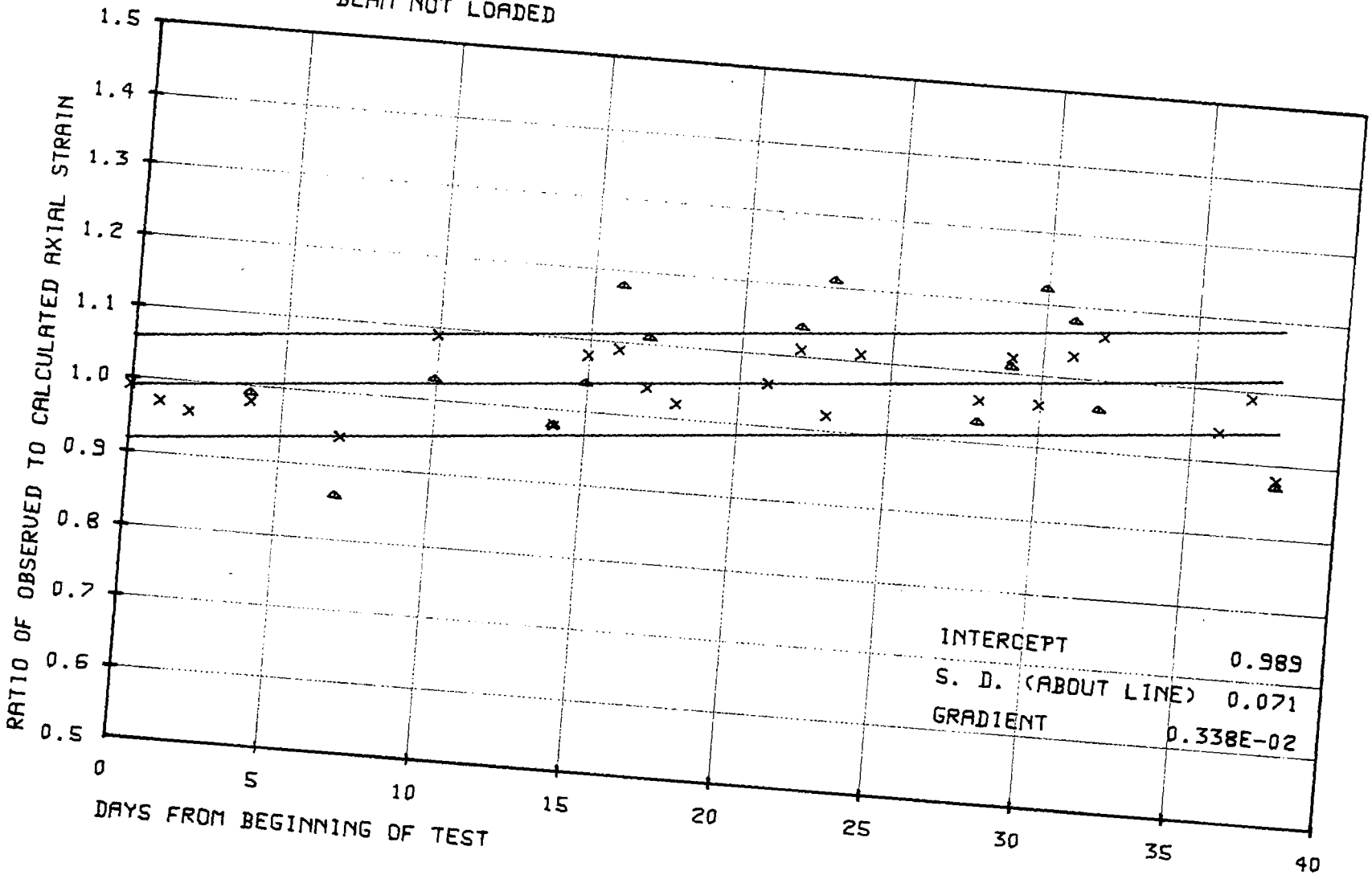

GRAPH 41. RATIOS OF OBSERVED TO CALCULATED CURVATURE
SECOND SINGLE SPAN TEST
BEAM NOT LOADED

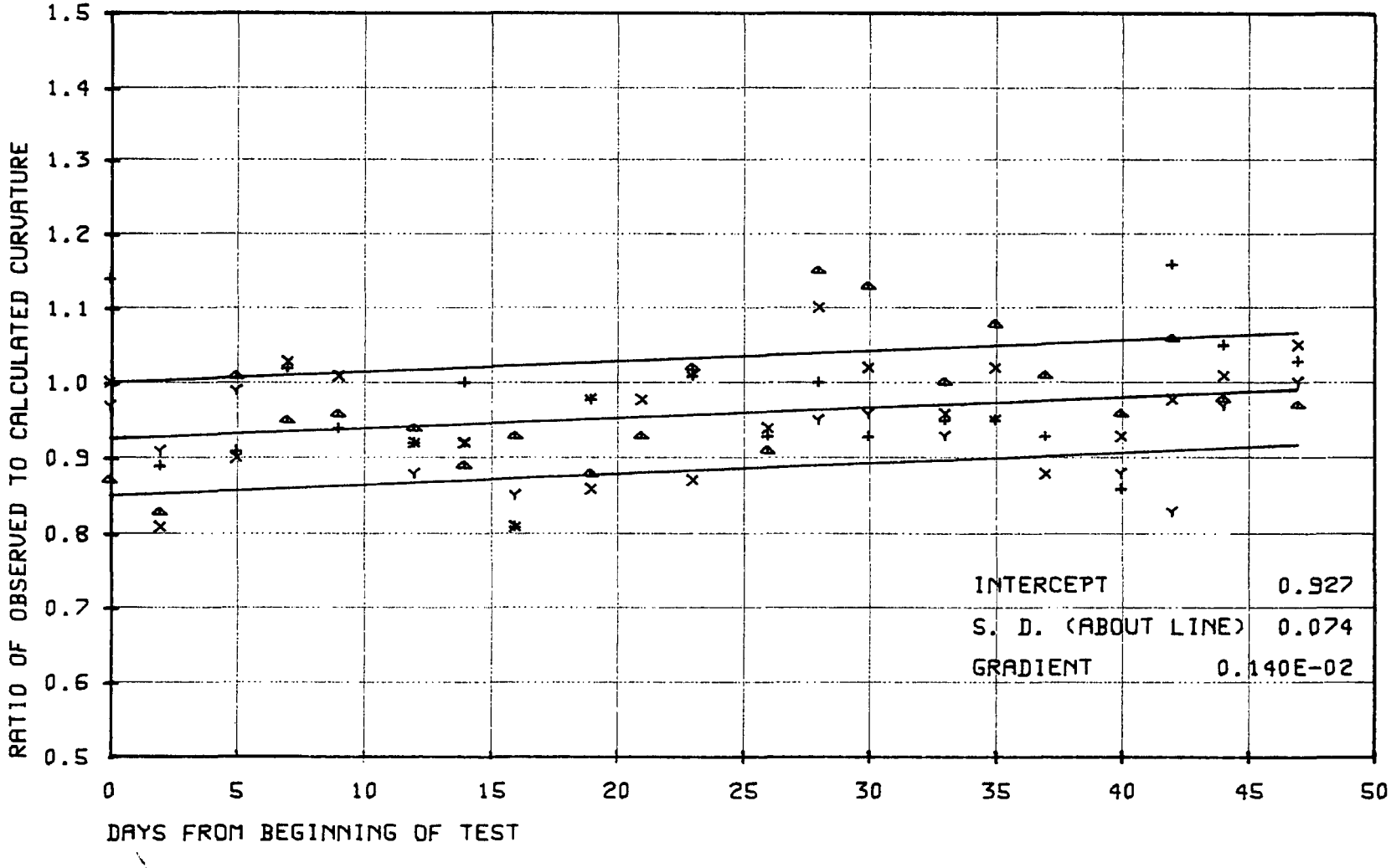

GRAPH 42. RATIOS OF OBSERVED TO CALCULATED CURVATURE
THIRD SINGLE SPAN TEST
BEAM NOT LOADED

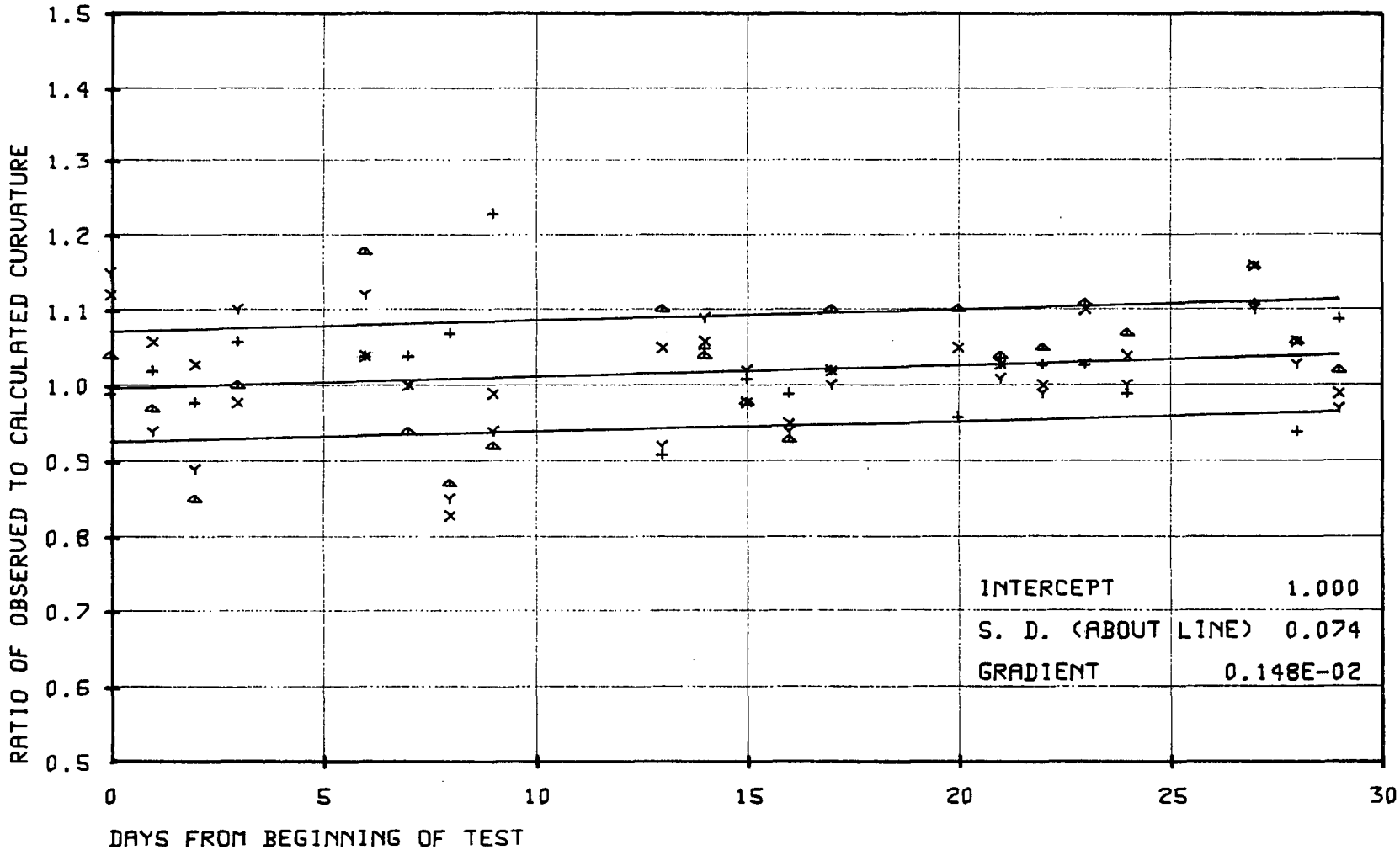

GRAPH 43. RATIOS OF OBSERVED TO CALCULATED CURVATURE
DEEP BEAM TEST
BEAM NOT LOADED

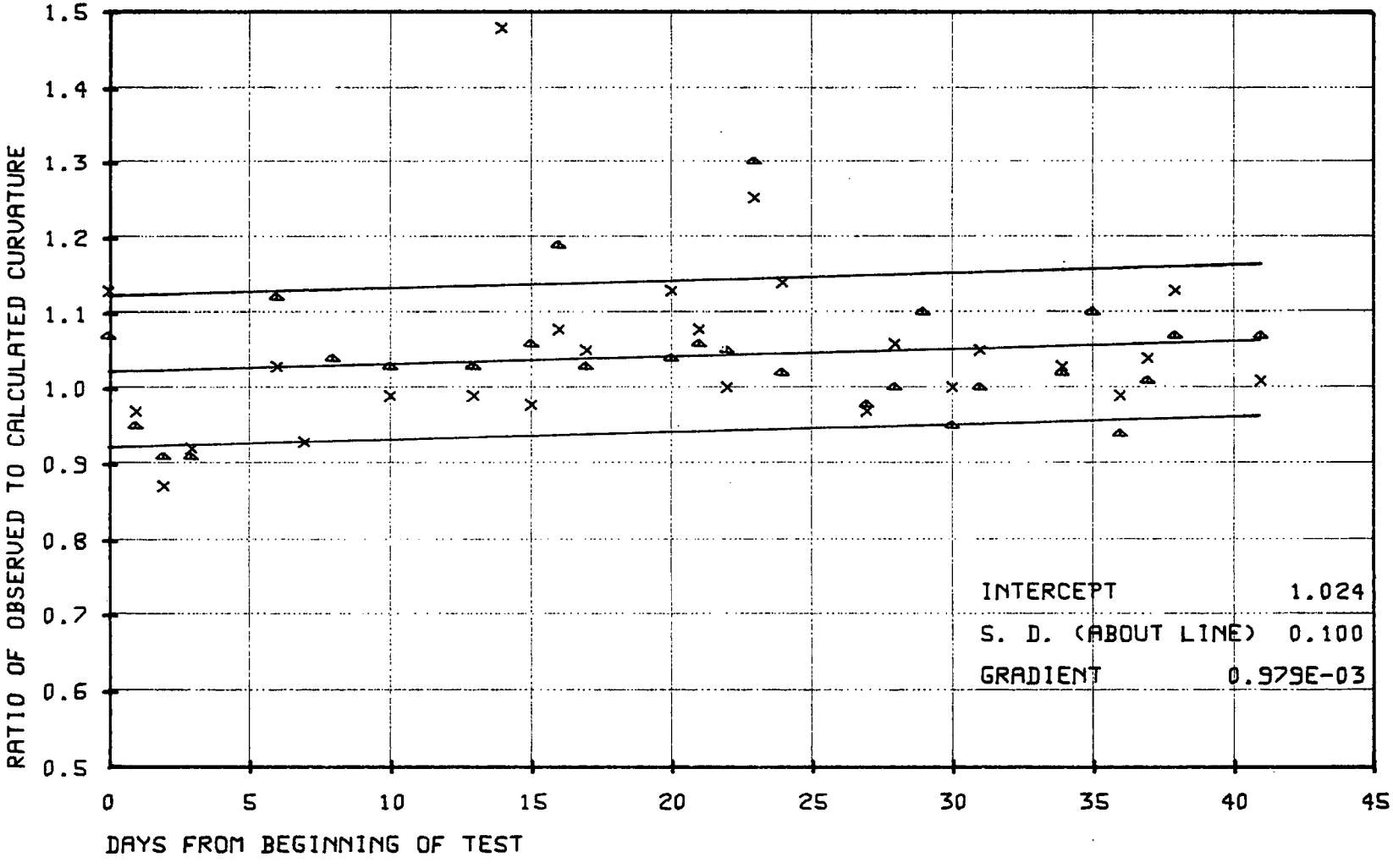

GRAPH 44. RATIOS OF OBSERVED TO CALCULATED CURVATURE
T-SECTION BEAM TEST
BEAM LOADED ON DAY 19 ... UNCRACKED ANALYSIS

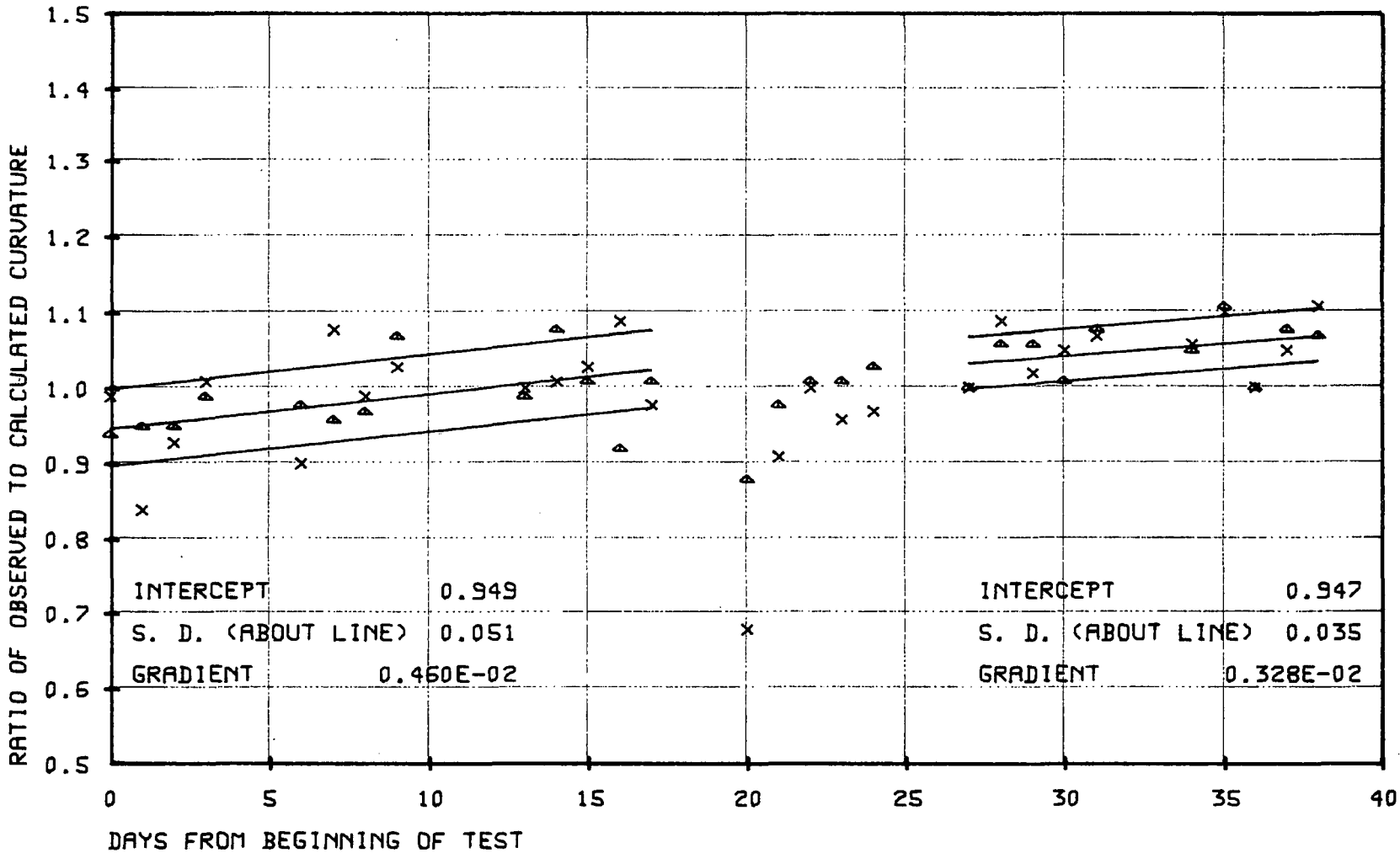

GRAPH 45. RATIOS OF OBSERVED TO CALCULATED CURVATURE
SECOND TWO SPAN TEST
BEAM NOT LOADED

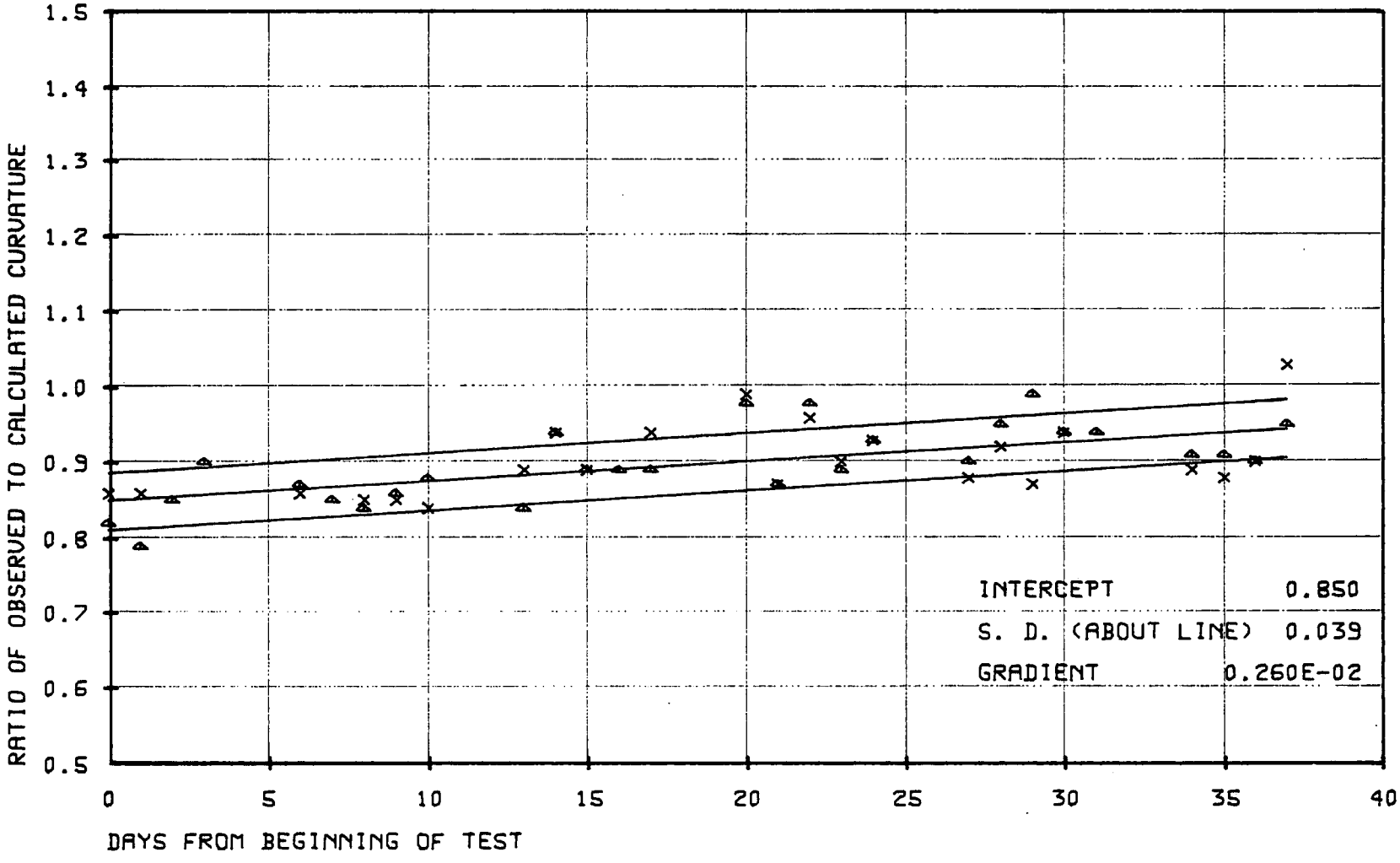

GRAPH 46. RATIOS OF OBSERVED TO CALCULATED CURVATURE
THIRD TWO SPAN TEST
BEAM NOT LOADED

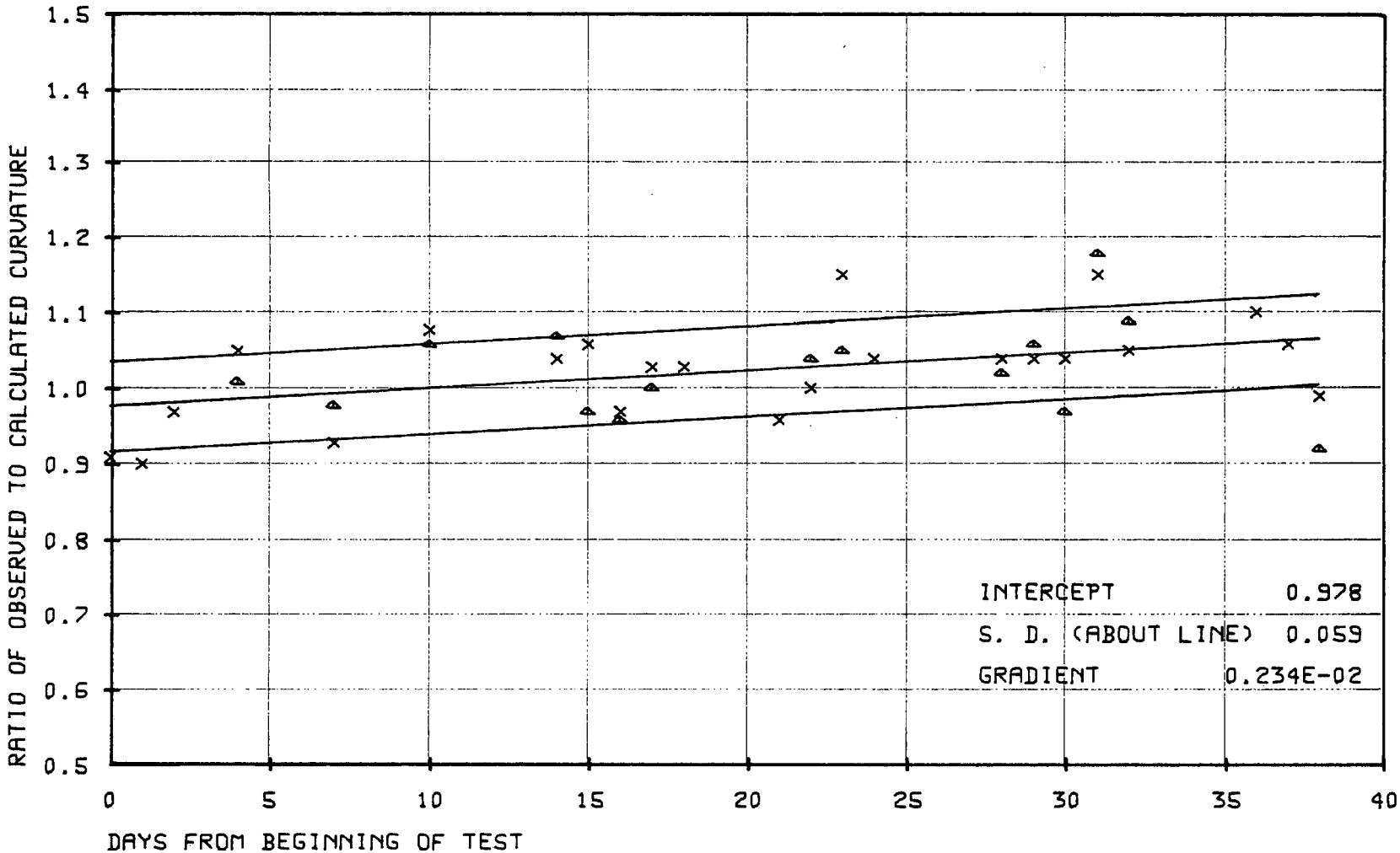

GRAPH 47. RATIOS OF OBSERVED TO CALCULATED AXIAL STRAIN
FIRST SINGLE SPAN TEST
BEAM LOADED ... UNCRACKED ANALYSIS

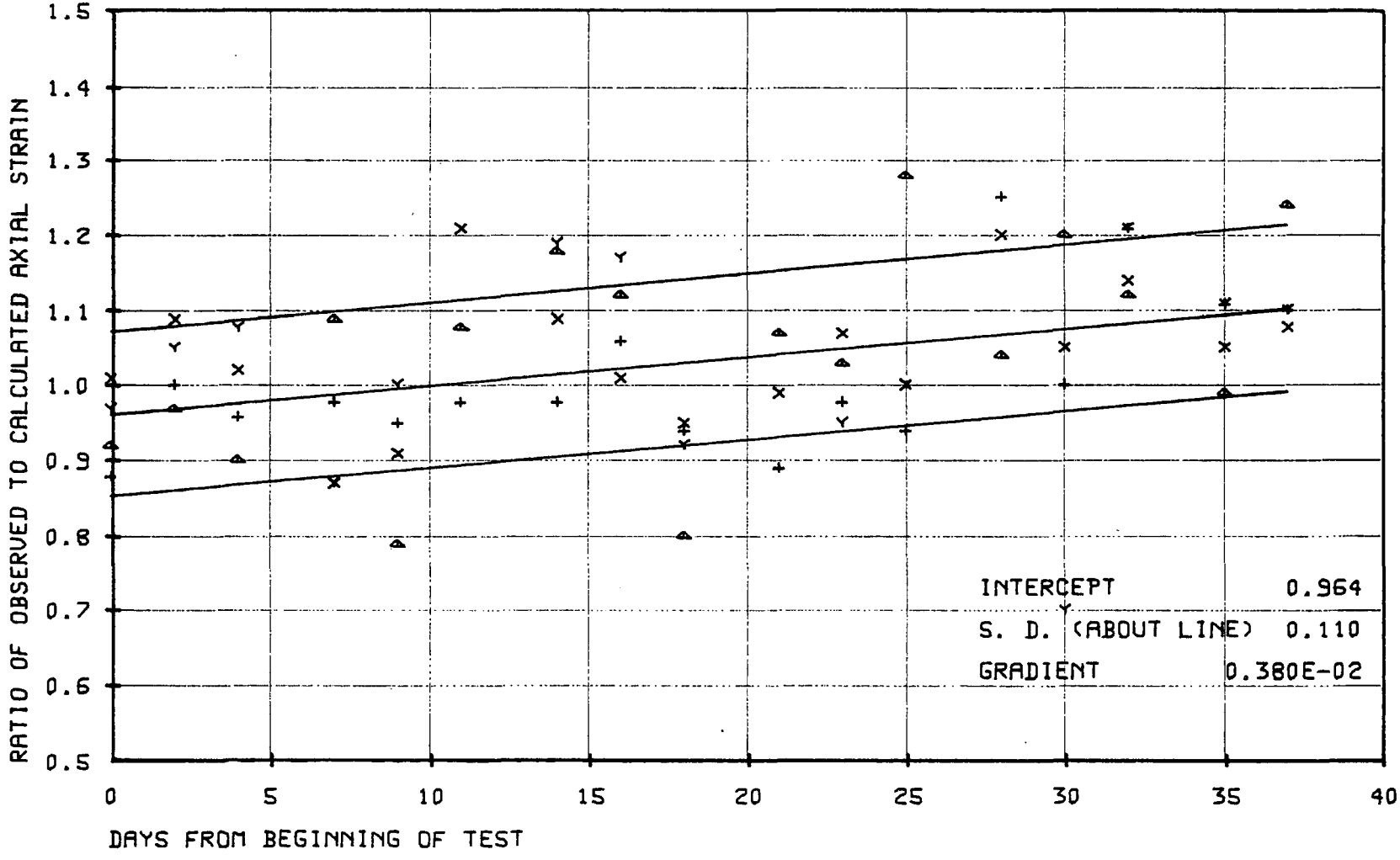

GRAPH 48. RATIOS OF OBSERVED TO CALCULATED AXIAL STRAIN
SECOND SINGLE SPAN TEST
BEAM LOADED ... UNCRACKED ANALYSIS

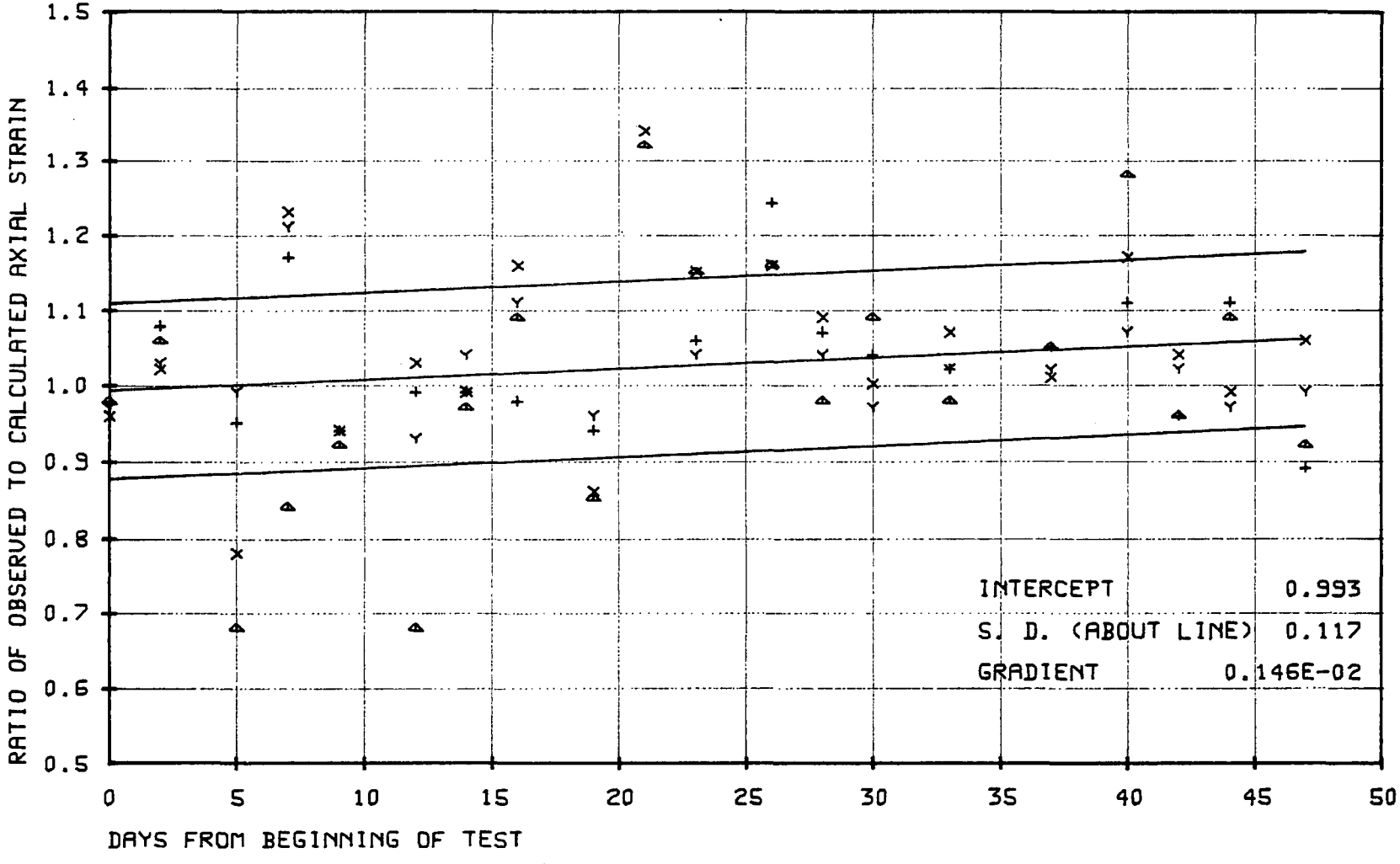

GRAPH 49. RATIOS OF OBSERVED TO CALCULATED AXIAL STRAIN
THIRD SINGLE SPAN TEST
BEAM LOADED ... UNCRACKED ANALYSIS

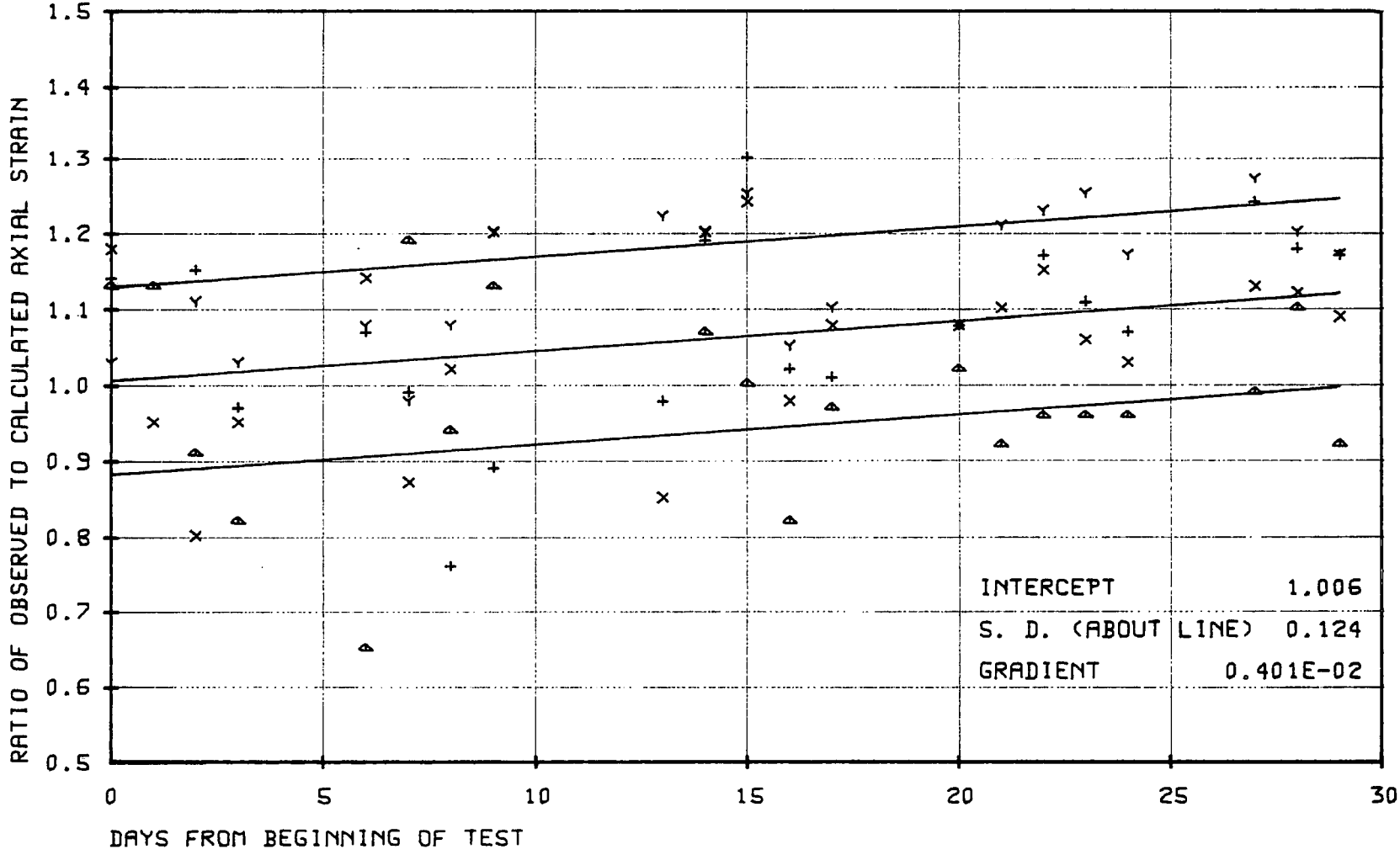

GRAPH 50. RATIOS OF OBSERVED TO CALCULATED AXIAL STRAIN
DEEP BEAM TEST
BEAM LOADED ... UNCRACKED ANALYSIS

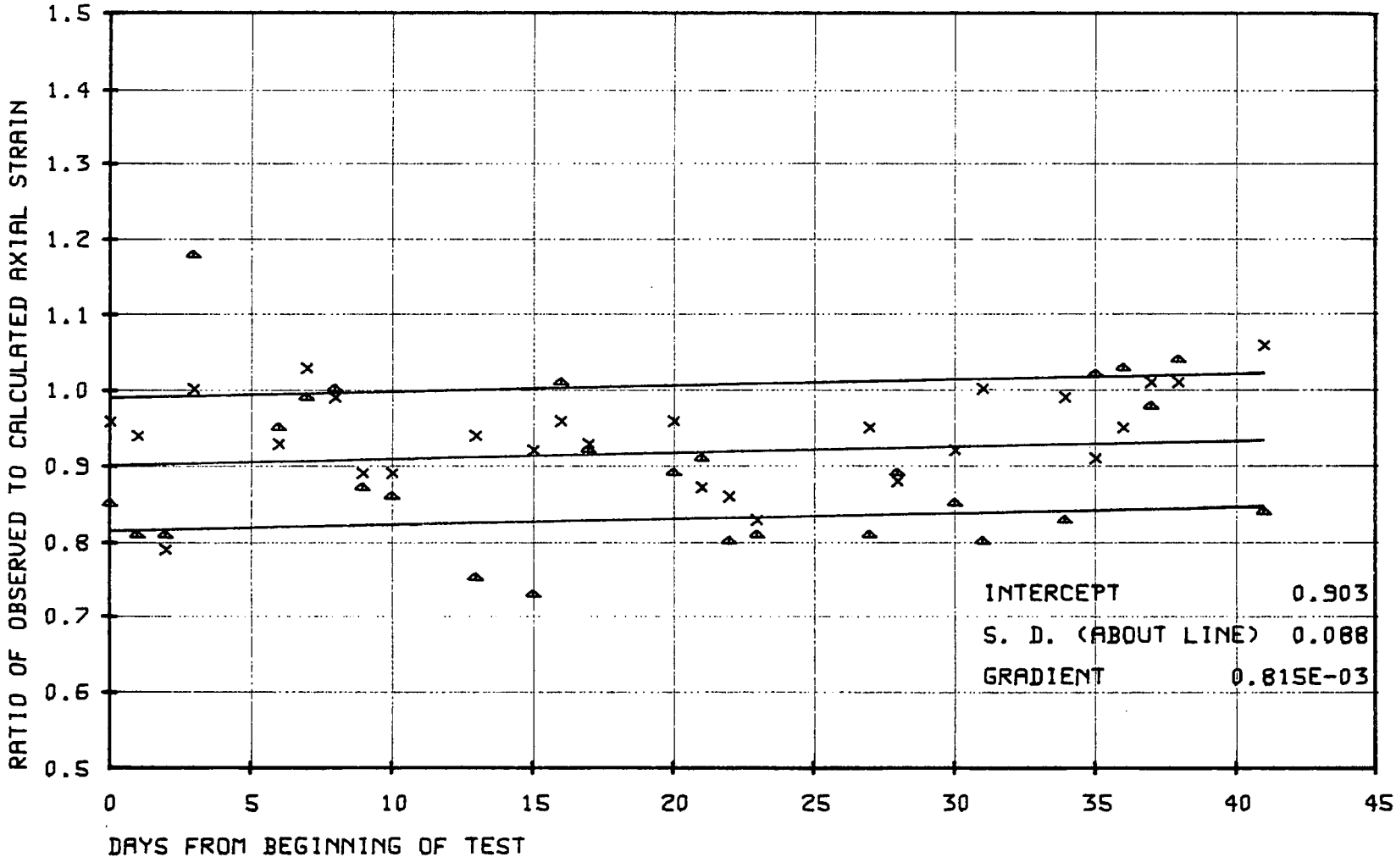

GRAPH 51. RATIOS OF OBSERVED TO CALCULATED CURVATURE
FIRST SINGLE SPAN TEST
BEAM LOADED ... UNCRACKED ANALYSIS

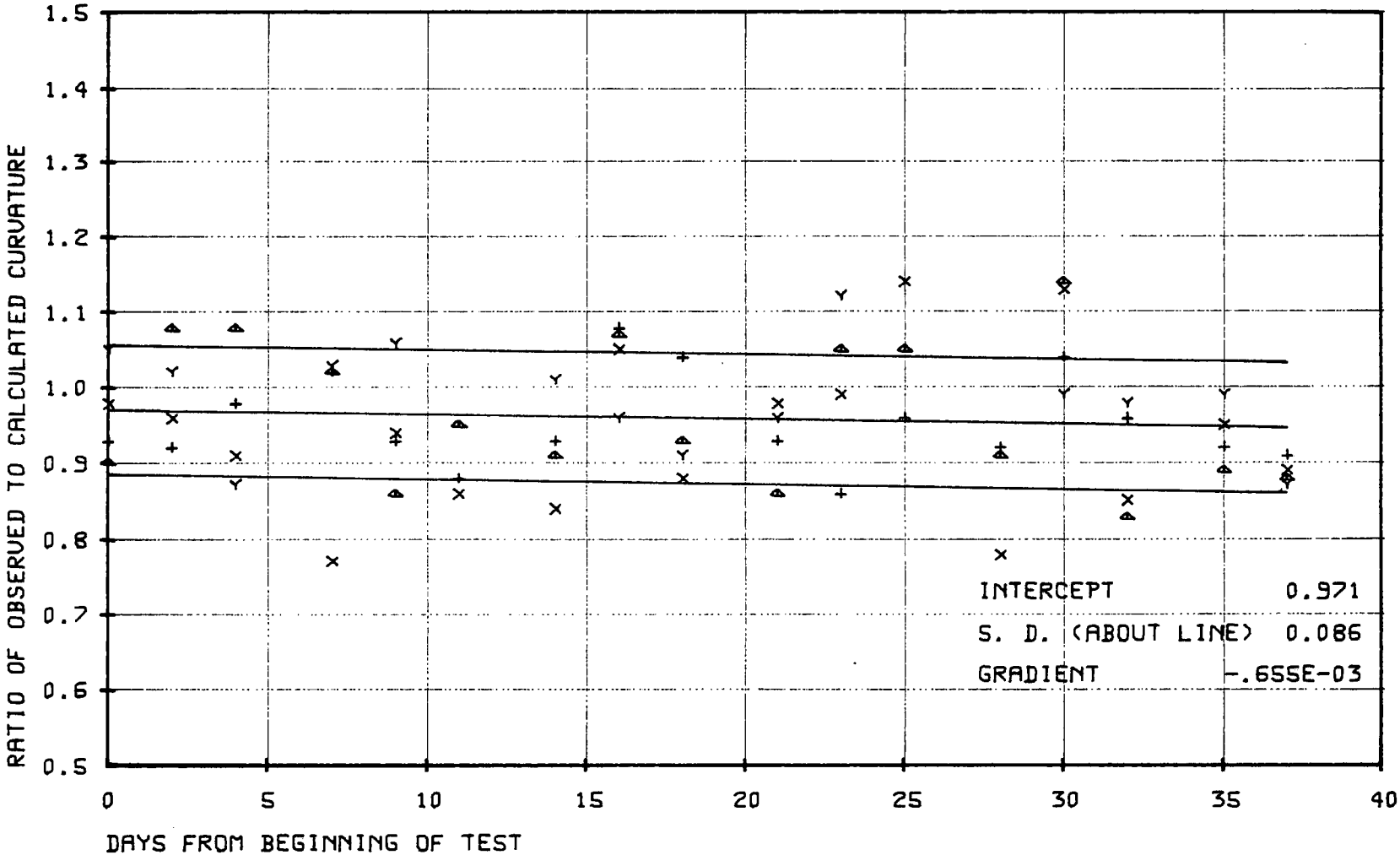

GRAPH 52. RATIOS OF OBSERVED TO CALCULATED CURVATURE
SECOND SINGLE SPAN TEST
BEAM LOADED ... UNCRACKED ANALYSIS

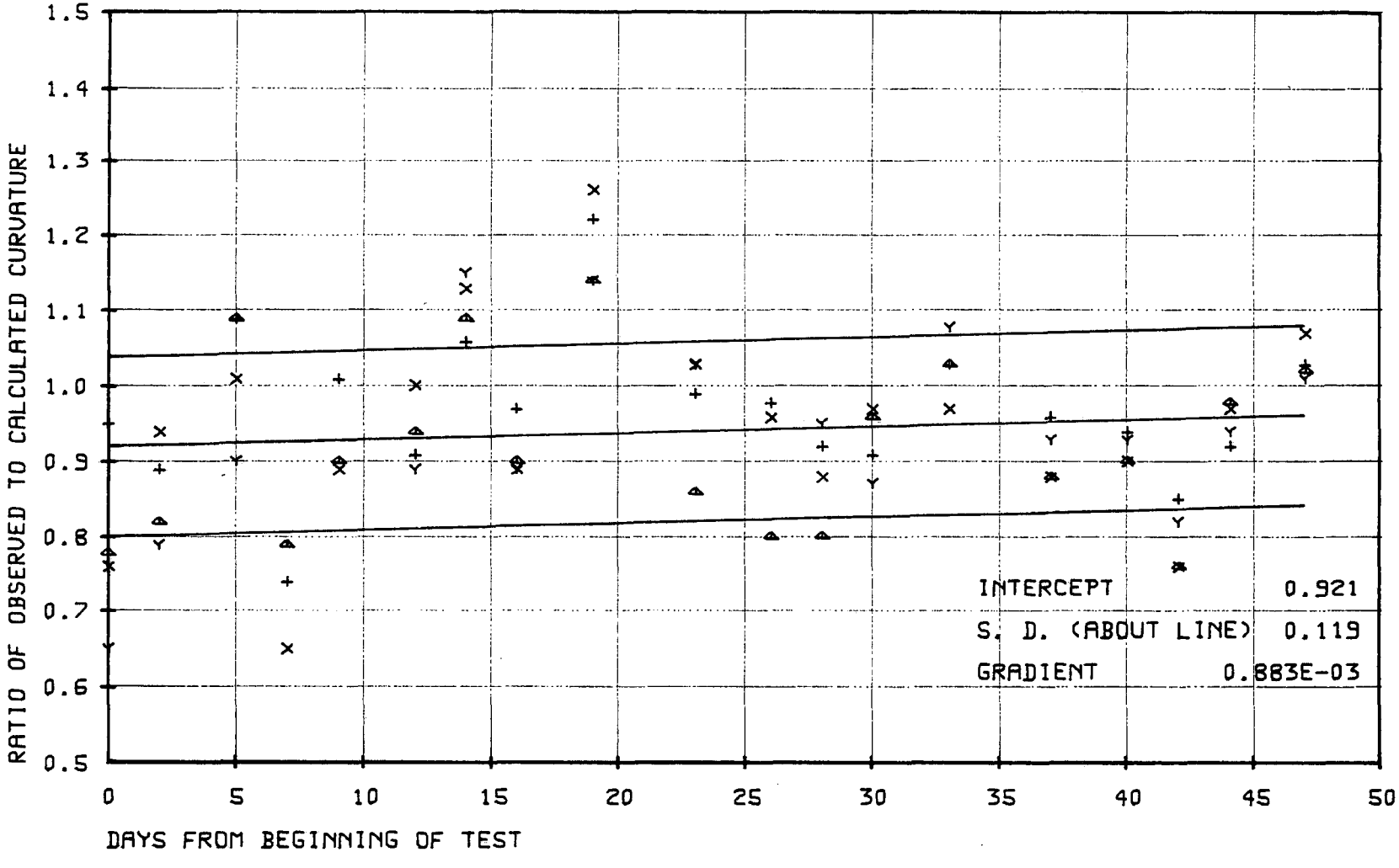

GRAPH 53. RATIOS OF OBSERVED TO CALCULATED CURVATURE
THIRD SINGLE SPAN TEST
BEAM LOADED ... UNCRACKED ANALYSIS

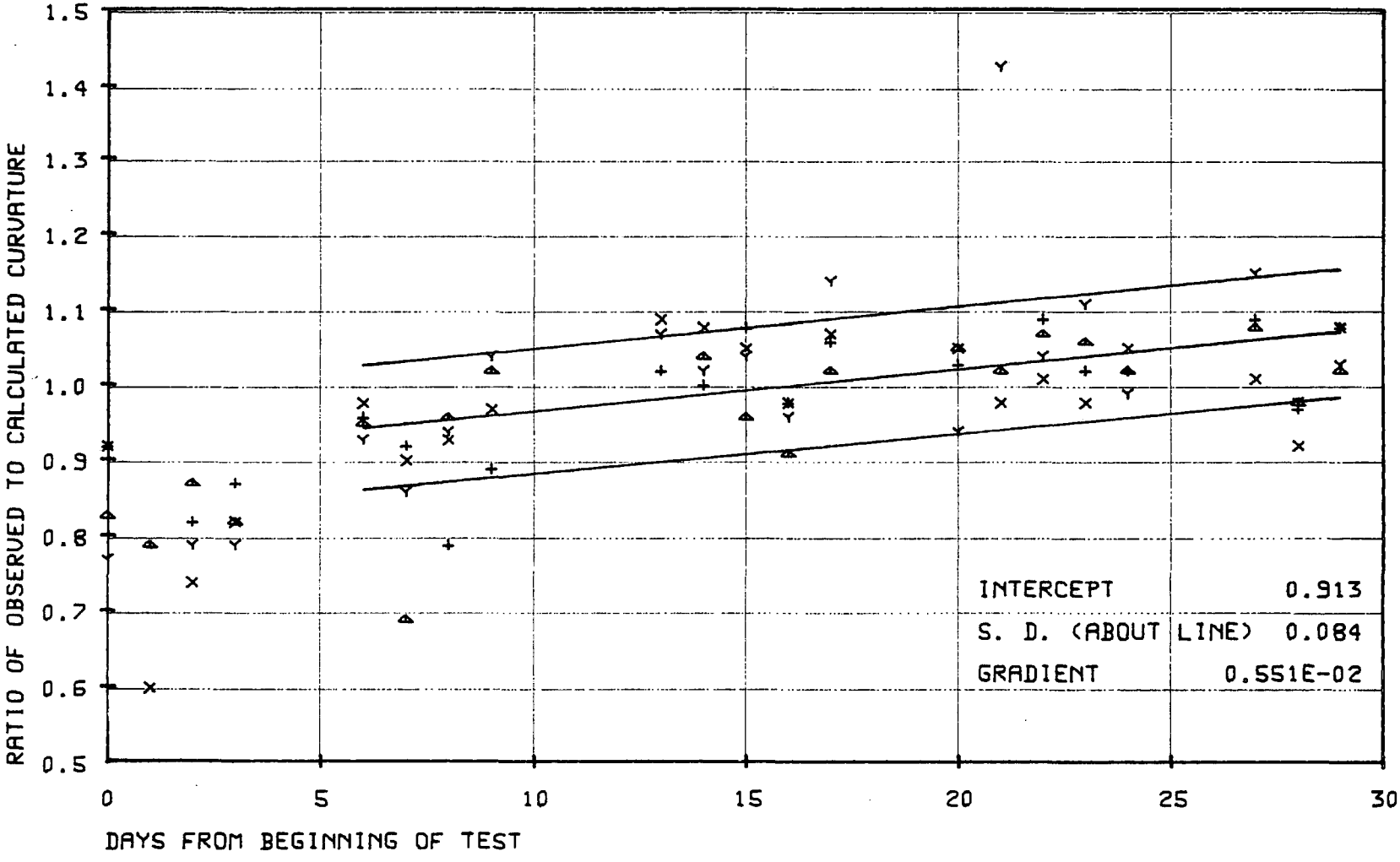

GRAPH 54. RATIOS OF OBSERVED TO CALCULATED CURVATURE
DEEP BEAM TEST
BEAM LOADED ... UNCRACKED ANALYSIS

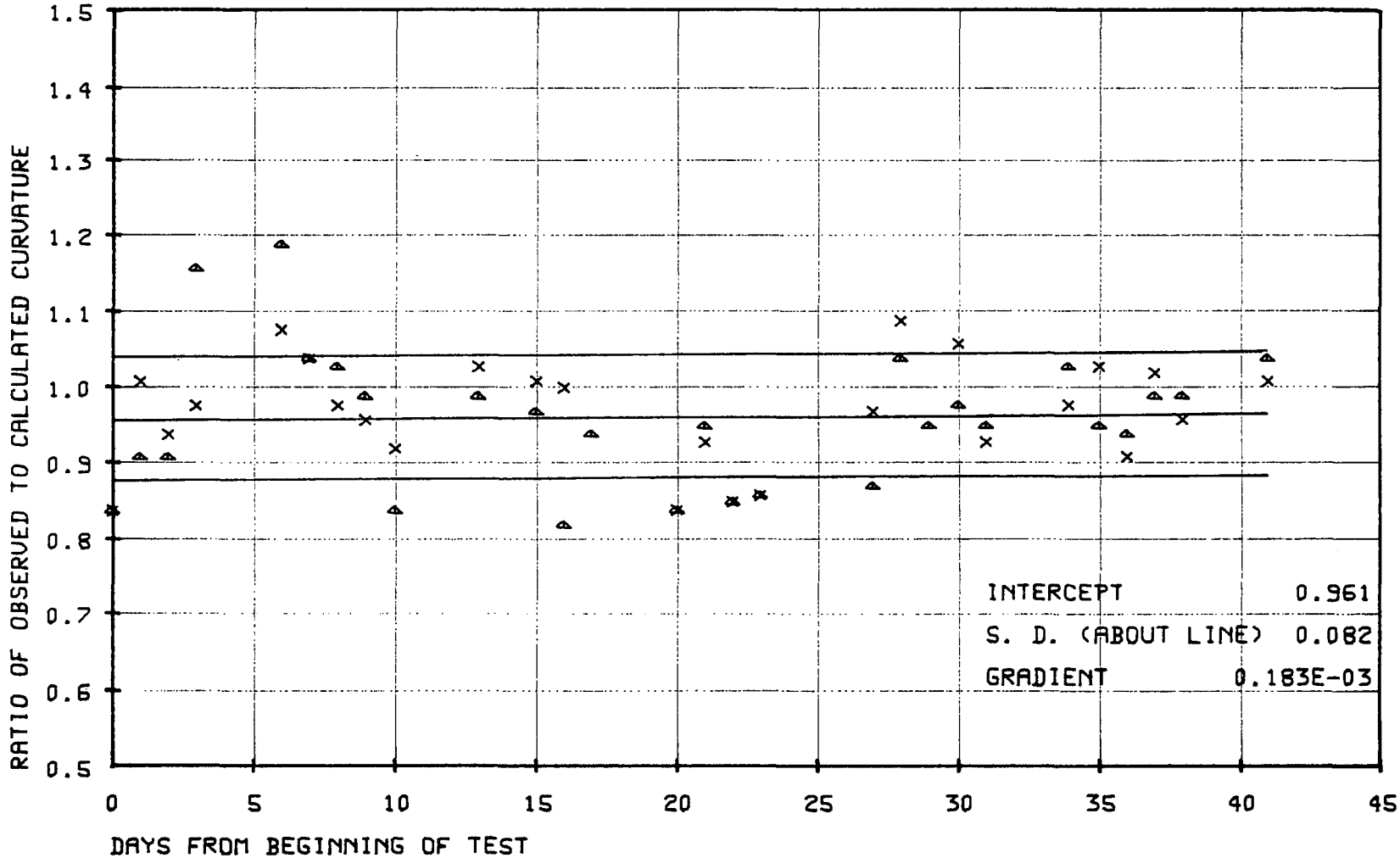

GRAPH 55. RATIOS OF OBSERVED TO CALCULATED CURVATURE
FIRST SINGLE SPAN TEST
BEAM LOADED ... CRACKED ANALYSIS

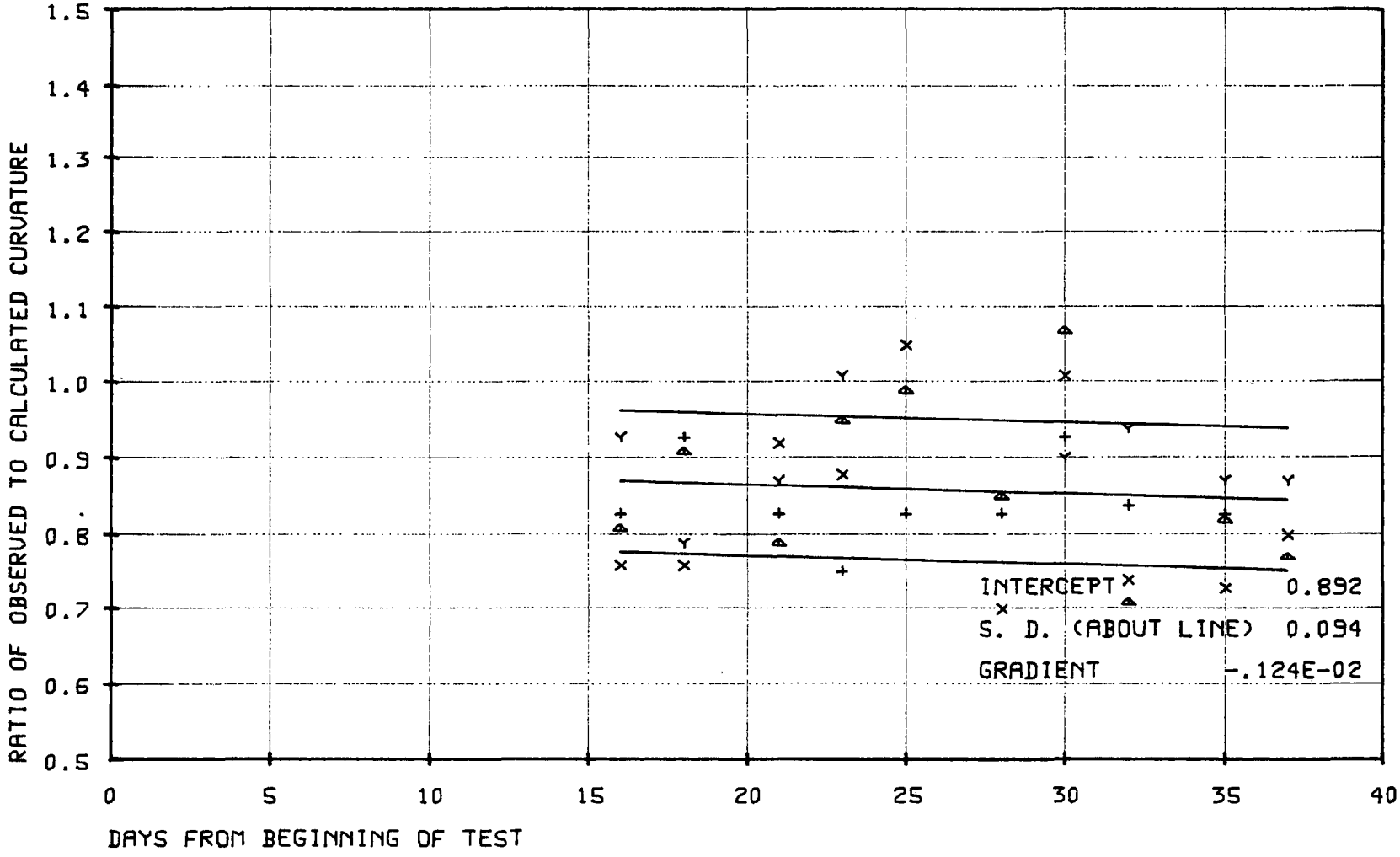

GRAPH 56. RATIOS OF OBSERVED TO CALCULATED CURVATURE
SECOND SINGLE SPAN TEST
BEAM LOADED ... CRACKED ANALYSIS

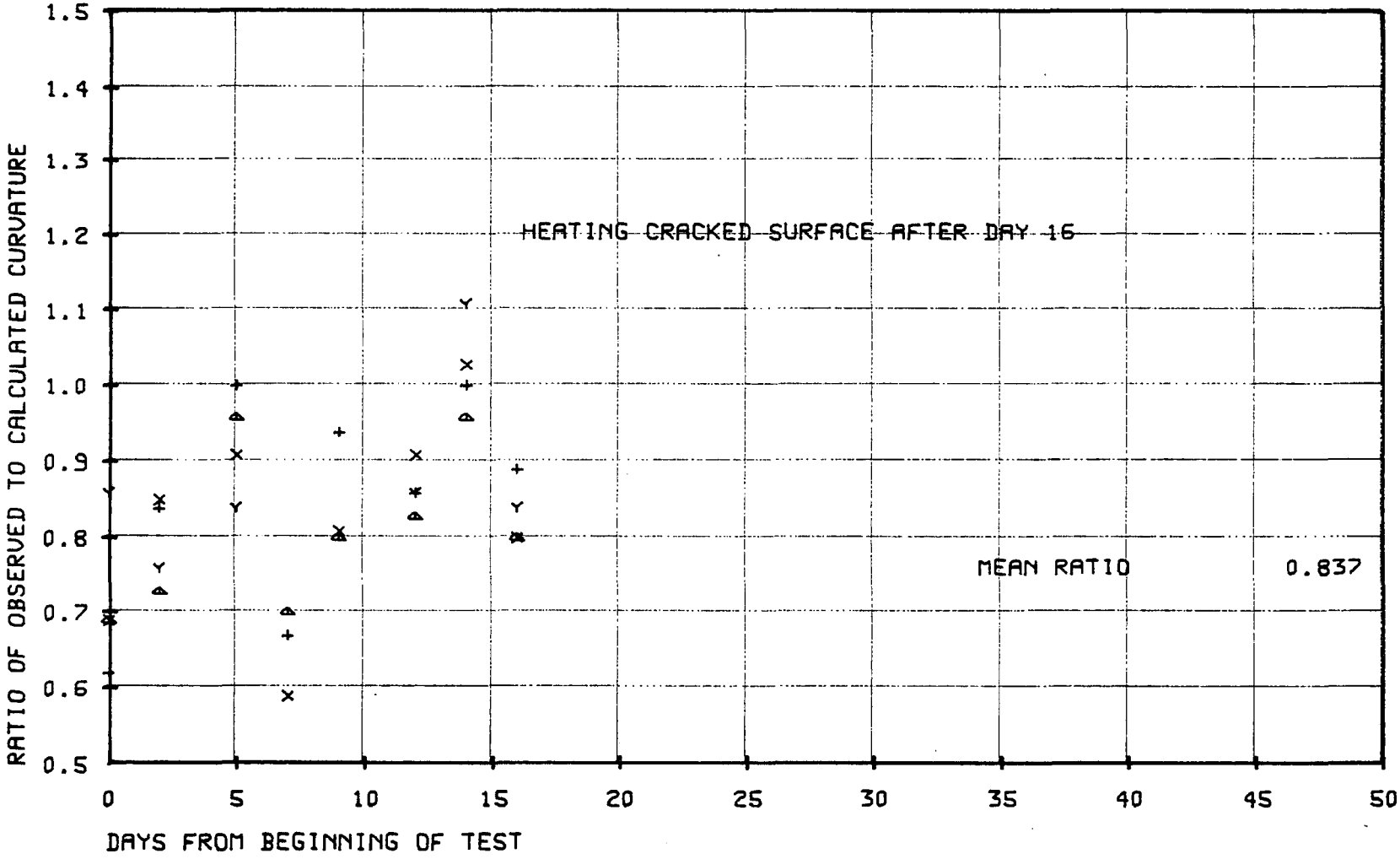

GRAPH 57. RATIOS OF OBSERVED TO CALCULATED CURVATURE
THIRD SINGLE SPAN TEST
BEAM LOADED ... CRACKED ANALYSIS

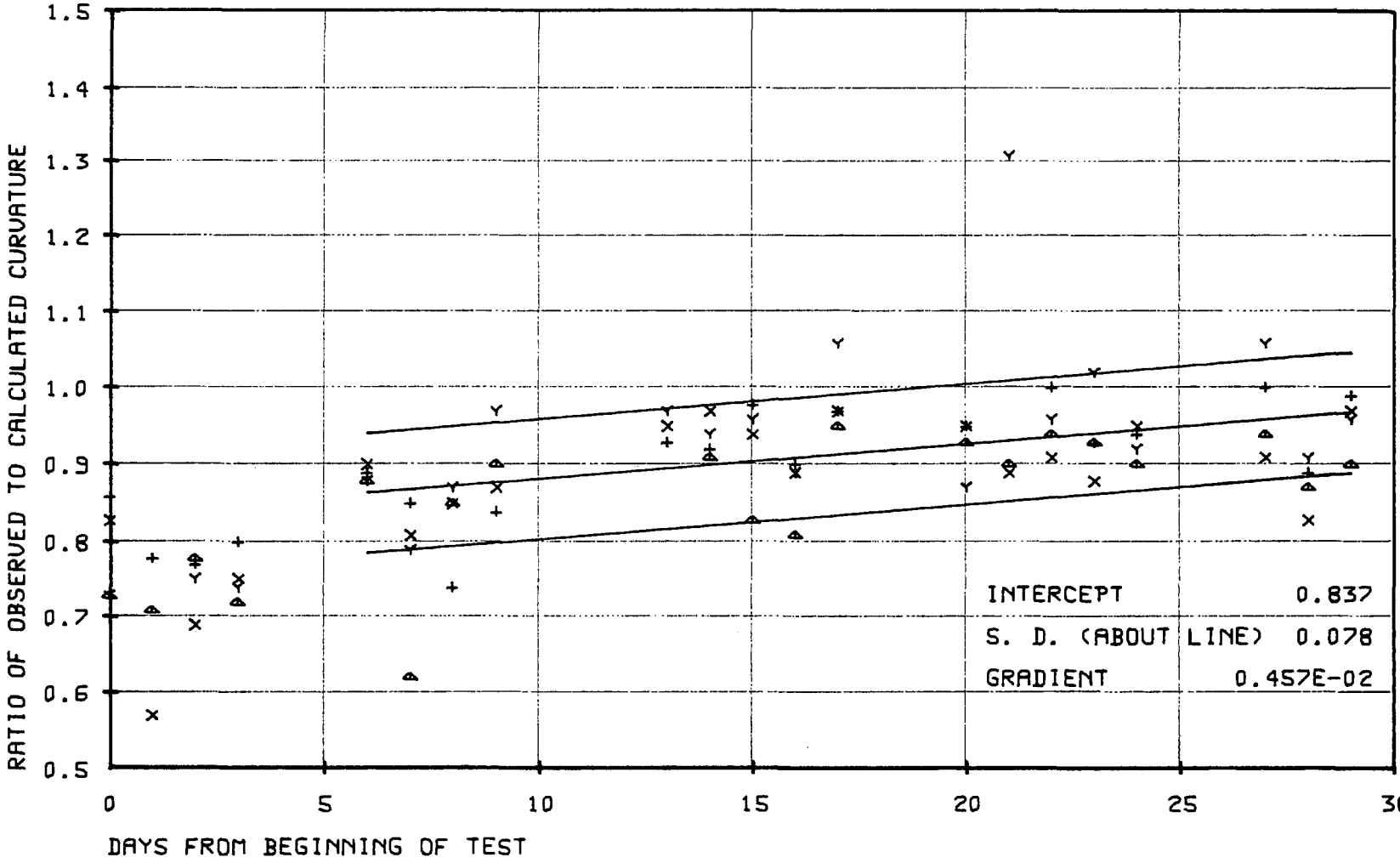

GRAPH 58. RATIOS OF OBSERVED TO CALCULATED CURVATURE
DEEP BEAM TEST
BEAM LOADED ... CRACKED ANALYSIS

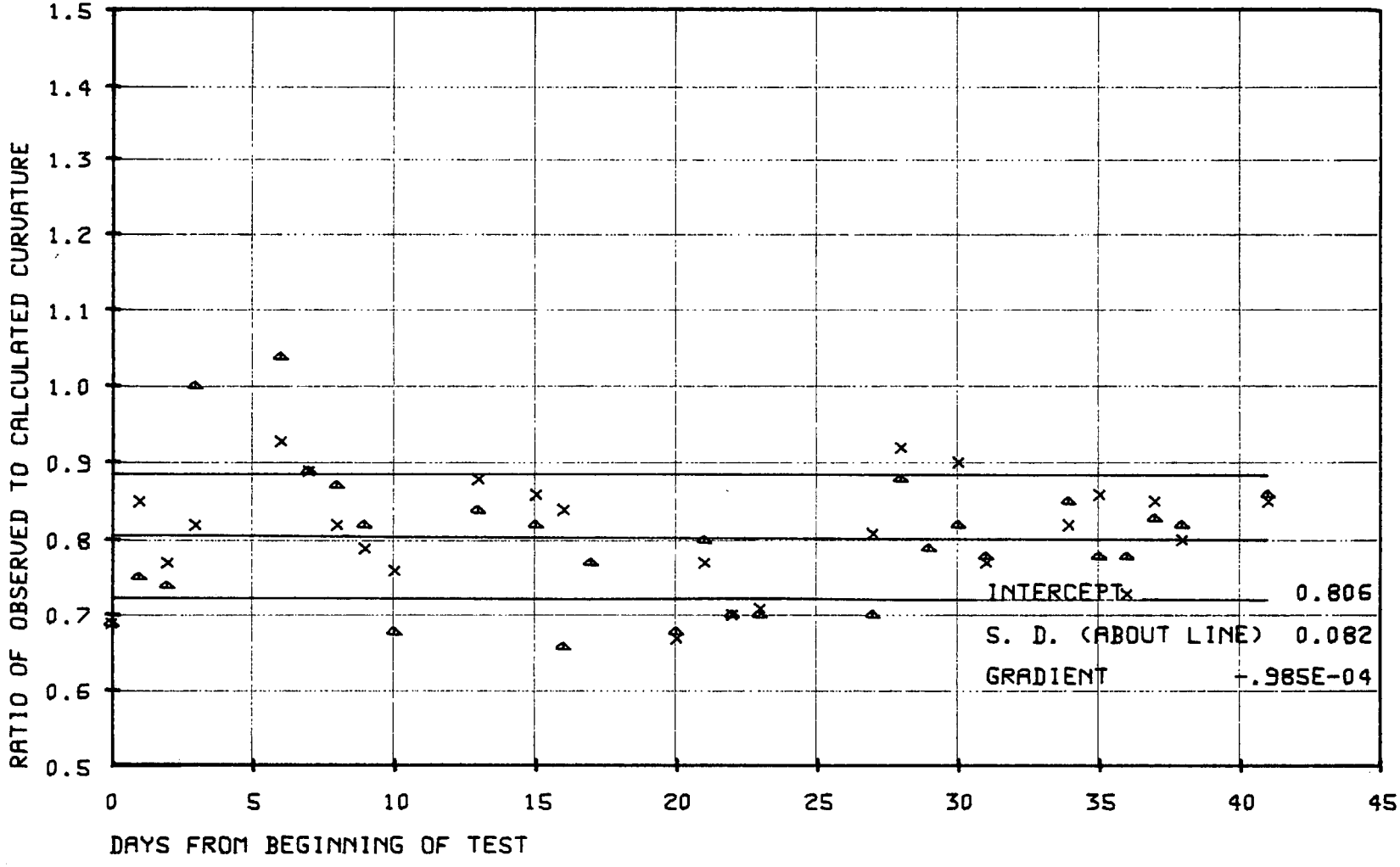

GRAPH 59. RATIOS OF OBSERVED TO CALCULATED CURVATURE
T-SECTION BEAM TEST
BEAM LOADED ... CRACKED ANALYSIS

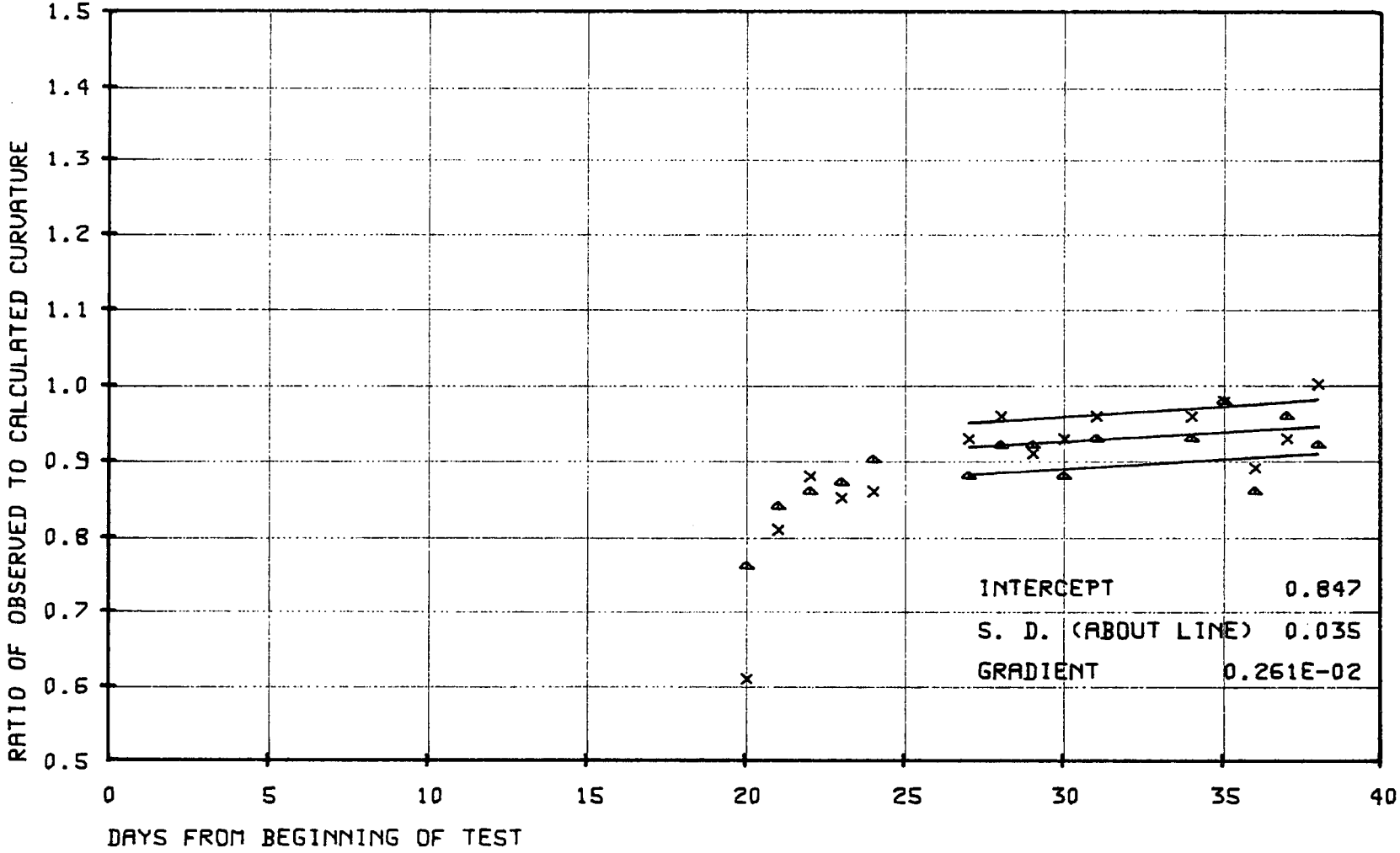

GRAPH 60. RATIOS OF OBSERVED TO CALCULATED AXIAL STRAIN
SECOND TWO SPAN TEST
BEAM LOADED

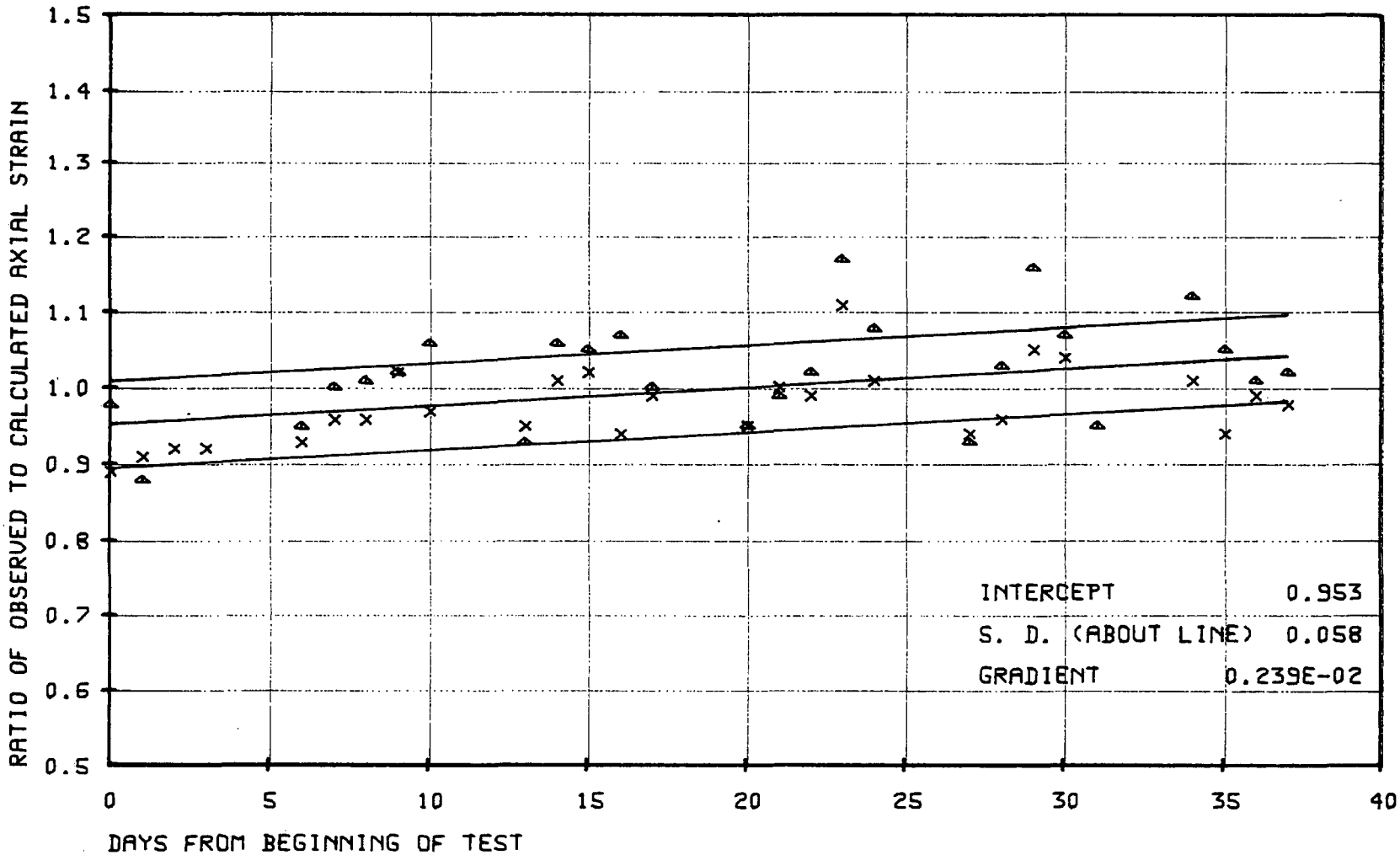

GRAPH 61. RATIOS OF OBSERVED TO CALCULATED AXIAL STRAIN
THIRD TWO SPAN TEST
BEAM LOADED

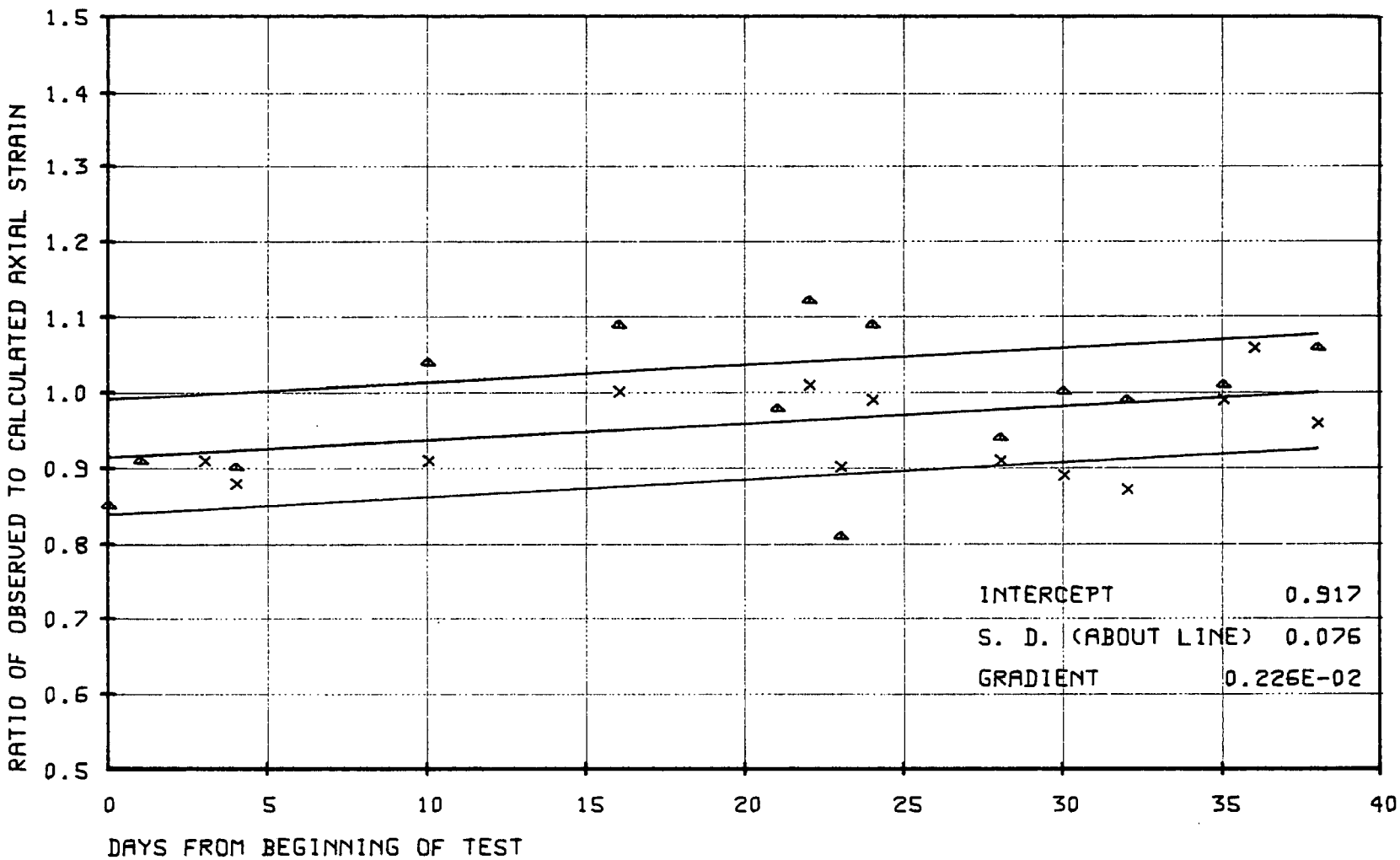

GRAPH 62. RATIOS OF OBSERVED TO CALCULATED REACTION
SECOND TWO SPAN TEST
BEAM LOADED ... CENTRAL SUPPORT REACTION

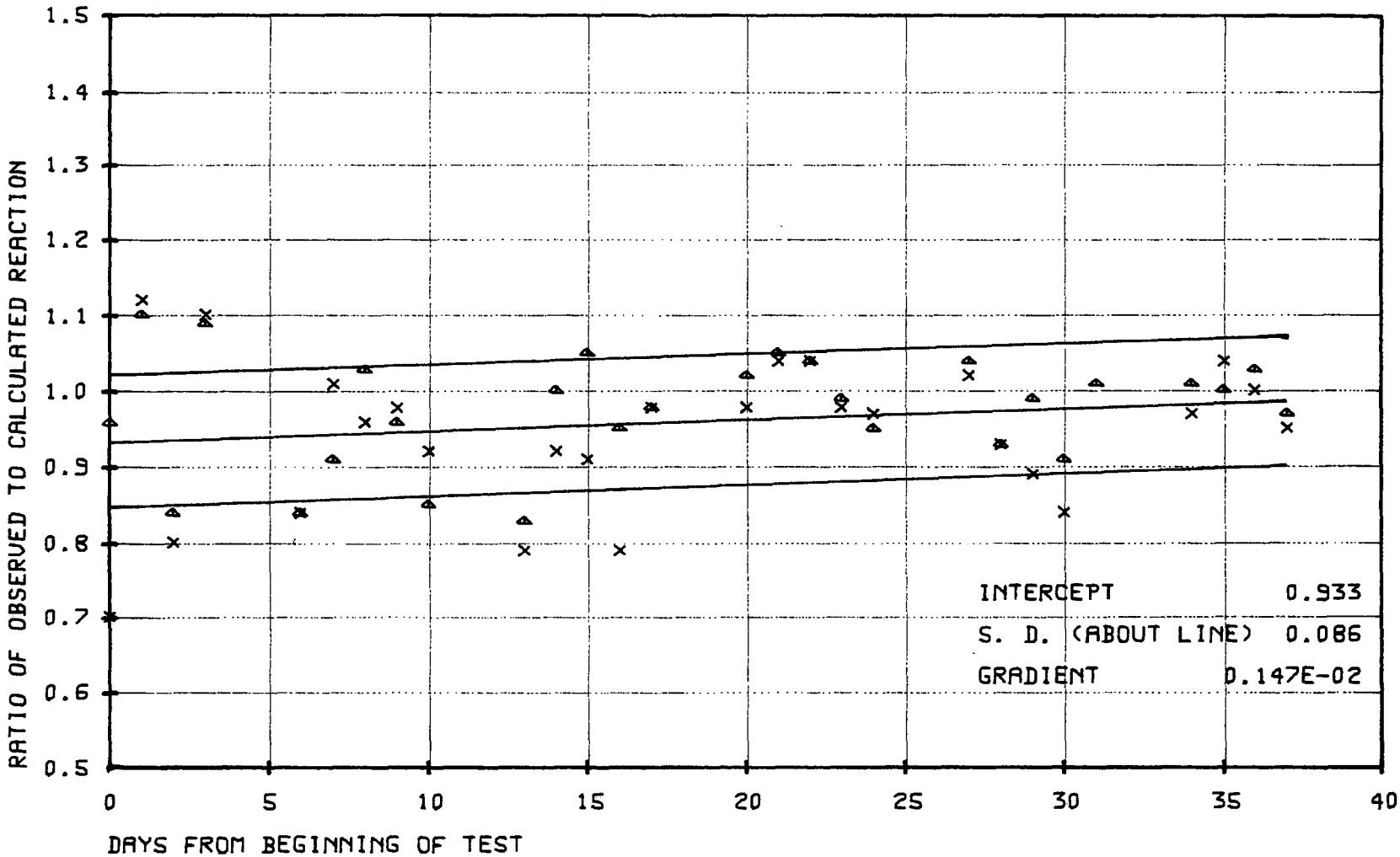

GRAPH 63. RATIOS OF OBSERVED TO CALCULATED REACTION
THIRD TWO SPAN TEST
BEAM LOADED ... CENTRAL SUPPORT REACTION

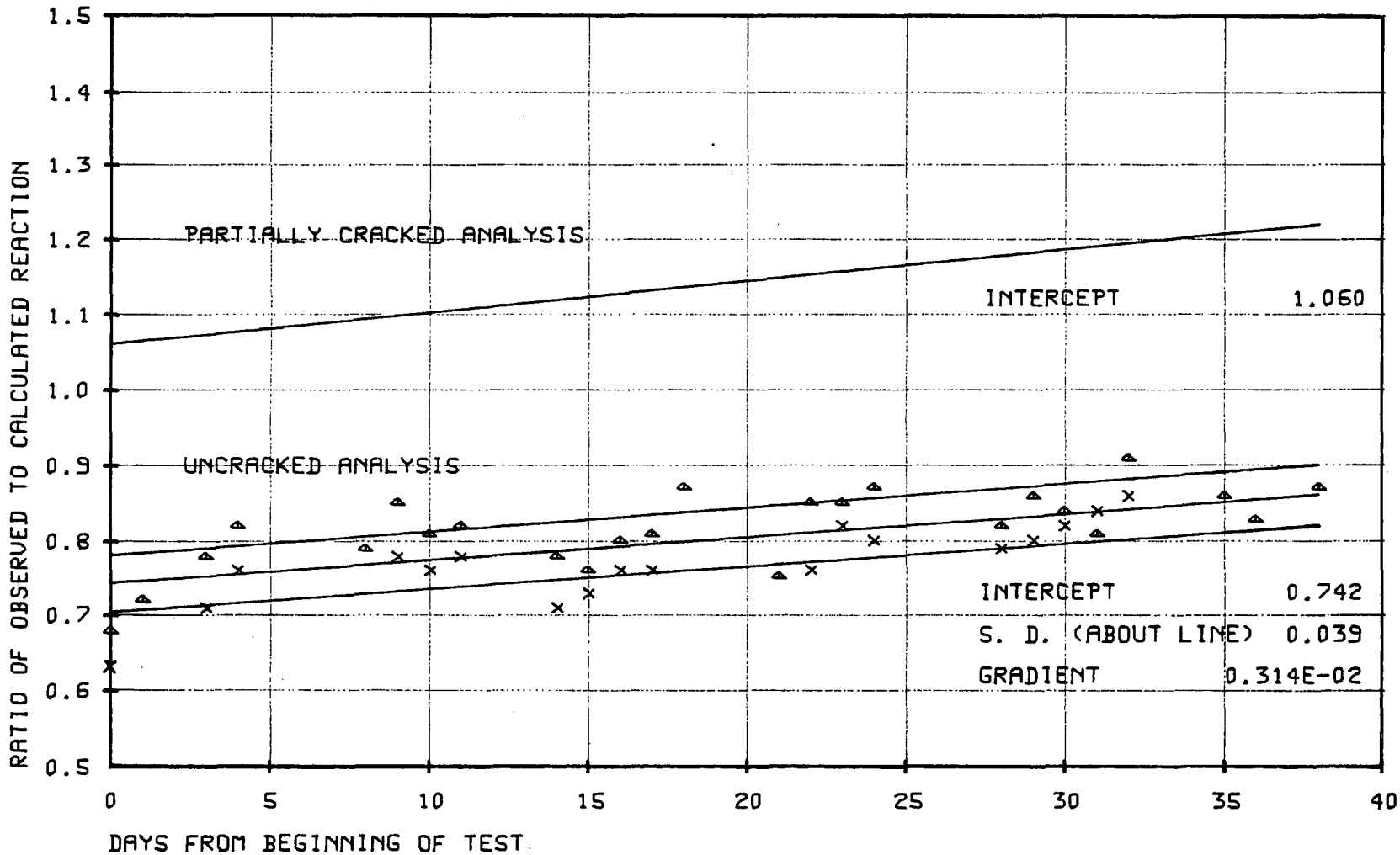

GRAPH 64. RATIOS OF CENTRAL SUPPORT TO END SUPPORT REACTION
SECOND TWO SPAN TEST

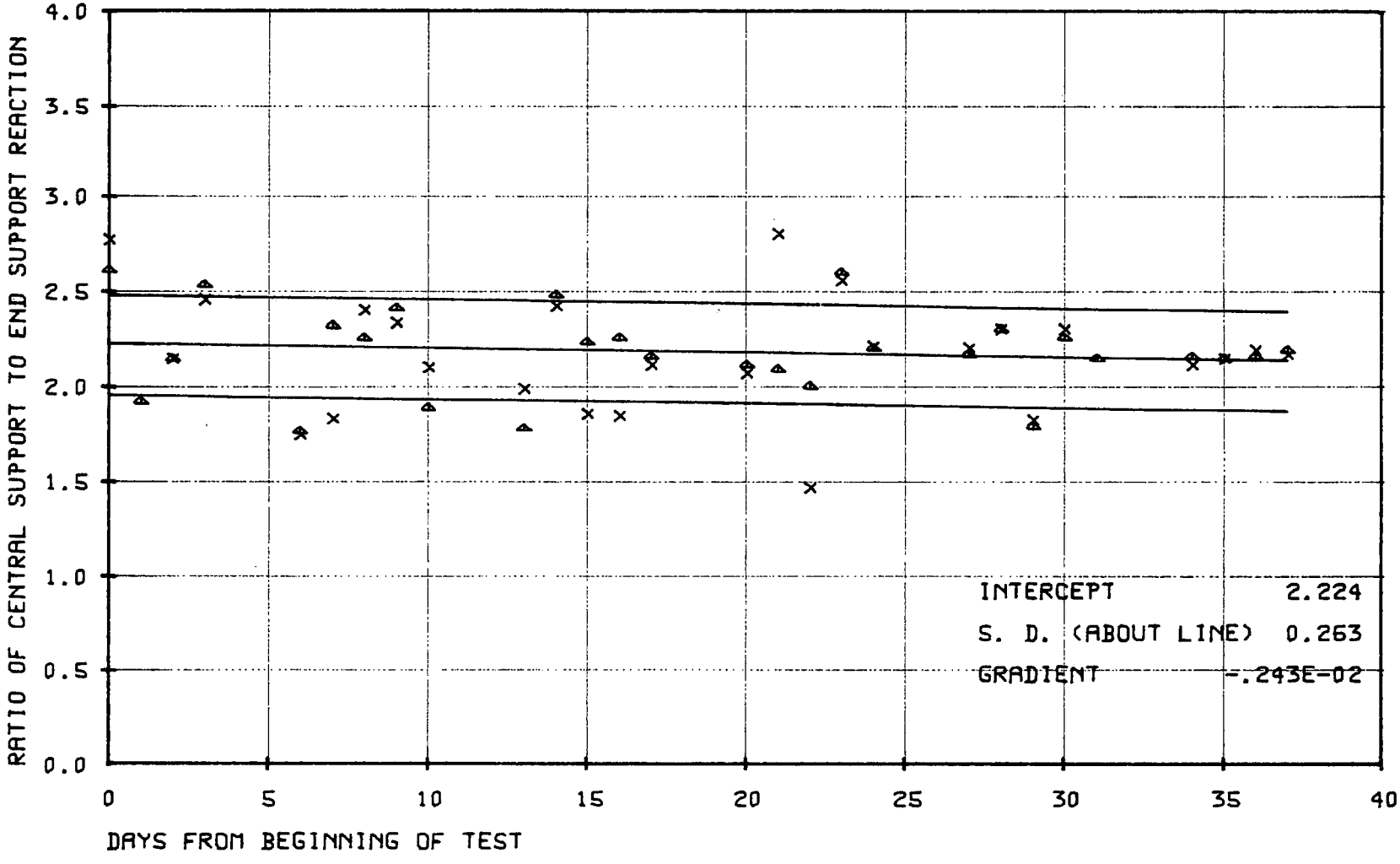

GRAPH 65. RATIOS OF CENTRAL SUPPORT TO END SUPPORT REACTION
THIRD TWO SPAN TEST

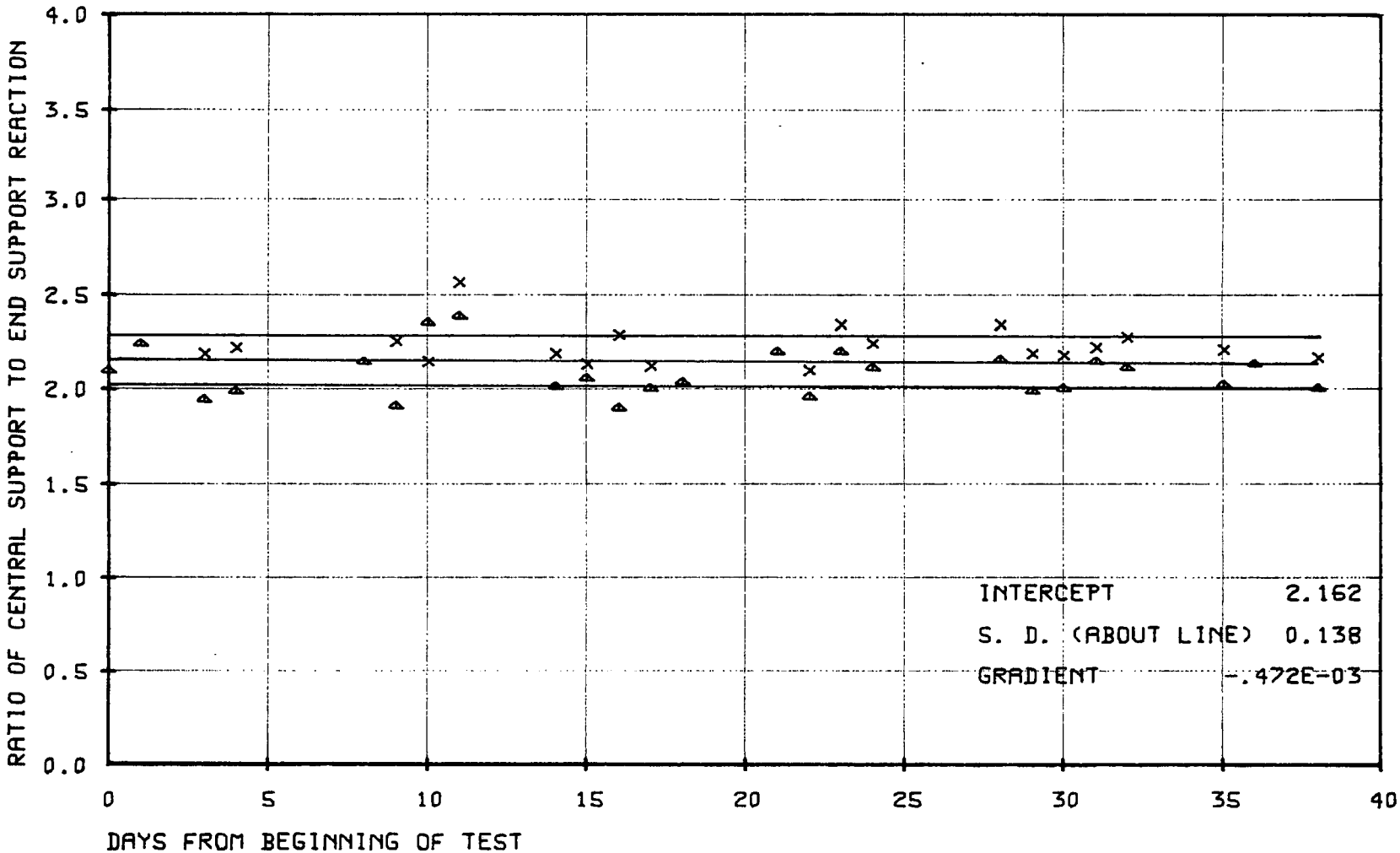

GRAPH 66. LONG-TERM AXIAL STRAINS
THIRD SINGLE SPAN TEST

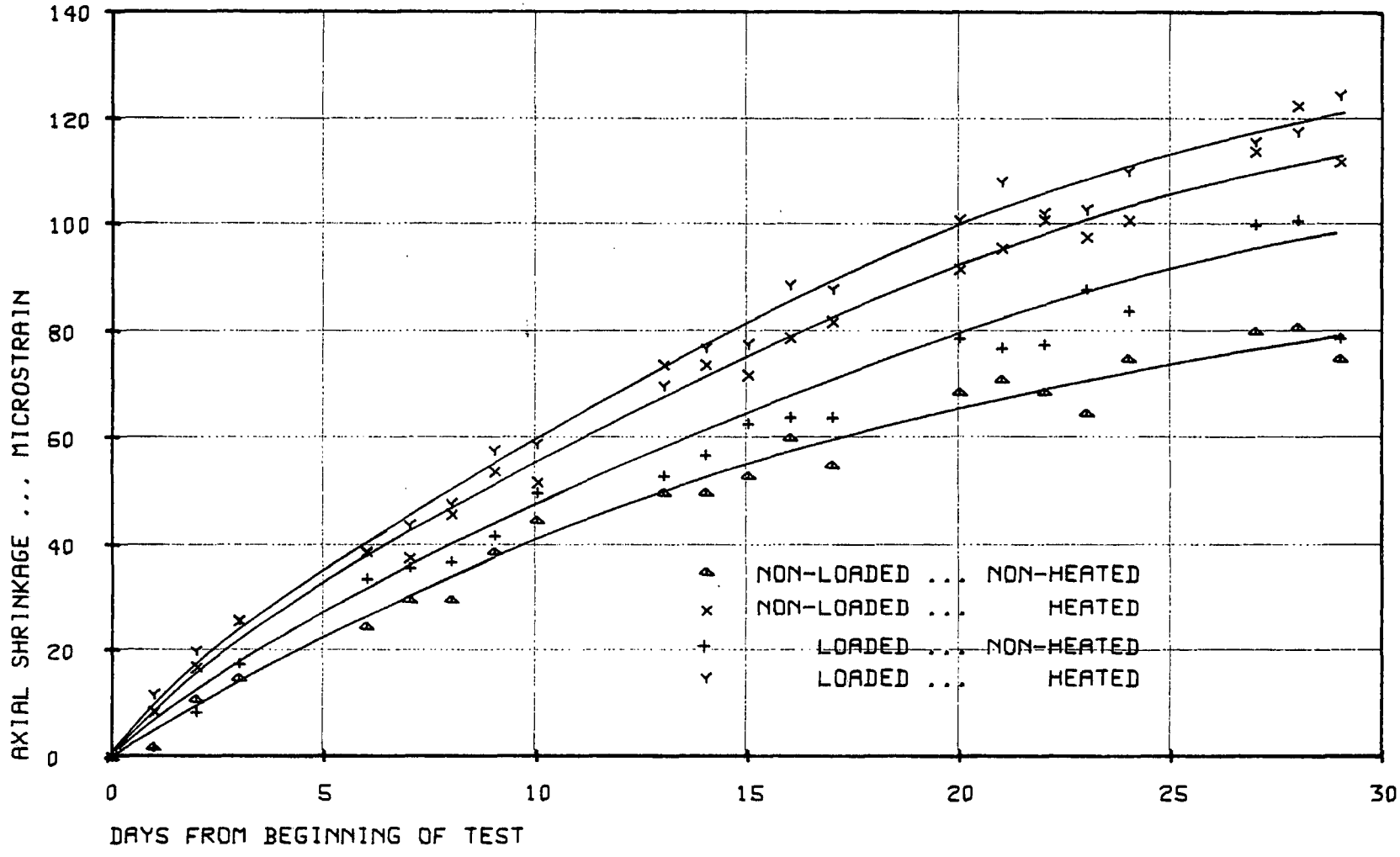

GRAPH 67. LONG-TERM RESULTS FROM FIRST SINGLE SPAN TEST

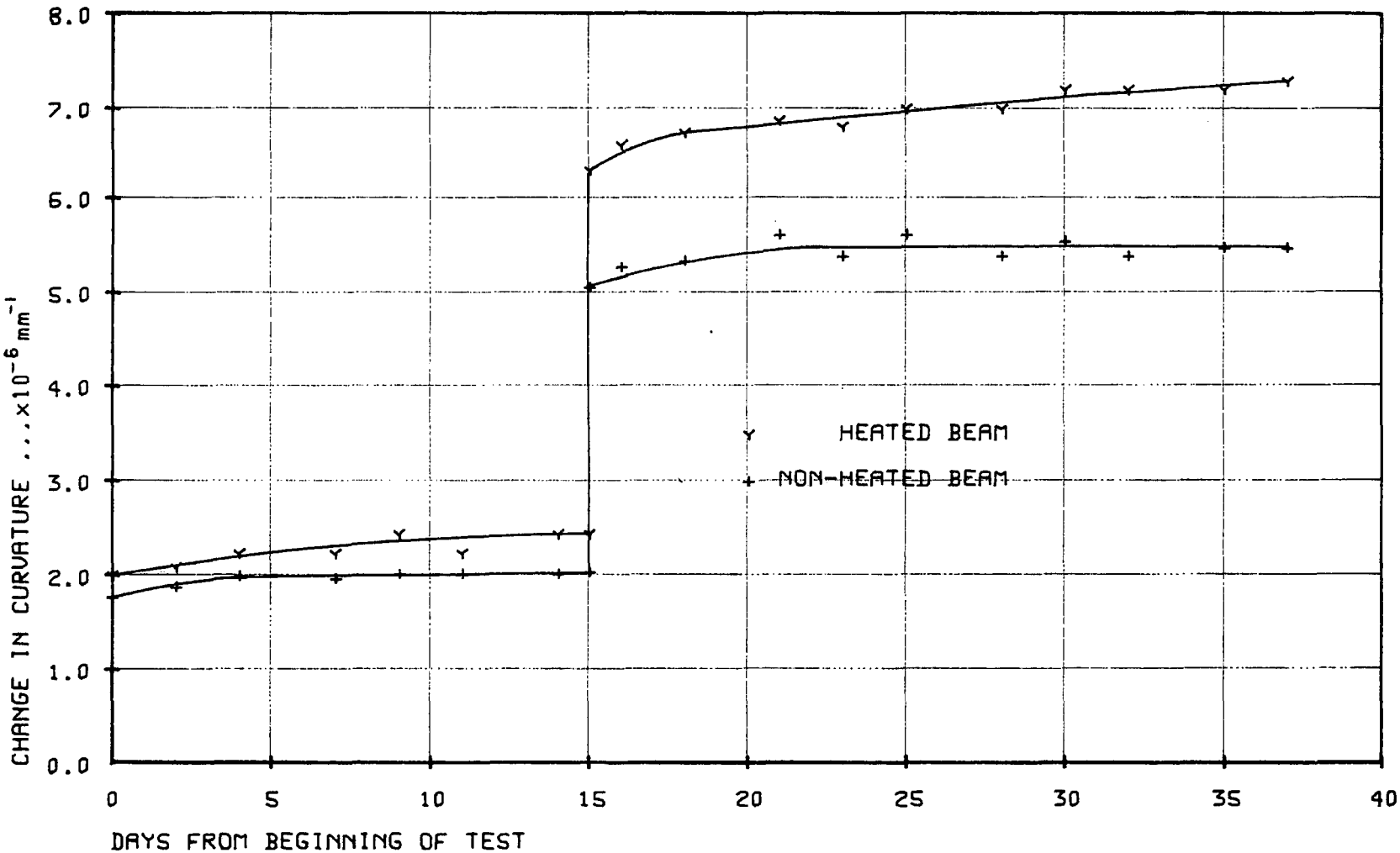

GRAPH 68. LONG-TERM RESULTS FROM SECOND SINGLE SPAN TEST

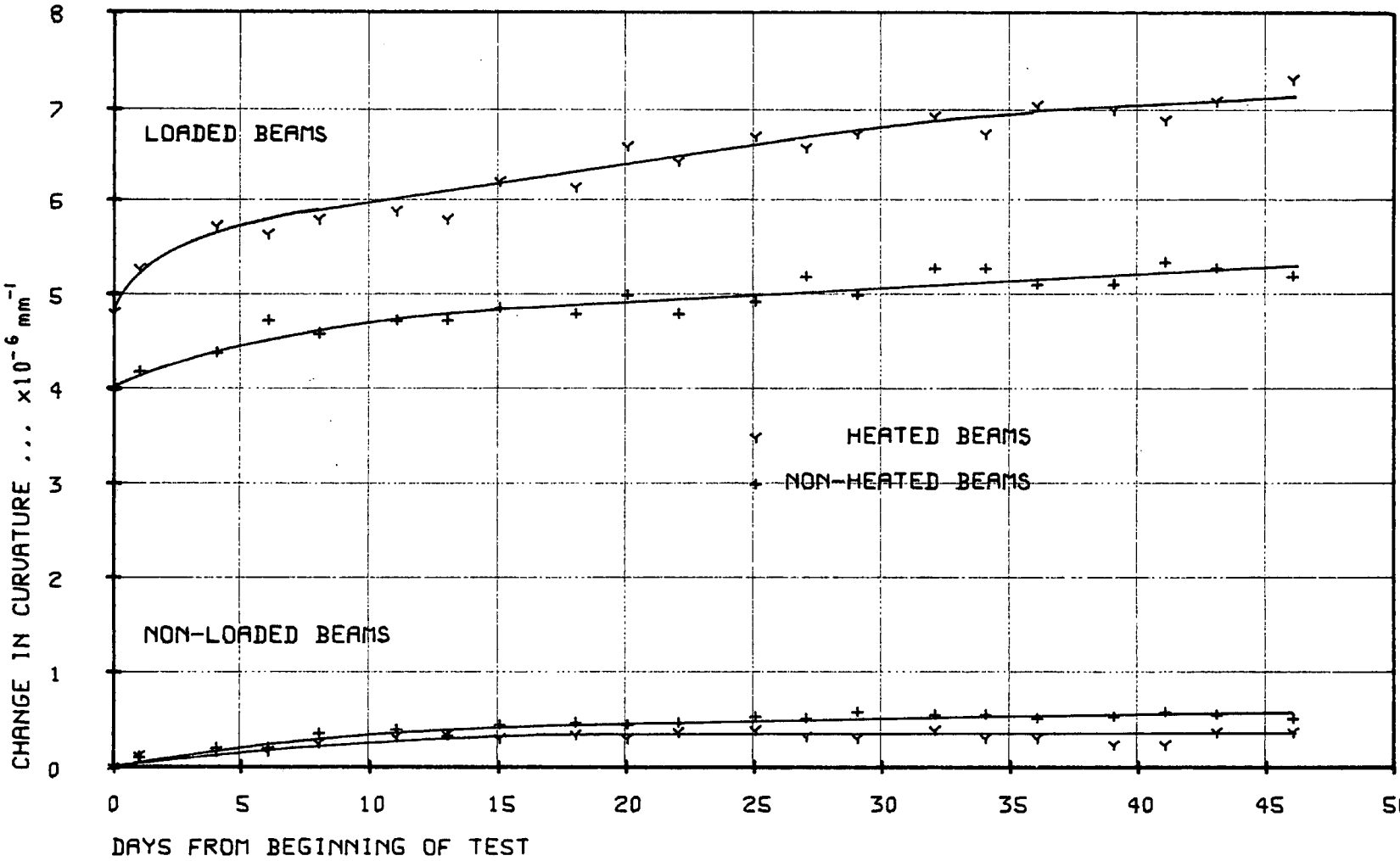

GRAPH 69. LONG-TERM RESULTS FROM THIRD SINGLE SPAN TEST

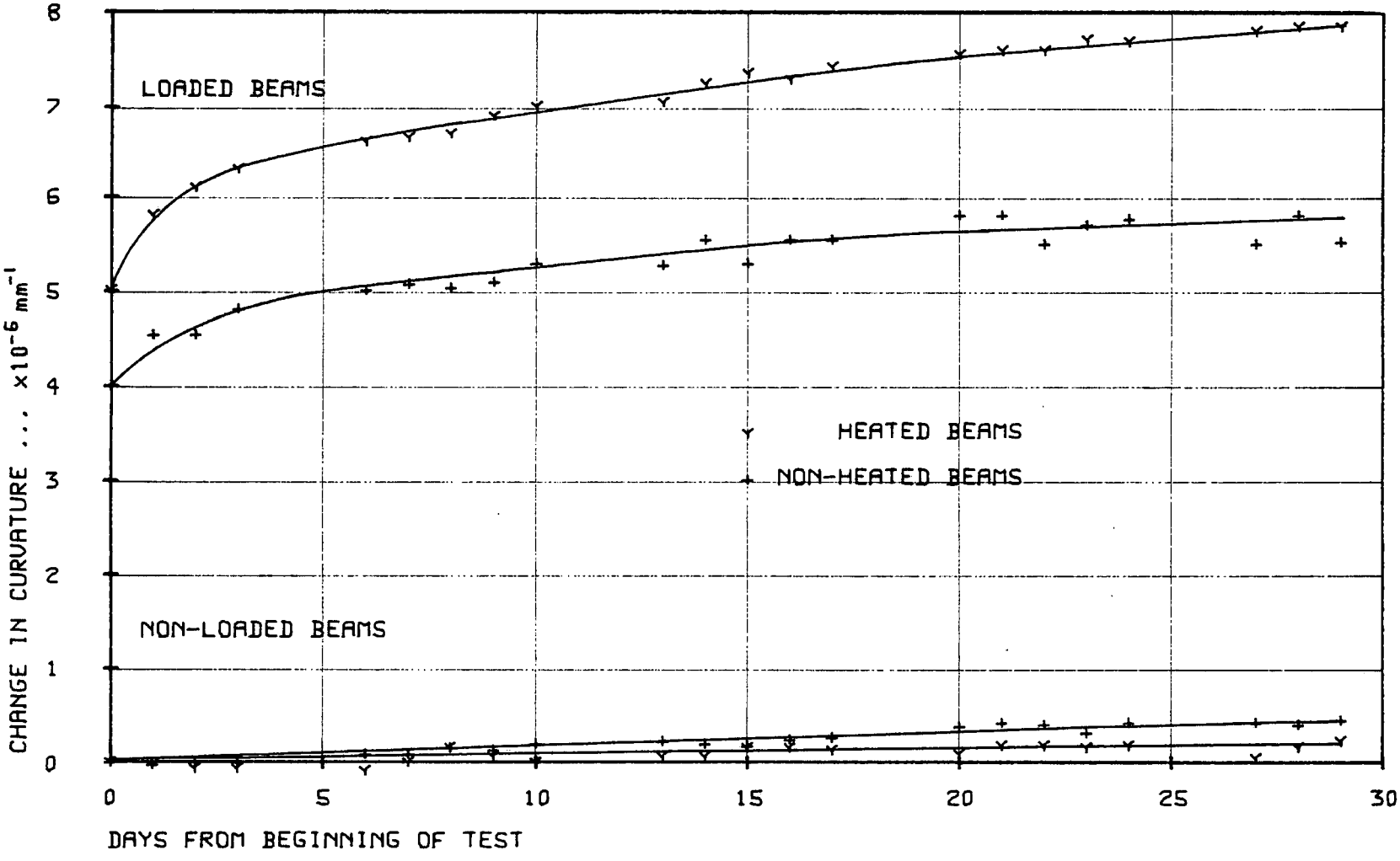

GRAPH 70. LONG-TERM RESULTS FROM DEEP BEAM TEST

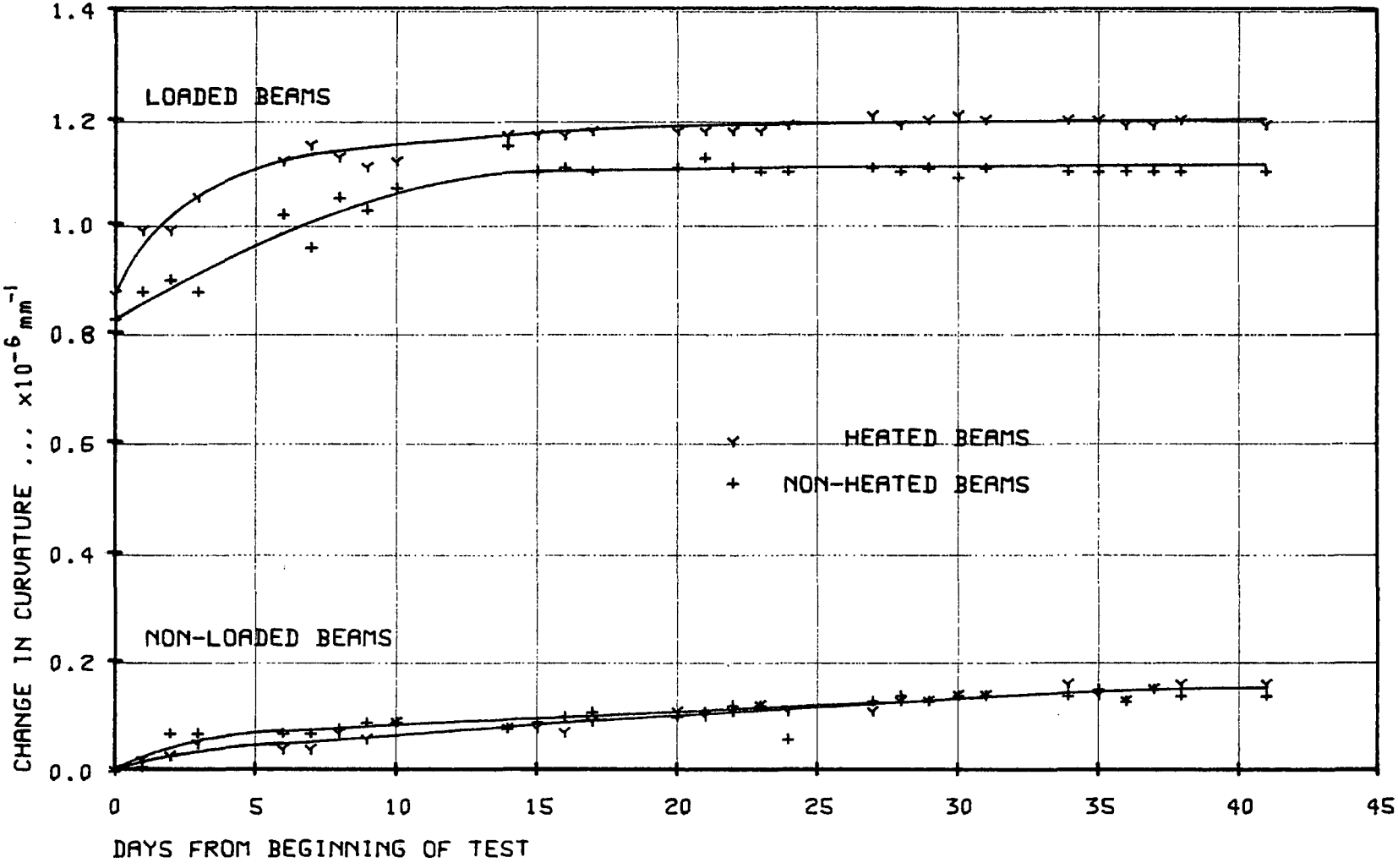

GRAPH 71. LONG-TERM RESULTS FROM T-SECTION BEAM TEST

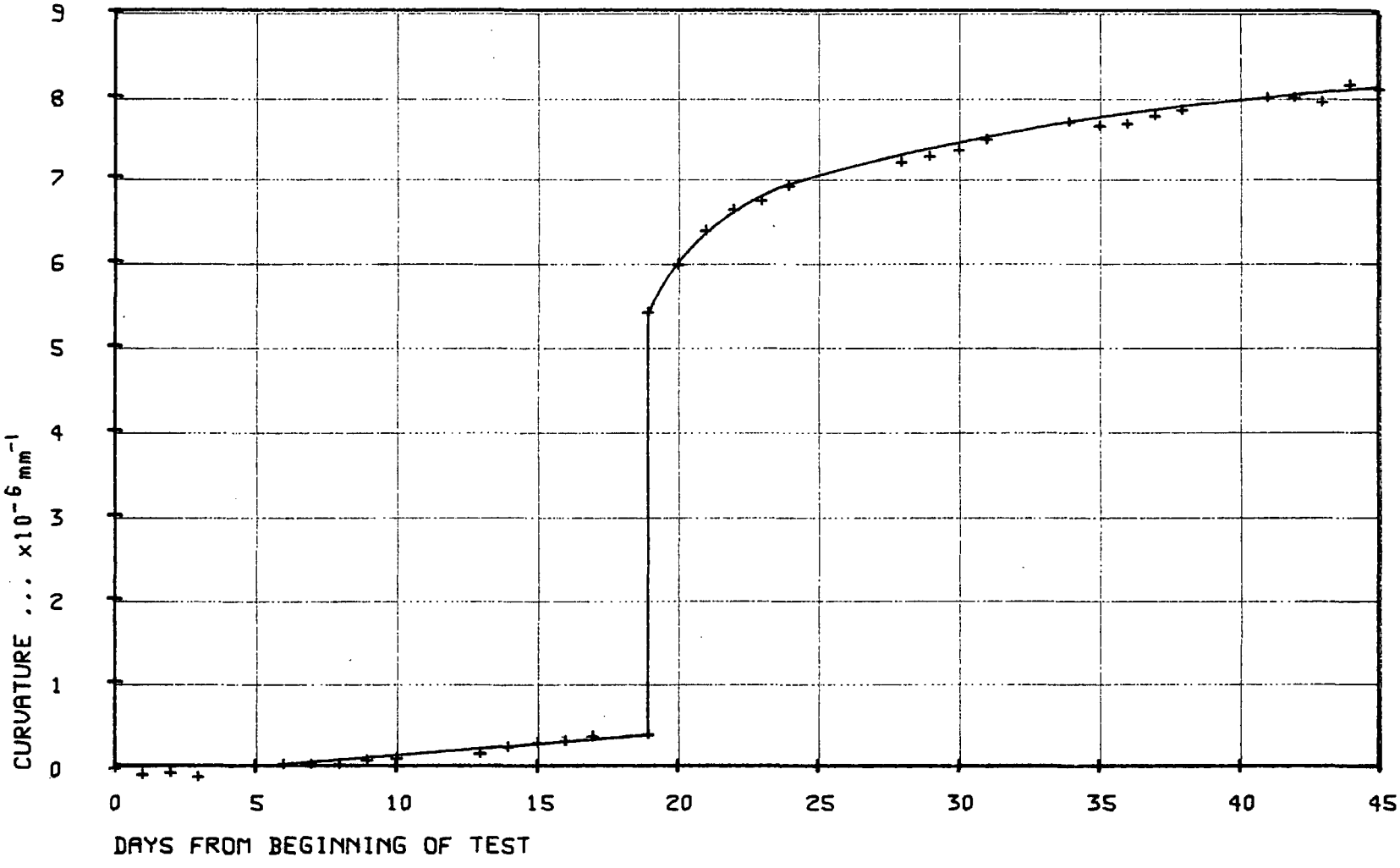

GRAPH 72. LONG-TERM CHANGES IN SUPPORT REACTIONS
SECOND TWO SPAN TEST

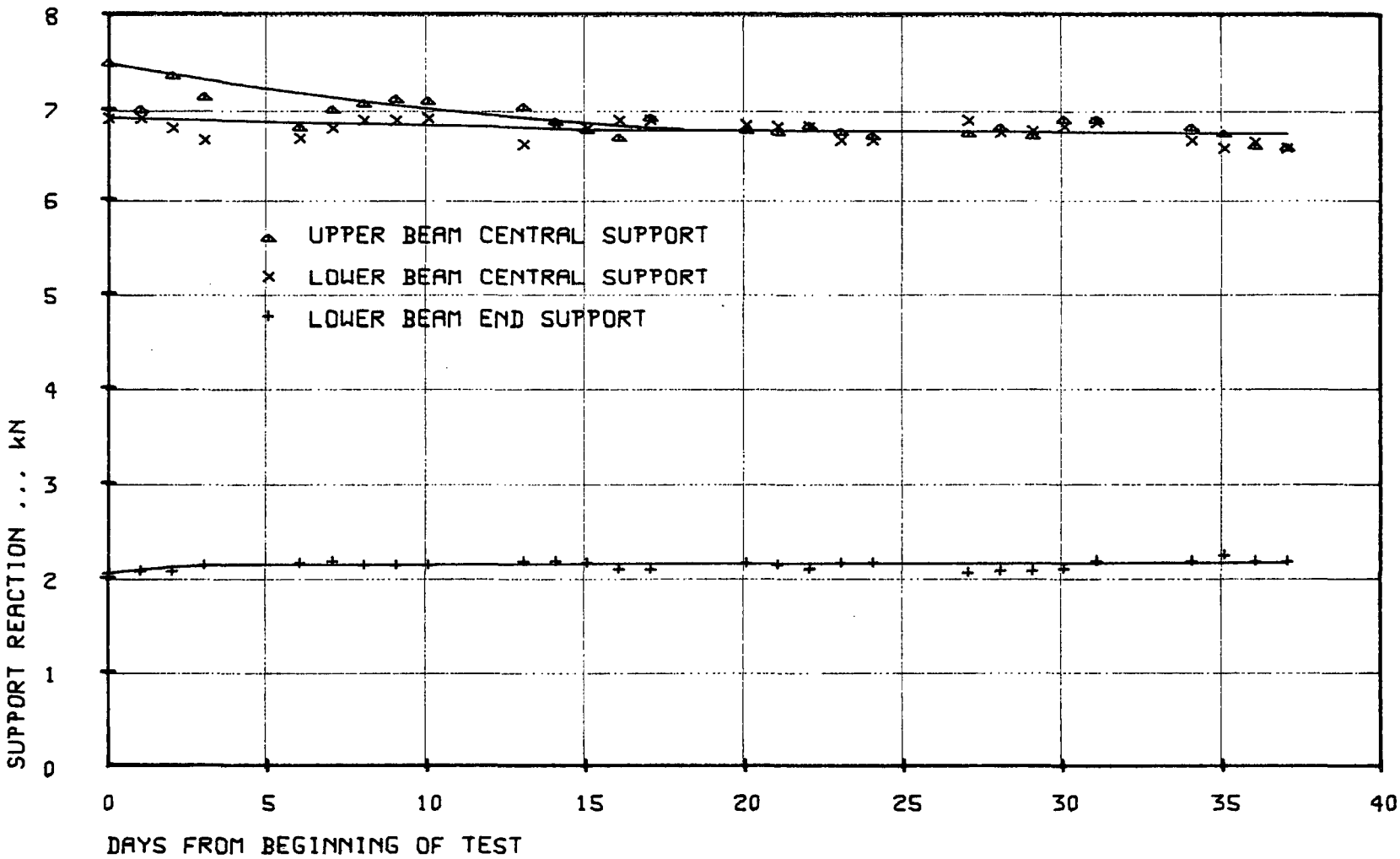

GRAPH 73. LONG-TERM CHANGES IN SUPPORT REACTIONS
THIRD TWO SPAN TEST

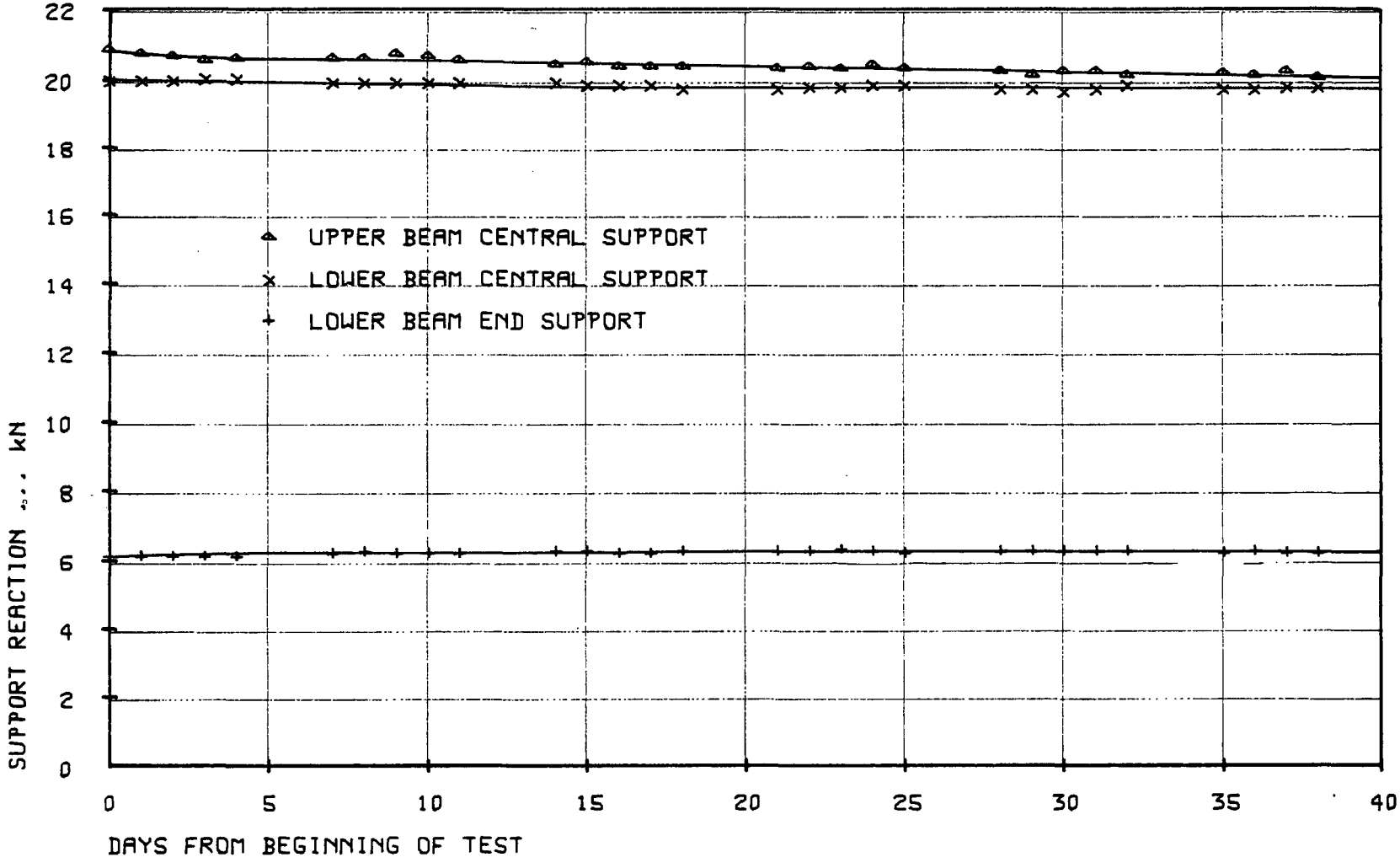

GRAPH 74. SPECIFIC THERMAL CREEP
FIRST TEST

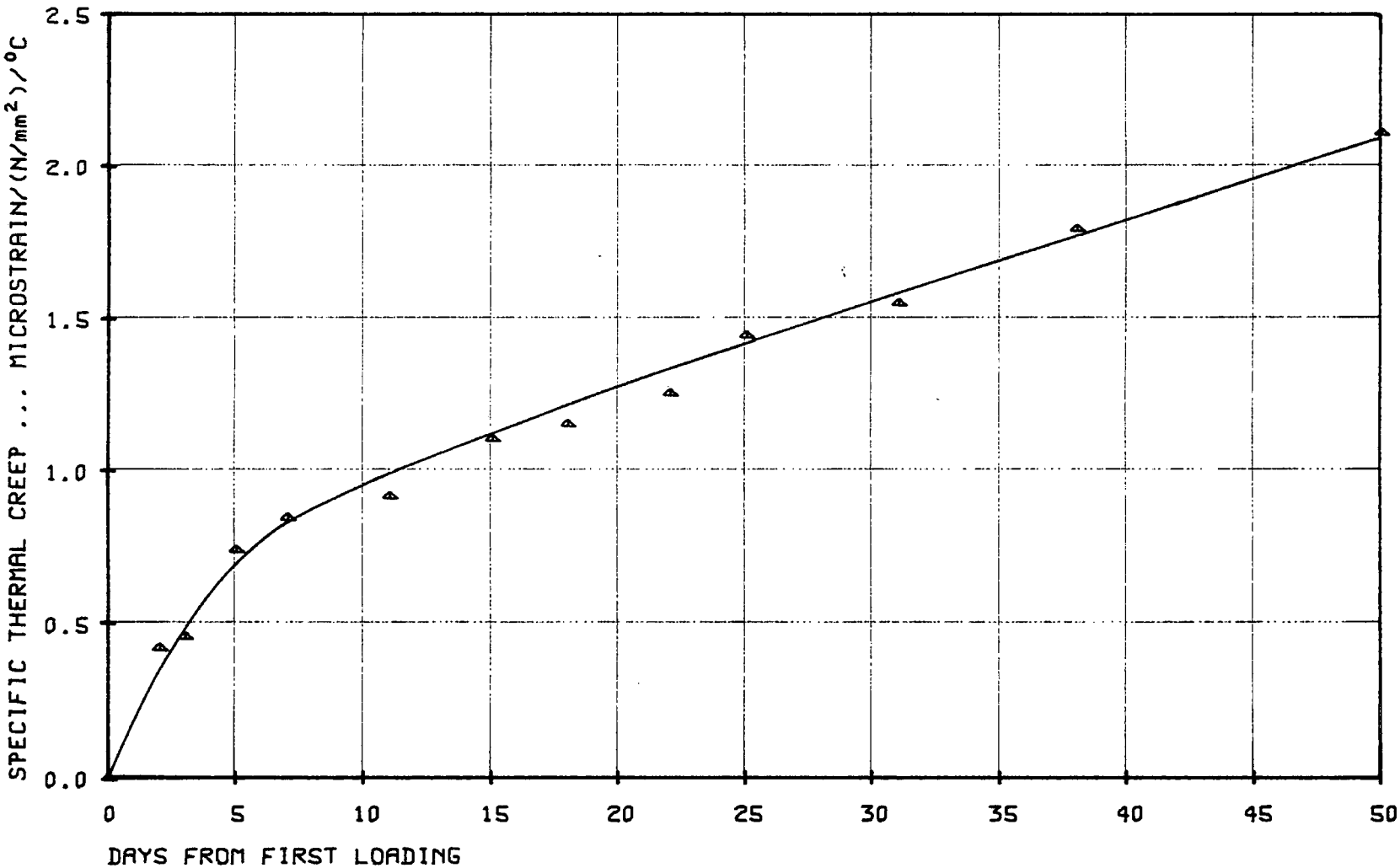

GRAPH 75. CREEP AND SHRINKAGE
SECOND TEST